TEAM tAO

Science

Table of Contents

15 April 2005
Volume 308
Number 5720

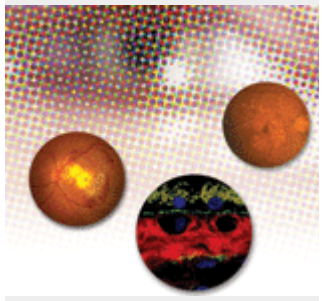

NEW THIS WEEK:

SPECIAL FEATURE

RESEARCH

Damming Analysis

Many large river systems that support a wide variety of ecosystems have been impacted by human needs. **Nilsson *et al.*** (p. 405) present a global overview of how dams have fragmented the world's largest river systems. Nearly half of the world's large river systems have major dams or diversions that either fragment ecosystems or reduce or regulate flow. **Syvitski *et al.*** (p. 376) describe a method for quantifying the impacts of anthropogenic activity, such as building dams, on the delivery of sediments to the coasts. They present an analysis of how sediment fluxes have changed between the past, when human influence was negligible, and the present. Their quantitative, global, river-by-river survey of the majority of the world's rivers reveals that human activities, like irrigation or agriculture, have increased fluvial sediment erosion, but that the rate of sediment delivery to the coasts has decreased because of trapping in artificial reservoirs.

Tracking a Solid-Liquid Transition

A number of studies have examined the ultrafast or nonthermal melting of crystals induced by ultrafast excitation. Shortening of the excitation and probe pulses should allow for greater mechanistic insights into the disordering process. **Lindenberg *et al.*** (p. 392) studied the optically induced melting of an indium antimonide crystal with sub-100-femtosecond x-ray pulses from an accelerator-based source. They modeled the decreases in diffraction intensity of (111) and (220) reflections at the crystal melted. At short times after the optical excitation, the atoms appear to move along a barrierless potential, with their velocities determined by their initial conditions.

Limits on Spin Entanglement?

Many schemes for quantum information processing are based on spin manipulation, but could the interactions between spins place limitations on processing capabilities? **Rønnow *et al.*** (p. 389) look to a solid-state system that may provide some answers. Tuning the magnetic insulator $LiHoF_4$ to a quantum critical point, they monitor the dispersion relation by neutron scattering and show that there is coupling between the electronic and nuclear spins of the ensemble. Such coupling, they suggest, may place limitations on quantum information processing, such as the distance over which spin excitations can be entangled.

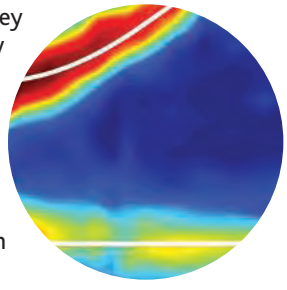

CREDITS (TOP TO BOTTOM): HENDERSON, RØNNOW *ET AL.*

Open Access to Sea Levels

Sea level has varied by amounts well in excess of 100 meters during recent 100,000-year-long glacial cycles. However, smaller but still substantial variations of tens of meters occurred on time scales of only tens of thousands of years. Corals are the best absolute indicators of sea level, but they often exchange uranium with seawater after they have died, which makes it difficult to perform the uranium-thorium radiometric dating needed to establish their ages and the timing of associated sea-level changes. **Thompson and Goldstein** (p. 401; see the Perspective by **Henderson**) have circumvented this problem by developing an analytical method that allows them to correct for the open system behavior of U-series nuclides in corals. They generated a sea-level curve for the last glacial period with sufficient temporal resolution to reveal variations that were not previously clear.

Tetracyclines from Scratch

Pharmaceutical chemists try constantly to modify the structures of antibiotic compounds as bacteria develop resistance to the drugs currently in use. In the case of tetracycline, which treats a broad range of infections including pneumonia, efficient synthetic routes to derivatives have proven hard to develop. **Charest *et al.*** (p. 395; see the Perspective by **Khosla and Tang**) have now found a strategy to access a broad range of structural variants (all of them 6-deoxytetracyclines) in sufficient quantity for bacterial testing in culture. Tetracyclines consist of four consecutively fused carbon rings, labeled A through D, and D-ring variations have shown particular promise against resistant bacteria. The authors prepared the AB fragment first, and then use the same reaction sequence to attach any of six distinctly modified D rings, forming the C ring in the process. The overall routes proceed in 5 to 7% net yield in 14 steps from benzoic acid.

Last Gasps

The cause of the end-Permian extinctions has remained unclear. Reconstructions show that oxygen levels, which were extreme earlier, may have declined markedly around as Earth's overall climate warmed. **Huey and Ward** (p. 398; see the news story by **Kerr**) present a physiological model of the likely effects of such low oxygen levels and show that the only habitable zone may have been at or near sea level.

Blinded by a Complement

Age-related macular degeneration (AMD) is the leading cause of blindness in the developed world and is characterized by a breakdown of light-sensitive cells in the retina. Both genetic and environmental factors are thought to contribute to the disorder, but its molecular pathogenesis has been unclear. Three research groups [**Klein *et al.*** (p. 385), see the cover; **Edwards *et al.*** (p. 421); and **Haines *et al.*** (p. 419)—all published online 3 March 2005] have identified a sequence-specific variant in the genome that increases an individual's risk of developing AMD by three-to sevenfold and that may explain 20 to 60% of AMD incidence in older adults (see the Perspective by **Daiger**). The culprit gene, located on chromosome 1q32, encodes complement factor H, a protein involved in inflammation. This finding opens the door for the development of presymptomatic tests that would allow earlier detection of AMD, which in turn may lead to better treatments.

CONTINUED ON PAGE 323

Published by AAAS

Let's Get Together

Cells fuse in a great variety of circumstances during normal development, such as during the fertilization of the egg by sperm or the formation of mature muscle fibers from individual precursor cells. Cell fusion has also complicated interpretations of experiments involving stem cells. **Chen and Olson** (p. 369) review the mechanics of cell fusion and the variety of circumstances where cell fusion is normally seen, and comment on some of the circumstances surrounding aberrant cell fusion.

Keeping Up Defenses

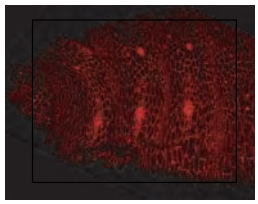

Protective barriers in animals, whether the skin of mammals or cuticle in insects, help prevent dehydration and protect against injury. A conserved innate immune system functions in both vertebrates and invertebrates to combat infectious microbes introduced by epidermal injury. However, less is known about the mechanisms for the aseptic wounding response (see the Perspective by **Harden**). **Mace *et al.*** (p. 381) now describe a wound response pathway in *Drosophila*, which is mediated by the factor grainyhead, and which senses aseptic breaks in the epidermis. The grainyhead mediated response provides cross-linking molecules to fix the cuticular barrier. Complementary work by **Ting *et al.*** (p. 411) suggests that this type of barrier wound response pathway is conserved—mice with a mutation in a mouse grainyhead ortholog show defects in epidermal wound repair.

Malaria Membrane Protein Structure

Apical membrane antigen 1 (AMA1) is an integral membrane protein in malaria-causing *Plasmodium* parasites and is currently in clinical trials against *P. falciparum*, the species that causes the most serious forms of malaria in humans. Although AMA1 is essential for host cell invasion, its molecular function is unknown. **Pizarro *et al.*** (p. 408, published online 24 February 2005) have solved the crystal structure of the three-domain ectoplasmic region of AMA1 from *P. vivax* at 1.8 angstrom resolution. Domains I and II belong to the PAN motif, a protein fold that functions in receptor binding.

The Making of a Simple Timepiece

Cyanobacteria operate under a circadian clock unlike those found in other organisms. It is driven by periodic phosphorylation of a core clock protein, rather than by periodic transcription or translation. **Nakajima *et al.*** (p. 414) now show that this oscillator can be reconstituted in vitro with only three clock proteins and a phosphate source, adenosine triphosphate. This supports the notion that biological time measurement in this simple organism is not rooted in the control of gene or protein expression, but on the dynamics of a complex of three proteins in a mechanism that requires little energy.

Keep Your Eyes on the Ball

Under normal conditions, we are generally not consciously aware of how stimuli arriving via multiple input pathways (such as sight and sound) are integrated into a single percept; this kind of processing can be uncovered when illusory stimuli are presented (for instance, in the McGurk effect: seeing one word being spoken while hearing a related one). **Indovina *et al.*** (p. 416) have adapted this approach to explore the interaction between visual and vestibular systems. Although superb at all sorts of tasks, our visual processing centers do not work quite so well in estimating the accelerations of objects. However, our vestibular system learns to cope with gravity at an early age. Behavioral and brain imaging data suggest that the vestibular system relies on an internal model of how the motions of objects are influenced by gravity and passes that information on to the visual processing centers when subjects estimate the time to collision of a falling ball.

CREDIT: MACE *ET AL.*

Published by AAAS

In Search of a Lifeline

Several recent studies have independently come to a consistent and deeply troubling conclusion: The diversity of life on our planet is declining rapidly, and in the absence of well-targeted conservation efforts, that trend will surely accelerate in the decades ahead. Loss of habitat, invasive species, global warming, pollution, overexploitation, disease, and perhaps other unidentified stressors present a massive threat to global biodiversity. The world's ecosystems provide services whose estimated value is in the trillions of dollars annually. The loss of a significant fraction of these services would have far-reaching biological and economic consequences. Preventing that outcome will require a global response that far exceeds current actions.

This past December, results from the first global assessment of amphibians were reported in *Science* (Stuart *et al*., 3 December 2004, p. 1783). The findings were chilling: More than 43% of all amphibians are in decline, 34 species are reported extinct, and another 113 species have almost or completely disappeared since 1980. Nearly one-third of amphibians worldwide are threatened. Also in December, a Stanford University group reported that 21% of bird species are extinction-prone and 6.5% are functionally extinct. Other studies show that 23% of mammals are threatened. These results are consistent with a comprehensive analysis of biodiversity in the United States, completed 5 years ago by NatureServe and The Nature Conservancy, indicating that one-third of plant and animal species are at risk of extinction. Beyond species, the recent Millennium Ecosystem Assessment paints a bleak picture of human impacts on the world's ecosystems. The assessment found that about 60% of the ecosystem services that support life are being degraded or used unsustainably.

These data are disconcerting at best and alarming at worst, but equally troubling is the reality that governments throughout the world are poorly equipped to address these declines. That's the dilemma of global change: Political processes are slow to recognize and respond to challenges that play out over decades. In some policy areas, dramatic one-time events of less consequence focus government attention and lead to aggressive action. Species and ecosystems are declining rapidly in the context of natural history, but relatively slowly in terms of human history. Hence, governments are slow to respond.

Although the United States has often led in addressing past environmental challenges, today it lags behind other countries in formulating environmental policies to protect species. The United States has not ratified the Convention on Biological Diversity developed at the Rio Earth Summit in 1992, nor is it a party to the Kyoto accords. And even if the world were united behind the Convention on Biological Diversity, its provisions alone are insufficient to stem the rapid decline in global biodiversity. What new approaches might make it possible to attack these issues more aggressively, and what form should they take?

Scientists must work harder to inform political leaders about the urgency of environmental challenges, aid them in developing solutions, and urge them to respond. However, placing the future of life on Earth in the hands of governments alone is a risky strategy.

Lasting societal change usually depends on actions by one or more of these institutions: governments, nongovernmental organizations, corporations, and universities. We may need to depend more heavily on the latter three sectors of society by exploring an unprecedented partnership among them. The objective would be to identify ways of working collaboratively to stem biodiversity decline. Academic scientists already team with nongovernmental organizations in directed efforts; more of the same could greatly expand the global database on biodiversity loss and build our international capacity to deal with the growing environmental challenge. Corporate participation in such partnerships adds an especially valuable element: the possibility of enhancing the innovative efforts already under way by harnessing the power of the marketplace. Measuring the value of ecosystems and the services they provide to human societies has already begun to demonstrate to policy-makers the importance of biodiversity and of building conservation values into planning processes and the price of commercial products. Ultimately, we must engage the tremendous power of individual action and consumer choice through information and economic incentives. Otherwise, the decline in Earth's biodiversity will continue with each tick of the clock.

Mark Schaefer

Mark Schaefer is president and chief executive officer of NatureServe in Arlington, Virginia (www.natureserve.org).

10.1126/science.1113309

edited by Gilbert Chin

EARTH SCIENCE

Forecast: Rain, Less and More

One of the most important aspects of global climate is precipitation, and variations in its timing or amount can have an enormous impact on human resources and activities. A pair of papers illustrate two different aspects of this type of variability. El Niño and La Niña events have dramatic effects on patterns of precipitation all across the globe and are often cited as the cause of large economic losses, because these events are associated with extremes of weather. However, Goddard and Dilley find that climate anomalies during these events are not greater than those that occur in the intervening periods. Moreover, because climate forecasts during El Niño and La Niña events are more accurate than those in the intervening periods, greater preparedness should actually lead to a diminished economic impact.

Jain *et al.* focus on regional hydrologic change in western North America during the late 20th century. They find a trend toward increasing year-to-year variance of stream flow in the major river basins, which coincides with an increase in the synchrony of stream flow changes across basins. These trends are closely related to the atmospheric circulation regimes of the late 20th century. They discuss the implications of this regional hydrologic change on the vulnerability of water resources and raise concerns about the adequacy of water resource planning and operations in this region. — HJS

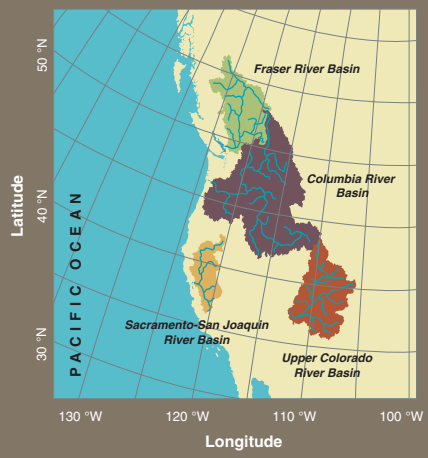

Western North America river basins.

J. Clim. **18**, 651; 613 (2005).

CHEMISTRY

Flexible Dendrimer Synthesis

The formation of dendrimers, in which branching polymer chains extend from a central core, normally involves the covalent attachment of the dendrons to a central core. Leung *et al.* report a dynamic covalent chemistry strategy for the mechanical attachment of dendrons to a core; this pathway, unlike earlier forays, proceeds in high yield. The core bears $-CH_2NH_2^+CH_2-$ centers on each arm that act as binding sites for crown ether groups terminated with two primary amines. These amines are then bridged by a dialdehyde-bearing dendron, producing two imine linkages and forming the ring that locks the macrocycle-dendrimer onto the core. These kinetically stable dendrimers form in >90% yields and can be fixed in place by reduction of the C=N bonds with BH_3 in tetrahydrofuran and subsequent deprotonation with aqueous NaOH. The formation of each generation (0, 1, and 2) of dendrimer products, which reach molecular weights of up to ~5000, was verified by mass spectrometry. — PDS

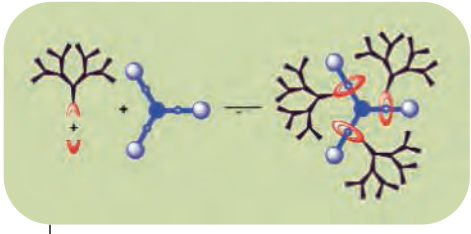

A representation of the synthesis process and the generation 1 dendrimer.

J. Am. Chem. Soc. 10.1021/ja0501363.

PLANT BIOLOGY

Closing the Wound

In the normal cut and thrust of everyday life, nonfatal injuries are common, and organisms rely on rapid repair mechanisms to stanch the loss of fluids. Adolph *et al.* have studied the invasive tropical green alga *Caulerpa taxifolia*, which lives as single polyploid multinucleated cells. In the early 1980s, *Caulerpa* invaded the Mediterranean, and its mechanism of wound repair may have contributed to its high growth rates. When the algal cells are mechanically broken, a gelatinous material consisting of cross-linked proteins rapidly plugs the wound and results in two cells, each with a full genomic inheritance. Polymer formation depends on the enzymatic unmasking of caulerpenyne, the dominant secondary metabolite of the alga. Its 1,4-bis-enoylacetate moiety is transformed into a dialdehyde, which reacts with nucleophilic groups of algal proteins, forming a life-saving plug. — SMH

Angew. Chem. Int. Ed. **44**, 10.1002/anie.200462276 (2005).

ECOLOGY/EVOLUTION

Too Much of a Good Thing

The widespread agricultural use of nitrogenous fertilizers in recent decades has doubled the amount of available nitrogen in the global ecosystem. Although higher levels of N generally cause an increase in primary productivity (the rate at which new plant growth is produced via photosynthesis), they also cause a loss of diversity.

To understand the mechanisms linking N supply to diversity, Suding *et al.* conducted a series of N fertilization experiments across a range of North American ecosystems and assessed the functional and ecological correlates of declining diversity in nearly 1000 plant species. One-third of species losses from the experimental plots were attributable to the initial rarity of these plant species. In most other cases, losses could be attributed to physiological or morphological traits of species. In particular, perennials and species with N-fixing symbioses (such as legumes) were more prone to local extinction after N fertilization, and native species tended to fare worse than non-natives. The relative importance of the trait-specific effects (versus initial abundance) varied across ecosystems; for example, there was a disproportionate loss of legumes from tallgrass

CREDITS: (TOP) JAIN *ET AL.*, *J. CLIM.* **18**, 651; 613 (2005); (BOTTOM) LEUNG *ET AL.*, *J. AM. CHEM. SOC.* 10.1021/JA0501363

prairie. Thus, these experiments generate predictions of how patterns of plant diversity will decline as N loading continues to increase. — AMS

Proc. Natl. Acad. Sci. U.S.A. **102**, 4387 (2005).

CHEMISTRY

Stitching Siloxanes

Siloxane polymers are widely used for their rubbery character. The stiffness and durability of the materials are influenced by the side groups pendant from the main Si-O chain. However, polymerization conditions often restrict the structural versatility of the monomers.

Chauhan and Rathore use platinum nanoclusters as a hydrosilation catalyst to append terminal olefins to the Si-H branches of (methylhydro)siloxane polymers. The reaction proceeds in benzene at room temperature with 0.1% catalyst loading and shows remarkable functional group tolerance. In addition to aromatic and alkyl groups, olefins bearing carbonyls, epoxides, and ferrocene were all successfully incorporated. Analysis of the products by nuclear magnetic resonance spectroscopy revealed strong regioselection (99:1 for nonaromatics) for Si bonding to the terminal carbon. — JSY

J. Am. Chem. Soc. 10.1021/ja042824c (2005).

PSYCHOLOGY

Genes and Environment

A classic approach to assessing the relative contributions of genes and environment to human behavior is to interrogate identical and fraternal twins. Hughes *et al.* have recruited 1116 pairs of twins (56% of whom are identical) in England and Wales and measured their performance at 5 years of age on a battery of theory-of-mind tasks, which collectively probe an understanding that beliefs can be false representations of reality (see also Perner and Ruffman, Perspectives, 8 April, p. 214). They find that genetic factors account for very little of the variance in task performance, and that shared (for example, siblings and social-economic status) and nonshared environmental factors each explain about half of the variance. The nonshared influences may come either from within the home, in the form of contrasting parental care, or from without, via interactions with socially skilled peers. It will be of interest to revisit these children in order to explore the relation between their theory-of-mind skills and their social development. — GJC

Child Dev. **76**, 356 (2005).

CELL BIOLOGY

Front and Back

Mammalian neutrophils and the amoebalike cells of the slime mold *Dictyostelium discoideum* respond to chemoattractants by engaging specific signaling mechanisms at the front and rear ends of the cell. During chemotaxis, two members of the Rho family of small GTPases, Rac and Cdc42, control actin dynamics at the leading edge of the cell. Meanwhile, RhoA controls contraction at the trailing end, which is where the phosphatase PTEN resides (which has the effect of restricting its phosphatidylinositol trisphosphate substrate to the front end).

Li *et al.* discovered that treatment of neutrophils or human embryonic kidney (HEK) cells with an inhibitor of RhoA-associated kinase (ROCK) blocked PTEN localization in response to a chemoattractant. Further analysis of HEK cells revealed that PTEN translocation and

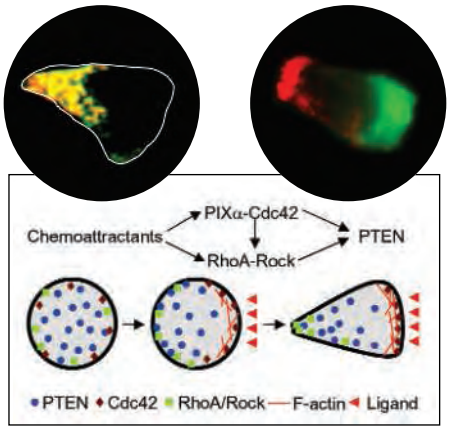

A model for GTPase regulation of PTEN, and localizations of Rho (left, green), Cdc42 (right, green), and PTEN (red).

activation could be induced by a constitutively activated form of RhoA and also by active Cdc42. A mutant PTEN that lacked four putative phosphorylation sites failed to rescue the chemotactic defects of cells lacking PTEN, and the mutant form also lacked lipid phosphatase activity when expressed with constitutively activated RhoA, suggesting that a RhoA-ROCK signaling pathway is required for phosphorylating and activating PTEN. Because neutrophils that were unable to activate Cdc42 in response to a chemoattractant also failed to localize RhoA and PTEN to the cell posterior, these two GTPase signaling pathways may cooperate to control PTEN during chemotaxis. — LDC

Nat. Cell Biol. 10.1038/ncb1236 (2005).

CREDITS: LI *ET AL., NAT. CELL BIOL.* 10.1038/NCB1236 (2005)

NetWatch

edited by Mitch Leslie

IMAGES

Electron Visions

Under the electron microscope, the surface of a cat's tongue (above) resembles a doormat, with rows of the backward-pointing tines, known as papillae, that come in handy for primping the creature's fur. The micro world comes into focus at this Web gallery from microscopist and professional photographer Dennis Kunkel of Kailua, Hawaii. The more than 1500 colorized and black-and-white electron micrographs expose a flea's face, the wrinkles on the surface of a stem cell, the bacteria speckling a patch of human skin, and many more hidden details. Teachers and researchers can use the images for free by contacting Kunkel.

education.denniskunkel.com

WEB TEXT

On the Defensive

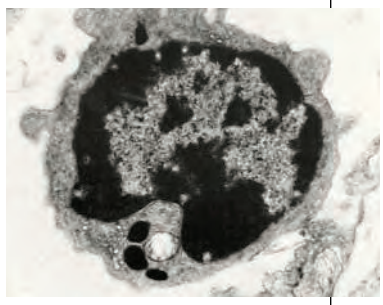

Signs of our protracted struggle against pathogens show up in our genome—up to 10% of our genes may help build or operate body defenses. Learn more about the molecular and genetic underpinnings of the immune system in this primer written by medical student Daniele Focosi of the International Centre for Genetic Engineering and Biotechnology in Trieste, Italy. Packed with links and original pages, Molecular Immunology is an outline-style guide aimed at upper-division college students and above. Readers can start by touring our border defenses, learning about, say, the 20 varieties of gooey mucin molecules that trap pathogens trying to sneak in through the nose, mouth, and other entryways. Other topics include the origin of infection-fighting cells such as this T cell (above) and the immune systems of fruit flies and other model organisms.

www.mi.interhealth.info

DATABASE

Who's Your (Chemistry) Daddy?

Much like genealogy buffs piecing together their ancestry, science historians compile intellectual genealogies that unravel researchers' influences and impact by mapping out their mentors and students. This site reconstructs the intellectual family trees of more than 1500 chemists from the 15th century through the late 20th century. For example, a line runs from chemist Larry Faulkner, who is now the president of the University of Texas, Austin, to the Italian scholar Nicolo da Lonigo (1428–1524). Vera Mainz and Gregory Girolami of the University of Illinois, Urbana-Champaign, compiled the database by working backward from faculty lists for 10 major universities, including the Massachusetts Institute of Technology, the University of California, Berkeley, and their own. Click on each chemist to download a PDF with biographical details, a career synopsis, and references.

www.scs.uiuc.edu/~mainzv/Web_Genealogy

COMMUNITY SITE

Beneath the Bark

By parsing the rings in this red oak trunk (*Quercus rubra*; below), a sharp-eyed dendrochronologist can read the tree's life story, deducing past fires, droughts, and other growth-changing events. These wooden records can help researchers track global warming, investigate the collapse of ancient civilizations, and more. Featuring everything from a jobs board to a gallery, the Ultimate Tree Ring Pages from dendrochronologist Henri Grissino-Mayer of the University of Tennessee, Knoxville, brims with information for professionals and initiates into the fellowship of the rings. Visitors can download a slew of software for analyzing tree-ring records and browse a giant bibliography with more than 10,000 listings stretching back to 1737. A list of recommended supplies explains why even pacifist dendrochronologists need gun-cleaning kits. (They're ideal for dislodging gunk from the long tube of an increment borer, the standard tool for removing cores.) Links include tree-ring databases and a tutorial on cross-dating, the technique for matching sequences from different trees to ascribe a year to each ring.

web.utk.edu/%7Egrissino/default.html

EXHIBITS

Sickle Cell Mystery

When he wasn't probing the secrets of chemical bonds or championing vitamin C, chemist Linus Pauling was often puzzling over hemoglobin. "It's in the Blood!" from Oregon State University in Corvallis chronicles the chemist's more-than-60-year fascination with the blood's oxygen-hauling molecule. The high point came in 1949, when Pauling and his colleagues discovered that hemoglobin from patients with the hereditary illness sickle cell anemia behaves differently than hemoglobin from healthy people does, inaugurating the concept of a molecular disease. The low point came in the 1960s, when Pauling campaigned for laws regulating childbearing by sickle cell disease carriers and urged that they be tattooed on the forehead for easy recognition.

osulibrary.oregonstate.edu/specialcollections/coll/pauling/blood/index.html

Send site suggestions to netwatch@aaas.org. Archive: www.sciencemag.org/netwatch

CREDITS (TOP TO BOTTOM): DENNIS KUNKEL MICROSCOPY INC.; DANIELE FOCOSI; HENRI GRISSINO-MAYER

Published by AAAS

NEWS

This Week

PAGE 338
A European Mars wish list

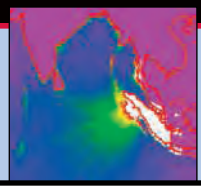

341
Islands damp second Sumatra tsunami

STEM CELLS

Restiveness Grows at NIH Over Bush Research Restrictions

Dissatisfaction within the National Institutes of Health (NIH) is growing over the Bush Administration's restrictions on funding for work with human embryonic stem (ES) cells. Meanwhile, measures to loosen restrictions may finally make it to the floor this year in Congress.

Reluctant defender? NIH's Elias Zerhouni.

At a hearing last week by a Senate appropriations subcommittee chaired by Arlen Specter (R–PA), NIH Director Elias Zerhouni seemed to defend the policy only reluctantly, citing "mounting evidence" that as the 22 approved cell lines age, an increasing number of problems are arising because of genetic instability. "Clearly, from a scientific standpoint, more might be helpful," said Zerhouni, who pointed out that the Bush policy forbidding the use of cell lines derived after 9 August 2001 is based on moral and ethical concerns. Asked by Specter "where is the moral issue" for embryos that are slated for disposal anyway, Zerhouni responded, "I think you'll have to ask that from those who hold that view."

Specter also released letters from several institute directors chafing at restrictions and warning that NIH could be falling behind in the field. Specter got some unvarnished sentiment by telling the directors to answer a set of questions he posed "without editing, revision, or comment by the Department of Health and Human Services." The following are some excerpts:

• Elizabeth G. Nabel, director of the National Heart, Lung, and Blood Institute: "NIH has ceded leadership in this field to the new California agency. … Because U.S. researchers who depend on Federal funds lack access to newer hESC lines, they are at a technological disadvantage. … The restricted access will hamper NIH's ability to recruit … young scientists."

"NIH has ceded leadership in this field to the new California agency."

Elizabeth G. Nabel

—Elizabeth G. Nabel
Director, NHLBI

• James Battey, director of the National Institute on Deafness and Other Communication Disorders (and until last month chair of the NIH Stem Cell Task Force): "The science is evolving very rapidly, and limitations of the President's policy [have] become more apparent since I last testified. … It is likely that there will be a movement of some of the best stem cell biologists to California."

• Duane Alexander, director of the National Institute of Child Health and Human Development: "NICHD scientists report some problems in obtaining … cell lines, [including] inadequate quantity and quality, … high prices, 'cumbersome' procedures, and long waiting times."

Battey—who said last week that the new conflict-of-interest rules that forbid many NIH managers and their families from owning stock in biomedical companies are compelling him to leave NIH—agrees that frustration over stem cell research constraints has been growing steadily at the agency. "I think many of our finest scientists are troubled by the policy," he told *Science*. He points out that ▶

AIDS RESEARCH

IOM Panel Clears HIV Prevention Study

An Institute of Medicine (IOM) panel has found no major improprieties in the conduct of a key HIV trial in Uganda to prevent mother-to-child transmission in the late 1990s, essentially validating the use of a cheap, effective, and simple anti-HIV drug: nevirapine. The report also helps clear the names of Johns Hopkins University pathologist Brooks Jackson and more than a dozen colleagues.

In two papers published in *The Lancet* in 1999 and 2003, National Institutes of Health (NIH)–funded researchers reported that giving a pregnant woman a single dose of nevirapine, and her infant a single dose immediately after birth, dramatically cut mother-to-child transmission rates. Since then, nevirapine has become the cornerstone of HIV prevention efforts in infants across Africa and beyond. But last year the work came under fire from an NIH staffer, Jonathan Fishbein, who charged that the investigators failed to adhere to regulatory standards governing data collection and record keeping (*Science*, 24 December 2004, p. 2168). He argued in an interview that "you cannot use this trial as part of the knowledge about how that drug works."

The nine-member IOM committee agreed that the study wasn't foolproof. But "we feel firmly that the findings and the conclusion … are valid," said committee member Mark Kline, a pediatric infectious disease specialist at Baylor College of Medicine in Houston, Texas. The committee had primary medical records sent from Uganda and focused on a sampling of 49 infants in the study. About 10% of adverse events went unreported in that sample, they noted.

Fishbein immediately blasted the IOM report as "an apologist's statement" that supported NIH's point of view. At a tense press conference, he and his brother, Rand Fishbein, a defense and foreign policy consultant, asked how the IOM committee could be unbiased, given that six of its members receive NIH grants.

IOM president Harvey Fineberg called that accusation "preposterous," adding that "there is nothing financially at stake for the individuals on this committee."

Some in the AIDS prevention field, who have worried that African governments would abandon nevirapine, are hoping that the IOM report will end the controversy. The Ugandan trial "was a critical pilot study" of nevirapine that has been confirmed by at least a half-dozen others, says Arthur Ammann, a pediatric immunologist and president of Global Strategies for HIV Prevention in San Francisco.

—Jennifer Couzin

CREDIT: RICK KOZAK

Published by AAAS

342 A new European research plan

346 What happens when a forest dries out?

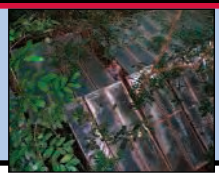

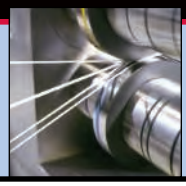

348 Prospects brighten for superconducting wire

newer cell lines are being grown free of contamination from animal products, and that one of scientists' goals—creating ES cell lines that can be used as models to study diseases—is being fulfilled at the Reproductive Genetics Institute in Chicago, Illinois. That fertility clinic claims it has created 50 cell lines representing six genetic diseases, including muscular dystrophy, from fertilized eggs that otherwise would have been discarded. But none of them can be touched by a U.S. government-funded researcher.

Battey is most worried about the effect of the federal restrictions on young scientists. "Young people are now electing to stay away" from research with human ES cells, he says. Mahendra Rao, who does stem cell research at the National Institute on Aging, says he's experiencing that firsthand: "I have four postdoc positions vacant in my lab." He says he knows of at least three colleagues—not counting Battey and Arlene Chiu (who just accepted a job in California; see p. 351)—who have interviewed for jobs in California.

"Limitations of the President's policy [have] become more apparent since I last testified in April 2004."

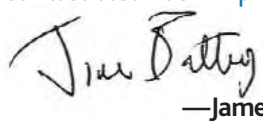

—James F. Battey Jr.
Director, NIDCD

The White House continues to stand firm against any revision in the policy, but pressure continues to grow in Congress. Last month, the moderate Republican sponsor of a bill to expand stem cell availability, Michael Castle (DE), got House Speaker Dennis Hastert (R–IL) to agree to schedule a vote on it this year.

–Constance Holden

With reporting by Jocelyn Kaiser.

NUCLEAR WASTE

Academy Gets the Word Out After Tussle With Agency

The National Academies (NAS) released a report last week that says dry storage of aging spent nuclear fuel offers "inherent security advantages" over submerging the rods in pools at reactor sites. The fact that a sponsor, the Nuclear Regulatory Commission (NRC), disagrees with that message is not unusual. What makes this report stand out is that the two sides spent 8 months negotiating a public version, and that the NRC preempted the academy by going public with a point-by-point rebuttal of the document while it was still under wraps. The episode is the latest illustration of ongoing problems between NAS and the government over handling of sensitive but unclassified data (*Science*, 22 November 2002, p.1548).

With no active repository for radioactive materials, some 54,000 tons of nuclear fuel have accumulated at U.S. reactors since the 1970s. Most of the fuel sits in pools, raising the concern that a terrorist attack could drain the water from the pools, causing the fuel to ignite and emit radioactive material over a large area. Congress called for the study after a 2003 paper said pools posed a safety threat "worse than … Chernobyl," a conclusion the NRC said lacked a "sound technical basis."

Last July the academy panel sent Congress a classified version of its report that raised concerns about the pools and urged NRC to take a fresh look at the problem. Separate dry casks, it said, are more robust than pools and would allow plants to disperse the older fuel. It also suggested redistributing hot fuels and installing water-cooling systems to cope with leaks. Daniel Dorman, NRC deputy director for nuclear security, says that pools and dry storage "both provide adequate protection" and that new steps to protect spent fuel are under way. At the same time, he says NRC agrees with the report's call for more outside review of the issue and its assertion that any theft of rods to make dirty bombs is unlikely.

The academy panel then turned to producing a public version. Getting the word out, however, proved arduous. In December, NRC rejected a draft version despite the fact that NAS left out data on how fuel rod fires could overheat, potential radiation releases, and specific attack scenarios. That material had been withheld as a precaution, according to panel members, but NRC told the academy that the draft was still "permeated with sensitive information" and requested an entirely new version. "That's not the way we operate," says committee director Kevin Crowley, who asked NRC for specific security concerns.

In March, before the parties could agree on a public version, NRC released a point-by-point response to much of the classified report. The academy, officials wrote, was asking for "more than what was needed." Last week NRC officials admitted that the document overstated a finding of the academy report by claiming that the committee had called for "earlier movement of spent fuel from pools into dry storage" when it had not.

After the dustup hit the papers, legislators demanded a public version. Last week it appeared, in a version that panelists and academy officials say is substantially unchanged from the November draft. This week, NRC said the public report "alleviated [its] concerns about sensitive information."

Hot rods. Academy report points to security flaws in keeping spent nuclear fuel in pools long after it has cooled.

"The academy clearly doesn't want to provide information that could be damaging to the country," says NAS Executive Officer E. William Colglazier. But without clearer rules governing what should be secret, he adds, "I wouldn't say we're not going to have this problem again."

–Eli Kintisch

CREDIT: NEI

Published by AAAS

GEOCHEMISTRY

Gasping for Air in Permian Hard Times

Life late in the Permian period certainly sounds unhealthy. More than 250 million years ago, the world was overheating under a growing greenhouse. The great Siberian Traps eruptions were spewing acid haze. Within the seas, noxious gases were building as oxygen dwindled. And something was about to trigger the worst mass extinction in the history of life. How could conditions have been any worse?

On page 398, researchers count some of the ways, from the standpoint of evolutionary biology. On land, atmospheric oxygen was sliding from a heady 30% toward a lung-sapping 15% or below. Low atmospheric oxygen would have squeezed land animals into smaller, more fragmented areas at low altitudes, inducing extinctions while driving down diversity. The hypothesis "adds another dimension" to the role of oxygen in evolution, says biologist Robert Dudley of the University of California, Berkeley. It also complicates the question of how the end-Permian extinction took place.

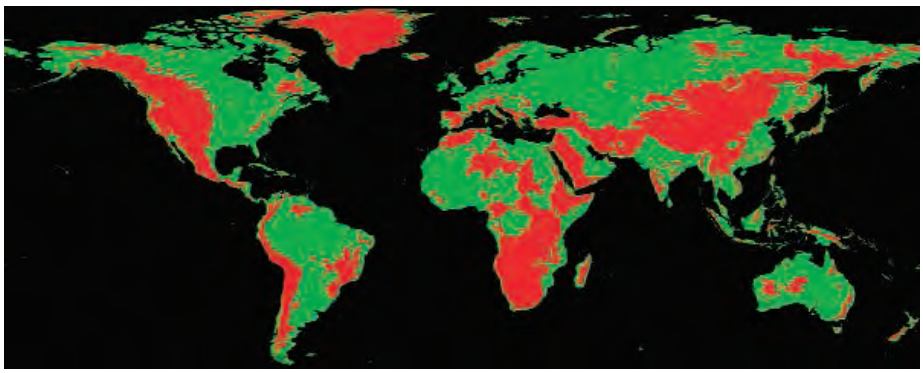

Too high. If the low atmospheric oxygen levels of the late Permian period prevailed today, few vertebrate animals could live much above an altitude of 500 meters (red).

CREDIT: R. HUEY *ET AL.*

Geochemists can gauge past oxygen levels by taking account of organic matter and reduced sulfur compounds stored in sediments—in effect, the byproducts of oxygen generation. In 2002, geochemist Robert Berner of Yale University calculated that during the past 600 million years, atmospheric concentrations of oxygen were stable near present-day levels of 20% until about 400 million years ago, rose sharply to a peak above 30% about 300 million years ago, and then dove to 12% by 240 million years ago.

Paleontologist Gregory Retallack of the University of Oregon, Eugene, and colleagues suggested in 2003 that such a precipitous decline could have determined winners and losers at the end of the Permian. One of the few large animals to survive the end-Permian extinction, a dog-sized burrowing creature called *Lystrosaurus*, appears to have been well-adapted already for breathing oxygen-poor air, says Retallack. Like humans adapted to living at high altitudes, *Lystrosaurus* had developed a barrel chest for deeper breathing, among other adaptations, apparently in order to "breathe its own breath" more easily in its underground lairs (*Science*, 29 August 2003, p. 1168).

On less well prepared animals, losing more than half of the normal oxygen supply would have had far-reaching effects, say evolutionary physiologist Raymond Huey and paleontologist Peter Ward of the University of Washington, Seattle. Every animal has its own minimum oxygen requirement, they note. That's why each species has a particular altitude beyond which it doesn't live. For example, humans live and reproduce no higher than 5.1 kilometers, in the Peruvian Andes. So, "if oxygen is 12%, sea level would be like living at 5.3 kilometers," says Huey.

With oxygen at the mid-Permian's peak of 30%, animals probably could have breathed easily at any altitude on Earth, says Huey. But as oxygen levels dropped, animals capable of living at 6.0 kilometers in the mid-Permian would have been driven down to 300 meters. Perhaps half of the Permian land area would have been denied to animals. Species specialized to live in upland habitats would have perished, assuming they couldn't adapt their relatively unsophisticated breathing systems. Survivors would have been squeezed down into smaller, more isolated areas, where overcrowding and habitat fragmentation would have driven up extinctions and diminished the number of species the land could support. "We can explain some big part of land extinction with this," says Ward.

Extinction by crowding into lowlands "is a very interesting idea," says Dudley, but "it's pretty hypothetical. None of the assumptions is yet testable." Further studies of breathing physiology and geographical patterns in the fossil record should help size up just how bad life might have been. **–RICHARD A. KERR**

ScienceScope

Zerhouni Hopes to Revise Stock Limits

Two months after announcing new conflict-of-interest rules, National Institutes of Health (NIH) Director Elias Zerhouni is rethinking the strict limits on owning biomedical stock.

The ethics rules were imposed after revelations that some NIH researchers had received hefty consulting payments from industry. But the stock limits are deterring some from joining NIH and persuading others to leave, including James Battey, director of the National Institute on Deafness and Other Communication Disorders, Zerhouni told a Senate subcommittee last week (see p. 334). He explained that the stock rule was imposed by the Department of Health and Human Services (HHS) and Office of Government Ethics, which felt that NIH should be treated like a regulatory agency. "We need to reevaluate" the stock provision "quickly," Zerhouni said.

Last week, a group of senior NIH scientists asked the U.S. Court of Appeals for the District of Columbia to review the rules in part because HHS didn't collect comments first. **–JOCELYN KAISER**

Hungarian Faculty Face Layoffs

Already squeezed by cuts to the national granting agency (*Science*, 26 November 2004, p. 1455), hundreds of Hungary's scientists now face layoffs stemming from a $21 million shortfall across higher education. A government-mandated 7.5% pay raise for faculty went into effect on 1 January this year, but funding increases for universities, which are overwhelmingly government-supported, have not kept pace. Science classes are more expensive than are the humanities, notes George Kampis of Eötvös Loránd University in Budapest, whose department of history and philosophy of science is under the gun. **–GRETCHEN VOGEL**

Trying Again on ITER

TOKYO—Japan and the European Union last week set an early July deadline to resolve the 15-month stalemate over which one will host the $5 billion International Thermonuclear Experimental Reactor (ITER). Japan's Education, Culture, Sports, Science, and Technology Minister Nariaki Nakayama and European Commissioner for Science and Research Janez Potočnik discussed how to iron out the main sticking point, that is, what to give the loser in exchange for not hosting the reactor. An agreement on how to split responsibilities for the mammoth project will hopefully set the stage for a unanimous selection of either the French or Japanese site. **–DENNIS NORMILE**

Published by AAAS

EUROPEAN SCIENCE

A Second Entry in the Mars Sweepstakes

LONDON—More than 100 European scientists met last week in Birmingham, U.K., to define Aurora, a solar system exploration venture that faces a critical decision this year. The workshop on 6 to 7 April began with one certainty: Europe wants its own Mars program. The scientists endorsed a one-way robotic trip to Mars in 2011 and hashed out the types of instruments they want onboard to search for signs of life and study geology. They also backed a follow-on sample-return mission. But big issues remain to be settled, such as whether governments will pay, and how they will coordinate the work with an ambitious U.S. Mars program.

Aurora's head at the European Space Agency (ESA), Bruno Gardini, said at a press conference here that he was pleased with the workshop's outcome. "It has given us a very focused target," he said. Doug McCuistion, director of NASA's Mars Exploration Program, an observer at the workshop, agrees: "It's very important that they were able to narrow their options so they can go forward."

Three proposals were on the table at the outset. The scientists recommended plucking out elements of each and rolling them into one mission, as yet unnamed. One piece of heavy equipment made it onto their consensus wish list: a drill to take samples at a depth of up to 2 meters below Mars's oxidized surface. NASA does not have a drill on its agenda, McCuistion says. The scientists also recommended including a rover with sensors to look at ratios of isotopes for traces of past or present life, modeled after those on Beagle 2, the United Kingdom's ill-fated robot that went missing in December 2003 during its descent to Mars. The scientists also want to include a seismograph to detect possible "marsquakes" that could show that the planet is geologically active.

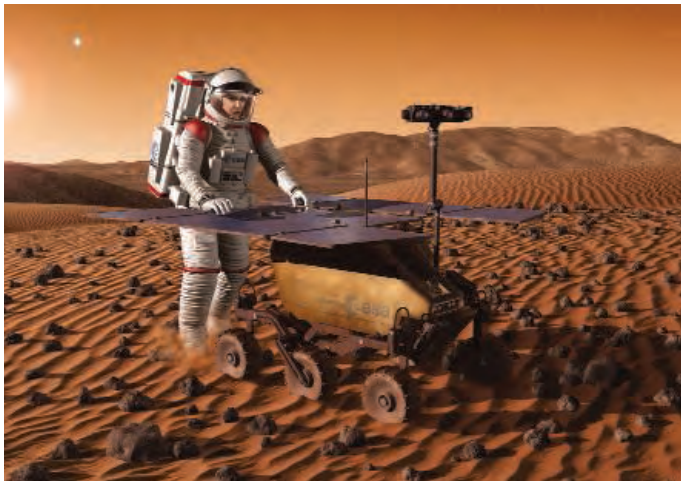

Long haul. Europe's vision for space exploration calls for sending first robots, then humans, to Mars.

Before the plans get much more specific, ESA needs some of its member countries to pony up for the mission, which carries a price tag of €500 million ($650 million). ESA members make voluntary contributions to Aurora, described at its launch in 2001 as a search for signs of life beyond Earth and a start to crewed exploration of the solar system. By June, Aurora's staff will put together a more detailed plan for a complete funding review, in which countries will choose whether to pledge support to carry the 2011 project through to completion. The total ▶

JAPAN

Space Vision Backs Peer-Reviewed Science

TOKYO—Space scientists here are reacting favorably to a new strategic plan from the Japan Aerospace Exploration Agency (JAXA) that endorses a bottoms-up approach to scientific exploration (*Science*, 1 April, p. 33). Many had feared the worst when Japan's space science agency was merged with two commercially oriented government organizations in 2003 to form JAXA. But "a number of former NASDA [National Space Development Agency] people are now listening to what space scientists say and realizing that there is a different approach to [scientific] missions," says Kazuo Makishima, an astrophysicist at the University of Tokyo.

The Long Term Vision report, issued last week, looks ahead for 20 years. It calls for strengthening efforts in basic space science, with the missions to be determined using the same grassroots approach to proposals adopted by the Institute for Space and Astronomical Science (ISAS), now a component of JAXA. The report discusses the possibility of crewed missions and a lunar base, but only after an additional 10 years of research and study. The plan also cites the need for satellites that could monitor natural disasters, facilitate rescue efforts, and provide a closer look at ongoing environmental problems, as well as for better launch technologies, a private-sector space industry, and supersonic aircraft. "For space science, we have to work with the scientific community, including university-based scientists," says Keiji Tachikawa, JAXA president.

Teamwork. JAXA's Keiji Tachikawa wants scientists to help chart a course for space exploration.

Tachikawa says that JAXA hopes to use the report to develop more detailed operational plans, to motivate employees, and to build public support for space exploration. The report recommends postponing any decision to pursue crewed flight until halfway through the 20-year cycle. "We believe that what can be accomplished with robotics is not sufficient to realize the potential of using space," says Tachikawa, noting Japan's participation in the international space station. The delay also puts off the need for an immediate ramp up in funding, however, with the report calling instead for a modest rise in annual spending from the current $2 billion to $2.6 billion over the next decade. Crewed activities will require more money, Tachikawa says, and "a good proposal [that would] gain the consent of Japanese citizens."

Scientists say they would welcome any new efforts by JAXA to build public support for space activities. "We've not been good at advertising the activities and accomplishments of Japan's space science," says Kozo Fujii, an astronautical engineer who headed a delegation to the vision committee from ISAS. A larger JAXA budget built upon growing public support for space, he predicts, would also be a boon for science.

–DENNIS NORMILE

CREDITS (TOP TO BOTTOM): ESA; D. NORMILE

Published by AAAS

budget is "a very challenging target," Gardini said. "We are trying very hard to get support from NASA to reduce the cost and risk of the mission." Canada, Japan, and Russia might also take part in the mission, he added.

European researchers see the 2011 mission as preparation for a much more ambitious round trip to return samples of Mars rock, soil, and atmosphere. Space scientist John Zarnecki of The Open University in the United Kingdom, a participant in the workshop, said the group recommended working toward such a mission in 2016, which would fit with NASA's timing for such a mission. "I think everyone hopes and expects that this is going to be a big international push with ESA, NASA, and possibly other agencies," Zarnecki says.

This work is designed to prepare for possible international crewed missions to Mars, which ESA hopes will begin around 2030. Gardini said the sample-return mission would be valuable practice in making the round trip. Aurora faces a big test in December, when ESA's governing council will vote on funding.

–MASON INMAN

PARTICLE PHYSICS

Magnetic Scope Angles for Axions

After 2 years of staring at the sun, an unconventional "telescope" made from a leftover magnet has returned its first results. Although it hasn't yet found the quarry it was designed to spot—a particle that might or might not exist—physicists say the CERN Axion Solar Telescope (CAST) is beginning to glimpse uncharted territory. "This is a beautiful experiment," says Karl van Bibber, a physicist at Lawrence Livermore National Laboratory in California. "It is a very exciting result."

CAST is essentially a decommissioned, 10-meter-long magnet that had been used to design the Large Hadron Collider, the big atom smasher due to come on line in 2007 at CERN, the European high-energy physics lab near Geneva. When CERN scientists turn on the magnet, it creates a whopping 9-tesla magnetic field—about five times higher than the field in a typical magnetic resonance imaging machine. From a particle physicist's point of view, magnetic fields are carried by undetectable "virtual" photons flitting from particle to particle. The flurry of virtual photons seething around CAST should act as a trap for particles known as axions.

Axions, which were hypothesized in the 1970s to plug a gap in the Standard Model of particle physics, are possible candidates for the exotic dark matter that makes up most of the mass in the cosmos. Decades of experiments have failed to detect axions from the depths of space, and many physicists doubt the particles exist (*Science*, 11 April 1997, p. 200). If axions do exist, however, oodles of them must be born every second in the core of the sun and fly away in every direction.

That's where CAST comes in. "When an axion comes into your magnet, it couples with a virtual photon, which is then transformed into a real photon" if the axion has the correct mass and interaction properties, says Konstantin Zioutas, a spokesperson for the project. "The magnetic field works as a catalyst, and a real photon comes out in the same direction and with the same energy of the incoming axion." An x-ray detector at the bottom of the telescope is poised to count those photons.

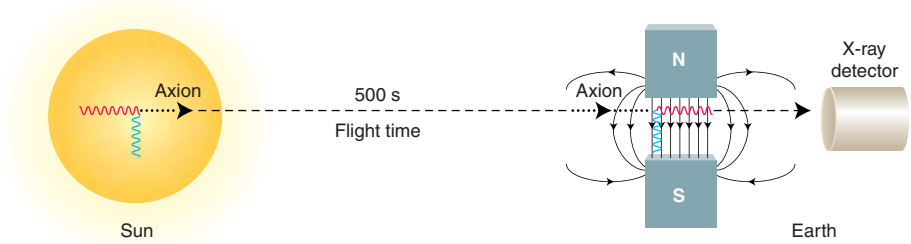

X-files. CAST "telescope" hopes to detect hypothesized particles from the sun by counting the x-rays they should produce on passing through an intense magnetic field.

The first half-year's worth of data, analyzed in the 1 April *Physical Review Letters*, showed no signs of axions. But CAST scientists say the experiment is narrowing the possible properties of the particle in a way that only astronomical observations could do before. "It's comparable to the best limits inferred from the stellar evolution of red giants," van Bibber says, and he notes that plans to improve the sensitivity of the telescope will push the limits further. Even an improved CAST would be lucky to spot axions, van Bibber acknowledges, because most of the theoretically possible combinations of the particle's properties would slip through the telescope's magnetic net. Still, he's hoping for the best. "Maybe Nature will deal a pleasant surprise," he says.

–CHARLES SEIFE

CREDIT: P. HUEY/*SCIENCE*

ScienceScope

Lockheed Boosts Los Alamos Bid

U.S. aerospace giant Lockheed Martin strengthened its bid to run Los Alamos National Laboratory in New Mexico this week by recruiting a key senior scientist. Sandia National Laboratories Director C. Paul Robinson, who spent 18 years at Los Alamos before moving to Sandia in 1990, has joined the proposal team for the Bethesda, Maryland–based company.

Lockheed officials want Robinson, 63, to head Los Alamos if they beat out the lab's current contractor, the University of California. Final competition details are expected soon, with bids in the summer. Meanwhile, former weapons chief Thomas Hunter has been promoted to director of Sandia, which has facilities in California and New Mexico.

–ELI KINTISCH

Pig Flu Scare—Case Closed?

The World Health Organization (WHO) hopes that the results of a new study will put to rest suspicions that pigs in South Korea have become infected with a potentially dangerous flu strain.

Last fall, Sang Heui Seo of Chungnam National University in Daejeon, Korea, deposited flu sequences in GenBank that suggested that Korean pigs carried WSN/33, a flu strain widely used in labs but not known to occur in nature. Several experts and WHO dismissed the findings as the result of lab contamination (*Science*, 4 March, p. 1392); now, Yoshi Kawaoka of the University of Wisconsin, Madison, and his colleagues have tested 400 samples from two Korean pig farms, WHO says, and found no trace of WSN/33.

Seo declined to comment. Henry Niman, a business owner in Philadelphia who backs Seo's claim, says Kawaoka's study wasn't broad enough to refute the theory. But, says WHO flu expert Klaus Stöhr, "we've spent too much time on these speculations already."

–MARTIN ENSERINK

Plant Center to Cut Jobs

The John Innes Centre in Norwich, U.K., one of Europe's top plant science institutions, plans to cut up to 35 researchers from its 800-person staff. Director Christopher Lamb announced on the center's Web site last week that the center began losing money 18 months ago when two funders—the European Union and private industry—became "less reliable sources." Income to the center, which has a $40 million annual budget, has dropped by $5.7 million.

This is "a big blow," says plant geneticist Michael Wilkinson of the University of Reading, U.K., adding that the institution produces an "astonishing number" of widely cited basic science papers.

–ELIOT MARSHALL

Published by AAAS

GEOCHEMISTRY

Gasping for Air in Permian Hard Times

Life late in the Permian period certainly sounds unhealthy. More than 250 million years ago, the world was overheating under a growing greenhouse. The great Siberian Traps eruptions were spewing acid haze. Within the seas, noxious gases were building as oxygen dwindled. And something was about to trigger the worst mass extinction in the history of life. How could conditions have been any worse?

On page 398, researchers count some of the ways, from the standpoint of evolutionary biology. On land, atmospheric oxygen was sliding from a heady 30% toward a lung-sapping 15% or below. Low atmospheric oxygen would have squeezed land animals into smaller, more fragmented areas at low altitudes, inducing extinctions while driving down diversity. The hypothesis "adds another dimension" to the role of oxygen in evolution, says biologist Robert Dudley of the University of California, Berkeley. It also complicates the question of how the end-Permian extinction took place.

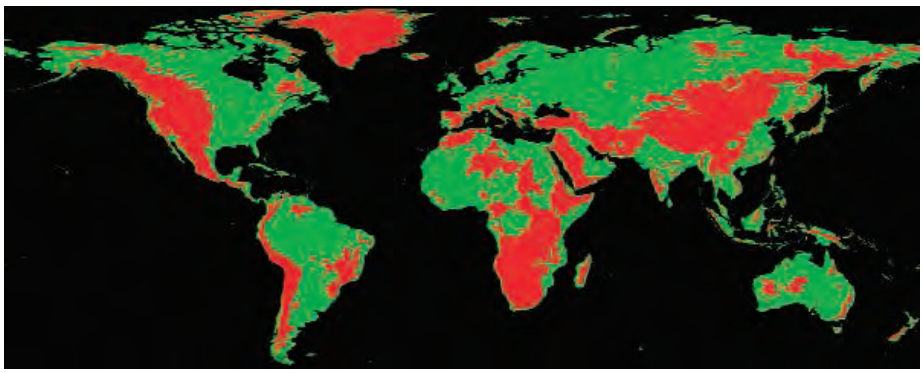

Too high. If the low atmospheric oxygen levels of the late Permian period prevailed today, few vertebrate animals could live much above an altitude of 500 meters (red).

CREDIT: R. HUEY *ET AL.*

Geochemists can gauge past oxygen levels by taking account of organic matter and reduced sulfur compounds stored in sediments—in effect, the byproducts of oxygen generation. In 2002, geochemist Robert Berner of Yale University calculated that during the past 600 million years, atmospheric concentrations of oxygen were stable near present-day levels of 20% until about 400 million years ago, rose sharply to a peak above 30% about 300 million years ago, and then dove to 12% by 240 million years ago.

Paleontologist Gregory Retallack of the University of Oregon, Eugene, and colleagues suggested in 2003 that such a precipitous decline could have determined winners and losers at the end of the Permian. One of the few large animals to survive the end-Permian extinction, a dog-sized burrowing creature called *Lystrosaurus*, appears to have been well-adapted already for breathing oxygen-poor air, says Retallack. Like humans adapted to living at high altitudes, *Lystrosaurus* had developed a barrel chest for deeper breathing, among other adaptations, apparently in order to "breathe its own breath" more easily in its underground lairs (*Science*, 29 August 2003, p. 1168).

On less well prepared animals, losing more than half of the normal oxygen supply would have had far-reaching effects, say evolutionary physiologist Raymond Huey and paleontologist Peter Ward of the University of Washington, Seattle. Every animal has its own minimum oxygen requirement, they note. That's why each species has a particular altitude beyond which it doesn't live. For example, humans live and reproduce no higher than 5.1 kilometers, in the Peruvian Andes. So, "if oxygen is 12%, sea level would be like living at 5.3 kilometers," says Huey.

With oxygen at the mid-Permian's peak of 30%, animals probably could have breathed easily at any altitude on Earth, says Huey. But as oxygen levels dropped, animals capable of living at 6.0 kilometers in the mid-Permian would have been driven down to 300 meters. Perhaps half of the Permian land area would have been denied to animals. Species specialized to live in upland habitats would have perished, assuming they couldn't adapt their relatively unsophisticated breathing systems. Survivors would have been squeezed down into smaller, more isolated areas, where overcrowding and habitat fragmentation would have driven up extinctions and diminished the number of species the land could support. "We can explain some big part of land extinction with this," says Ward.

Extinction by crowding into lowlands "is a very interesting idea," says Dudley, but "it's pretty hypothetical. None of the assumptions is yet testable." Further studies of breathing physiology and geographical patterns in the fossil record should help size up just how bad life might have been. **–RICHARD A. KERR**

ScienceScope

Zerhouni Hopes to Revise Stock Limits

Two months after announcing new conflict-of-interest rules, National Institutes of Health (NIH) Director Elias Zerhouni is rethinking the strict limits on owning biomedical stock.

The ethics rules were imposed after revelations that some NIH researchers had received hefty consulting payments from industry. But the stock limits are deterring some from joining NIH and persuading others to leave, including James Battey, director of the National Institute on Deafness and Other Communication Disorders, Zerhouni told a Senate subcommittee last week (see p. 334). He explained that the stock rule was imposed by the Department of Health and Human Services (HHS) and Office of Government Ethics, which felt that NIH should be treated like a regulatory agency. "We need to reevaluate" the stock provision "quickly," Zerhouni said.

Last week, a group of senior NIH scientists asked the U.S. Court of Appeals for the District of Columbia to review the rules in part because HHS didn't collect comments first. **–JOCELYN KAISER**

Hungarian Faculty Face Layoffs

Already squeezed by cuts to the national granting agency (*Science*, 26 November 2004, p. 1455), hundreds of Hungary's scientists now face layoffs stemming from a $21 million shortfall across higher education. A government-mandated 7.5% pay raise for faculty went into effect on 1 January this year, but funding increases for universities, which are overwhelmingly government-supported, have not kept pace. Science classes are more expensive than are the humanities, notes George Kampis of Eötvös Loránd University in Budapest, whose department of history and philosophy of science is under the gun. **–GRETCHEN VOGEL**

Trying Again on ITER

TOKYO—Japan and the European Union last week set an early July deadline to resolve the 15-month stalemate over which one will host the $5 billion International Thermonuclear Experimental Reactor (ITER). Japan's Education, Culture, Sports, Science, and Technology Minister Nariaki Nakayama and European Commissioner for Science and Research Janez Potočnik discussed how to iron out the main sticking point, that is, what to give the loser in exchange for not hosting the reactor. An agreement on how to split responsibilities for the mammoth project will hopefully set the stage for a unanimous selection of either the French or Japanese site. **–DENNIS NORMILE**

Published by AAAS

budget is "a very challenging target," Gardini said. "We are trying very hard to get support from NASA to reduce the cost and risk of the mission." Canada, Japan, and Russia might also take part in the mission, he added.

European researchers see the 2011 mission as preparation for a much more ambitious round trip to return samples of Mars rock, soil, and atmosphere. Space scientist John Zarnecki of The Open University in the United Kingdom, a participant in the workshop, said the group recommended working toward such a mission in 2016, which would fit with NASA's timing for such a mission. "I think everyone hopes and expects that this is going to be a big international push with ESA, NASA, and possibly other agencies," Zarnecki says.

This work is designed to prepare for possible international crewed missions to Mars, which ESA hopes will begin around 2030. Gardini said the sample-return mission would be valuable practice in making the round trip. Aurora faces a big test in December, when ESA's governing council will vote on funding.

–MASON INMAN

PARTICLE PHYSICS

Magnetic Scope Angles for Axions

After 2 years of staring at the sun, an unconventional "telescope" made from a leftover magnet has returned its first results. Although it hasn't yet found the quarry it was designed to spot—a particle that might or might not exist—physicists say the CERN Axion Solar Telescope (CAST) is beginning to glimpse uncharted territory. "This is a beautiful experiment," says Karl van Bibber, a physicist at Lawrence Livermore National Laboratory in California. "It is a very exciting result."

CAST is essentially a decommissioned, 10-meter-long magnet that had been used to design the Large Hadron Collider, the big atom smasher due to come on line in 2007 at CERN, the European high-energy physics lab near Geneva. When CERN scientists turn on the magnet, it creates a whopping 9-tesla magnetic field—about five times higher than the field in a typical magnetic resonance imaging machine. From a particle physicist's point of view, magnetic fields are carried by undetectable "virtual" photons flitting from particle to particle. The flurry of virtual photons seething around CAST should act as a trap for particles known as axions.

Axions, which were hypothesized in the 1970s to plug a gap in the Standard Model of particle physics, are possible candidates for the exotic dark matter that makes up most of the mass in the cosmos. Decades of experiments have failed to detect axions from the depths of space, and many physicists doubt the particles exist (*Science*, 11 April 1997, p. 200). If axions do exist, however, oodles of them must be born every second in the core of the sun and fly away in every direction.

That's where CAST comes in. "When an axion comes into your magnet, it couples with a virtual photon, which is then transformed into a real photon" if the axion has the correct mass and interaction properties, says Konstantin Zioutas, a spokesperson for the project. "The magnetic field works as a catalyst, and a real photon comes out in the same direction and with the same energy of the incoming axion." An x-ray detector at the bottom of the telescope is poised to count those photons.

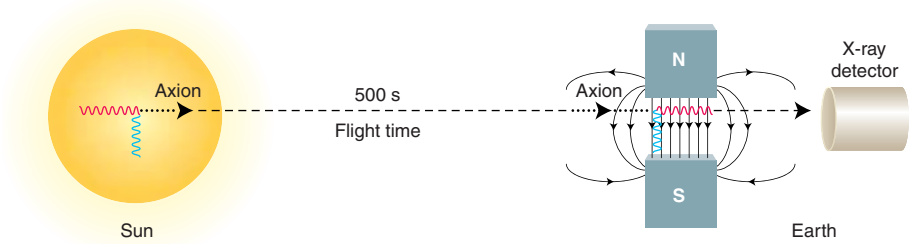

X-files. CAST "telescope" hopes to detect hypothesized particles from the sun by counting the x-rays they should produce on passing through an intense magnetic field.

The first half-year's worth of data, analyzed in the 1 April *Physical Review Letters*, showed no signs of axions. But CAST scientists say the experiment is narrowing the possible properties of the particle in a way that only astronomical observations could do before. "It's comparable to the best limits inferred from the stellar evolution of red giants," van Bibber says, and he notes that plans to improve the sensitivity of the telescope will push the limits further. Even an improved CAST would be lucky to spot axions, van Bibber acknowledges, because most of the theoretically possible combinations of the particle's properties would slip through the telescope's magnetic net. Still, he's hoping for the best. "Maybe Nature will deal a pleasant surprise," he says.

–CHARLES SEIFE

CREDIT: P. HUEY/*SCIENCE*

ScienceScope

Lockheed Boosts Los Alamos Bid

U.S. aerospace giant Lockheed Martin strengthened its bid to run Los Alamos National Laboratory in New Mexico this week by recruiting a key senior scientist. Sandia National Laboratories Director C. Paul Robinson, who spent 18 years at Los Alamos before moving to Sandia in 1990, has joined the proposal team for the Bethesda, Maryland–based company.

Lockheed officials want Robinson, 63, to head Los Alamos if they beat out the lab's current contractor, the University of California. Final competition details are expected soon, with bids in the summer. Meanwhile, former weapons chief Thomas Hunter has been promoted to director of Sandia, which has facilities in California and New Mexico.

–ELI KINTISCH

Pig Flu Scare—Case Closed?

The World Health Organization (WHO) hopes that the results of a new study will put to rest suspicions that pigs in South Korea have become infected with a potentially dangerous flu strain.

Last fall, Sang Heui Seo of Chungnam National University in Daejeon, Korea, deposited flu sequences in GenBank that suggested that Korean pigs carried WSN/33, a flu strain widely used in labs but not known to occur in nature. Several experts and WHO dismissed the findings as the result of lab contamination (*Science*, 4 March, p. 1392); now, Yoshi Kawaoka of the University of Wisconsin, Madison, and his colleagues have tested 400 samples from two Korean pig farms, WHO says, and found no trace of WSN/33.

Seo declined to comment. Henry Niman, a business owner in Philadelphia who backs Seo's claim, says Kawaoka's study wasn't broad enough to refute the theory. But, says WHO flu expert Klaus Stöhr, "we've spent too much time on these speculations already."

–MARTIN ENSERINK

Plant Center to Cut Jobs

The John Innes Centre in Norwich, U.K., one of Europe's top plant science institutions, plans to cut up to 35 researchers from its 800-person staff. Director Christopher Lamb announced on the center's Web site last week that the center began losing money 18 months ago when two funders—the European Union and private industry—became "less reliable sources." Income to the center, which has a $40 million annual budget, has dropped by $5.7 million.

This is "a big blow," says plant geneticist Michael Wilkinson of the University of Reading, U.K., adding that the institution produces an "astonishing number" of widely cited basic science papers.

–ELIOT MARSHALL

Published by AAAS

POPULATION GENETICS

Private Partnership to Trace Human History

In an unusual twist for population genetics research, two giants, one in publishing and the other in computing, have teamed up to trace human history. As *Science* went to press, the National Geographic Society in Washington, D.C., and IBM Corp. in White Plains, New York, were scheduled to announce the 5-year Genographic Project, which will collect 100,000 human DNA samples and from them determine patterns of human migration. In addition, the partnership will sell $99 DNA kits to people who want details about their past or want to contribute their genetic samples. Researchers are eager to see such an extensive survey done, but several wonder whether its organizers can avoid the problems that overwhelmed a similar survey of the world's populations.

DNA prospector. Spencer Wells's (*center*) new human diversity project needs indigenous people to donate DNA.

National Geographic's Spencer Wells, a population geneticist and popularizer of human history studies, will lead the new study, coordinating 10 research groups across the world. The teams will collect DNA samples locally, focusing on about 1000 indigenous populations. Alan Cooper of the University of Adelaide, Australia, also plans to gather DNA from preserved human remains found throughout the world.

Led by IBM's Ajay Royyuru, the company's Computational Biology Center will store the data and analyze them for trends indicative of how people moved from region to region. Wells says the project's information will be placed in a publicly available database after the project has published its analyses. He estimates that the effort, which is funded by National Geographic, IBM, and the Watt Family Foundation, will cost about $40 million.

The new project is reminiscent of the Human Genome Diversity Project (HGDP), which has limped along for more than a decade because of technical and political challenges. "It could generate all the ethical issues that stopped the HGDP," says Ken Weiss, a geneticist at Pennsylvania State University, University Park. When it was conceived in the early 1990s, HGDP was to be a global effort with regional components, involving DNA samples from 500 populations. But neither the U.S. National Institutes of Health nor the U.S. National Science Foundation has been willing to foot the $30 million bill for HGDP, in a large part because of outcries by indigenous groups worried about the commercial exploitation of their tissue and DNA. "It was certainly much harder [to do] than we expected," says Hank Greely, a Stanford University law professor who helped promote HGDP.

The Genographic Project may sidestep some of the ethical landmines with a pledge not to use its data for biomedical research. The Genographic Project will just stockpile DNA, whereas HGDP also maintains cell lines, which make the collection more valuable for biomedical research, says Stanford's L. Luca Cavalli-Sforza, who came up with the HGDP concept.

To date, however, HGDP has amassed only about 1000 cell lines. Almost all had been previously collected by researchers for independent projects. "The Genographic Project [would be] 100 times more powerful than the present HGDP collections, and this makes it extremely interesting," says Cavalli-Sforza, who was Wells's mentor and is on the Genographic advisory board.

The new project, notes Weiss, "is privately funded, which probably removes some constraints, controls, and monitoring." Wells argues that his teams and local residents will work out a satisfactory protocol for DNA collection and analysis. HGDP proposed to do the same, Weiss points out, but never won the confidence of indigenous groups. Wells and his colleagues are hopeful that that bit of human history won't repeat itself. —ELIZABETH PENNISI

TOXICOLOGY

EPA Kills Florida Pesticide Study

The nominee to head the Environmental Protection Agency (EPA) last week cancelled a controversial study to measure the exposure of children to pesticides 1 day after two legislators threatened to derail his appointment if the study went ahead. Some scientists who see value in the study are worried that acting EPA Administrator Stephen L. Johnson has placed politics above science in making his decision. EPA says that the controversy scared away potential participants and made the research impossible to carry out.

The Children's Health Environmental Exposure Research Study (CHEERS) aimed to follow 60 children in Duval County, Florida, living in homes where pesticides were already being used. Last fall, environmental and patient activist groups complained that the study, although approved by several ethics boards, was fatally flawed by an offer of $970 and a camcorder to families as an inducement to participate (*Science*, 5 November 2004, p. 961). Critics also objected to a $2 million contribution from the American Chemistry Council, an industry lobby, that would have allowed EPA to measure exposures to other chemicals, such as flame retardants. Responding to the outcry, EPA suspended the 2-year, $9 million study pending review by a special advisory panel.

That review was to begin in May. But on 8 April, 1 day after senators Barbara Boxer (D–CA) and Bill Nelson (D–FL) blasted the study at Johnson's nomination hearing and put a hold on any vote to confirm him, Johnson declared that the study "cannot go forward" because of "gross misrepresentation" of it. EPA spokesperson Richard Hood says agency scientists told Johnson—a 24-year EPA employee who would be the agency's first leader with a scientific background—that they didn't think they could enroll enough families because of the "furor" over the study in Duval County. Hood says the researchers feel "badly burned" by the uproar.

Some outside researchers are disappointed, too. A properly designed study would have filled critical gaps in understanding whether children absorb pesticides mainly through the skin, by inhalation, or by ingestion, says environmental health researcher Timothy Buckley of the Johns Hopkins University Bloomberg School of Public Health in Baltimore, Maryland. "We need that kind of data to protect kids," Buckley says. Kristin Shrader-Frechette, an ethicist at the University of Notre Dame in Indiana who was to chair EPA's special review panel, says she personally thinks the study contained "fixable" scientific and ethical flaws. Instead of being improved, however, the study became what she calls a "political football."

—JOCELYN KAISER

CREDIT: PHOTO BY MARK READ

Published by AAAS

POPULATION GENETICS

Private Partnership to Trace Human History

In an unusual twist for population genetics research, two giants, one in publishing and the other in computing, have teamed up to trace human history. As *Science* went to press, the National Geographic Society in Washington, D.C., and IBM Corp. in White Plains, New York, were scheduled to announce the 5-year Genographic Project, which will collect 100,000 human DNA samples and from them determine patterns of human migration. In addition, the partnership will sell $99 DNA kits to people who want details about their past or want to contribute their genetic samples. Researchers are eager to see such an extensive survey done, but several wonder whether its organizers can avoid the problems that overwhelmed a similar survey of the world's populations.

DNA prospector. Spencer Wells's (*center*) new human diversity project needs indigenous people to donate DNA.

National Geographic's Spencer Wells, a population geneticist and popularizer of human history studies, will lead the new study, coordinating 10 research groups across the world. The teams will collect DNA samples locally, focusing on about 1000 indigenous populations. Alan Cooper of the University of Adelaide, Australia, also plans to gather DNA from preserved human remains found throughout the world.

Led by IBM's Ajay Royyuru, the company's Computational Biology Center will store the data and analyze them for trends indicative of how people moved from region to region. Wells says the project's information will be placed in a publicly available database after the project has published its analyses. He estimates that the effort, which is funded by National Geographic, IBM, and the Watt Family Foundation, will cost about $40 million.

The new project is reminiscent of the Human Genome Diversity Project (HGDP), which has limped along for more than a decade because of technical and political challenges. "It could generate all the ethical issues that stopped the HGDP," says Ken Weiss, a geneticist at Pennsylvania State University, University Park. When it was conceived in the early 1990s, HGDP was to be a global effort with regional components, involving DNA samples from 500 populations. But neither the U.S. National Institutes of Health nor the U.S. National Science Foundation has been willing to foot the $30 million bill for HGDP, in a large part because of outcries by indigenous groups worried about the commercial exploitation of their tissue and DNA. "It was certainly much harder [to do] than we expected," says Hank Greely, a Stanford University law professor who helped promote HGDP.

The Genographic Project may sidestep some of the ethical landmines with a pledge not to use its data for biomedical research. The Genographic Project will just stockpile DNA, whereas HGDP also maintains cell lines, which make the collection more valuable for biomedical research, says Stanford's L. Luca Cavalli-Sforza, who came up with the HGDP concept.

To date, however, HGDP has amassed only about 1000 cell lines. Almost all had been previously collected by researchers for independent projects. "The Genographic Project [would be] 100 times more powerful than the present HGDP collections, and this makes it extremely interesting," says Cavalli-Sforza, who was Wells's mentor and is on the Genographic advisory board.

The new project, notes Weiss, "is privately funded, which probably removes some constraints, controls, and monitoring." Wells argues that his teams and local residents will work out a satisfactory protocol for DNA collection and analysis. HGDP proposed to do the same, Weiss points out, but never won the confidence of indigenous groups. Wells and his colleagues are hopeful that that bit of human history won't repeat itself. —ELIZABETH PENNISI

TOXICOLOGY

EPA Kills Florida Pesticide Study

The nominee to head the Environmental Protection Agency (EPA) last week cancelled a controversial study to measure the exposure of children to pesticides 1 day after two legislators threatened to derail his appointment if the study went ahead. Some scientists who see value in the study are worried that acting EPA Administrator Stephen L. Johnson has placed politics above science in making his decision. EPA says that the controversy scared away potential participants and made the research impossible to carry out.

The Children's Health Environmental Exposure Research Study (CHEERS) aimed to follow 60 children in Duval County, Florida, living in homes where pesticides were already being used. Last fall, environmental and patient activist groups complained that the study, although approved by several ethics boards, was fatally flawed by an offer of $970 and a camcorder to families as an inducement to participate (*Science*, 5 November 2004, p. 961). Critics also objected to a $2 million contribution from the American Chemistry Council, an industry lobby, that would have allowed EPA to measure exposures to other chemicals, such as flame retardants. Responding to the outcry, EPA suspended the 2-year, $9 million study pending review by a special advisory panel.

That review was to begin in May. But on 8 April, 1 day after senators Barbara Boxer (D–CA) and Bill Nelson (D–FL) blasted the study at Johnson's nomination hearing and put a hold on any vote to confirm him, Johnson declared that the study "cannot go forward" because of "gross misrepresentation" of it. EPA spokesperson Richard Hood says agency scientists told Johnson—a 24-year EPA employee who would be the agency's first leader with a scientific background—that they didn't think they could enroll enough families because of the "furor" over the study in Duval County. Hood says the researchers feel "badly burned" by the uproar.

Some outside researchers are disappointed, too. A properly designed study would have filled critical gaps in understanding whether children absorb pesticides mainly through the skin, by inhalation, or by ingestion, says environmental health researcher Timothy Buckley of the Johns Hopkins University Bloomberg School of Public Health in Baltimore, Maryland. "We need that kind of data to protect kids," Buckley says. Kristin Shrader-Frechette, an ethicist at the University of Notre Dame in Indiana who was to chair EPA's special review panel, says she personally thinks the study contained "fixable" scientific and ethical flaws. Instead of being improved, however, the study became what she calls a "political football."

—JOCELYN KAISER

CREDIT: PHOTO BY MARK READ

Published by AAAS

ASIAN TSUNAMIS

Model Shows Islands Muted Tsunami After Latest Indonesian Quake

In the first days after a magnitude 8.7 earthquake leveled buildings on the Sumatran islands of Nias and Simeulue on 28 March, experts wondered why it failed to generate a significant tsunami. After all, the monster quake that struck just to the north in December spawned a tsunami that killed more than a quarter-million people. Now that they've had a chance to locate the fault rupture more precisely and to run some simulations, they believe that the islands that bore the brunt of the March quake largely stifled its tsunami.

Quakes generate tsunamis by moving the sea floor, along with a lot of overlying water. The March quake was not only about a third as large as its December predecessor, but it apparently had another disadvantage: It didn't reach as far, vertically. The December quake appears to have ruptured the fault—the inclined, deep-diving boundary between two tectonic plates—from tens of kilometers deep all the way up to the sea floor in the deep-sea trench off northern Sumatra, says seismologist Seth Stein of Northwestern University in Evanston, Illinois. The vertical displacement of the sea floor along the rupture would have transferred more of the quake's energy into heaving up the tsunami, he says. In contrast, the rupture caused by the March quake didn't breach the sea floor, which means that it would have transferred less energy to the water column.

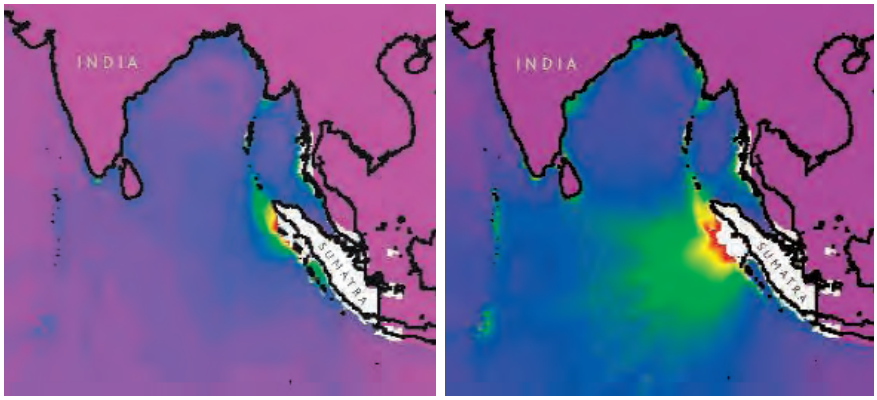

With and without. Simulations driven by the March quake off Sumatra fail to generate a far-ranging tsunami (green) until islands overlying the quake (included at left) were removed (*right*).

Further weakening any tsunami, the March quake occurred under relatively shallow water. (The deeper the water over a quake, the more water it will displace and the larger the tsunami will be.) The movements of the overlying islands, in fact, displaced no water at all—and that turned out to be a critical factor.

When hydrodynamicists Costas Synolakis of the University of Southern California in Los Angeles and Diego Arcas of the National Oceanic and Atmospheric Administration's Pacific Marine Environmental Laboratory in Seattle, Washington, simulated the March quake's tsunami with the islands removed from their model, the resulting tsunami was much larger. Significant waves reached the distant islands of the Maldives south of India in the islandless simulation. "Had the two islands not been there" off Sumatra, says Synolakis, "we would have had another damaging transoceanic tsunami, although smaller in impact than the December one."

Such vagaries of tsunami generation are reinforcing the tsunami community's conviction that it won't be able to predict tsunamis reliably anytime soon from seismic observations alone; only a dense network of tsunami detectors on the ocean floor will do.

—RICHARD A. KERR

INFECTIOUS DISEASES

Veterinary Scientists Shore Up Defenses Against Bird Flu

PARIS—It took just a few years for avian influenza to move from a veterinary backwater into the global spotlight. Now researchers are trying hard to catch up. At a meeting here last week, more than 200 bird flu scientists called for more aggressive research and control efforts—from improved surveillance to finding more humane ways of killing birds. They also launched a new international lab network to coordinate research and share virus strains.

Asia's lethal H5N1 is grabbing most of the headlines, but it's not the only strain of so-called highly pathogenic avian influenza (HPAI) on the march worldwide. There have been 15 known outbreaks of HPAI between 2000 and 2004, which killed or led to the culling of some 200 million birds, Ilaria Capua of the Istituto Zooprofilattico Sperimentale della Venezie in Italy said at the meeting. In the 40 years before, she said, there were just 18 outbreaks, affecting 23 million birds: "We've gone from a few snowflakes to an avalanche." Several strains other than H5N1—including H9N2 in China and Hong Kong, H7N2 in the United States, H7N3 in Canada, and H7N7 in the Netherlands—have also caused human infection, disease, or even death.

Researchers aren't exactly sure what triggered the change or how big a threat it poses to humans. That's why meeting participants called for more funding to study the panoply of strains. Most also welcomed a new network, proposed by the meeting organizers, the World Organization for Animal Health (OIE) and the Food and Agricultural Organization of the United Nations. Mirroring a similar network for human influenza, the new structure, dubbed OFFLU, would pool veterinary expertise, stimulate closer collaboration with human flu researchers, and facilitate the exchange of samples—often a thorny issue because of intellectual property concerns, says Capua, whose lab will host the network's secretariat for the first 3 years. "It's a great idea, if they can get it to work," says Nancy Cox, chief flu scientist at the U.S. Centers for Disease Control and Prevention in Atlanta, Georgia.

Other changes are afoot to limit the spread of avian influenza as well. OIE has proposed that countries be required to search for and report outbreaks of low-pathogenicity avian influenza (LPAI) as well as its higher-pathogenicity kin. LPAI outbreaks cause little mortality and are easy to miss, says OIE's Alejandro Thiermann—but they can evolve to become HPAI.

At the same time, OIE plans to introduce a new strategy called "compartmentalization" that could help protect international trade during an outbreak. Currently, entire regions or countries are shut off from the international market when they have bird flu. In the future, parts of the poultry industry could keep their disease-free status if they can show that their entire operation—including, for instance, feed supply, farm workers, and vets—operate within a biosafe "compartment" out of reach for the virus. Thiermann hopes the measure, which will be formally discussed by OIE's 167 member countries next month, will spur investment in flu-proof poultry facilities.

—MARTIN ENSERINK

CREDITS: DIEGO ARCAS/NOAA-PMEL AND COSTAS SYNOLAKIS/USC

Published by AAAS

European Union officials have proposed a €73 billion, 7-year funding program with money for individual grants and promises of less red tape. But will researchers believe them, and will political leaders foot the bill?

A Framework for Change?

Promising to mend its bureaucratic ways, the European Commission has unveiled what it hopes will be a new and improved version of its multiyear funding program known as Framework. "This is not just another Framework program," Research Commissioner Janez Potočnik promised several times as he pitched the proposal to the European Parliament on 6 April and to journalists a day later. "We want to do more."

Indeed, the proposal—Framework 7—is twice as big as previous programs, boosting yearly funding from just over €4 billion ($5.2 billion) to more than €10 billion ($13 billion). Scientists greeted the report with cautious enthusiasm, praising the increased budget and the plans to launch the long-desired European Research Council (ERC), a Europe-wide grantmaking body that will fund individual scientists instead of the large and often unwieldy collaborations supported by previous Framework programs.

The hopes are tempered, however, by two concerns: First, a pending battle over the size of the European Union's whole budget may scupper the grand plans for doubling research spending. Second, scientists have heard promises to simplify Brussels's bureaucracy before, without real results. "The problem with the commission is that they put out quite nice press releases, but they are not always able to follow up," says Bart Destrooper of the Catholic University of Leuven in Belgium, who led a petition campaign calling for reform of the Framework program. "Especially with Framework 6, it was clear that they wanted to have a less complicated system, but it turned out to be more complicated than ever." Nevertheless, he says, Brussels is making the right signals: "They are listening. That's very clear."

On the budget front, Potočnik hopes to convince Europe's heads of government and finance ministers that the expanded Framework program is vital to keep Europe competitive in the face of an aging population and limited natural resources. The Lisbon Agenda, a plan laid out in the Portuguese capital in 2000 to boost Europe's economy by 2010, makes research a key driver for growth, calling on member countries to spend 3% of their gross national products on research and development—half from industry and half from government sources. "This is a moment of truth for us," Potočnik told reporters at a press conference. "Will we be credible in implementing the things that we have agreed to in principle?"

Big plans. Research Commissioner Janez Potočnik seeks a doubling of E.U. research funding.

Support from the European Parliament seems strong, says Philippe Busquin, the former research commissioner turned parliamentarian. In March, the parliament endorsed the ideas of an ERC and a doubling of research spending. However, Europe's heads of government, who hold the E.U.'s purse strings, are gearing up for a bruising fight over the budget. The six countries that contribute more than they receive from Brussels—Germany, the United Kingdom, France, Sweden, Austria, and the Netherlands—want to cap their contributions to the E.U. at 1% of gross national income per year. The commission is proposing an average of 1.14% per year. If these net payers get their way in negotiations in the coming months, scientists' hopes could evaporate. "It all hinges on whether the money will be there or not," says Helga Nowotny of the Vienna Science Center, who chairs the European Research Advisory Board, a panel that advises the commission. Without an increase in the overall budget, €10 billion for Framework per year seems unlikely, she says.

The commission divides its proposal into four areas: Cooperation, Ideas, People, and Capacities. "Cooperation" projects—the networks of excellence and other large-scale projects familiar from previous Framework programs—take up nearly half the budget. The Cooperation money is split between nine themes—including health, energy, environment, transport, and space and security—and will be used to fund large collaborations, often involving dozens of labs. "Ideas" refers to the cutting-edge research the commission hopes the ERC will fund. Money for "People" will finance the Marie Curie program that helps European and international researchers study and work abroad. The program, which even critics say is a real success, is slated to receive just over €1 billion a year—twice as much as it has under Framework 6 (see sidebar, p. 343). "Capacities," which includes infra-

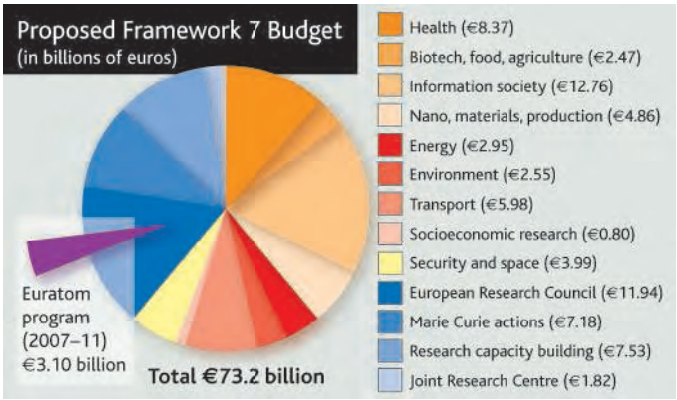

CREDITS (TOP TO BOTTOM): EUROPEAN COMMUNITY, 2005

Published by AAAS

structure projects such as genomics data banks, radiation sources, and observatories as well as funding for science-and-society programs, will also receive about €1 billion per year. The budget also includes €1.8 billion for the E.U.'s Joint Research Center, which does food and chemical safety testing as well as climate and some nuclear research. Because of political sensitivities, funding for nuclear energy research in the EURATOM program is calculated separately. It is slated to receive €3.1 billion through 2011.

The proposal includes funding for two new areas: socioeconomic research and security and space. Socioeconomics will receive nearly €800 million over 7 years. The €4 billion allotted for security and space will allow for closer cooperation with the European Space Agency, especially on the Galileo project to launch a fleet of global positioning satellites (*Science*, 25 April 2003, p. 571). It will also fund antiterrorism research, new border security technologies, and emergency-management strategies.

The €1.7 billion a year planned for the ERC is the result of an unprecedented grassroots movement initiated by scientists just 3 years ago (*Science*, 3 May 2002, p. 826). Fed up with the large projects that strangled their research in top-down bureaucracy, science leaders began calling for a European body more like the U.S. National Science Foundation or the National Institutes of Health.

That dream came true more quickly than many of its architects expected. Busquin championed the idea, and the commission endorsed it last June. Although some worried that the Brussels Eurocrats would take a solid-gold idea and transmute it into lead, most soon came to realize that the efficient path went through the commission. "There is no alternative" to having the commission involved, says Nowotny. "The times are gone when there was no E.U., and you could set up [international physics lab] CERN with treaties between governments. If you tried to do that now, it would take 20 years."

In recent months the pace has accelerated. In January the commission named a five-member Identification Committee to draw up a list of candidates for the 18-member governing council that will run the ERC. The committee issued a progress report in March outlining the qualities it is looking for in candidates. It promised to present its final list to the commission by June.

Second only to their hopes for an ERC is a call to cut down on the paperwork required to apply for and administer Framework money (see sidebar, p. 344). "If there is one word that I have heard from every scientist who has entered my office, it is 'simplify,' " Potočnik says. He promised that the commission will try. Although details won't be clear until later this year, the commission will propose that scientists

On the road. E.U. funds have paid for thousands of migrating fellows.

E.U. Wins Over Researchers With a Ticket to Ride

Although many European Union research programs are considered unwieldy and overbureaucratic, there is one that is universally popular, says longtime observer John Findlay of the University of Leeds, U.K. It works by encouraging young researchers to jump ship. This unusual effort, called the Marie Curie Fellowships program, gives researchers a taste of independence by funding them to leave home and move to a new place—all in the name of professional growth. Recognizing its appeal, E.U. Research Commissioner Janez Potočnik last week said the commission wants to double its funding—to €1 billion per year through 2013.

This "mobility initiative" got its more user-friendly name in 1996. The Marie Curie fellowships are now an important route for talented researchers to sidestep local constraints, or "inbreeding," as many say. Awarded by peer review, the fellowships go mainly to young researchers. They provide a few years' pay and are very attractive, says Jean-Patrick Connerade, president of the nonprofit advocacy group Euroscience, "because the research is untargeted" and relatively free of E.U. guidelines. According to E.U. data, applications nearly doubled between 2003 and 2004, to 4364, although only a small fraction will be funded.

The E.U.'s plan this year calls for "more of the same," according to Conor O'Carroll, Ireland's delegate to a Marie Curie oversight panel. The new Framework 7 plan is likely to expand support for non-E.U. researchers in Europe and allow more fellows to take their money outside Europe. To discourage fellows from disappearing, grantees from Europe must return home after several years or repay the total; they can get limited research support once they're back. The willingness to support outsiders reflects the E.U.'s growing confidence, says O'Carroll: It's a recognition that "science is international. … You have to be open to outsiders."

More controversial, says O'Carroll, is a proposal to have national institutions in Europe chip in 25% "cofunding" of Marie Curie schemes and other programs—"which is not universally accepted at all." This would expand the budget but also raise the pressure on national agencies to match the E.U.'s high standards for working conditions. (E.U. contracts promise health care, maternity leave, and other benefits.)

The E.U. laid the foundation for extending such benefits on 11 March in a new "European Charter for Researchers" and a "Code of Conduct for the Recruitment of Researchers." The code stipulates that all researchers, including Ph.D. candidates, should be recognized "as professionals," that "teaching responsibilities should not be excessive," and that researchers should have "equitable social security provisions." These are only recommendations, but they're part of the E.U.'s plan to build Europe into a formidable "knowledge economy."

Young researchers are enthusiastic about this dream—as well as the fellowships—but they are not blind to flaws. Toni Gabaldon of the Centre for Molecular and Biomolecular Informatics in Nijmegen, the Netherlands, and vice president of an advocacy group called EURODOC, is cheered by the doubling of the Marie Curie budget. But he warns that as the application success rate falls to a "very low" level of 10%, a lot of people are wasting their time. Mathematician Dagmar Meyer, who heads the Marie Curie Fellowship Association, a society of ex-fellows, says that grant processing has completely bogged down; months-long delays have cropped up. E.U. official Sieglinde Gruber acknowledges the problem but says it will be fixed soon.

Although technical glitches can be fixed, one thing is not likely to change quickly, Findlay says: the economic current that sweeps talented scientists from southern and eastern Europe to Scandinavia, Britain, and the United States. It's still the case, notes O'Carroll, that four out of five researchers who cross the Atlantic and stay in America for a few years never return. He's hoping the latest E.U. inducements will lower the ratio.

—ELIOT MARSHALL

CREDITS: BRYAN PICKERING/EYE UBIQUITOUS/CORBIS

Published by AAAS

The Dos and Don'ts of Getting an E.U. Grant

BRUSSELS—So you're an upwardly mobile European researcher and some European Union (E.U.) money might be just what your lab needs. But where to start? How do you get a piece of the €73 billion Framework 7 action?

The good news is that a whole industry of trainers, consultants, liaison officers, and research managers has sprung up across the continent to lend a hand. On the downside, they all caution that, although the rewards are enticing, learning to play the Brussels game is frustrating and requires a major, long-term commitment: It's less about filling out forms than a whole new career choice. And there are plenty of pitfalls.

For starters, your question is the wrong one, says Sean McCarthy, president of Hyperion, an Irish company specializing in Framework training. As he wrote in a paper posted on his Web site, "you don't go to Brussels looking for money for your research. You go there to help the European Commission solve a problem that *they* have identified." It's not enough, say, to show that you're an expert in detecting low-level toxic compounds in water, McCarthy explains; you have to know the politics, economics, and business of water quality and show how your research will result in the prototype of a new sensor that Europe needs to clean up its water.

Grants guru. Don't appear to promote your own ideas, says Lene Topp.

Finding good partners is also crucial. The vast majority of the E.U.'s research money is distributed in chunks as large as €12 million or €15 million to consortia of 15 institutes or more. You can try to become the lead partner for such a group, but only if you're a European heavyweight who can persuade colleagues across the continent to join and your institute is prepared to help with the dizzying paperwork, says Willem Wolters, an E.U. funding specialist at Wageningen University in the Netherlands. Smaller players are well-advised to identify the hot shots and see if they can fill a niche in existing schemes, Wolters says.

Once the European Commission issues a call for proposals that interests you, there are usually only 3 months to apply, says Lene Topp of Rambøll Management, a Danish company that organizes training programs; that's why it's important that you organize your consortium months or even years in advance. At the same time, it's crucial that the final proposal exactly fits the call, she says—don't try to slip in unrelated ideas, however brilliant. "Many applications go straight out of the window because they don't fit the criteria," Topp says.

The proposals that survive the first screening are then ranked by panels of independent experts, flown to Brussels by the commission. Try to get on one of these panels, Topp says, because it's a good way of getting to know the process and increasing your chances the next time around.

Applying political muscle to get proposals to the top of the pile is generally not appreciated, but it is very common to lobby earlier on, when the commission and the European Parliament establish research priorities—a phase that is just starting for Framework 7. But beware: "Lobbying is an American concept. In Brussels it is better to describe the process as briefing," McCarthy says. Whatever it's called, it can be worth it: Plant scientists, realizing 4 years ago that they were about to lose out in Framework 6, teamed up and very successfully briefed their way to a bigger share, Wolters recalls.

If you're a lead partner and your proposal is among the ones selected, you will be invited to Brussels for contract negotiations, which can last several months. Signing a contract doesn't end your worries, however. You have to make sure that all partners honor their part of the deal. (If not, the commission can and sometimes will ask for its money back.) Also, as a result of the E.U.'s past financial scandals, there's a crushing burden to account for every euro, Topp says. Be prepared to nag your partners about missing train tickets and flight coupons. Indeed, Wolters warns, "if you're a prominent researcher and you take on one of these projects, you can spend so much time on management that by the end you're no longer a prominent researcher."

Although Framework 7 promises some relief to the paperwork (see main text), none of the experts expect Brussels to become simple anytime soon. Yet, despite it all, many researchers do like to participate in European programs, says Menno van der Klooster of Utrecht University in the Netherlands, not just because of the money and the ability to attract staff, but also because it offers new perspectives on their research and an international network that can prove invaluable. So good luck. **–MARTIN ENSERINK**

applying for Framework 7 money go through a two-step process. The first application will require less paperwork and will involve only a concept proposal. Only those whose projects make a first cut will be asked to submit a full proposal.

In a staff working paper on simplification that, perhaps tellingly, runs nearly 10 pages, the commission also promises to establish an electronic database of applicants that should help speed the application and evaluation process. In his presentation to Parliament, Potočnik urged delegates to ease some of the legal restrictions that bind the commission, leading to complex legal contracts instead of grants. "I hope we will gain the courage to give scientists more trust and autonomy than we have in the past," he later told journalists. "We want this to happen."

The proposal outlined last week is far from the final say on Framework 7. The European Parliament now has a chance to scrutinize the commission's plan. Last time around, they weren't shy about sharing their opinion: The parliament offered hundreds of amendments to the Framework 6 proposal. The competitiveness council, comprising research ministers from all member states, will also offer comments. The commission will then submit a revised proposal, and the feedback loop will continue until the council of ministers adopts a final proposal.

That process could take up to a year and could face unexpected hurdles. In the months before Framework 6 was adopted, a coalition of countries threatened to block the entire program over funding for human embryonic stem cell research, which is restricted or even forbidden in some E.U. countries. Another fight over that issue is unlikely, because in the expanded E.U. the opponents no longer have enough votes to block the program. But some other burning issue of the day could flare to the surface.

As the process goes forward, scientists are likely to make some noise, says geneticist Kai Simons, a director of the Max Planck Institute for Molecular Cell Biology and Genetics in Dresden, Germany, and a longtime proponent of the ERC. "The change in atmosphere in the last 2 or 3 years is just incredible," he says. The commission has become more open, Simons says, but even more important is the fact that scientists have begun to make themselves heard in Brussels and are seeing real results: "Everyone realizes there are going to be real benefits from this. For the first time, they see a hope."

–GRETCHEN VOGEL

CREDIT: COURTESY OF LENE TOPP

Published by AAAS

Ibogaine Therapy: A 'Vast, Uncontrolled Experiment'

Despite potentially harsh side effects, an African plant extract is being tested in two public clinical trials—and many clandestine ones

On a snowy President's Day, an odd group of activists and scientists devoted to treating addiction gathered in an art gallery in the Chelsea warehouse district of New York City. As an all-night, all-day rave throbbed next door, panelists outlined the latest developments in a decades-long movement to mainstream a West African plant alkaloid, ibogaine, that purportedly interrupts addiction and eliminates withdrawal.

Sustained by true believers who operate largely outside the academic medical world, research on the vision-inducing drug is gaining attention, despite its U.S. status as a banned substance. The Food and Drug Administration (FDA) approved a clinical trial in 1993, but the National Institute on Drug Abuse (NIDA) decided not to fund it after consultants raised questions about safety.

Traditional high. Ibogaine is derived from a root bark used in the West African Bwiti religion as a way to "visit the ancestors."

CREDIT: LAURENT SAZY

The plant extract can be neurotoxic at high doses and can slow the heart. Yet a handful of scientists continue to study it for its potential in treating addiction. The enthusiasts who gathered in New York reviewed efforts to tease apart its antiaddictive and hallucinatory components.

Although a PubMed search for "ibogaine" pulls up some 200 articles on laboratory studies, clinical reports cover just a few dozen patients. That's because patients seek treatment clandestinely. "Whether the FDA likes it or not, the fact of the matter is that … hundreds, probably thousands of people … have been treated with ibogaine," said Stanley Glick, a physician and pharmacologist at the Albany Medical Center in New York who has documented ibogaine's antiaddictive potential in rodents. At the meeting, Kenneth Alper, a Columbia University assistant professor of psychiatry, estimated that more than 5000 people have taken ibogaine since an organized (but unregulated) clinic opened in Amsterdam in the late 1980s. Boaz Wachtel, an ibogaine advocate in Israel, believes that 30 to 40 clinics operate worldwide. Listed alongside heroin, LSD, and marijuana on the U.S. Drug Enforcement Administration's schedule I of banned substances, ibogaine is nevertheless legal in most of the world.

"There's basically a vast, uncontrolled experiment going on out there," said Frank Vocci, director of antiaddiction drug development at NIDA. The agency spent several million dollars on preclinical ibogaine work in the 1990s before dropping it.

Ibogaine's promoters yearn for the legitimacy that a successful clinical trial can bring. They may soon get their wish. Later this spring, neuroscientist Deborah Mash of the University of Miami in Coral Gables, Florida, will launch a phase I safety trial in Miami. A second safety and efficacy trial, of 12 heroin-addicted individuals, is slated to begin this fall at the Beer Yaakov Mental Health Center in Tel Aviv. Both are being funded in an unusual fashion: by anonymous donations—$250,000 for Mash, a smaller amount for the Israeli study.

Restarting

For Mash, a tenured professor who runs an Alzheimer's brain bank and won attention in the 1980s for research on how mixing alcohol and cocaine damages the brain, the donation marks a victory. The holder of a patent claim on ibogaine, she has been trying for 12 years to give the drug a scientific hearing. FDA approved Mash's phase I study in 1993, but she abruptly halted the trial when NIDA rejected her funding application.

Three years later, she moved offshore, opening a fee-for-service clinic on the Caribbean island of St. Kitt's. The standard fee per patient of several thousand dollars is adjusted based on ability to pay, according to Mash. Critics derided the unorthodox move as a money grab, but Mash maintains that her motivations were scientific. "You know, somebody ought to test it. Either the damn thing works or it doesn't," she said in a telephone interview.

At the New York meeting, Mash's physician colleague Jeffrey Kamlet presented snippets of data from the 400 patients he and Mash helped treat at St. Kitt's. (Patients took a single dose of ibogaine titrated to body weight and other factors.) He said that for up to 90 days posttreatment, patients reported "feeling wonderful"; physician evaluations also showed improvement in depression and drug-craving scores. The results mirror those from 27 cocaine- and heroin-addicted individuals treated with ibogaine at St. Kitt's published by Mash in 2000 in the *Annals of the New York Academy of Sciences*.

However, Mash has not published the bulk of her data. Her explanation: She does not want to stir up long-running controversies, including a patent dispute with Howard Lotsof, who discovered ibogaine's antiaddiction value as a young heroin addict in 1962.

Multiple effects

There is no consensus on precisely how ibogaine works, although researchers have shown that it inhibits the reuptake of the neurotransmitter serotonin, among other actions. In this way, "it's like supersticky, long-acting Prozac," said Kamlet, president of the Florida Society of Addiction Medicine in Pensacola.

It can also have effects similar to those of LSD or PCP. Like them, it jolts serotonin and glutamate systems and can cause hallucina-

Published by AAAS

tions and feelings of depersonalization. In Gabon, the Bwiti religion revolves around "visits to the ancestors" induced by eating root bark from the shrub *Tabernanthe iboga*, the source of ibogaine. Many patients in the West also report emotionally intense, sometimes frightening visions: scenes from childhood, or past mistakes and regrets replayed and somehow released. Debate rages over whether these experiences are key to ibogaine's antiaddictive potential or simply a psychedelic side effect.

Not every patient experiences visions, but animal and human pharmacokinetic data reveal a common physiological response: The liver converts ibogaine into its primary metabolite, noribogaine, which fills opiate receptors hungry for heroin or morphine. Mash believes that this dramatically reduces or eliminates withdrawal symptoms, and "that's why [addicts] don't feel dope sick anymore." Ibogaine also stimulates nicotinic receptors in the cerebellum, an action that, according to Glick, contributes to ibogaine's long-lasting antiaddictive properties by modulating the dopamine reward circuit in the midbrain.

Besides tweaking neurotransmitters, rodent studies suggest that ibogaine increases quantities of a protein in the brain called glial cell line–derived neurotrophic factor (GDNF). Researchers at the University of California, San Francisco, recently observed this effect in the brain's dopamine-producing areas. Dorit Ron and colleagues reported in the January issue of the *Journal of Neuroscience* that addicted rodents lose interest in opiates when given either ibogaine or GDNF. But after injecting an anti-GDNF antibody that scoops the growth factor out of play, the team found that the animals go dope-crazy again.

Ron goes further, suggesting that GDNF maintains and possibly even repairs frazzled dopamine receptors. She reported last year in the *Journal of Neuroscience* that genetically modified mice producing excess GDNF grow up to have denser dopamine connections in the ventral tegmental area, where the dopamine reward pathway begins.

Mash and others suggest that the effects of the St. Kitt's therapy lasted up to 3 months because unmetabolized ibogaine deposits in fat, creating a slow-release reservoir, and because metabolized ibogaine can stay in circulation for weeks. But government agencies are wary of ibogaine, in part because of its myriad effects. It slows the heart and, at very high doses, can destroy neurons in the cerebellum. FDA and NIDA cited these toxicity risks repeatedly in the 1990s.

Glick has been trying to develop cleaner-acting derivatives. The best-studied, 18-methoxycoronaridine (18-MC), exhibits strong action at nicotinic receptors but "seems to lack all of the actions that make ibogaine undesirable," said Glick. Mash and other ibogaine supporters claim that the neurotoxicity risks have been hyped. But the St. Kitt's team closely monitors heart activity of volunteers, excluding any with irregular rhythms.

While Glick tries to line up funding for clinical studies of 18-MC, Mash is betting on a formulation of the metabolite noribogaine. She and the University of Miami won patent rights to noribogaine in 2002 after a long-running dispute with Lotsof, who holds a patent claim on ibogaine. Mash hopes that, like 18-MC, noribogaine may offer antiaddictive effects without the scary trip.

Meanwhile, Vocci is disappointed that Mash has not published her data from St. Kitt's. "This big case series, no one knows what to make of it," he said. "I would expect to see a spectrum of responses. Even though it's not a controlled study, it would still give us some idea whether or not she has anything worth looking at." If Mash's new trial does produce promising data, ibogaine advocates will have a token of legitimacy to point to. But the circle of true believers seems to be expanding, Wachtel says, because users insist that ibogaine works.

–BRIAN VASTAG

Brian Vastag, a writer in Washington, D.C., is working on a book about ibogaine.

Ecology

Experimental Drought Predicts Grim Future for Rainforest

An extraordinary research effort in the Amazon starved a tropical forest of rain and provides a glimpse of the potential effects of climate change

For 5 years, Daniel Nepstad has been slowly killing trees throughout a hectare of his beloved Amazonian rainforest. In an elaborate experiment akin to an installation by the artist Christo, Nepstad's team set up a 1-hectare array of 5600 large plastic panels that diverted the rain and created an artificial drought. The point of the $1.4 million experiment is to provide the most detailed look ever at how tropical forests respond to such stress.

The good news, as Nepstad, an ecologist at the Woods Hole Research Center (WHRC) in Massachusetts, and colleagues have reported in recent papers, is that the forest is quite tough. Although that's no great surprise—forests in the eastern Amazon have long experienced regular droughts from El Niño events—the team is discovering clever tricks that the trees use to survive when the soil becomes parched.

What's worrisome is that when drought lasts more than a year or two, the all-important canopy trees are decimated. Everyone knows that a lack of water eventually kills plants. But by pushing the tropical forest to its breaking point, researchers now have a better idea of exactly how much punishment these forests can withstand.

These kinds of data will be indispensable for predicting how future droughts might change the ecological structure of the forest, the risk of fire, and how the forest functions as a carbon sink, experts say. Given that droughts in the Amazon are projected to increase in several climate models, the implications for these rich ecosystems is grim, says ecologist Deborah Clark of the University of Missouri, St. Louis, who works at La Selva Biological Station in Costa Rica. The forests are "headed in a terrible direction," she says. What's more, the picture includes a loss of carbon storage that might exacerbate global warming.

Parched. Thousands of panels prevented most rain from reaching the forest floor.

CREDIT: WOODS HOLE RESEARCH CENTER

Basement to attic

Nepstad got the idea for the experiment while working in the eastern Amazon in 1992 during

Extreme instrumentation. Towers and trenches revealed the inner workings of the forest.

an El Niño drought. Some forests there had dried out so much that they burned, apparently, for the first time. To find out more, Nepstad teamed up with Paulo Moutinho of the Institute for Environmental Research in the Amazon in Belém and Eric Davidson of WHRC. They chose a field site in the Tapajós National Forest, 67 km south of Santarém, Brazil, in the lowlands that are predicted to be especially vulnerable to climate change. It's not as wet as true rainforest and has an annual dry season that lasts for up to 6 months.

The setup required a year's worth of effort in hot, muggy conditions. With a crew of up to 15 local workers, the team outfitted two sites with four 30-meter-high towers, linked by catwalks to study the canopy. Working with hand tools to avoid disturbing the forest, the crew also dug five pits down to 11 meters in each site to enable researchers to regularly examine roots and soil water. "You can look from the basement to the attic of the forest," says Nepstad. Even more earth was moved as workers dug a 1.5-meter-deep trench around the hectare-sized experimental site to prevent rainwater from seeping in from the surrounding forest. To control for the impact of digging on tree roots, they excavated a similar trench around the comparison plot.

As has been done in similar but smaller experiments elsewhere, they then assembled a system of wooden rafters 1 to 4 meters above the forest floor. Some 5600 plastic panels, each 0.6 m by 3 m, rested on these rafters. "It's like the whole understory of the forest is wrapped in plastic," says team member Rafael Oliveira, a plant ecophysiologist now at the National Institute for Space Research in São Paulo. The panels caught about 80% of the rain that fell through the canopy and diverted it to wooden gutters that drain to the trench. To mimic natural conditions, workers flipped each panel three times a week to allow leaves and other material to reach the forest floor.

The forest was remarkably resilient—at first. As expected, photosynthesis slowed down to conserve water, and the roots drew water from ever deeper in the soil—ultimately as far down as 13 meters. These deep roots help irrigate the topsoil, the researchers found: At night, water flows from the tap roots and dribbles out of the larger network of shallow roots to be used after daybreak, as Oliveira and Todd Dawson of the University of California, Berkeley, will report in a paper accepted at *Oecologia*. This phenomenon, called hydraulic redistribution, had been seen in temperate forests but wasn't known to occur in the tropics.

The canopy also had tricks up its sleeve. No one would have expected leaves to absorb rainwater, says Gina Cardinot, a grad student at the Federal University of Rio de Janeiro, because of their adaptations to prevent water loss. But unpublished research by Cardinot and Leonel Sternberg of the University of Miami in Coral Gables, Florida, suggests otherwise. Stable isotope tracers applied during the drought experiment indicate that two of three common species take up some water through their leaves. "All of this adds up to a forest with enormous drought tolerance," says Nepstad.

That's not to say there weren't changes. Trees in the experimental plot slowed their growth, and many of the smaller trees stopped growing entirely. And then, 4 years after the drought began, they began to die. The mortality rate was especially high in tall, canopy trees—up to 9% per year—as Nepstad's team describes in a paper submitted to *Ecology*. "These are astonishing effects," says Clark, who says no one ever really knew exactly how much death was specifically due to drought.

The loss of large, centuries-old trees has big implications. Gaps in the canopy allowed more light to reach the forest floor, drying out the leaf litter and increasing the risk of fire. According to a model of fire risk that Nepstad has devised, in press at *Ecological Applications*, the control plot is highly flammable for about 10 days a year. The experimental plot, by contrast, is now highly vulnerable for 8 to 10 weeks each year. Intense fires not only convert tropical forest to savanna, they also release a lot of carbon and generate smoke that can further dry out remaining forest. Even without fires, dead trees release large amounts of carbon when the wood and roots decompose.

Severe drought also brought dramatic changes in the ability of the forest to store carbon, because of the slower plant growth. By the third year of drought, the experimental plot was storing only 2 tons of carbon as wood, whereas the control plot still tucked away 7 tons. "That's a profound reduction," says John Grace of the University of Edinburgh, U.K.

By putting hard numbers on these kinds of processes, the drought experiment will help refine climate models, says David Lawrence of the National Center for Atmospheric Research (NCAR) in Boulder, Colorado. Already, Jung-Eun Lee and Inez Fung of the University of California, Berkeley, have shown in unpublished research that incorporating the hydraulic redistribution of water into the NCAR climate model makes it more accurate.

One important question is how broadly Nepstad's results can be extrapolated. In contrast to the Tapajós forest, large swaths of tropical forest further west don't experience regular dry seasons. That could mean these forests haven't evolved coping strategies and might suffer even more dramatically when drought-stricken, Nepstad warns. On the other hand, wetter environments are more buffered. Nepstad deliberately picked a site with a water table so low that roots couldn't reach it. In contrast, Grace and Brazilian colleagues have finished a smaller scale experiment farther east where the water table was higher; they found less tree mortality.

Diversion. Panels and gutters caught rain, enabling Daniel Nepstad and his team to mimic a drought.

Another factor is the time scale. Five years is just a blink of an eye for a forest. Ariel Lugo, director of the U.S. Forest Service's International Institute of Tropical Forestry in Puerto Rico, suggests that climate change will be more gradual than the onset of this experiment, perhaps allowing forests to adapt: "You have to be aware those are worst-case scenarios."

The next step is to observe what happens after the end of a severe drought. Nepstad's team has removed the plastic panels and will study the two plots for another 2 years to see how—or whether—the forest recovers.

–ERIK STOKSTAD

CREDITS (TOP TO BOTTOM): KEMEL A. B. KALIF/INSTITUTO DE PESQUISA AMBIENTAL DA AMAZÔNIA; WOODS HOLE RESEARCH CENTER

New Wave of Electrical Wires Inches Closer to Market

The performance of wires made from yttrium, barium, copper, and oxygen is getting tantalizingly close to what is needed to compete with conventional conductors

SAN FRANCISCO, CALIFORNIA—In this era of high-tech wizardry, not every flashy new technology rises to the top. Case in point: a first generation of wire made from high-temperature superconductors (HTS). It's been on the market for years and can carry more than 100 times the current of a copper wire of the same size. But because it costs more than 100 times as much as copper wire, it has made few inroads into the mass market. Researchers worldwide are banking on a second generation of high-tech HTS wire to drop prices and improve performance. These second-generation wires—made from yttrium, barium, copper, and oxygen (YBCO)—have been difficult to make in long lengths. Now, after a decade of slow and fitful progress, YBCO wires appear to be on the cusp of reaching the market.

At a meeting here last month,* three companies reported that they've developed manufacturing techniques to turn out YBCO wires up to 100 meters long; a few years ago, the best the industry could do was a mere meter or so (*Science*, 1 February 2002, p. 787). What's more, some of the new wires can carry almost as much current as the best first-generation (1G) wires, and further improvement may be in the offing: Researchers have pushed the current-carrying capacity of short lengths of wire above 1400 amperes, and they are developing a slew of wiremaking techniques that promise to drop the costs of 2G wire considerably below those of its HTS predecessor.

"We're getting to the point where it's very interesting," says Dean Peterson, who directs the YBCO superconducting tape development program at Los Alamos National Laboratory in New Mexico. "We can start to think about tapes and coils." Adds David Larbalestier, a superconductivity researcher at the University of Wisconsin, Madison: "There's no doubt now it can work. Now it's all about the cost." But therein could lie the rub. Some electrical industry watchers worry that unless 2G HTS wire ends up vastly superior to conventional copper cables, ultraconservative utilities won't make the switch, leaving HTS companies high and dry. Smaller applications, such as making motors and magnets, may bolster the bottom line of HTS companies. But utilities represent the biggest bulk customers.

A cut above. Second-generation superconducting wires are slit from wide tapes into thin ribbons.

The switch to high-temperature superconductors seemed a foregone conclusion after researchers discovered them nearly 20 years ago. Unlike conventional low-temperature superconductors that conduct electricity without resistance at about 20 kelvin, in 1986 copper oxide ceramics were found to superconduct above a relatively balmy 77 K. That meant they could be cooled with relatively cheap liquid nitrogen rather than the more expensive liquid hydrogen. Pundits immediately promised everything from levitating trains to the ability to store power endlessly without losses. All these applications depended on turning the brittle materials into long, flexible wires and cooling the wires below the critical temperature at which they superconduct. Scientists created the first generation of wires by packing a powder of bismuth, strontium, calcium, copper, and oxygen (BSCCO) into silver tubes and then drawing them out into wires. That encased architecture, however, made it difficult to fine-tune the arrangement of the BSCCO superconductor for better performance. And the need for large amounts of silver has kept the price of those wires high.

Ten years ago, researchers at Los Alamos National Laboratory in New Mexico and Oak Ridge National Laboratory in Tennessee came up with different schemes for making potentially cheap high-current-carrying wires out of YBCO. At similar temperatures, YBCO wires carried higher currents than 1G bismuth wires did and retained their superconducting abilities better under magnetic fields. Those advantages held out hope that the materials could be useful for making high-powered magnets and motors that generate such high fields. YBCO could also work just fine atop nickel and other cheap substrates, and it could be laid down on top of the substrates with atomic precision using techniques borrowed from the semiconductor industry. That versatility gave the 2G conductors "all kinds of potential," says Jim Daley, who manages the superconductivity program at the U.S. Department of Energy in Washington, D.C. "You can completely engineer them."

Easier said than done. YBCO has proved a pain in the neck to work with. As it is deposited, YBCO forms an array of tiny grains. Unless the boundaries of those grains line up with one another more or less in the same direction, the pairs of electrons that make up a supercurrent find it impossible to hop from one grain to the next. The ability of the materials to superconduct drops, and the electrical resistance spikes.

To make matters worse, magnetic fields in many cases still cause trouble. Those fields penetrate top-down through a superconductor that passes current along a wire from one end to another. As they do, they create tiny magnetic whirlpools called vortices. As long as the vortices remain stationary, or "pinned," in HTS lingo, there's no problem, because superconducting electrons can simply wiggle their way around them. But as the current in a superconductor increases, the vortices start to meander. The moving barriers increase the material's resistance and choke off the supercurrent.

Such issues have to be controlled throughout the whole length of each wire. YBCO wires "are only as good as their weakest link," Peterson says. "Initially, there was some doubt whether we could get there and maintain the support we needed." But in the United States and Japan, support for YBCO wires has remained relatively steady, allowing researchers primarily at national labs and companies to work through their litany of challenges. "We had to roll up our sleeves and tackle the problems one by one," says Steve Foltyn, a 2G wire expert at Los Alamos. That has been the story of the past decade as

CREDIT: SUPERPOWER INC.

* Materials Research Society, 28 March–1 April.

Published by AAAS

researchers have sifted through dozens of changes to their materials and processes in search of the best combination.

Possible fixes include a pair of low-cost techniques to deposit YBCO atop nickel or other metal substrates both cheaply and quickly. Researchers discovered that topping this substrate with materials such as cerium oxide (CeO) helps orient the grains of YBCO that are grown on top. Finally, they came up with high-speed schemes to add a layer of copper or another normal conductor on top to carry the current in the event that the YBCO stopped superconducting.

Together, these advances have enabled companies for the first time to come within striking distance of the current-carrying benchmarks set down by the U.S. Department of Energy (DOE) and sister organizations in other countries. DOE's goals call for 2G wire to carry 300 amps over 100 meters by 2006 and 1000 amps over 1 kilometer by 2010. At the meeting, Thomas Kodenkandath of American Superconductor Corp. in Westborough, Massachusetts, reported that his company had used a high-speed wiremaking technique to make 10-meter lengths of wire that carry 272 amps at 77 K and 30-meter lengths that carry 186 amps. Venkat Selvamanickam of SuperPower in Schenectady, New York, reported that his company had turned out close to 100-meter lengths of wire that can carry up to 100 amps at 77 K, also using a high-speed process. Using a slower and thus probably more expensive process, researchers at the Nagoya Coated Conductor Center in Japan have turned out 105-meter-long wires that carry 159 amps throughout. "They're all getting to long lengths with higher currents," says Larbalestier. What's more, he and others add, it's far easier to scale up production from 100 meters to make kilometers of wire than it is to go from making 1-meter-long wires in a lab environment to creating a production process. "If you can do 100 meters, you have a process typical of reel-to-reel processing," Daley says.

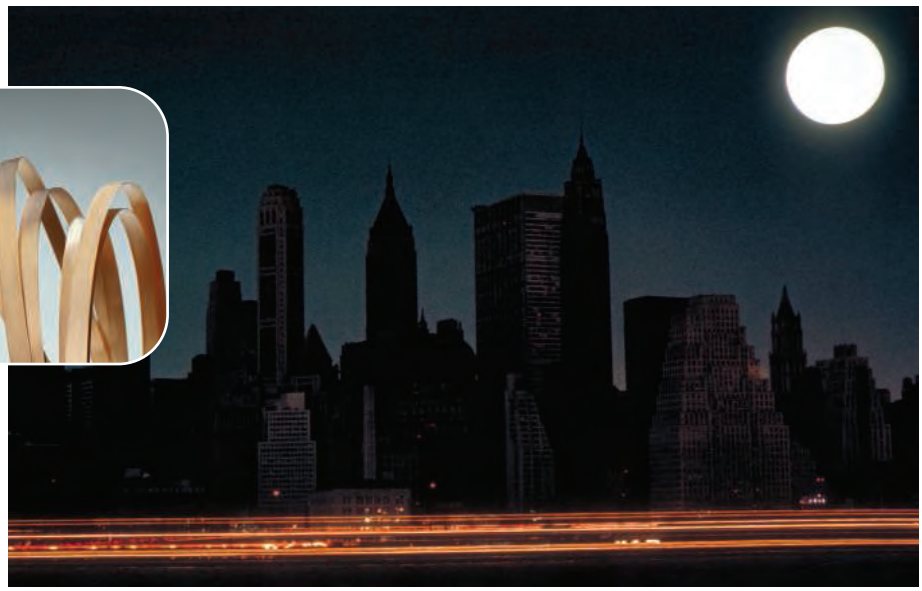

Bright future? Utility experts anticipate that high-current wires (*inset*) will help stabilize the power grid.

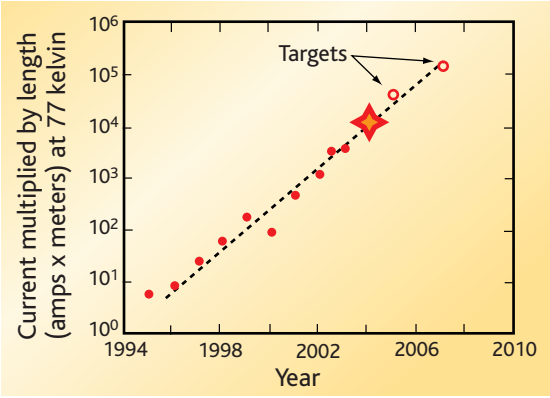

Ever closer. YBCO wires from the Japanese firm Fujikura are nearing the goals needed to compete with copper.

Improvements are still coming. At the meeting, Kodenkandath and others reported that by adding nanoscale impurities to their films, they can create "pinning centers" that grab hold of magnetic vortices and thereby allow wires to operate at higher magnetic fields. Foltyn also reported that his team at Los Alamos has come up with a new scheme for boosting the current-carrying capability of their wires. Researchers have tried for years to do that simply by growing thicker layers of YBCO in their wires, so that they can handle larger currents. But they've found that as they increase YBCO's thickness, the current-carrying capability drops off.

One possible culprit was that as the YBCO layer thickens, the grains in the film get progressively more out of alignment and therefore carry less current. To solve the problem, Foltyn and his colleagues split a single thick layer of YBCO into several layers separated with cerium oxide film to reorient the grains. The result was striking. In one club sandwich–like tape with six alternating YBCO-CeO layers, the current topped 1400 amps. "This is a terrific result," Larbalestier says. So far the new multilayer wire has been demonstrated only on a sample about a centimeter long. However, Larbalestier says, it's likely that the wire companies will pick up on the idea and begin trying it out on longer wires.

Heartened by their progress, HTS companies are working furiously to scale up production. Last month, American Superconductor raised $45 million on the stock market to build a 2G "prepilot" production plant in Ayer, Massachusetts. SuperPower has already built a YBCO wire-production factory in Schenectady, New York. Selvamanickam says his company plans to begin producing up to 1000 kilometers of 2G wire next year. And although it's too early to know how much it will cost, he says, "it will be significantly lower than 1G."

"This has been a story of wonderful science and incredible work" in universities, the national labs, and superconductivity companies, says Paul Grant, a longtime superconductivity watcher, who recently retired from the Electric Power Research Institute in Palo Alto, California, to start his own consulting business. However, Grant says the approaching commercialization belies deeper questions about whether electric utilities and other heavy industries will be willing to buy HTS products.

"What worries me is, where is the gold rush?" asks Grant. At best, he says, utilities are lukewarm in their interest in HTS products. Several times in the past, Grant argues, electric utilities have backed off even from new technologies that were widely expected to cost less in the long run. "You're dealing with an industry that is very lethargic and doesn't adopt new technology very easily," he says. Daley agrees: "We're dealing with a regulated industry. It's not as easy for them to make investments [in new technology]." However, Daley says he is encouraged by the fact that three utility companies are participating in three separate pilot projects to install 1G HTS power cables. "We can only hope they'll stay behind it and keep active," Daley says. Making motors and other devices from 2G wire should help HTS companies stay afloat. But if utilities bail on making the switch, all the high-tech prowess in the world might not be enough to turn HTS wires into true power players.

–ROBERT F. SERVICE

CREDITS (TOP TO BOTTOM): TIME LIFE PICTURES/GETTY IMAGES; (INSET) SUPERPOWER INC.; SOURCE: D. PETERSON/LOS ALAMOS NATIONAL LABORATORY

Published by AAAS

Random Samples

Edited by Constance Holden

Tsunami Uncovers Indian Shrines

For all the disaster the tsunami of last 26 December left in its wake, it also uncovered treasures: the remains of ancient, long-buried Indian seacoast shrines.

As the waters receded, three large rocks with elaborate carvings of animals as well as the vestiges of two temples emerged from the sands near the coastal town of Mahabalipuram in Tamil Nadu. They appear to be from a port city built in the 7th century.

Carved rock has emerged from the waves.

Mahabalipuram is well-known for its ancient, intricately carved stone temples along the shore. According to descriptions by early European writers, the area was home to seven temples, six of which were supposedly submerged.

The 2-meter rocks include an elaborately sculpted head of an elephant and a horse in flight. Above the elephant's head is a small niche with a statue of a deity. Another rock has a reclining lion. According to archaeologists, lions, elephants, and peacocks decorated temples during the Pallava period in the 7th and 8th centuries. Archaeologists from the Archaeological Survey of India are continuing excavations. Director of excavations Alok Tripathi says "there can be no doubt" that the finds are from 8th century Hindu religious structures.

Politics of Light

A scheme to celebrate the Einstein Centennial with an around-the-world light signal has been hijacked by a group of physicists hoping to shine a political spotlight on a little-known cluster of islets claimed by both Japan and South Korea.

The international undertaking, dubbed "Physics Enlightens the World," will relay light signals—using everything from flashlights to lasers—around the planet, starting in Princeton, New Jersey, on 18 April, the day Einstein died (*Science*, 15 October 2004, p. 403).

But a rogue group of South Korean researchers plans to extend the activities to a group of rocky islets long the subject of dispute between South Korea, where they are known as Dokdo, and Japan, which calls them Takeshima. A flotilla of fishing vessels will shine lights "signaling to the world that this territory is indisputably owned by Korea," according to a South Korean newspaper.

The incident is embarrassing the official sponsors. Max Lippitsch of the University of Graz, Austria, says he has "expressed my deep concern" to the South Korea coordinator of the venture, Chang Gil Han, a physicist at Pusan National University. Han's response: "We have no intention of using this peaceful and cooperative world event for any kind of political purposes." The Japanese have not yet responded. But Kazuo Kitahara, a physicist at International Christian University in Tokyo, notes Einstein's pacifism, adding, "If he saw what was going on, he would be disappointed."

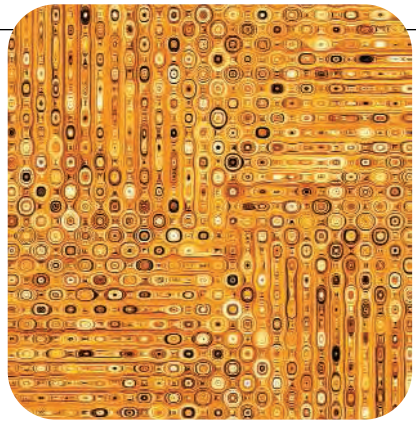

The Beauty of Electromagnetism

Reminiscent of designs by painter Gustav Klimt, this image by freshman Dan Yuan is one of the prizewinners in the annual "weird fields" contest for students at the Massachusetts Institute of Technology's introductory course on electricity and magnetism. Physicist John Belcher and colleagues developed a computer program into which his students can plug mathematical equations describing electromagnetic fields. The computer then churns out dramatic visual representations of the formulas.

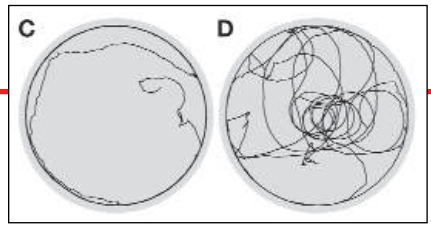

A fly's trajectory switches from lazy (L) to adventurous (R).

Fly Mind Control

Remote control isn't just for gadgets. Researchers have now made genetically engineered flies that can be ordered to leap, fly, and walk at the flash of a laser.

Neurobiologists Susana Lima and Gero Miesenböck of Yale University School of Medicine developed the new technique because they found traditional methods for studying the neural bases of behavior, such as electrode stimulation of neurons, cumbersome and unable to reach networks of cells. "Through this combination of optics and genetics, we can talk to whole populations of cells," says Miesenböck.

The scientists first inserted a rat's ion channel gene into the flies. This particular ion channel transmits electrical impulses by allowing charged particles to cross cell membranes in the presence of ATP, the ubiquitous energy-carrying molecule. The researchers then injected the flies with ATP inactivated by encaging it within another molecule. When hit with the laser, the ATP was released, triggering the ion channels and causing the neurons to fire, they report in the 8 April issue of *Cell*.

If the rat ion channel was expressed in the dopaminergic neurons, for example, the laser caused sedentary flies to become hyperactive. If the ion channel was expressed in the giant fiber neurons, which control the so-called escape pathway, the flies could be made to leap about, buzz their wings, and fly. The method could be used to study behaviors including mating and feeding, the authors say.

CREDITS (TOP TO BOTTOM): LIMA *ET AL.*, *CELL* **121**, 148 (2005); PALLAVA BAGLA; COURTESY DAN YUAN/MIT

Published by AAAS

Edited by Yudhijit Bhattacharjee

JOBS

Extended visit. German mathematical biologist Andreas Dress has been tapped to be one of the founding directors of a new computational biology institute in Shanghai, China. Dress, who is touring the country this month to learn more about China and its science, says he hasn't made a final decision, but "the people here are making it very difficult to decline." Leadership duties will be shared with Chinese population geneticist Li Jin, now at the University of Cincinnati in Ohio, and possibly a third co-director with expertise in computational neuroscience.

The institute, which will receive $11.5 million over 5 years from the Max Planck Society and the Chinese Academy of Sciences, is scheduled to open in October. If Dress accepts the position, he plans to continue collaborations with a group in Magdeburg, Germany, that uses antibodies to visualize the activity of hundreds of proteins in a suite of cells. Antibodies costing $1500 in Germany can be had for $15 in China, he notes.

Homecoming. Neurobiologist Arlene Chiu, a research administrator at the National Institutes of Health, has become the first scientist appointed to the new California Institute for Regenerative Medicine (CIRM). The 59-year-old California native will serve as the institute's director of scientific programs and review.

Chiu, currently associate director of the Office of Research Administration of the National Institute of Biomedical Imaging and Bioengineering, serves on the NIH Stem Cell Task Force and has overseen NIH-funded stem cell research programs aimed at treating neurological diseases. She calls the CIRM position "an incredible opportunity" as well as a chance to return home. She starts work on 1 May.

THEY SAID IT

"What's happening at NIH? Is it just a shell of its former self?"

—Senator Tom Harkin (D–IA) at a 6 April Senate hearing on the National Institutes of Health's budget. Harkin was expressing concern about the recent departure of some topflight researchers from NIH in the wake of new conflict-of-interest rules.

DEATHS

Exuding warmth. A disease to which he devoted his life has claimed cancer researcher Stanley Korsmeyer. He was 54.

Korsmeyer, who had directed the molecular oncology department at Harvard University's Dana-Farber Cancer Institute since 1998, was best known for his work linking apoptosis, or programmed cell death, to cancer. Korsmeyer's research earned him membership in the National Academy of Sciences and a host of other honors, including the General Motors Mott Award. And his optimism and warmth earned him many friends.

"He was admired and loved for who he was even more than for what he accomplished," says Edward Benz, Dana-Farber's president.

CELEBRATING HISTORY

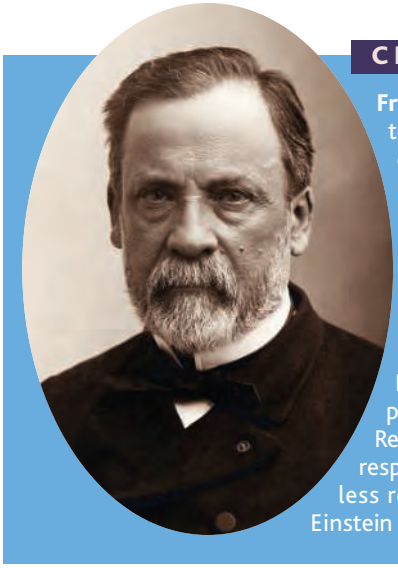

French idols. Three scientists have made the top 10 in a television competition to name the greatest French citizen of all time. Last week, microbiologist Louis Pasteur (left) grabbed second place, trailing only the revered founder of the Fifth Republic, Charles de Gaulle. Polish-born two-time Nobelist and feminist icon Marie Curie took the fourth spot, and oceanographer-filmmaker Jacques-Yves Cousteau came in ninth, topping singer Edith Piaf.

France is not alone in honoring its scientists. In 2002, British viewers ranked Charles Darwin fourth and Isaac Newton sixth on a similar all-time list, and microscope pioneer and microbiologist Antoni van Leeuwenhoek and Renaissance scholar Desiderius Erasmus ran fourth and fifth, respectively, in a 2004 Dutch election. German voters were less reverential in a 2003 poll, however, consigning Albert Einstein to 10th place—far behind Karl Marx, who came in third.

Got any tips for this page? E-mail people@aaas.org

CREDITS (TOP TO BOTTOM): SOURCE: ANDREAS DRESS; DANA-FARBER CANCER INSTITUTE; BILL BRANSON/NIH; CORBIS/BETTMANN

Published by AAAS

The Problem with Patents

SHUJI NAKAMURA'S PERCEPTION THAT THE United States is the land of opportunity for inventors ("Inventor knocks Japan's system after settlement," News of the Week, D. Normile, 21 Jan., p. 337) requires some qualification. Although it is true that some inventors capitalize on the value of the intellectual property they own by patenting their inventions, the majority of inventors realize very little monetary reward. A large percentage of the scientists and engineers producing inventions with potential commercial value in the United States are employed by companies that require, as a condition of their employment, that all intellectual property rights developed using company resources must be assigned to the company for a nominal quid pro quo.

Some inventors develop their ideas, reduce them to practice, and receive patents to protect their intellectual property using their own resources. Without the ability to manufacture, market, and distribute the fruits of their labors, however, these inventors must sell their concept to a company with the ability to bring their invention to market.

> "Although it is true that some inventors capitalize on the value of the intellectual property they own by patenting their inventions, the majority of inventors realize very little monetary reward."
>
> —CRONLUND

On rare occasions, an inventor has the right balance of technical innovation and entrepreneurial skills to make a thriving business out of his or her inventions. Success in these ventures requires dedication, hard work, and shrewd business acumen.

Nakamura should consider himself fortunate that he was able to get $8 million compensation for his inventions from a Japanese for-profit company. In the United States, he might have received $1 for each of his inventions. The contributions of inventors in corporate employment are inadequately compensated. Those scientists and engineers employed by U.S. companies would work day and night with little complaint if the companies rewarded them with a reasonable fraction of the profits realized from their inventions. Talk about incentive!

MALCOLM CRONLUND
958 Meadowbrook Drive, Huntingdon Valley, PA 19006, USA.

Defining the Concept of Public Information

IN THEIR REVIEW OF INFORMATION USE BY animals in social contexts ("Public information: from nosy neighbors to cultural evolution," 23 July 2004, p. 487), É. Danchin *et al.* do an excellent job of reviewing the importance of socially acquired information in a wide taxonomic range of animals. Nevertheless, I feel that discrepancies in the use of the term "information" by Danchin *et al.* warrant attention because they are symptomatic of a broader challenge facing biology, particularly organismal biology.

With the widespread acceptance of Darwinian and neo-Darwinian reasoning in the biological sciences, information has emerged as a central analytical concept (*1*–*4*), yet there are significant inconsistencies in its use. These stem largely from a reluctance to define it explicitly when formal definitions borrowed from communication theory and physics (*5*) do not apply (*6*). To their credit, Danchin *et al.* break ranks and attempt an explicit (albeit informal) definition: "Information is anything that reduces uncertainty" (p. 487). However, this definition suffers from similar limitations in its biological applicability as more formal entropy-based concepts of information (*5*) by implying that ambiguity reduction per se is valuable (since information is presumably valuable), which is at odds with the way that informational analogies are typically made (implicitly) in organismal biology. To see why ambiguity reduction on its own is not a sufficient property of information as referred to by Danchin *et al.*, consider an extreme example: If an individual is killed by a predator (or indeed anything else), uncertainty about its future is reduced, yet by dying it does not acquire information. Other examples of this limitation to the stated definition abound in the text. Yet, the value of the Review, focused as it is on socially acquired information, hinges on such information use having special biological implications; in other words, by using this type of information, rather than, say, personally acquired information, animals behave in ecologically and evolutionarily important ways, a conclusion Danchin *et al.* persuasively sustain. This paper is thus an excellent illustration of why "pragmatic" or "semantic" concepts of information are needed in biology (*3*); information as ambiguity-reduction per se is a "syntactic," meaning-free concept (*7*) and does not capture many of the ways that researchers think about information in organismal biology.

Recently, Maynard Smith (*1*, *2*) rekindled interest in developing a biologically meaningful concept of information, emphasizing the need for an explicitly evolutionary perspective. Jablonka (*3*) subsequently took up the challenge to extend Maynard Smith's deliberations to accommodate nongenetic information, focusing on the crucial link between information and its use by emphasizing that information must have the potential to "change the state of the receiver in a… functional manner…" (p. 582). Thus, in keeping with philosophical traditions in biology, evolved entities in the form of information receivers are assigned a central role, along with their functioning from an evolutionary perspective. I feel that recent developments such as these, together with the conceptual issues they raise, deserve attention in any discussion of information use by individual organisms, such as that by Danchin *et al*. It is only by exploring such ideas explicitly, as well as developments in formal semantic-pragmatic information theory (*8*) and how animals actually use information, that progress will be made toward a scientifically useful definition of information for the biological sciences. After all, information is an integrative concept in biology that has yet to be integrated coherently.

SASHA R. X. DALL*
Department of Zoology, University of Cambridge, Downing Street, Cambridge CB2 3EJ, UK. E-mail: sashadall@iname.com
*Present address: Centre for Ecology and Conservation, University of Exeter in Cornwall, Penryn, Cornwall TR10 9EZ, UK.

References

1. J. Maynard Smith, *Q. Rev. Biol.* **74**, 395 (1999).
2. J. Maynard Smith, *Philos. Sci.* **67**, 177 (2000).
3. E. Jablonka, *Philos. Sci.* **69**, 578 (2002).
4. R. Dawkins, *A Devil's Chaplain, Reflections on Hope, Lies, Science and Love* (Houghton Mifflin, New York, 2003), pp. 91–103.
5. See, for example, C. E. Shannon, W. Weaver, *The Mathematical Theory of Communication* (Univ. of

Illinois Press, Urbana, IL, 1949).
6. See, for example, S. R. X. Dall, R. A. Johnstone, *Philos. Trans. R. Soc. London Ser. B.* **357**, 1519 (2002).
7. J. C. A. van der Lubbe, *Information Theory* (Cambridge Univ. Press, Cambridge, UK, 1997).
8. See, for example, E. D. Weinberger, *BioSystems* **66**, 105 (2002).

IN THEIR REVIEW "PUBLIC INFORMATION: from nosy neighbors to cultural evolution" (23 July 2004, p. 487), É. Danchin *et al.* illustrate convincingly that animals can use information about the behavior of other individuals in their decision-making and that such use can trigger cultural evolution. Yet, their suggested unified concept of "public information" (PI) remains somewhat vague, possibly for two reasons.

First, in their attempt to highlight the implications of PI, they expand the meaning of this term from merely describing a potential resource (a type of information) to a term that also describes a "phenomenon," and a "tool" for research (p. 490). As a result, it is not clear whether the concept of PI represents a theory, a process, or merely a potential resource. We believe that the latter, less complicated designation would in fact be more constructive. The existence of PI as a potential resource is hardly disputed, and the open issues for research are (i) the extent to which this resource is actually being used by animals and (ii) the extent to which it is being transmitted culturally across generations.

The second problem in defining PI is the authors' exclusion of information derived from animals' locations and signaling behaviors (see their fig. 1). This narrow definition may be impractical. For example, information about location may frequently be correlated with information about performance or quality (e.g., feeding site or male's position on a lek), so it seems difficult to distinguish between PI and information about location in practice. Signaling behavior, such as bird singing, in addition to containing cues for male quality, likely also provides information about male density: Is such information not PI? The exclusion of signaling comes to a real paradox when we have to deal with teaching, which is the most advanced form of information transmission in cultural evolution and which clearly involves communication: What are we to make of such intentional information transmission? Rather than viewing what we teach as nonpublic information, it would seem that there is room for considering a variety of public information sources available to animals and for using a more practical definition of PI that includes any information derived from the behavior of other individuals.

ARNON LOTEM[1] AND DAVID W. WINKLER[2]
[1]Department of Zoology, Faculty of Life Sciences, Tel-Aviv University, Tel-Aviv 69978, Israel. E-mail: lotem@post.tau.ac.il. [2]Department of Ecology and Evolutionary Biology, Cornell University, Corson Hall, Ithaca, NY 14853, USA. E-mail: dww4@cornell.edu

IN THEIR STIMULATING REVIEW "PUBLIC information: from nosy neighbors to cultural evolution" (23 July 2004, p. 487), É. Danchin *et al.* combine a sweeping survey of behavior and culture with a focused advocacy for public information's role in cultural evolution. In my reading, these elements are in tension. The examples given often go beyond the definition that public information is about the quality (rather than location) of a resource and is revealed by the performance of other individuals. Scrub jays only need to learn the location of other jays' caches to rob them, and fish do not need to observe any behavior to avoid an area containing alarm substance. These examples reveal that many interesting and important aspects of behavior may not strictly involve public information.

Although the authors couch their conclusions in terms of public information, this term is mentioned only sporadically in the second half of the Review. I found many instances where the broader terms "social information" or "inadvertent social information" could be substituted for "public information" without loss of meaning. It may be useful to discuss the relative importance of communication and inadvertent social information to cultural evolution, but it seems unnecessary and potentially counterproductive to advocate for one form of information while ignoring others.

PETER A. BEDNEKOFF
Biology Department, Eastern Michigan University, Ypsilanti, MI 48197, USA.

WE ENDORSE É. DANCHIN *ET AL.*'S EMPHASIS on public information, both as a taxonomically widespread source of adaptive behavior and as a driver of social evolution ("Public information: from nosy neighbors to cultural evolution," Review, 23 July 2004, p. 487). However, we feel it is important to stress the costs of public information and to consider why some species of vertebrates do not exploit this reservoir of knowledge. In our study of public-information use in two closely related species of sticklebacks (*1*), we found that nine-spined sticklebacks (*Pungitius pungitius*), after watching conspecific or heterospecific demonstrators feeding at two patches and then tested alone, tend to approach the former location of the richer patch. As their observational experience was restricted to the relative success of their demonstrators, and potential alternative explanations could be ruled out, we surmised that nine-spined sticklebacks were capable of public-information use. However, three-spined sticklebacks (*Gasterosteus aculeatus*), when subject to the same test, swam with equal frequency to the former locations of rich and poor patches. Why should one species and not the other rely on public information?

The answer to this conundrum comes from a mathematical analysis of the adaptive advantages of human culture. Boyd and Richerson (*2*) postulate a costly information hypothesis, which proposes an evolutionary trade-off between reliable but costly self-acquired information and potentially less reliable but cheap socially transmitted information. The relative cost of acquiring personal information varies between the two stickleback species, which determines the value of public information. Three-spines have large spines and armored body plates—robust structural defenses that allow them to sample alternative food patches directly, in relative safety. Such sampling by nine-spines, which have weaker physical defenses, would leave them vulnerable to predation and hence, in fitness terms, would be extremely costly. Consequently, nine-spines spend much of their time in refuge, from where selection seemingly has favored the ability to monitor the foraging success of others. Considerable evidence is accumulating among fish, birds, and mammals that animals will ignore public information under specific circumstances (*3*). For example, nine-spines will ignore public information if they have reliable, up-to-date personal information, yet switch to exploiting public information if their personal information is unreliable or outdated (*4*). In turn, the costs associated with public information can stimulate the collection of personal information that refreshes the cultural knowledge pool (*5*), providing the variation required for cultural evolution.

KEVIN N. LALAND,[1] ISABELLE COOLEN,[2] RACHEL KENDAL[3]
[1]School of Biology, University of St. Andrews, Bute Medical Building, Queen's Terrace, St. Andrews, Fife KY16 9TS, Scotland. [2]Institut de Recherche sur la Biologie de l'Insecte, Université de Tours, Avenue Monge, 37200 Tours, France. [3]Department of Biological Sciences, Stanford University, Stanford, CA 94305, USA.

References

1. I. Coolen, Y. van Bergen, R. L. Day, K. N. Laland, *Proc. R. Soc. London Ser. B* **270**, 2413 (2003).
2. R. Boyd, P. J. Richerson, *Culture and the Evolutionary Process* (Univ. of Chicago Press, Chicago, IL, 1985).

Letters to the Editor

Letters (~300 words) discuss material published in *Science* in the previous 6 months or issues of general interest. They can be submitted through the Web (www.submit2science.org) or by regular mail (1200 New York Ave., NW, Washington, DC 20005, USA). Letters are not acknowledged upon receipt, nor are authors generally consulted before publication. Whether published in full or in part, letters are subject to editing for clarity and space.

3. R. L. Kendal, I. Coolen, Y. van Bergen, K. N. Laland, *Adv. Study Behav.*, in press.
4. Y. van Bergen, I. Coolen, K. N. Laland, *Proc. R. Soc. London Ser. B* **271**, 957 (2004).
5. T. Kameda, D. Nakanishi, *Evol. Human Behav.* **23**, 373 (2002).

Response

THE LETTER WRITERS RAISE SEVERAL questions that provide us with the opportunity to clarify important points about public information (PI) and cultural evolution. Four major issues are raised.

What is information? We agree with Dall that a biological definition of information should be linked to the fitness consequences of having it. Our definition that information is "anything that reduces uncertainty for the observer" (our fig. 1) is set in an evolutionary context. Information thus changes the state of the receiver in a functional way: It improves fitness when a more effective response is made possible by the reduced uncertainty about current environmental conditions. A more specific definition of information is "anything that reduces uncertainty, potentially allowing a more adaptive response."

What is Public Information? While Dall questioned the definition of information generally, Lotem and Winkler and Bednekoff each question our definition of public information as information derived from the "performance of other individuals sharing similar environmental requirements." They suggest that this definition is too specific because in general use, "public" usually refers to commodities that are available to all. Our application of PI accounts for its long-term use in the literature. However, we agree with the need for a broader perspective, which is why we introduced the term inadvertent social information (ISI), which includes PI. Furthermore, Lotem and Winkler propose that PI should incorporate signaling and teaching, both of which are deliberate transmissions of information. However, it was our goal to highlight the fact that cues inadvertently produce information, while signals produce information deliberately. By viewing cues separately from signals, our aim was to explore the consequences of inadvertent information alone. We recognize the existence of interactions between cues and signals (our fig. 1), both of which, for example, contribute to culture and reputation. We also stated that cues "may be viewed in some contexts as the platform from which signals evolve." Thus, by separating cues and signals, we can better understand both in order to subsequently synthesize them.

Lotem and Winkler also criticized our unified concept of PI as being vague because we have described it as both a "tool" and a "phenomenon." Here we specify that clear definitions of phenomena are important tools that can be used in experiments. Lotem and Winkler further interpret our paper to suggest that PI can also be viewed as a resource. However, we do not state this and suggest here that it may not be useful to view information as a resource because unlike most resources, the use of information does not usually result in its depletion.

Is using PI always adaptive? Laland *et al.* note that the use of PI may sometimes be costly. Although many forms of PI use may be beneficial, we acknowledge that its benefits are by no means universal. In instances where the gathering of personal and public information are incompatible activities, animals must choose continuously which type of information to gather. When everybody is watching everybody else, there is nobody to produce PI. This frequency-dependence is akin to producer-scrounger games (*1*) where stable equilibrium mixtures of the two alternatives are expected (*2*). The paradoxical outcome of this frequency-dependence is that even though using PI could be advantageous, it spreads within a group until it does not pay any more than using personal information only (*3*). PI is used not because it provides a benefit over its alternative, but because it would be costly not to use it (*2*). The potential for such a trade-off highlights the importance of ascertaining the relative value of public versus personal information. Another potential constraint to the use of PI concerns informational cascades, which occur when public information overrides personal information such that all decisions are based on the behavior of others, irrespective of one's own personal information (*4*). Although cascades may be produced by adaptive decision-making, they can sometimes lead to incorrect responses. Thus, as Laland *et al.* underline, we expect variation in PI use across species, with that one factor explaining variation in the cost of acquiring it.

The importance of public information and its potential to trigger culture. Bednekoff questions our emphasis on PI in relation to cultural evolution. Our goal was not to advocate ignoring other contributors to cultural evolution, but rather to explain how ISI in general, and PI in particular, can be important contributors to cultural evolution. Culture can be viewed as a by-product of learning from others (*5*, *6*), and our Review shows that many major fitness-enhancing decisions do involve PI, that is, learning from others. In our fig. 3, we used the broader expression ISI to save space. However, elsewhere we made explicit that we view PI as a major component of ISI that contributes to cultural evolution.

Finally, evidence exists for the occurrence of traditions even in invertebrates (*5*). The existence of cultural processes in taxa other than vertebrates would considerably increase the potential role of culture in the evolution of life. We reiterate that evolutionary biologists should consider the possibility that cultural evolution plays a significant role in evolutionary processes and that PI may provide an important concept for studying cultural evolution in animals.

ÉTIENNE DANCHIN,[1]* LUC-ALAIN GIRALDEAU,[2] THOMAS J. VALONE,[3] RICHARD H. WAGNER[4]

[1]U.P.M.C. CNRS-UMR7625, Bât A, 7è étage, Case 237, 7 quai Saint Bernard, 75252 Paris Cédex 05, France. [2]Groupe de Recherche en Écologie Comportementale et Animale, Département des Sciences Biologiques, Université du Québec à Montréal, Case Postale 8888, Succursale Centre-Ville, Montréal, QC H3C 3P8, Canada. [3]Department of Biology, St. Louis University, St. Louis, MO 63103, USA. [4]Konrad Lorenz Institute for Ethology, Austrian Academy of Sciences, Savoyenstrasse 1a, A-1160 Vienna, Austria.

*To whom correspondence should be addressed. E-mail: edanchin@snv.jussieu.fr

References

1. L. A. Giraldeau, T. Caraco, *Social Foraging Theory, Monographs in Behavior and Ecology* (Princeton University Press, Princeton, 2000).
2. L. A. Giraldeau, T. J. Valone, J. J. Templeton, *Philos. Trans. R. Soc. B* **357**, 1559 (2002).
3. T. Kameda, D. Nakanishi, *Evol. Hum. Behav.* **24**, 242 (2003).
4. S. Bikhchandani, D. Hirshleifer, I. Welch, *J. Econ. Perspect.* **12**, 151 (1998).
5. S. Blackmore, *The Meme Machine* (Oxford Univ. Press, Oxford, 1999).
6. E. Avital, E. Jablonka, *Animal Traditions-Behavioural Inheritance in Evolution* (Cambridge Univ. Press, Cambridge, 2000).

PLOS Position on NIH Public Access Policy

THE RECENT NEWS ARTICLE "NIH WANTS public access to papers 'as soon as possible'" (J. Kaiser, News of the Week, 11 Feb., p. 825) misrepresents the Public Library of Science's position on the National Institutes of Health's new Public Access Policy. It is not the case that we are "pleased with the wording." To the contrary, our view is that the policy should have been stronger in several respects (*1*).

For one thing, to serve the public interest more effectively, the agency's language should have been to "require" or "expect" rather than "request" the deposition of NIH-funded articles in the National Library of Medicine's free-to-use Internet repository, PubMed Central. For another, the maximum allowable delay before articles' public release should have been at most 6, rather than 12 months—particularly since no publisher has presented evidence that the free availability of a fraction of its journals' articles half a year after publication would adversely affect subscription revenues.

ANDY GASS AND HELEN DOYLE

Public Library of Science, 185 Berry Street, Suite 1300, San Francisco, CA 94107, USA.

Reference

1. See www.plos.org/news/announce_nihpapolicy.html.

CORRECTIONS AND CLARIFICATIONS

News of the Week: "Unnoticed amendment bans synthesis of smallpox virus" by M. Enserink (11 Mar., p. 1540). The story stated that Peter Jahrling studied variola at the U.S. Army Medical Research Institute of Infectious Diseases (USAMRIID) in Fort Detrick, Maryland. While Jahrling was employed by USAMRIID at the time, the experiments were carried out at the Centers for Disease Control and Prevention in Atlanta.

Netwatch: "Breaking down diabetes" (4 Mar., p. 1385). This item incorrectly listed the sponsors of the T1DBase. The site is is funded by the Juvenile Diabetes Research Foundation (JDRF) and is a collaboration between the JDRF/Wellcome Trust Diabetes and Inflammation Laboratory and the Institute for Systems Biology.

News of the Week: "Report puts Pasteur move on hold" by M. Enserink (4 Mar., p. 1391). The story misspelled the name of a building on the Pasteur Institute campus in Paris. The building is named Duclaux.

This Week in Science: "A tamed radical" (14 Jan., p. 177). In the 12th line, "rhenium" should instead read "rhodium."

TECHNICAL COMMENT ABSTRACTS

COMMENT ON "Grain Boundary–Mediated Plasticity in Nanocrystalline Nickel"

Mingwei Chen, Xiaoqing Yan

Shan *et al.* (Reports, 30 July 2004, p. 654) reported transmission electron microscopy observations of nanograin rotation and claimed that the plasticity of nanocrystalline nickel is mediated by this grain boundary behavior. Our analysis of Shan's results suggests that the contrast change more likely results from nanograin growth rather than plastic deformation.

Full text at www.sciencemag.org/cgi/content/full/308/5720/356c

RESPONSE TO COMMENT ON "Grain Boundary–Mediated Plasticity in Nanocrystalline Nickel"

Zhiwei Shan, E. A. Stach, J. M. K. Wiezorek, J. A. Knapp, D. M. Follstaedt, S. X. Mao

Chen and Yan propose that the contrast changes we observed likely do not result from plastic deformation. We provide specific reasons why we disagree and why their measurement approaches are inappropriate, as well as further evidence supporting our original conclusion of grain boundary–mediated deformation.

Full text at www.sciencemag.org/cgi/content/full/308/5720/356d

Published by AAAS

Comment on "Grain Boundary–Mediated Plasticity in Nanocrystalline Nickel"

Nanograin rotation via grain boundary sliding has been predicted as an important deformation mode in nanocrystalline materials as grain sizes approach less than 10 nm (*1*–*3*). However, definite experimental evidence beyond molecular dynamics (MD) simulations has been long sought. Recently, Shan *et al*. (*4*) reported in situ straining dark-field transmission electron microscope (DFTEM) observations of grain rotation in nanocrystalline Ni and claimed that the plastic deformation of nano-Ni is mediated by this grain boundary behavior. Although the experimental results reported by Shan *et al*. are interesting, their assessment and analysis of the TEM images are problematic. Using the images presented in (*4*), we have quantitatively measured the relative displacements and grain sizes. Both results suggest that the grain rotation and associated contrast change reported by Shan *et al*. more likely come from low-temperature nanograin growth, caused by electron-beam irradiation and applied stresses, than from plastic deformation.

In Fig. 1, we show contrast-inverted images from figure 3 in (*4*). Small grains with less contrast change are linked with lines to form a trapezoidal frame surrounding grain G, which exhibited significant contrast change during loading. Overlaying the trapezoidal frame in Fig. 1, B to F, shows that all the joint points of the frame match well with the original small grains. Precise measurements of the line lengths were performed using NIH Image (*5*), and the dependence of the line lengths on loading time was plotted (Fig. 2). The mean error of these measurements is about ±1 nm and the corresponding strain smaller than 0.5%. The measurements do not suggest any systematic length changes and, thus, any relative displacements and strains.

To rule out the possible bending and torsion deformation, which might not significantly alter the line lengths, we measured the angles marked in Fig. 1B. We were also unable to observe any systematic angle changes with time. These measurements unambiguously show that no detectable deformation occurred during loading. If the significant contrast change of grain G were caused by plastic deformation, relative displacements, either in plane or out of plane, should have been observed among the surrounding grains, because plastic deformation cannot be accomplished solely by a single grain rotation.

As several attempts have well demonstrated (*6*–*8*), it is extremely difficult to get uniform plastic deformation in nanocrystalline samples, and localized deformation and cracking cannot be avoided during in situ straining TEM observations. Although the data in Fig. 1 were recorded during in situ tensile tests, it is quite possible that the region observed by Shan *et al*. did not experience visible plastic deformation and that the observed contrast change came mainly from nanograin growth caused by electron-beam irradiation and applied stresses. The time-related size change of grain G, measured using the NIH Image (*5*), revealed a linear relation between grain size in the area (S) and time (t) (Fig. 2C) that is exactly consistent with the classical grain growth equation (*9*), $S - S_0 = kt$, where S_0 is the initial grain size and k is a constant.

The diffraction patterns shown in figure 2, B and D, in (*4*) also indicate nanograin growth during DFTEM observations. Slightly adjusting the brightness of figure 2D in (*4*) to be close to that of figure 2B in (*4*) (fig. S1)

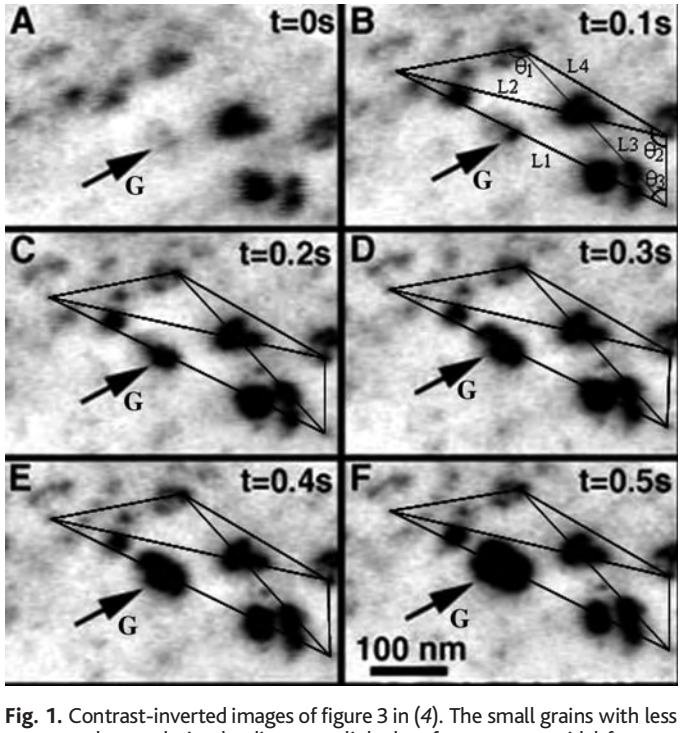

Fig. 1. Contrast-inverted images of figure 3 in (*4*). The small grains with less contrast change during loading were linked to form a trapezoidal frame.

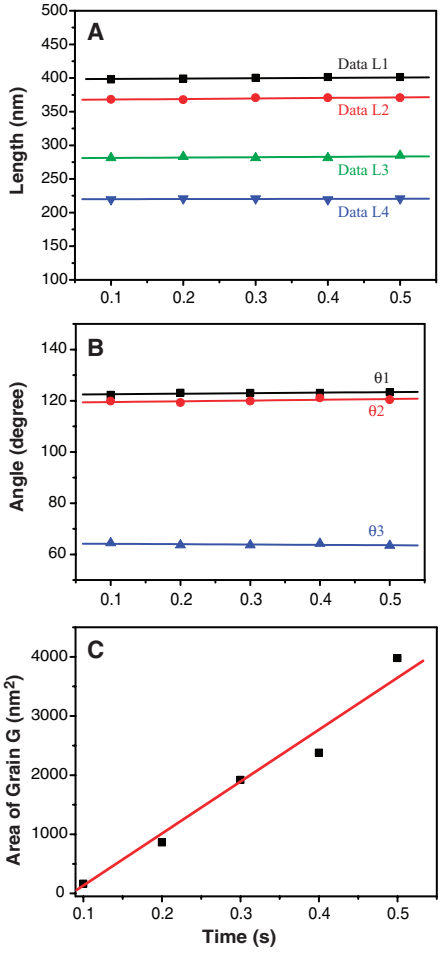

Fig. 2. Measurements of line lengths, angles, and grain areas using NIH Image. (**A**) The distance changes between the smaller grains around the marked grain G as a function of loading time (see Fig. 1B). The slope of each line approaches zero, which suggests that no systematic deformation occurs accompanying the continuous contrast changes of grain G. (**B**) The relation between the angles (see Fig. 1B) and loading time. (**C**) Changes in the area of grain G as a function of time. The linear relation between S and t is consistent with the classical grain growth equation.

reveals continuous rings with an increasing number of bright spots that correspond to coarsened grains; this, in turn, suggests that the change of diffraction patterns results from the grain growth, rather than the thickness decrease claimed by Shan *et al*. (*4*). Additionally, the contrast in the DFTEM [figure 2E in (*4*)] cannot be solely attributed to the grain boundaries. Crystal defects—for example, dislocations, as revealed by their high-resolution electron microscope image [figure 4C in (*4*)]—can provide the similar contrast caused by their elastic strain fields (*10*). After contrast inversion of figure 2E in (*4*), the dark contrast that Shan *et al*. suggested represented grain boundaries shows discontinuous features (fig. S2) that are characteristic of dislocations in bright-field TEM. It is not surprising to see dislocations in the nanograin because the grain size, at around 50 nm in diameter, is large enough to contain a number of perfect dislocations. Actually, the appearance of the edge dislocations as observed by Shan *et al*. is also consistent with the rotation growth theory, as suggested by recent MD simulations (*11*, *12*) and the classical rotation growth model (*13*).

In summary, the TEM results reported in (*4*) can be interpreted as nanograin growth caused by electron-beam irradiation and applied stresses. Although nanograin growth may not be the whole story, and although a small amount of deformation through grain boundary mediation may occur accompanying the observed grain rotation, the grain contrast change reported by Shan *et al*. appears to result mainly from nanograin coalescence and growth rather than visible plastic deformation.

Mingwei Chen* and Xiaoqin Yan
Institute for Materials Research
Tohoku University
2-1-1 Katahira, Aoba-ku,
Sendai 980-8577, Japan
**E-mail: mwchen@imr.tohoku.ac.jp*

References and Notes

1. J. Schiøtz, F. D. Di Tolla, K. W. Jacobsen, *Nature* **391**, 561 (1998).
2. H. Van Swygenhoven, *Science* **296**, 66 (2002).
3. J. Schiøtz, K. W. Jacobsen, *Science* **301**, 1357 (2003).
4. Z. Shan *et al.*, *Science* **305**, 654 (2004).
5. NIH Image is free software for image processing and quantitative measurements; http://rsb.info.nih.gov/nih-image.
6. C. J. Youngdahl, J. R. Weertman, R. C. Hugo, H. H. Kung, *Scripta Mater.* **44**, 1475 (2001).
7. R. C. Hugo *et al.*, *Acta Mater.* **51**, 1937 (2003).
8. K. S. Kumar, S. Suresh, M. F. Chisholm, J. A. Horton, P. Wang, *Acta Mater.* **51**, 387 (2003).
9. J. E. Burke, D. Turnbull, *Prog. Metal Phys.* **3**, 220 (1952).
10. M. W. Chen *et al.*, *Science* **300**, 1275 (2003).
11. A. J. Haslam, S. R. Phillpot, D. Wolf, D. Moldovan, H. Gleiter, *Mater. Sci. Eng. A* **318**, 293 (2001).
12. D. Moldovan, V. Yamakov, D. Wolf, S. R. Phillpot, *Phys. Rev. Lett.* **89**, 206101 (2002).
13. J. C. M. Li, *J. Appl. Phys.* **33**, 2958 (1962).

Supporting Online Material

www.sciencemag.org/cgi/content/full/308/5720/356c/DC1
Figs. S1 and S2

4 November 2004; accepted 15 March 2005
10.1126/science.1107143

Response to Comment on "Grain Boundary–Mediated Plasticity in Nanocrystalline Nickel"

Our study (*1*) reported on the deformation response of nanocrystalline Ni during in situ dark-field transmission electron microscopy (DFTEM) straining experiments and showed what we view as direct and compelling evidence of grain boundary–mediated plasticity. Based on their analysis of the limited experimental data we presented, however, Chen and Yan (*2*) propose that the reported contrast changes more likely resulted from grain growth caused by electron irradiation and applied stress rather than from plastic deformation. Here, we give specific reasons why their assertions are incorrect and discuss how the measurement approaches they have used are inappropriate. Additionally, we present further evidence that supports our original conclusions.

The method Chen and Yan employed to measure displacement merely probes the in-plane (two-dimensional) components of incremental strain occurring during the very short time interval shown [figure 3 in (*1*)] instead of the accumulated strain. As we noted explicitly in the supporting online material in (*1*), the loading was applied by pulsing the displacement manually. After each small displacement pulse, the monitored area always moved significantly within or even out of the field of view. Clear images could be obtained only when the sample position stabilized within the field of view, and at that time severe deformation was nearly complete. Thus, little incremental strain occurs during this short image sequence [figure 3 in (*1*)], as one might expect.

We believe that the images shown in figure 3 of (*1*) are particularly valuable in understanding deformation in nanocrystalline materials. In general, the formation process of grain agglomerates simply occurred too fast to be recorded clearly. Moreover, instead of remaining constant after formation, the sizes of the grain agglomerates changed in a rather irregular manner in responding to the deformation and fracture process (see, for example, Fig. 1, B to D). This indicates that strong grain boundary–related activity occurred inside the grain agglomerates. Figure 3 in (*1*), a short (0.5 s) extract from more than 6 hours of videotaped experimentation (imaged ahead of cracks), not only reveals the formation process of a grain agglomerate, but also shows conclusive evidence for grain rotation and excludes the effect of overall sample rotation.

It should be noted that other small grains still exhibit some minor contrast changes in figure 3 in (*1*). Hence, using them as reference points yields measurements that may not be accurate to ±1 nm [as Chen and Yan (*2*) claim in their analysis] and limits the accuracy of their conclusions. Chen and Yan also claim that no deformation has occurred, yet simultaneously state that the analysis has a deformation measurement error of 0.5%. This is simply not consistent; even small strains of this order may cause plastic deformation.

In contrast with previous in situ TEM experiments (*3*–*5*), the special sample design adopted in our investigation (*1*) ensured that all deformation was primarily concentrated in a bandlike area ahead of the propagating crack. We found that these grain agglomerates were observed only in this bandlike thinning area as a response to the applied loads (Fig. 1B). No similar phenomena were detected under the electron beam alone or in stressed areas apart from the main deformation area, and these phenomena have not been reported during in situ observations of this same material made by other researchers (*5*). Subsequent cracks were always observed to follow this deformation area upon further displacement pulses (Fig. 1, C and D). This clearly indicates that the enlarged agglomerates do not result simply from electron irradiation plus stress, but rather from stress-induced deformation.

In their comment, Chen and Yan claimed a linear relation between "grain" area and time based on their measurements made from figure 3 in (*1*) and claimed that these measurements are exactly consistent with the classical grain growth equation. However, as we noted (*1*), the growth in size of this agglomerate is not isotropic and occurs in an irregular manner. For example, after bright contrast emerged from a grain about 6 nm in diameter, it remained well defined in size as a single, approximately equiaxed grain until t = 0.1 s (fig. S1). We have reproduced the "grain growth" plot of Chen and Yan (Fig. 2) using our entire video image sequence (fig. S1). Clearly, the growth in area of the agglomerate is not consistent with linear grain growth. (Unfortunately, only a portion of these data could be included in the original paper for reasons of space.) Notably, Chen and Yan did not apply a similar "grain growth" analysis to nearby grains; this would have yielded no information in support of their argument, as those grains show essentially no growth.

In addition, if classical grain growth were occurring during our observations—even though it is not expected at ambient temperature in nanocrystalline nickel (*6*, *7*)—the initial displacement pulse might have added mechanical driving force to overcome an apparent activation barrier that exists for the thermally activated process of grain growth. This additional mechanical contribution would diminish over time. However, once the appropriate larger grains would have grown to about 6 to 10 times the size of the average grain (see, for example, the large grains in figs. S1 and S2), their growth would be expected to continue at the expense of the

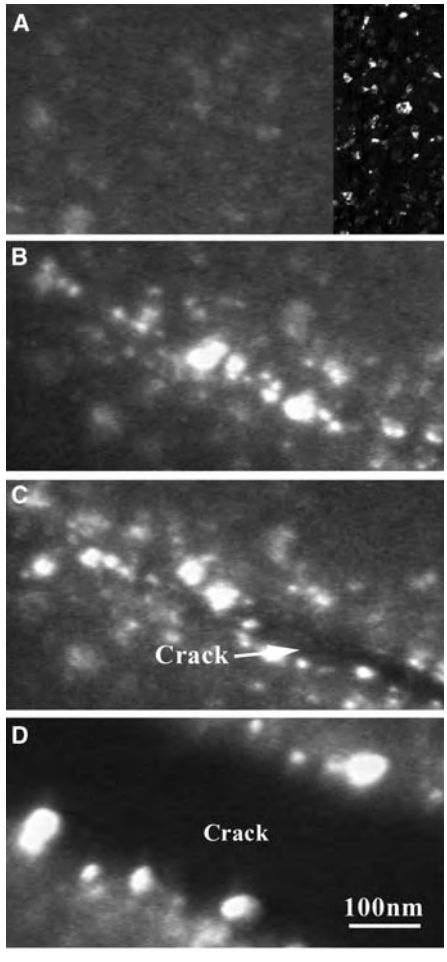

Fig. 1. Dark-field TEM images showing deformation and fracture of nanocrystalline Ni in response to an applied tensile displacement pulse. Note the growth of larger grain agglomerates along the propagating crack path. Inset in (A) is an image from an undeformed area that has been prethinned with low-temperature ion thinning to show more clearly the presence of small grains as well as the narrow grain size distribution.

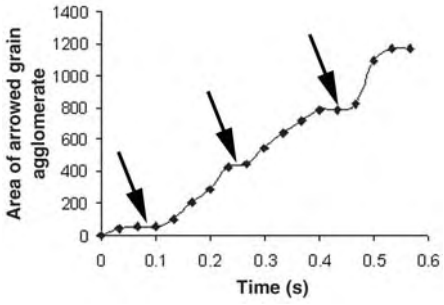

Fig. 2. Changes in the area of the grain agglomerate as a function of time. Clearly, the growth in area of the agglomerate is not consistent with linear grain growth. Note the "terraces" indicated by black arrows, which suggest an "incubation" time between grain rotations.

smaller grains in their vicinity, because the curvature-derived driving force would be greater, more strongly favoring their continued growth and the reduction of the free energy of the material. However, this was not the case [see, for example, fig. S2, which was extracted immediately after the sequence shown in figure 3 in (*1*)]. Without any further displacement pulses, the key grain agglomerate stopped growing and then appeared to split with time. Further loading leads to crack propagation in the bandlike deformation area in an inter- or intra-agglomerate manner. Again using the nearby features as references, this subsequent splitting is further conclusive evidence of grain boundary–mediated plasticity and argues against classical grain growth.

The image shown as figure 2E in (*1*) allowed us to state that grain agglomerates, instead of individual large grains, resulted from the applied displacement pulse. To directly compare the undeformed and deformed states, the two diffraction patterns that appeared in our paper [figure 2, B and D, in (*1*)] were taken under identical conditions—that is, using the same illumination intensity, the same selected-area aperture size, and the same exposure time. Simply boosting the contrast, as Chen and Yan have done, fundamentally alters the information in these patterns and thus yields an inaccurate conclusion. Presumably they have mistakenly chosen to alter the images out of concern over whether we had taken them in an equivalent manner; unfortunately, their alteration of contrast removes the difference in background intensity, which demonstrates that the material has also thinned and thus has been plastically deformed.

When considering how DFTEM images are formed, it is clear that the smaller grains in the agglomerates exhibit essentially edge-on orientations of their {111} lattice planes, their {200} lattice planes, or both (*1*). From a thermodynamic view, it is very possible that these grains are divided by small-angle grain boundaries (which would consist of dislocation arrays) or even that some coalescence occurred (*8*). However, considering that grain agglomerates, after being formed, change their sizes in a rather irregular way in response to the deformation (for example, Fig. 1, B to D), classical grain rotation–induced grain growth, if it exists, is not likely to be prominent.

The contrast-inverting method used by Chen and Yan (*2*) on figure 2E in (*1*) is poorly chosen. A bright-field image is formed by selecting the direct beam in the selected-area diffraction pattern, which will include contrast information from all diffracting lattice planes. Alternatively, a dark-field image of the type we have used is formed by selecting a small part of the diffraction rings (for polycrystalline materials) using the objective lens aperture. The dark-field image only includes the contrast information from those grains that are oriented such that they contribute to the specific diffraction vectors (direction and length) contained in the small region of the diffracting rings that is selected by the objective lens aperture. Therefore, to obtain bright-field contrast by inverting the dark-field contrast is simply incorrect; bright-field and dark-field TEM images give strictly inverse intensity only when considering a two-beam diffraction condition in the kinematic electron diffraction limit (*9*). Moreover, diffraction-contrast TEM images display true grain sizes only when the diffraction condition, exposure time, and image intensities are selected correctly. Manipulation of TEM images by software is easy but is fraught with scientific peril and should be done only with great care.

In sum, it is unfortunate that only part of the video frames from our experiments could be included in (*1*), as this omission led to the incorrect deduction by Chen and Yan (*2*) of a false linear grain growth by subsequent measurements. However, the remaining supporting evidence that they present stems largely from inappropriate image contrast adjustments and a misreading of our original paper.

Zhiwei Shan
Department of Mechanical Engineering
University of Pittsburgh
Pittsburgh, PA 15261, USA

E. A. Stach
School of Materials Engineering
Purdue University
West Lafayette, IN 47907

J. M. K. Wiezorek
Department of Materials Science and Engineering
University of Pittsburgh
Pittsburgh, PA 15261, USA

J. A. Knapp *and* ***D. M. Follstaedt***
Sandia National Laboratories
Albuquerque, NM 87185–1056, USA

S. X. Mao*
Department of Mechanical Engineering
University of Pittsburgh
Pittsburgh, PA 15261, USA
**To whom correspondence should be addressed.*
E-mail: smao@engr.pitt.edu

References and Notes

1. Z. W. Shan *et al.*, *Science* **305**, 654 (2004).
2. M. W. Chen, X. Yan, *Science* **308**, 356 (2005); www.sciencemag.org/cgi/content/full/308/5720/356c.
3. C. J. Youngdahl, J. R. Weertman, R. C. Hugo, H. H. Kung, *Scripta Mater.* **44**, 1475 (2001).
4. K. S. Kumar, S. Suresh, M. F. Chisholm, J. A. Horton, P. Wang, *Acta Mater.* **51**, 387 (2003).
5. R. C. Hugo *et al.*, *Acta Mater.* **51**, 1937 (2003).
6. R. Dannenberg, E. A. Stach, J. R. Groza, B. J. Dresser, *Thin Solid Films* **370**, 54 (2000).
7. N. Wang, Z. Wang, K. T. Aust, U. Erb, *Acta Mater.* **45**, 1655 (1997).
8. A. J. Haslam *et al.*, *Acta Mater.* **52**, 1971 (2004).
9. P. B. Hirsch *et al.*, *Electron Microscopy of Thin Crystals* (Krieger, Malabar, FL, 1977).
10. Supported by NSF grant CMS-0140317 to University of Pittsburgh. The work at the National Center for Electron Microscopy of Lawrence Berkeley National Laboratory and at Sandia was supported by the Division of Materials Sciences and Engineering, Office of Basic Energy Sciences, of the U.S. Department of Energy. Sandia is a multiprogram laboratory operated by Sandia Corporation, a Lockheed Martin Company, for the U.S. Department of Energy's National Nuclear Security Administration under contract DE-AC04-94AL85000.

Supporting Online Material

www.sciencemag.org/cgi/content/full/308/5720/356d/DC1
Fig. S1 and S2

22 November 2004; accepted 29 March 2005
10.1126/science.1107389

NEUROSCIENCE

Treasures from a Golden Age

Robert Wurtz

The cerebral cortex performs the highest level of processing in the brain, and the last half century has seen a revolution in our understanding of this superficial gray matter. David Hubel and Torsten Wiesel played a major role in this revolution, one that they chronicle in *Brain and Visual Perception*.

Brain and Visual Perception
The Story of a 25-Year Collaboration
by David H. Hubel and Torsten N. Wiesel
Oxford University Press, New York, 2004. 737 pp. $49.50, £29.99. ISBN 0-19-517618-9.

We can best understand the excitement generated by the authors' work by remembering how little was known about cerebral cortex in the 1950s, when they started their research. Anatomical studies using stains of fibers and cells had divided cortex into discrete areas. Measurements of the electrical potentials evoked by stimulating peripheral nerves had mapped the cortical regions related to touch, hearing, and vision, and stimulation of the cortex itself had revealed the areas related to movements of the body and eyes. Clinical neurology, brain stimulation during human surgery, and ablations in experimental animals had identified additional regions of cortex related to such higher functions as speech, attention, and memory. Whereas localization of function was firmly established, what remained a mystery was the production of something as complex as visual perception from the activity of individual cortical neurons.

Hubel and Wiesel's first experiments, reported in 1959 and 1962, provided initial answers by demonstrating a plausible hierarchy of visual processing from "concentric cells" to "simple cells" to "complex cells," with each level's output being the input to the next level. The authors went on to identify a columnar organization in visual cortex, the organization Vernon Mountcastle had found in somatosensory cortex (*1*); cells in each column required the same stimulus orientation, and different orientations were represented in different columns. This organization was complemented by an independent one for the inputs from the two eyes. Their experiments led Hubel and Wiesel to the concept of a cortical module (hypercolumn) that did all the processing needed for one region of the visual field—the most complete description of a functional unit in cerebral cortex. Intertwined with this work on organization, they completed striking experiments exploring the development of the system, the alterations with visual deprivation, and the importance of critical periods. Research continues to this day on all these topics, but Hubel and Wiesel provided the first insights.

Brain and Visual Perception recounts this sequence of experiments and much more. The book begins with autobiographical sketches and the authors' descriptions of their research background and the environment of their collaboration (at Johns Hopkins and then at Harvard). Hubel and Wiesel include fond and grateful recollections of their mentor Steve Kuffler, who played a critical role in their research careers and whose work (*2*) was the inspiration for theirs. In the book's epilogue, the authors reflect on the current state of neurophysiology and comment that their 25-year collaboration lasted so long because, in analogy to Gilbert and Sullivan, they were equals with different talents.

The bulk of the book comprises a selection of research papers from the authors' enviable series of elegant experiments, with a foreword and afterword for each. The papers are grouped around the two major contributions for which Hubel and Wiesel received the 1981 Nobel Prize in physiology and medicine: "Normal Physiology and Anatomy" (14 papers) concentrates on the experiments that provided the first insights into the nature of transformations of visual information in cerebral cortex. "Deprivation and Development" (10 papers) centers on how the system forms and the consequences of disruption, topics of considerable clinical relevance. The book's final section supplements the research reports with three appropriate summary articles: the authors' individual Nobel lectures and their joint Ferrier lecture (published in 1977). If one wants to read a single paper to grasp the totality of their work, the Ferrier lecture should be it.

The book's glory is that the commentaries sandwiching each paper illuminate the workings of one of the most productive collaborations in the history of biology. Hubel and Weisel describe the joy of mom-and-pop science where the collaborators do the work and weigh what to do next. One cannot help but feel nostalgia for their model of doing science with infrequent but well-wrought papers that can be profitably read after almost 50 years. The original papers provide an unvarnished report, and the commentaries offer pithy insights into the why and the how of the experiments. For those of us who think that the best way to understand the principles of our field is to read the original scientific reports, the book brings their work all together—complete with the authors' retrospective evaluations of their work.

Mixed among the comments on the authors' many successes are remarks on disappointments and omissions. Hubel and Wiesel had hoped to find progressively higher orders of processing beyond the primary visual cortex (V1), but did not. They missed the structural feature referred to as blobs within V1, and they did not pursue in detail color vision or depth perception. Their comments on roads not taken emphasize the critical role of experimental strategy, one that in their case let them concentrate on the organization of V1 and on visual development. Even with the benefit of hindsight, few would contest their decisions.

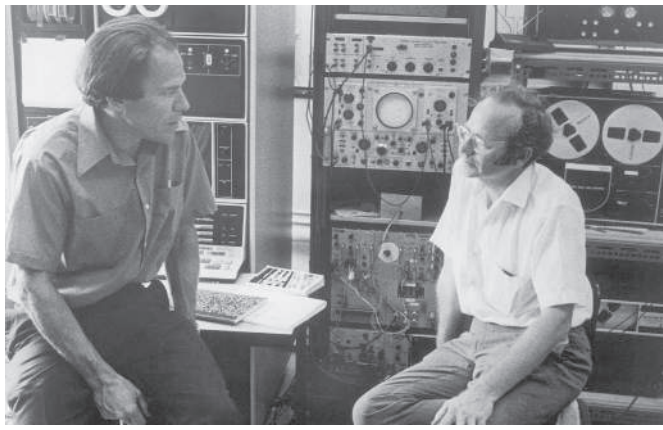

The Gilbert and Sullivan of visual cortex (1970).

Many of us now investigating the visual system were attracted by the beauty of the organization Hubel and Wiesel laid out and by the hope of exploring higher levels of cognition through the window they opened into the visual system. *Brain and Visual Perception* consolidates the basis for this surge of interest. The book is not intended for the general

The reviewer is at the Laboratory of Sensorimotor Research, National Eye Institute, NIH, Building 49, Room 2A50, Bethesda, MD 20892–4435, USA. E-mail: wurtzr@nei.nih.gov

Published by AAAS

reader curious about perception, because it presents the original scientific reports in all of their technical detail. But for neuroscientists interested in vision, it is a gem in the history of the field and a core resource for understanding the roots of what we now know about the mammalian visual system.

References
1. V. B. Mountcastle, *J. Neurophysiol.* **20**, 408 (1957).
2. S. W. Kuffler, *J. Neurophysiol.* **16**, 37 (1953).

10.1126/science.1109968

MARINE ECOLOGY

Toward Ecosystems Oceanography

Philippe Cury

In ecology, stimulating fields of research can emerge from observed patterns. Analyzing the very irregular numbers of young herring and cod in the North Atlantic, the Norwegian marine biologist Johan Hjort noted that "the renewal of the [fish] stock…must depend upon highly variable natural conditions" (*1*). With those words in 1914, fisheries oceanography was born. Since then, the discipline has made considerable progress in relating environmental processes, and the spatial scales at which they act, to fish recruitment and the success or failure of fisheries. In their summary chapter in *Marine Ecosystems and Climate Variation*, the Norwegian ecologists Nils Chr. Stenseth and Geir Ottersen remark that "although the variation in North Atlantic cod stocks throughout the last decades is reasonably well known, the possibly major *indirect* community effects of the varying abundance of cod have not been studied with equal intensity." Their statement reflects the book's ambitious objective: to explore a wide range of ecological patterns in the North Atlantic driven by climate and involving phytoplankton, zooplankton, benthos, and seabirds as well as fish.

Disentangling the consequences of climate variation at an ecosystem level is not a simple task. We lack a general ecological theory that can adequately elucidate the functioning of marine ecosystems. But we ecologists can track patterns and processes. The book presents numerous examples that highlight apparent links between climate and marine ecology. It also elaborates concepts, models, and statistical and simulation techniques for quantifying species interactions. Readers are treated to an overview of what happened in the North Atlantic during the last decades of the 20th century and of our current understanding of the causes of those changes. (The authors also include insights from the Pacific as well as from freshwater and terrestrial perspectives.)

The volume contains 16 chapters, with contributions from 40 authors. One might therefore worry about a lack of homogeneity in both presentation style and content, but the editors and authors have succeeded in producing a coherent, integrated treatment rather than a collection of disjointed chapters. An introduction effectively links the chapters to one another, and a unified conceptual framework structures the entire volume. This structure is grounded in the argument that large-scale climate indices (e.g., the North Atlantic Oscillation or NAO) may serve as simplified proxies that capture the essence of the overall physical variability better than the complex of local observational details—the "package of weather" sensu Stenseth (*2*).

Marine Ecosystems and Climate Variation
Nils Chr. Stenseth, Geir Ottersen, James W. Hurrell, and Andrea Belgrano, Eds.
Oxford University Press, Oxford, 2004. 266 pp. $124.50, £68. ISBN 0-19-850748-8.

Nature is intricate. The effects of climate fluctuations on ecology may be nonlinear, can act with time lags that are difficult to detect, and may have both direct effects on life history traits and indirect effects through the food web. The contributors disentangle many ecological interactions in rather simple and convincing ways, producing what I consider to be ecological enlightenment.

The fish that changed marine ecology. Atlantic cod (*Gadus morhua*).

The book focuses quite naturally on cod, a key predator species that has a central role in the ecosystem dynamics of the North Atlantic. The authors show how a given NAO pattern can correspond to varying levels of cod recruitment (good or poor) in different areas, which yield apparently contradictory results. Comparative analysis of the factors (e.g., air and water temperatures, ice cover, and winds) that appear to control cod recruitment at an ecosystem level among the different environmental settings of the Barents Sea, the North Sea, and Canadian waters offers an elegant approach to unraveling this paradox. The chapters on phytoplankton, birds, and benthos offer intriguing insights into the subtle balances among direct and indirect environmental effects on species abundance.

The approach elaborated in the book supports the idea that the environment exerts significant controls on ecosystem dynamics. On the other hand, it is also abundantly clear that by greatly reducing the abundance of large predators such as cod, fisheries can have major direct effects on the structure and functioning of ecosystems—the resulting ecological patterns of such "top-down control" can be found in Daniel Pauly and Jay Maclean's recent book (*3*). I believe that future work on the North Atlantic will benefit from a synthesis of these two viewpoints (climate change and overexploitation), presented as a unified treatment and not separately. However, the present book certainly kick-starts the process.

Recently the world ocean was subdivided into 64 large marine ecosystems (www.edc.uri.edu/lme), and the book's conceptual framework should help stimulate research in these ecosystems. The book should also contribute to the efforts of several current international programs that address ecosystem integration (e.g., Global Ocean Ecosystem Dynamics and the European Network of Excellence for Ocean Ecosystems Analysis). In addition, the book provides a comprehensive approach to acknowledging ecological interactions between exploited and nonexploited species in the context of climate change. This is an important step, particularly given the recognized need to move toward an ecosystem approach to fisheries (*4*).

Will the book's ecosystem oceanography become a new field of research? Time will tell. What can definitely be said is that *Marine Ecosystems and Climate Variation* excellently illustrates the issues of controls in marine ecosystems, addressing them in a convincing and organized manner. "Who controls whom" in marine ecosystems is a stubborn and intricate issue, but potentially solvable. At least that is the message of the Norwegian scientists and their colleagues.

The reviewer is at the Institut de Recherche pour le Développement, Centre de Recherche Halieutique Méditerranéenne et Tropicale, Boite Postale 171, 34203 Sète Cedex, France. E-mail: philippe.cury@ird.fr

References
1. J. Hjort, *Rapp. P.-v. Cons. Perm. Int. Explor. Mer.* **20**, 1 (1914).
2. N. C. Stenseth *et al.*, *Proc. R. Soc. London Ser. B* **270**, 2087 (2003).
3. D. Pauly, J. MacLean, *In a Perfect Ocean: The State of Fisheries and Ecosystems in the North Atlantic Ocean* (Island, Washington, DC, 2003).
4. E. K. Pikitch *et al.*, *Science* **305**, 346 (2004).

10.1126/science.1108868

ECOLOGY

Importing Timber, Exporting Ecological Impact

Audrey L. Mayer,[1]* Pekka E. Kauppi,[2] Per K. Angelstam,[3] Yu Zhang,[1] Päivi M. Tikka[2]

Covering 32% of all forest area, boreal forests are one of the last relatively intact terrestrial biomes and are a critical carbon sink in global climate dynamics (*1*, *2*). Naturally dynamic forest landscapes, with mature and old-growth boreal forests, provide products that are culturally and economically important, from wood-based lumber, pulp, and fuelwood to nonwood products, such as animal meat and fur, mushrooms, nuts and berries, resins, and medicinal extracts (*3*). Intensive wood harvest and conservation of naturally dynamic intact forests tend to be mutually exclusive. In protected areas, where biodiversity is highly valued, wood harvests are limited or banned outright.

Enhanced online at www.sciencemag.org/cgi/content/full/308/5720/359

Increasing domestic forest protection without simultaneously decreasing demand for wood necessitates an increase in foreign imports, introducing a negative impact on forest biodiversity elsewhere (*4*). On an international scale, a net gain in forest protection is questionable if local protection shifts logging pressure to natural forests in less privileged areas of the world (*5*–*7*). This is especially problematic as conservation area networks usually function better in landscapes with a shorter land-use history (*8*). Increasing demand for both wood products and forest conservation in Asian and European countries, such as China and Finland, has placed increasing pressure on neighboring forests in Russia.

Russia

Russia supports over half of the boreal forest on the planet and has 20% of global wood resources (*1*, *9*). As of 2000, there were 135 national parks and strict federal nature reserves in Russia, with a total of 40 million ha (*10*). To meet increasing demand for environmental protection, the government has set a goal of 150 parks and reserves, but administrative organization and resources are inadequate and forest protection is progressing slowly (see figure, this page). Although Russia's remote northern forests are relatively intact, forests in northwest Russia decrease by about 3% annually.

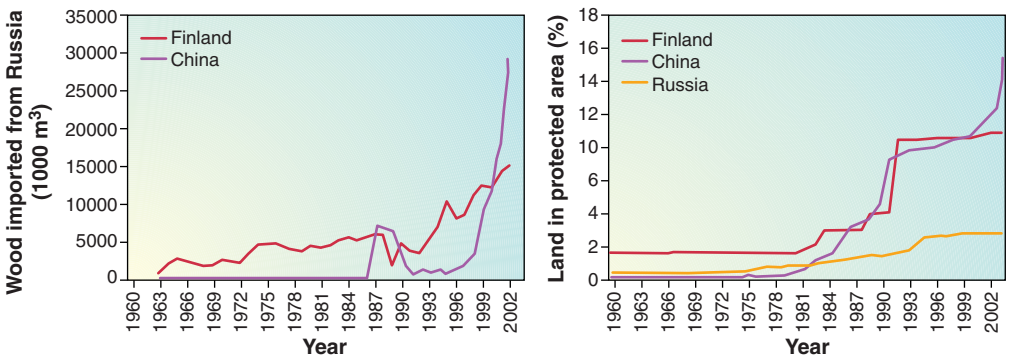

Concurrent growth in timber imports and protected areas. Imports of industrial round wood, sawn wood, and wood pulp from Russia into Finland and China (*32*) have increased concurrently with the cumulative area of forest protected from logging [IUCN Categories Ia through VI (*33*)]. Russian data include only federal-level parks and preserves.

The industrial forest sector accounts for 4% of Russia's Gross Domestic Product (GDP) (*9*). Russian forests are state owned and leased to logging companies (both domestic and foreign) for timber harvest, through contracts lasting from 1 to 49 years (*11*). Forest management policies (especially with respect to sustainable harvest and reforestation) often differ among regional governments, and display wide post harvest variation in both wood production and biodiversity conservation. Although the use of more economically efficient timber auctions is increasing, the prevalent system of flat stumpage fees typically values Russian wood at 10% of European prices (*12*).

China

Less than 20% of China is forested, predominantly in the northeastern and southern regions of the country (*13*). Deforestation for cropland, fuelwood, and industrial wood use has accelerated soil erosion and desertification and has caused flooding over large areas. In response, the Chinese government established the Natural Forest Conservation Program (NFCP) in 1998 (*14*). This program bans or restricts logging across more than half of the country and compensates rural communities for reforestation activities and emigration out of heavily impacted areas. The Chinese government has spent an estimated 50 billion yuan (U.S.$6 billion) on the program (*15*), and plans to spend 100 billion yuan (U.S.$12 billion) over 10 years in the NFCP and other programs, to increase China's overall forest area to 26% (*13*, *16*).

China's rapidly growing economy and demand for housing have increased consumption of lumber and other wood products. Decreased tariffs on imported wood, due partly to membership in the World Trade Organization, and limited domestic supply due to the NFCP have made the import of logs from Russia for further processing in China more profitable (*17*) (see figure above, left). In particular, domestic production of high-quality logs has declined since the implementation of the NFCP, and consequently logging in southeastern Russia has targeted predominantly large, mature trees to meet this demand (*11*).

Finland

Boreal forest covers two-thirds of Finland. The forestry sector is responsible for roughly 25% of Finland's exports and 5% of its GDP (*18*, *19*), and products are exported chiefly to western European countries such as the United Kingdom, Germany, and the Netherlands. Less than 10% of Finnish paper and lumber is used domestically. Finnish logging companies procure roundwood throughout northwest Russia, and export both coniferous and decid-

[1]U.S. Environmental Protection Agency, Office of Research and Development, National Risk Management Research Laboratory; Cincinnati, OH 45268, USA. [2]University of Helsinki, Department of Biological and Environmental Sciences, 00014 Helsinki, Finland. [3]Swedish University of Agricultural Sciences, Faculty of Forest Sciences, School for Forest Engineers, Sweden.

*To whom correspondence should be addressed. E-mail: mayer.audrey@epa.gov

Published by AAAS

uous species for mills in Finland, although Finn-owned mills have recently been established in Russia. Wood consumption of Finnish industries has increased steadily, more recently based on wood exports from Russia (see left side of figure, p. 359). The Finnish-Russian border marks the transition from Finnish landscapes dominated by intensively managed, privately owned, smaller forest fragments, to Russian landscapes where intact forests with large mature and old-growth stands are delineated by large, clear-cut areas in various stages of succession.

The majority of protected forest is in northern Finland, where large tracts of old-growth forest are more prevalent. However, concern over biodiversity loss in southern Finland [where species richness is higher (*20*)] has initiated conservation incentive programs for private landowners, such as those advanced by the Forest Biodiversity Program for Southern Finland ("METSO program"). Income and demand for forest protection are high in Finland, and Finns have expressed a high willingness to pay for domestic forest protection and species conservation (*21*). In 2004 alone, the Finnish government spent over €50 million (U.S.$62 million) for purchase and maintenance of areas reserved for nature protection in Finland (*22*). Although potential loss of remnants of intact natural forest in northwest Russia has prompted some conservation effort by environmental groups and the Finnish government, many of the proposed protected areas lie along the Finnish-Russian border (*23*).

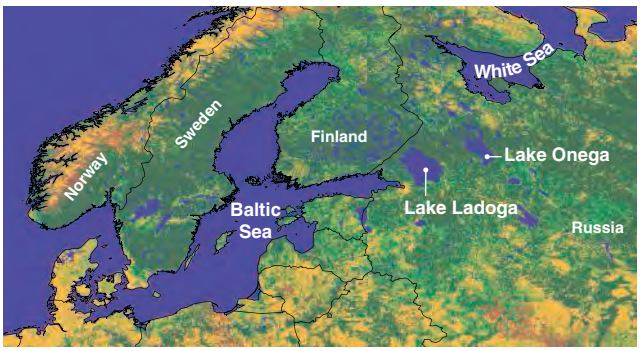

A potential boomerang. Logging in northwest Russia, particularly in three critical forested corridors between the White Sea, lakes Onega and Ladoga, and the Baltic Sea, may sever the ecological connectivity of Fennoscandian forests to the large forests in Russia (closed and open forests are in dark and light green, other land cover types are in brown and yellow). [Source: (*34*)]

A Potential Boomerang Effect

Finnish forests interact with Russian forests through species dispersal and migration, mainly across three key corridors (see figure, above) (*24*). For some species such as the rare white-backed woodpecker (*Dendrocopos leucotos*), a focal species of late successional stages in deciduous forest, populations in Finland depend on periodic immigrants from Russia to maintain population size and genetic diversity (*25*, *26*).

Forests in northern Finland are a major pathway for boreal species to disperse from Russia into Sweden and Norway (*24*, *26*). If current logging rates continue and harvest patterns fail to mimic natural disturbances and structural diversity (*8*, *27*), northwest Russia will suffer a net loss of large forest patches and a reduction in overall forest age (*23*). The effect of thus altered, more impacted forests in northwest Russia on the long-term diversity and viability of conserved forests in Finland is likely to be negative. Nordic countries therefore have an ecological incentive to assure that forest conservation area networks in northwest Russia are suitably protected and managed and that the activities of timber companies (regardless of origin) do not "boomerang" and degrade conservation efforts in Finland.

Successful forest conservation efforts will be based on a mix of several factors. Intensification of forestry on plantations can increase wood yields on hectares already in use, reducing land used for wood production and sparing existing natural forests for biodiversity conservation. This approach already provides over a third of industrial harvests globally (*28*). Gains in efficiency can be realized through improved logging practices and industrial processes, requiring fewer trees per ton of products manufactured (*29*). Reducing consumption of wood-based products can reduce pressure on forests, as can using alternative materials [although these also have environmental impacts (*5*)]. Finally, emulation of natural forest disturbance regimes in sustainable forest management (*8*, *27*), and spatial landscape scale planning can be used to improve functionality of forest habitat networks and the surrounding matrix (*30*).

The import of wood to meet domestic demand for both conservation targets and consumption is not unique to the countries discussed here [e.g. (*31*)]. Nature conservation policy must therefore acknowledge biogeography and the interaction between domestic protection and international markets, which can cause exported environmental damage to boomerang into countries with high environmental standards. Net conservation of nature (and sustainable forest management) will not occur when natural resource harvests are simply exported abroad.

References and Notes

1. P. J. Burton *et al.*, in *Towards Sustainable Management of the Boreal Forest*, P. J. Burton, C. Messier, D. W. Smith, W. L. Adamowicz, Eds. (NRC Research Press, Ottawa, Ontario, Canada, 2003), pp. 1–40.
2. J. Liski *et al.*, *Clim. Change* **61**, 89 (2003).
3. H. G. Lund, B. Pajari, M. Korhonen, Eds., "Sustainable development of non-wood goods and benefits from boreal and cold temperate forests," Proceedings of the International Workshop, Joensuu, Finland, 18 to 22 January 1998 (European Forest Institute, Joensuu, Finland, 1998).
4. E. B. Barbier, in *World Forests, Society and Environment*, M. Palo, J. Uusivuori, Eds. (Kluwer Academic Publishers, Dordrecht, Netherlands, 1999), pp. 106–117.
5. R. A. Sedjo, *J. For.* **93**, 25 (1995).
6. B. Sohngren, R. Mendelsohn, R. Sedjo. *Am. J. Agric. Econ.* **81**, 1 (1999).
7. M. M. Berlik, D. B. Kittredge, D. R. Foster, "The illusion of preservation: A global environmental argument for the local production of natural resources" (Harvard Forest Pap. no. 26, Harvard Univ., Petersham, MA, 2002).
8. P. Angelstam, M. Dönz-Breuss, J.-M. Roberge, Eds., *Ecol. Bull.* **51** (2004).
9. A. Moiseyev, J. Uusivuori, N. Burdin, in *World Forests, Society and Environment*, M. Palo and J. Uusivuori Eds. (Kluwer Academic Publishers, Dordrecht, Netherlands, 1999), pp. 351–358.
10. A. N. Filiptchouk *et al.*, "Forest and forest products country profile: Russian Federation" (Geneva Timber and Forest Study Pap. No. 18, United Nations Economic Commission for Europe, New York, 2001).
11. G. Dudarev, S. Boltramovich, D. Efremov, "From Russian forests to world markets: A competitive analysis of the northwest Russian forest cluster" (ETLA Series B 195, Taloustieto Oy, Helsinki, 2002).
12. Pertti Veijola, personal communication.
13. S. Wang, G. C. van Kooten, B. Wilson, *For. Policy Econ.* **6**, 71 (2004).
14. P. Zhang *et al.*, *Science* **288**, 2135 (2000).
15. Xinhua News Agency, "50 billion yuan poured into Natural Forest Protection Project" (1 December 2003); available at http://forests.org/articles/reader.asp?linkid=27354.
16. U.S. Embassy, Beijing, *Forests Vs. People? PRC Natural Forest Protection* (August 2000 report); available at www.usembassy-china.org.cn/sandt/yunnan-forest-one.htm.
17. A. L. Hammett, X. Sun, M. Barany, *J. For.* **99**, 4 (2001).
18. Ministerial Conference on the Protection of Forests in Europe (MCPFE), *State of Europe's Forests 2003: The MCPFE Report on Sustainable Forest Management in Europe* (MCPFE, Vienna, Austria, (2003), 115 pp.
19. Finnish Forest Industries Federation, see http://english.forestindustries.fi.
20. I. Hanski, *Ann. Zool. Fenn.* **37**, 271 (2000).
21. E. Lehtonen, J. Kuuluvainen, E. Pouta, M. Rekola, C-Z Li. *Environ. Sci. Policy* **6**, 195 (2003).
22. Statistics Finland; see www.tilastokeskus.fi/tk/tt/ymparisto_en.html.
23. C. Burnett, A. Fall, E. Tomppo, R. Kalliola, *Conserv. Ecol.* **7**(2), 8 (2003); available at www.ecologyandsociety.org/vol7/iss2/art8/index.html
24. H. Lindén *et al.*, *Wildlife Biol.* **6**, 179 (2000).
25. A. Carlson, *For. Ecol. Manag.* **131**, 215 (2000)
26. Ø. Flagstad *et al.*, *Mol. Ecol.* **12**, 869 (2003).
27. Y. Bergeron, *For. Chron.* **80**, 458 (2004).
28. R. A. Sedjo. *For. Chron.* **77**, 221 (2001).
29. I. K. Wernick, P. E. Waggoner, J. H. Ausubel. *J. Forest.* **98**, 8 (2000).
30. P. Angelstam *et al.*, *Ambio* **32**, 527 (2003).
31. D. L. Dekker-Robertson, W. J. Libby, *BioScience* **48**, 471 (1998).
32. European Forest Institute, European Forestry Information and Data Analysis System, available at www.efi.fi/efidas/fpstf.html
33. U.N. Environmental Programme, World Conservation Monitoring Centre; available at http://sea.unep-wcmc.org/wdbpa/toplevelindex_new.cfm.
34. Global Forest Resources Assessment, U.S. Geological Survey available at http://edcdaac.usgs.gov/glcc/fao/index.asp.
35. We gratefully acknowledge a grant from *Metsämiesten säätiö* to P.E.K.; Y.Z. is a postdoctoral research Fellow through the Oak Ridge Institute for Science and Education; P.M.T. was supported by the Marjatta and Eino Kolli Foundation. We are grateful for comments from R. Sedjo and two anonymous reviewers. Policies addressed here represent the opinions of the authors, not necessarily those of the U.S. Environmental Protection Agency.

10.1126/science.1109476

OCEAN SCIENCE

Coral Clues to Rapid Sea-Level Change

Gideon M. Henderson

Like coffee in your morning mug, or beer in your evening pint, the level at which the sea rests is controlled both by the shape of the vessel and by the volume of liquid it contains. Ocean basins change shape only slowly, but on page 401 of this issue, Thompson and Goldstein show that the amount of seawater they contain changes more frequently than previously thought (*1*).

At the time of the last glacial maximum, about 20,000 years ago, continental ice sheets locked up large amounts of water. As a result, sea level was about 130 m below that of today. If all the ice that remains on the continents today were to melt, it would cause sea level to rise by a further 70 m. Such changes are an integral part of the global climate system and, like the rest of that system, are influenced by regular cycles in Earth's orbit. By altering the seasonal distribution of incoming solar radiation, these orbital changes lead to changes in sea level with a frequency of 21,000 years and longer. Orbital frequencies are clearly visible in the record of past sea-level change, although they cannot fully explain either its timing or its amplitude.

Climate records recovered from the Greenland ice cores in the 1980s show that climate can also change at a higher, millennial, frequency—too fast to be caused by orbital cycles. But ice sheets have inertia and take time to melt or grow. Did this inertia enable ice sheets to damp out millennial climate changes, such that sea level varied only on the longer orbital frequencies? Or does sea level change more rapidly?

Corals provide the most widely used sea-level archive with which to address this question. Because many coral species survive only in shallow water, fossil corals (see the first figure) found above or below present reefs demonstrate variations in past sea level. Corals can also be dated by radiocarbon for the past 40,000 years and by the formation of ^{230}Th through radioactive decay of uranium for the past 500,000 years. The longer a coral sits around waiting for a passing geochemist to take it back to the lab, however, the more likely it is to be altered, causing addition or loss of uranium or thorium and making uranium-thorium ages inaccurate. Coral alteration can often be detected by changes in mineralogy, but a more subtle geochemical alteration commonly affects the uranium-thorium ages of corals that appear mineralogically pristine. Such alteration changes the uranium isotope ratio of the coral and can thus be screened for, but for periods older than about 70,000 years, few samples pass this screening.

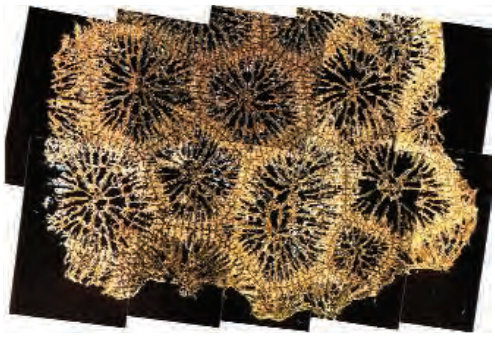

Coral structure. The calcium carbonate deposited by corals, such as this *Goniastrea*, incorporates uranium during growth, but not thorium. Subsequent decay of uranium to ^{230}Th allows the coral to be dated, but the large surface area of the coral structure often allows for addition of uranium and thorium, making the dates inaccurate. The approach of Thompson and Goldstein (*1*) corrects for such addition. The field of view is 6 cm high.

For the period from 55,000 to 30,000 years ago, enough corals pass the screening to indicate millennial sea-level changes of 10 to 15 m (*2*). The validity of these shifts is supported by modeling of oxygen isotope records in the Red Sea (*3*). Suborbital changes in sea level are therefore well established for this period, when global sea levels were low and millennial changes in climate had a large amplitude.

Thompson and Goldstein now demonstrate the presence of similar millennial sea-level changes at times of high sea level and relative climate stability (*1*). The key to their success has been the development of a geochemical model to date corals that have not behaved as chemically closed systems. Rather than using uranium isotopes simply to reject samples, they use them to correct ages, thereby enabling dating of many altered corals for the interval from 250,000 to 70,000 years ago. For a single reef, ages that once scattered widely cluster tightly when corrected by the model, supporting its validity.

The new open-system ages provide a high-resolution sea-level record for the interval from 250,000 to 160,000 years ago, for which data were previously sparse. Substantial swings in sea level are seen (see the second figure), only some of which can be explained by orbital changes. Perhaps most surprising is that 185,000 years ago—at a time

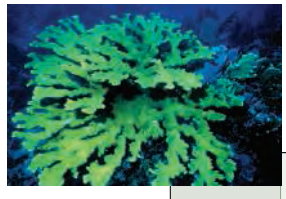

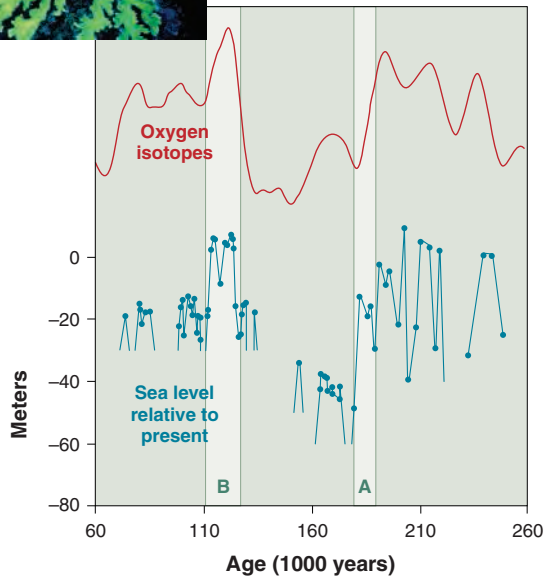

Beyond orbital cycles. (**Top**) The SPECMAP oxygen isotope record (*5*) reflects both ice volume and temperature. The influence of orbital cycles is clearly seen. (**Bottom**) The sea-level record reported by Thompson and Goldstein (*1*) shows millennial sea-level changes that are too frequent to be caused by orbital changes. Inset: Photograph of *Acropora palmata*, the coral most widely used in sea-level reconstructions.

The author is in the Department of Earth Sciences, University of Oxford, Oxford OX1 3PR, United Kingdom. E-mail: gideon.henderson@earth.ox.ac.uk

Published by AAAS

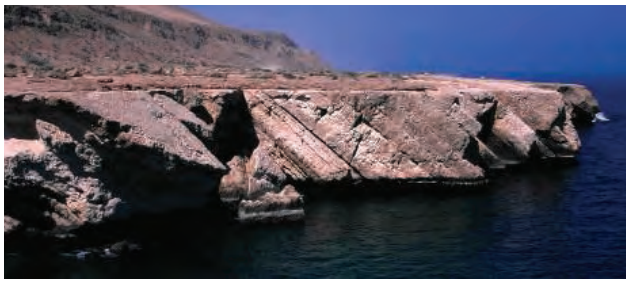

Marine terraces. Past sea level is recorded at coastlines, as in this example from Oman, by horizontal erosion of marine terraces and by growth of reefs. Reef material on top of the terrace includes corals, dating of which indicates that sea level was 5 meters above its modern position 125 thousand years ago during the last interglacial.

when orbital parameters and climate proxies indicate cold conditions—sea level was only about 20 m below its present level (see band A in the second figure). This event challenges our understanding of the conditions required for ice growth.

Between 130,000 and 90,000 years ago, the record provides clear evidence for sea-level change at higher frequency than can be explained by orbital changes. A 10-m lowering of sea level in the middle of the last interglacial period is a good example (see band B in the second figure). The possibility of two distinct sea-level highstands during this period has been discussed before (*4*), but was never fully accepted due to insufficiently precise chronology. The new results reignite this controversy. What might cause significant sea-level lowering when most records, from the oceans at least, show the last interglacial to be a time of considerable climate stability?

Such questions are enough to turn you back to that evening pint. If you take too long to drink it, though, it warms and expands so that you have a fuller glass. This change is not something that most drinkers notice. But for the oceans, with an average depth of 3700 m, it can make important differences to sea level. Most of the ~0.5 m of sea-level rise expected by 2100 will be due to heating of the oceans. On millennial time scales, temperature change extends to the deep ocean and might cause several meters of sea-level change (see the third figure). Some lowstands in the record of Thompson and Goldstein (*1*) are defined not by dated corals, but on the basis of field evidence for breaks in coral growth. Small sea-level changes caused by temperature change might explain such breaks. Elsewhere in the record, larger sea-level changes are well constrained by lower corals. They must be generated by changes in global ice volume, even if there is no evidence for climate change at these times.

There is still much to learn about how moisture transport and seasonal temperatures interact to control the volume of continental ice. We may have been fooled by the relative stability of the present sea-level highstand into assuming that sea-level change is always slow. With their improved chronological method, Thompson and Goldstein force a reappraisal. The challenge now is to understand the processes that caused rapid sea-level change in the past and will continue to do so in the future.

References

1. W. G. Thompson, S. J. Goldstein, *Science* **308**, 401 (2005).
2. Y. Yokoyama, T. M. Esat, K. Lambeck, *Earth Planet. Sci. Lett.* **193**, 579 (2001).
3. M. Siddall *et al.*, *Nature* **423**, 853 (2003).
4. B. White, H. A. Curran, M. A. Wilson, *Carbonates Evaporites* **13**, 10 (1998).
5. D. G. Martinson *et al.*, *Quat. Res.* **27**, 1 (1987).

10.1126/science.1110550

GENETICS

Was the Human Genome Project Worth the Effort?

Stephen P. Daiger

One of the promises of the Human Genome Project was that it would provide tools for identifying genetic factors that contribute to common, complex diseases such as cancer and diabetes. Finding these factors would, in turn, suggest possible targets for drug therapy and other forms of treatment. Three papers in this week's issue—by Edwards *et al*. (*1*) on page 421, Haines *et al*. (*2*) on page 419, and Klein *et al*. (*3*) on page 385—deliver on this promise for a debilitating, blinding disease called age-related macular degeneration (AMD). Using several genome-derived tools applied to nonoverlapping groups of AMD patients, the three groups report that a common variant in the complement factor H gene (*CFH*) on human chromosome 1q31 contributes a substantial fraction of the difference between affected and unaffected individuals. AMD afflicts more than 10 million Americans and is the leading cause of blindness among the elderly. The complement system is the target of a number of modulatory drugs and treatments. Together with the new findings, these facts confirm the broad potential health benefits of "genome science."

The macula is a circular area at the center of the retina that contains a high density of cone cells—these are photoreceptor cells that are specialized for distinguishing colors, resolving closely spaced objects, and detecting motion. The macula accounts for the central 30% of our visual fields and is critical for the full vision that enriches our lives (see the figure). AMD results in progressive damage to the macula, ultimately leading to patients becoming legally blind. This disorder principally affects individuals over age 50, although in certain inherited forms of macular degeneration symptoms appear at a much younger age. Macular degeneration diminishes the quality of life of those afflicted and is a major burden on society.

This complex disease has diverse symptoms and multiple contributing factors. It is a truism that complex diseases are the result of interactions between environmental factors, genetic factors, and stochastic effects. For AMD, smoking and dietary intake of lipids are known environmental risk factors (*4*); age alone is an additional risk factor. There is also strong evidence indicating a genetic contribution. Concordance between identical twins, family clustering, and increased risk to first-degree relatives all show that genetic differences play a major role in the life-time risk of AMD (*5*). But how do we find these genetic factors?

Broadly speaking, there are three methods for finding genes contributing to complex diseases: candidate gene screening, linkage mapping, and association (case-control) studies. Candidate gene screening relies on selecting potential disease-causing genes—for example, genes causing inherited forms of disease—and sequencing these genes in patients with complex diseases. Linkage mapping follows the segregation of chromosomal regions marked by random genetic variants in families with complex diseases, in search of regions that cosegregate with the disease trait. For AMD, the "families" range from simple sib-pairs to large extended pedigrees. Finally, case-con-

The author is at the Human Genetics Center, the University of Texas Health Sciences Center, Houston, TX 77030, USA. E-mail: stephen.p.daiger@uth.tmc.edu

CREDIT: GIDEON HENDERSON

trol association studies look for differences in the frequencies of common genetic variants between ethnically matched cases and controls to find variants that are strongly associated with the disease. The eventual goal of each method is to identify either mutations—that is, rare genetic variants with a strong causal relation to the disease—or polymorphic variants—that is, common, weakly causal variants that affect the lifetime risk of disease. These are extremes of a continuum, of course. For AMD, each of these methods and possibilities has been applied and advocated.

Genes causing several inherited forms of macular degeneration have been screened as candidates for AMD. For example, mutations in the *ABCA4* gene cause recessive Stargardt disease, an early-onset form of macular degeneration. An earlier *Science* paper suggested an association between variants in the *ABCA4* gene and AMD (*6*). However, it has been difficult to validate this claim, in part because of the exceptional degree of genetic variation between humans. Although we are 99.9% identical, we differ from each other at millions of nucleotide sites. Many of these differences change an amino acid within a protein, or affect protein function in other ways. For ABCA4, there are at least 11 polymorphic amino acid substitutions within the gene and many more rare variants (*7*). It is extremely difficult to detect a signal against this noisy background.

Linkage mapping comes to the rescue. The "signal" in this case is summed across families and combines different variants within a gene, if the variants each contribute to the trait. Genetic markers that cover all human chromosomes have been tested for segregation in several independently ascertained sets of AMD families. Several of these genomewide linkage scans implicate a region on chromosome 1q31 (*8*–*12*). Suggestively, the gene causing an inherited, late-onset form of macular degeneration, the *ARMD1* locus, also maps to this region (*13*). The problem with linkage mapping, however, is that the delimited regions are large, typically tens of millions of base pairs in length, harboring scores of genes. The haystack is smaller, but still daunting.

The current trio of *Science* papers (*1*–*3*) take off from this point. One recent product of the Human Genome Project is a collection of well-defined, genomewide polymorphic variants called single-nucleotide polymorphisms (SNPs). To date, more than 1 million human SNPs have been identified (*14*). Klein *et al.* used gene chips from Affymetrix Corporation to test for association among more than 100,000 SNPs in 96 AMD cases and 50 controls. The strongest signal mapped to chromosome 1q31. They then saturated the region with additional SNPs. Edwards *et al.* followed up on earlier linkage mapping to the 1q31 region, testing 86 SNPs in 400 cases and 202 controls. Haines *et al.* conducted additional linkage testing within the 1q31 region and followed up with 61 SNPs in 495 cases and 185 controls. (Cases and controls were Americans of European origin.) All three studies pointed to the *CFH* gene…but which specific variant or variants within this gene are associated with AMD?

A recent goal of the Human Genome Project has been to determine the haplotype structure of human chromosomes in various ethnic groups, a goal embodied in the International HapMap Project (*15*). Haplotypes are sets of specific DNA variants that are so close together on a chromosome that they undergo recombination only very rarely. The pattern of nonrecombining variants, known as haplotype blocks, reflects the evolutionary history of humans over the past 50,000 to 100,000 years. Haplotype blocks typically span tens of thousands of base pairs. One immediate benefit of the HapMap Project is that it provides a bridge between linkage mapping at millions of base pairs and SNPs mapped to single base pairs.

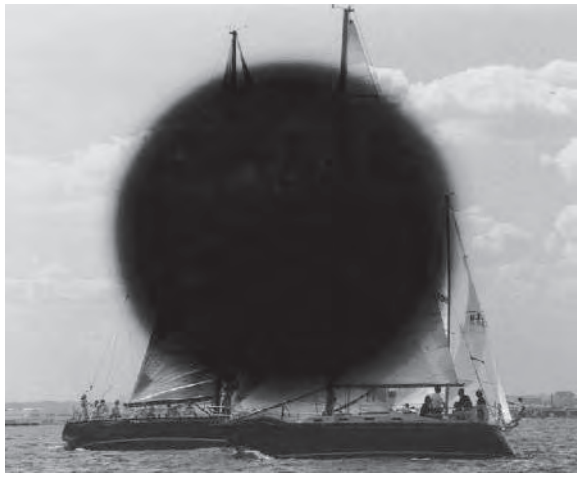

A view from the periphery. Age-related macular degeneration has a devastating effect on central vision. Peripheral vision is often spared, but objects in the center of vision are blurred or completely blocked. Central vision allows us to read, to recognize faces, and to enjoy our surroundings, as in this sailboat scene. The picture is altered to show the vision lost to the millions of individuals afflicted with age-related macular degeneration.

Klein *et al.* made explicit use of HapMap data to disentangle the SNPs in the *CFH* region. Edwards *et al.* and Haines *et al.* developed haplotype data on the basis of their tested samples. In all three cases, the haplotype data point to a specific *CFH* SNP (rs1061170) that results in replacement of the amino acid tyrosine with histidine at amino acid 402 (Tyr402His). Individuals who carry a single copy of the histidine allele in the Tyr402His polymorphism have a two- to fourfold increased risk of AMD; individuals who carry two copies of the allele have a five- to sevenfold increased risk. Within this retrospective study population, the histidine allele accounts for 20 to 50% of the overall risk of developing AMD.

Does evidence from biology support the statistical findings? The complement system is the innate component of the immune response. Initiation of complement-mediated immunity by a microorganism triggers a cascade of protein interactions in blood that eventually results in opsonization and destruction of the invading organism. Host tissues can also trigger the complement cascade, causing chronic inflammation and tissue damage. Complement factor H modulates the complement cascade by inactivating components of the cascade and by binding initiation factors such as C-reactive protein (*16*). The CFH protein consists of 20 repeat units of 60 amino acids each, called complement control modules; module 7 contains the Tyr402His polymorphism. This module interacts with cell surface markers such as heparin and sialic acid. A switch from tyrosine to histidine at this site is predicted to weaken this interaction. Thus, the polymorphism is likely to affect complement activity.

A role for complement in AMD has long been suggested (*17*). Clinical hallmarks of AMD include multiple drusen, geographic atrophy, and choroidal neovascularization. Drusen, the defining feature of AMD, are small, yellowish, extracellular deposits of lipid, protein, and cellular debris, formed beneath the retinal pigment epithelium (RPE), a tissue that underlies the photoreceptor cells. Drusen contain complement proteins. Geographic atrophy is a consequence of the degeneration of the photoreceptor cells and the RPE. Choroidal neovascularization—disruptive growth of capillaries from the choroid, a tissue at the back of the eye that nourishes the retina—occurs in 10% of cases. Atrophic tissue damage and neovascularization are potential consequences of chronic inflammation, mediated by the complement system. Further, the known AMD risk factors—smoking, diet, and age—all correlate with complement activity.

Taken together, the three new studies and preexisting information on complement factor H suggest a direct, causal connection

between the polymorphic histidine allele and life-time risk for AMD. What next? These were retrospective studies, so there needs to be more research into prospective risks for individuals who carry one or two copies of the histidine allele. It will be extremely interesting to learn whether the histidine allele is found in other ethnic groups, and whether this allele, or others, contribute to AMD in non-Caucasians. Complement activity is responsive to drug therapy and life-style changes. Will these have differential effects on AMD risks in individuals with one or two copies of the histidine allele? Do other complement factors contribute to AMD? Finally, detecting the CFH Tyr402His type in human DNA is an easy assay to perform. How will this test be incorporated into the diagnosis and treatment of AMD?

As promised, the Human Genome Project provides powerful new insights into human diseases and raises many challenging questions.

References

1. A. O. Edwards *et al. Science* **308**, 421 (2005); published online 10 March 2005 (10.1126/science.1110189).
2. J. L. Haines *et al. Science* **308**, 419 (2005); published online 10 March 2005 (10.1126/science.1110359).
3. R. J. Klein *et al. Science* **308**, 385 (2005); published online 10 March 2005 (10.1126/science.1109557).
4. L. Hyman, R. Neborsky, *Curr. Opin. Ophthalmol.* **13**, 171 (2002).
5. E. M. Stone, V. C. Sheffield, G. S. Hageman, *Hum. Mol. Genet.* **10**, 2285 (2001).
6. R. Allikmets *et al. Science* **277**, 1805 (1997).
7. A. R. Webster *et al., Invest. Ophthalmol. Vis. Sci.* **42**, 1179 (2001).
8. G. R. Abecais *et al., Am. J. Hum. Genet.* **74**, 482 (2004).
9. S. K. Iyengar *et al., Am. J. Hum. Genet.* **74**, 20 (2004).
10. J. Majewski *et al., Am. J. Hum. Genet.* **73**, 540 (2003).
11. J. M. Seddon *et al. Am. J. Hum. Genet.* **73**, 780 (2003).
12. D. E. Weeks *et al. Am. J. Hum. Genet.* **75**, 174 (2004).
13. M. L. Klein *et al. J. Ophthalmol.* **116**, 1082 (1998).
14. R. Sachidanandam *et al. Nature*, **409**, 928 (2001).
15. The International HapMap Consortium, *Nature* **426**, 789 (2003).
16. S. R. de Córdoba *et al. Mol. Immunol.* **41**, 355 (2004).
17. G. S. Hageman *et al., Prog. Retinal Eye Res.* **20**, 705 (2001).

Published online 10 March 2005
10.1126/science.1111655
Include this information when citing this paper.

CELL BIOLOGY

Of Grainy Heads and Broken Skins

Nicholas Harden

Whether you're a fly or a mouse, it's a dangerous world out there, full of sharp objects and nasty microbes trying to pierce your bodily armor. To deal with these threats, multicellular organisms are equipped with a tough waterproof barrier that protects them from physical damage and invasion by unfriendly microbes. In the fruit fly *Drosophila*, the barrier consists of an epidermis, a single cell layer thick, that secretes a cuticle at its apical surface. The cuticle is made rigid through cross-linking of proteins and chitins by quinones (*1*). In mammals, the epidermis is composed of several cell layers, the outermost of which, the stratum corneum, consists of dead squamous epithelial cells. Each of these cells is encased in a cornified cell envelope, a robust structure composed of covalently cross-linked proteins and lipids (*2*).

Numerous studies in vertebrates and invertebrates have examined the signaling pathways that regulate reepithelialization, the process in which epithelial cells migrate to seal holes in damaged epithelia. These studies have looked at a diverse collection of "wounds," ranging from holes in epithelia that are a natural consequence of embryonic development, to wounds in the epidermis induced by physical injury. What emerges from these studies is the striking conservation of signaling events centered around a mitogen-activated protein kinase (MAP kinase) pathway called the c-Jun N-terminal kinase (JNK) cascade, which leads to activation of the AP-1 transcription factor (*3*). Reepithelialization is one component of epidermal wound healing, but how is the outer layer of the surface barrier—the cuticle in insects and the stratum corneum in mammals—repaired? Two papers in this issue, by Mace *et al*. on page 381 (*4*) and Ting *et al*. on page 411 (*5*), reveal that the wound-healing response that repairs damage to the outer layer is also attributable to a highly conserved family of transcription factors. The studies, in flies and mice, show that members of the Grainy head transcription factor family drive expression of proteins that participate in cross-linking of barrier components. The investigators demonstrate the existence of an ancient system for regulating the transcription of genes required for both the formation and repair of the outer layer of the surface barrier.

Among the genes required for *Drosophila* cuticle formation are *Ddc* and *pale* (*ple*), which encode DOPA decarboxylase and tyrosine hydroxylase, respectively. Both enzymes catalyze the production of the quinones that cross-link cuticle components (*1*). In their study of late-stage fly embryos, Mace *et al.* (*4*) show that the *Ddc* and *ple* genes are switched on in the epidermal cells surrounding wounds that were generated either genetically or physically using a sterile needle. Thus, not only do *Ddc* and *ple* participate in the formation of the cuticle during development, but they are also called into action in the appropriate epidermal cells when the cuticle is breached. The induction of *Ddc* and *ple* expression within 30 min of wounding suggested to Mace *et al*. the existence of direct transcriptional regulation by a wound-induced signaling pathway. So, the authors set out to look for wound response regulatory elements in the control regions of these genes. The authors identified upstream stretches of DNA from both genes that were capable of driving reporter gene expression in the epidermis around wound sites. But which transcription factors activate these wound response enhancers? The Grainy head (Grh) transcription factor is expressed in the fly epidermis where it is required for *Ddc* expression, and *grh* fly mutants have a defective cuticle (*6*). Both wound response enhancers contain consensus binding sites for Grh, and mutation of one of the Grh binding sites in the *Ddc* enhancer abolishes its ability to drive reporter gene expression around wound sites (*4*). Furthermore, the *Ddc* wound response enhancer only operates weakly in wounded *grh* mutant fly embryos.

In a complementary study, Ting *et al*. demonstrate that, similar to Grh in *Drosophila*, a Grainy head–like transcription factor in mice (Grhl3) drives expression of a protein that cross-links barrier components (*5*). This study seems to have progressed in the opposite direction to that of Mace *et al*., because the authors started out by looking at the phenotypes of *Grhl3* mutant mice. This led them to the enzyme transglutaminase 1 (TGase1), which cross-links proteins and lipids in the mouse stratum corneum (*2*). In *Grhl3* mutant mice, defects in the stratum corneum are similar to those seen in *TGase1* mutant mice. In addition, *TGase1* expression in the epidermis of *Grhl3* mutant mice is greatly reduced, indicating that TGase1 is regulated by Grhl3. To determine whether this regulation is direct, Ting *et al*. first needed to define a consensus binding site for

The author is in the Department of Molecular Biology and Biochemistry, Simon Fraser University, Burnaby, BC, V5A 1S6 Canada. E-mail: nharden@sfu.ca

Grhl3. They used Grhl3 to screen a population of random sequences for Grhl3-binding clones that were subsequently amplified by polymerase chain reaction. Alignment of the sequences of these clones revealed a Grhl3 consensus binding site identical to that of *Drosophila* Grh. There are two good matches to this consensus site upstream of the *TGase1* transcription start site, and preliminary data suggest that these sequences bind to Grhl3.

The Mace *et al*. and Ting *et al*. studies reveal a conserved role for the Grainy head family of transcription factors in forming and maintaining the tough outer covering of multicellular organisms. This conclusion is driven home by the finding that impairment of a Grainy head family member, Ce-GRH-1, in the roundworm *Caenorhabditis elegans* by RNA interference results in worms with a defective cuticle (*7*). But does Grainy head have additional tasks in wound repair? The phenotype of *Grhl3* mutant mice suggests that Grainy head, like AP-1, may be important in the reepithelialization of wounds. *Grhl3* mutant mouse embryos fail to close induced epidermal wounds and display defects in neural tube closure (*5*, *8*). Neural tube closure involves the sealing of epithelial sheets, and is an example of a developmental "wound healing" event similar to dorsal closure of the *Drosophila* embryo and eyelid fusion in the mouse embryo (*3*, *9*). All of these processes show parallels with the healing of induced wounds, including a requirement for the JNK cascade. Involvement of *Drosophila* Grh in epithelial fusion has not been reported, but overexpression of Grh in the *Drosophila* embryo causes failure of dorsal closure (*10*). Grainy head joins AP-1 as a key transcriptional mediator of the wound response. Is there any evidence that AP-1 and Grainy head cooperate in the induction of wound-healing genes? The *Ddc* wound response enhancer has three AP–1-like consensus sequences. Mutation of these three sites together with the predicted binding site for the CREB-A protein (cAMP response element–binding protein–A) abrogates the function of the wound response enhancer. This suggests that AP-1 may indeed cooperate with Grh in driving *Ddc* expression (*4*).

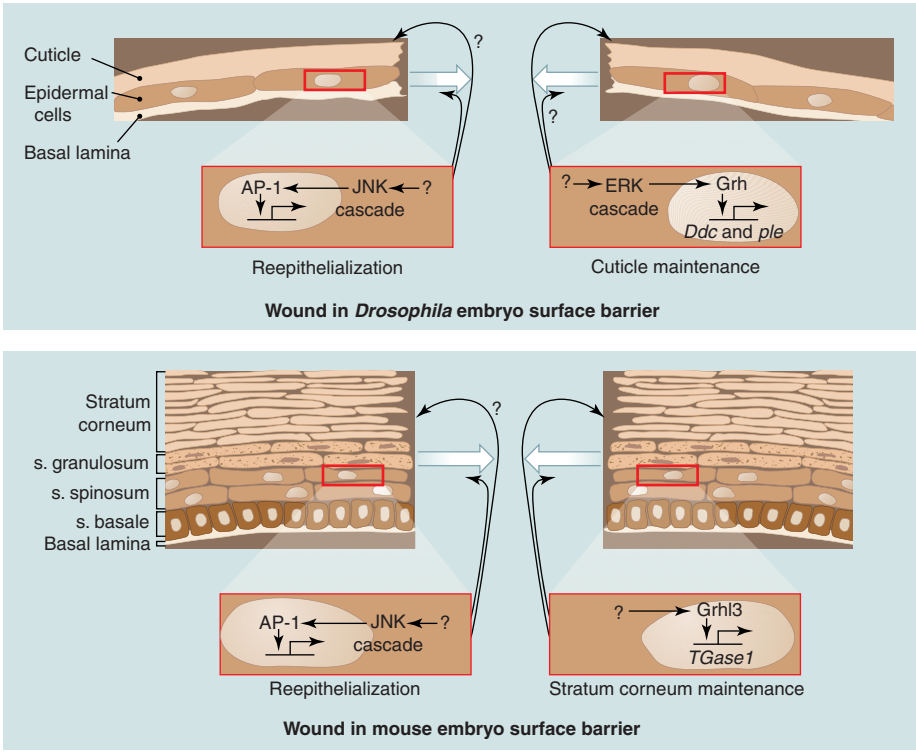

Healing transcription factors. Reepithelialization and repair of the outer layer of the surface barrier in a wounded *Drosophila* embryo (**top**) and mouse embryo (**bottom**). Repair of wounds in the outer layer of the surface barrier is regulated by conserved transcription factors of the Grainy head family: Grh in the fruit fly and Grhl3 in the mouse. JNK cascade activation of AP-1–mediated transcription participates in reepithelialization, the movement of epidermal cells to seal the breach in damaged epithelia (white arrows). Grh and Grhl3 drive the expression of genes whose products are required for cross-linking components in the tough outer layer of the surface barrier (cuticle in *Drosophil*a, stratum corneum in mouse). There is evidence that Grhl3 also may be involved in reepithelialization, presumably by regulating the expression of genes other than *TGase1*.

How does a breach in the *Drosophila* surface barrier signal Grh to activate expression of *Ddc* and *ple* in epidermal cells around the wound? The JNK pathway that activates AP-1 in wounding does not appear to be required. But preliminary results from Mace *et al*. suggest that another MAP kinase cascade—the extracellular signal–regulated kinase (ERK) pathway—may be involved (*4*). One of the elusive goals of wound-healing research is the identification of signals that emanate from the wound to trigger such intracellular signaling pathways. In the case of induction of the innate immune response after wounding, invading microbes contribute to the initiation of this signal (*4*). For wound repair mediated by AP-1 and Grainy head, however, the activating signals must be generated by a diversity of wounds, that is, both developmentally and physically induced. The wound response enhancers studied by Mace *et al*. are activated around wounds induced either by mutations in the embryo or through needle puncture. These authors ruled out bacteria as an activating signal for Grh, because they wounded their embryos under aseptic conditions that did not trigger the innate immune response. For any kind of wound, the tension applied to cells at the wound edge will be different from that elsewhere in the epithelium. An interesting possibility is that mechanical signals are involved in triggering wound response pathways (*3*).

Whatever signaling pathways are found to trigger activation of Grainy head, it is clear that this transcription factor was conscripted very early in metazoan evolution to form part of a vital defense mechanism. The Grainy head studies represent an important addition to the literature. They show that although the structure of the surface barrier varies considerably across taxa, the signaling pathways that direct repair of this barrier are evolutionarily conserved.

References and Notes

1. T. R. Wright, *J. Hered.* **87**, 175 (1996).
2. Z. Nemes, P. M. Steinert, *Exp. Mol. Med.* **31**, 5 (1999).
3. P. Martin, S. M. Parkhurst, *Development* **131**, 3021 (2004).
4. K. A. Mace, J. C. Pearson, W. McGinnis, *Science* **308**, 381 (2005).
5. S. B. Ting *et al*., *Science* **308**, 411 (2005).
6. S. J. Bray, F. C. Kafatos, *Genes Dev.* **5**, 1672 (1991).
7. K. Venkatesan, H. R. McManus, C. C. Mello, T. F. Smith, U. Hansen, *Nucleic Acids Res.* **31**, 4304 (2003).
8. S. B. Ting *et al*., *Nat. Med.* **9**, 1513 (2003).
9. P. Martin, W. Wood, *Curr. Opin. Cell Biol.* **14**, 569 (2002).
10. L. D. Attardi, D. Von Seggern, R. Tjian, *Proc. Natl. Acad. Sci. U.S.A.* **90**, 10563 (1993).
11. I thank E. Verheyen and R. Conder for helpful comments, and the Canadian Institutes of Health Research and the Natural Sciences and Engineering Research Council of Canada for support.

10.1126/science.1112050

Life on the Early Earth: A Sedimentary View

Frances Westall

Fifty years after the discovery of fossil microorganisms in 2-billion-year-old rocks from the Gunflint Formation in Ontario (*1*), Canada, there is renewed interest in the history of life on the early Earth. This resurgence of interest is in part due to the burgeoning field of astrobiology and the recognition of the importance of studying Earth's early environment and seeking life on other planets. Such renewed interest necessitates a better understanding of the problems surrounding the identification of very ancient traces of life and the development of more sophisticated methods of investigation. Resolution of such problems is crucial if we are to obtain reliable evidence for traces of life on other planets, such as Mars, with any reasonable degree of certainty.

When searching for evidence of past life, sedimentary environments are considered the most suitable because they are often formed in association with water, a fundamental requirement for life. There are only three known locations that host exposures of ancient sediments: Isua and Akilia in southwest Greenland, which are 3.8 to 3.7 billion years old (Ga), the Pilbara in northwestern Australia (3.5 to 3.3 Ga), and Barberton in eastern South Africa (3.5 to 3.3 Ga). These sediments, however, formed almost 1 billion years after the formation of the Earth (4.56 Ga). Any older sedimentary deposits, and with them any potential information on the origin of life and its initial evolution, have been destroyed by tectonic activity. Of the existing three exposures of ancient sediments, the Isua and Akilia rocks have been so altered by metamorphic changes over the past 3.8 billion years that they are no longer useful for microfossil studies. In contrast, large parts of the Pilbara and Barberton ancient terrains are exquisitely preserved, representing veritable goldmines for microfossil hunters.

Until recently, investigations of early life on Earth concentrated on the search for fossils of cyanobacteria (*2*). These relatively large microorganisms (from a few to tens of micrometers in size) evolved a sophisticated metabolism for obtaining energy from sunlight (photosynthesis), producing oxygen as a by-product (oxygenic photosynthesis). The attention lavished on these microorganisms stems from early discoveries of fossil cyanobacteria (*1*), but since then the study of early life has moved into a more contentious, if more realistic, sphere. New questions are being raised: (i) What characteristics of life (structural and biogeochemical) also are produced by abiogenic processes and, consequently, how can we distinguish between signatures of past life and signatures of nonlife? (ii) What is the nature of the earliest preserved microorganisms, and (iii) what environments did they inhabit? The first question is a particularly thorny one—and is especially pertinent to the search for life on other planets—because we have no examples of the transition from nonlife to life. The life forms preserved in the oldest terrestrial sediments were already highly evolved compared with the earliest cell and with LUCA (last universal common ancestor).

Owing to the difficulties in distinguishing between life and nonlife, no one signature of life—for example, the fractionated isotopic ratio, the molecular carbon composition, or an isolated microfossil—should be considered unequivocal evidence for traces of past life. Hence, the most realistic approach to identifying evidence of past life is a global strategy that includes relevant environmental (habitat), structural (morphology), and biogeochemical (chemical composition, isotopic fractionation) information. Analyzing the geological context of rocks that potentially contain microfossils is crucial. Also needed is a better understanding of the differences in the spatial and temporal scale of interactions between microbes and their environment, and geological processes. For example, some microenvironments (such as volcanic rocks or hydrothermal veins) provide habitats suitable for microbes even though the overall environment may be inhospitable to life. Indeed, extreme environments were the norm on the early Earth. Furthermore, although micro-

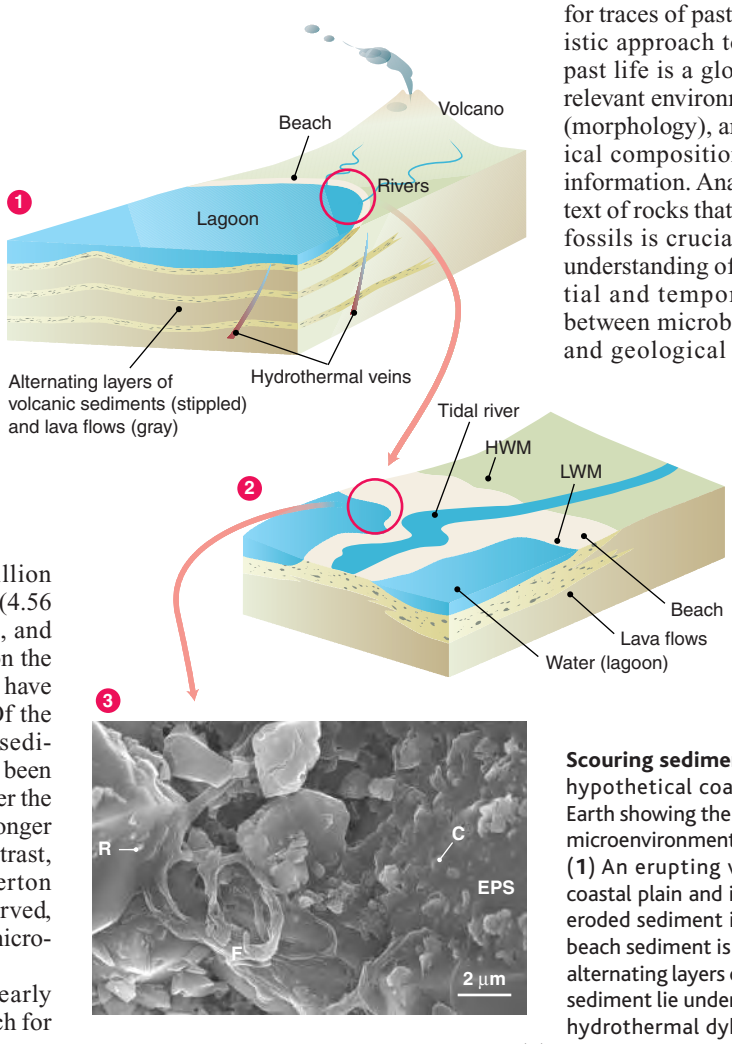

Scouring sediments for signs of early life. A hypothetical coastal landscape on the early Earth showing the global geological context and microenvironments that could have hosted life. (**1**) An erupting volcano spreads ash onto a coastal plain and into a lagoon; rivers transport eroded sediment into the lagoon and a strip of beach sediment is laid down around the lagoon; alternating layers of lava flows and thin layers of sediment lie under the lagoon and coastal plain; hydrothermal dykes or veins cut through the lava and sediment layers to reach the surface. (**2**) Enlargement of the beach area showing a meandering tidal channel that cuts through the beach sediment. HWM, high-water mark; LWM, low-water mark. (**3**) High-resolution image of the surface of sediment at the water's edge showing a microbial biofilm. R, rod-shaped microbe; F, filamentous microbe; C, coccoidal microbe; EPS, extracellular polymeric substances. [Image from figure 4 of (*16*)]

CREDIT: FRANCES WESTALL; PRESTON HUEY/*SCIENCE*

The author is at the Centre de Biophysique Moléculaire, CNRS, Rue Charles Sadron 45071 Orléans cedex 2, France. E-mail: westall@cnrs-orleans.fr

Published by AAAS

biological time scales are very short, microorganisms can be preserved in ephemeral environments, such as mud flats, through rapid fossilization. Another consideration is that, given the difficulty in distinguishing between the fossil remains of Bacteria, Archaea, and unicellular Eukaryotes, the term fossil "microorganism" or "microbe" should be used instead of fossil "bacteria." Micropaleontologists are now beginning to search for fossil microorganisms in the context of their specific microecosystems, rather than for microfossils in isolation.

Recent reports of abiogenic structures (bacteriomorphs) that mimic microbial morphologies (*3*, *4*) and of abiogenic imitations of biogenic fractionation, especially of carbon (*5*), have made investigators more cautious in their interpretations of evidence of past life. Contamination of ancient rocks by recent endolithic microorganisms further complicates the task of identifying the original signatures of life (*6*). Despite such pitfalls, the use of in situ imaging and analytical methods (*3*, *7*, *8*) has produced exciting new results. For example, microbial biofilms and mats—colonies of filamentous, coccoid, or rod-shaped microbes—have been found in sediments that formed in shallow-water basins in littoral (marine coastal) environments from the Pilbara and Barberton (both 3.5 to 3.3 billion years old) (*9*–*11*). The type of mat structure and its formation in a sunlit environment that lacked oxygen suggest a primitive form of photosynthesis (anoxygenic photosynthesis). Other microenvironments, such as hydrothermal veins and the surfaces of lava flows (*12*–*14*), may have hosted microbial life. However, the lack of evidence for biofilms in these environments complicates the identification of biogenic structures (*15*). This problem is compounded by the possibility of abiogenic carbon formation and isotopic fractionation through Fischer-Tropsch synthesis in hydrothermal veins or by metamorphic processes (*3*, *5*).

We have come a long way in our understanding of abiogenic mimics of biogenic signatures, and the nature of early life and its distribution. This success is partly attributable to the development of instrumentation with the fine scales of resolution necessary for studying communities of microorganisms that have an individual size range between 0.1 and 10 μm. Yet a vast amount of work lies before us if we are to understand (i) the boundary between abiogenic and biogenic structures (nonlife versus life); (ii) the variety and distribution of early life, given that the earliest traces of life represent a large evolutionary step from LUCA; (iii) further evolution of life on Earth (especially the appearance of oxygenic photosynthesis and the branching of the Eukaryote Kingdom from those of Bacteria and Archaea according to microfossil evidence). (iv) We also need to search not only for evidence of life on Mars, but also for the part of the earliest rock record that is missing on Earth, because the lack of plate tectonics on Mars means that rocks are preserved from the earliest period (4.56 Ga). Developing instrumentation capable of in situ analyses on a submicrometer scale of the concentration and distribution of carbonaceous and noncarbonaceous chemical biomarkers, for example, will be crucial for resolving questions about biogenicity and the nature of early life. The degree of sophistication necessary in the search for reliable traces of life makes it clear that current in situ instrumentation will not work on Mars. However, laboratory analyses of suitably selected samples returned from Mars should be possible and will benefit from knowledge gleaned about life on early Earth during the period when life may have appeared on Mars.

References

1. S. A. Tyler, E. S. Barghoorn, *Science* **119**, 606 (1954).
2. J. W. Schopf, *Science* **260**, 640 (1993).
3. M. Brasier *et al.*, *Nature* **416**, 76 (2002).
4. J. M. Garcia-Ruiz *et al.*, *Science* **302**, 1194 (2003).
5. M. Van Zuilen, A. Lepland, G. Arrhenius, *Nature* **418**, 627 (2002).
6. F. Westall, R. Folk, *Precambrian Res.* **126**, 313 (2003).
7. J. W. Schopf *et al.*, *Nature* **416**, 73 (2002).
8. F. Westall *et al.*, *Precambrian Res.* **106**, 93 (2001).
9. M. M. Walsh, *Precambrian Res.* **54**, 271 (1992).
10. F. Westall, in *Astrobiology: Future Perspectives*, P. Ehrenfreund *et al.*, Eds. (Kluwer, Doordrecht, Netherlands), pp. 287–316.
11. M. Tice, D. R. Lowe, *Nature* **431**, 549 (2004).
12. Y. Ueno, Y. Isozaki, H. Yurimoto, S. Maruyama, *Int. Geol. Rev.* **43**, 196 (2001).
13. B. Rasmussen, *Nature* **405**, 676 (2000).
14. H. Furnes *et al.*, *Science* **304**, 578 (2004).
15. M. M. Walsh, *Astrobiology* **4**, 429 (2004).
16. F. Westall, *C. R. Palevol* **2**, 485 (2003).

10.1126/science.1107227

CHEMISTRY

A New Route to Designer Antibiotics

Chaitan Khosla and Yi Tang

Like all good tools, antibiotics need periodic upgrades, but their structural complexity can make the task daunting. Nowhere is this dilemma more acutely felt than in the search for new antibacterial agents, because the most effective antibiotics usually have exceptionally complex structures. There are signs, however, that synthetic chemistry is increasingly well poised to decode the relation between structure and function of these invaluable but poorly understood jewels from nature. On page 395 of this issue (*1*), Charest *et al.* present an excellent example by developing a practical synthetic route to tetracycline, an important antibacterial, and using it to prepare an unprecedented series of tetracycline analogs, including one with properties superior to those of the natural product.

To date, all useful tetracyclines are either natural products or semisynthetic analogs composed of four fused rings, designated A, B, C, and D (see the figure). Charest *et al.* have developed efficient methods for separately constructing an AB-ring precursor and a D-ring precursor (see the figure, top panel). The most amazing feature of their synthesis is the exquisite precision with which these two pieces are joined to yield an ABCD-ring tetracycline. In theory, this elegant transformation (known as the Michael-Dieckmann reaction) could have yielded four stereoisomers with all possible chiral combinations at carbons 5a and 6 (see the figure). Instead, Charest *et al.* found a way to steer the reaction to yield mainly tetracycline-like compounds, even for the particular AB precursor that yields the more challenging 5-deoxytetracyclines, which are sought after for their improved chemical stability and biological activity.

The synthesis presented in (*1*) is not just a synthetic tour de force; it enormously expands the armamentarium of the tetracycline medicinal chemist. Tetracyclines exert their antibacterial action by binding to the 30*S* subunit of the bacterial ribosome. Over the past half-century, extensive use of tetracycline antibiotics in animals and humans has led to the emergence of at least two clinically important resistance mechanisms: one that cleanses

C. Khosla is in the Departments of Chemistry, Chemical Engineering, and Biochemistry, Stanford University, Stanford, CA 94305, USA. E-mail: khosla@stanford.edu Y. Tang is in the Department of Chemical Engineering, University of California, Los Angeles, CA 90095, USA. E-mail: yitang@ucla.edu

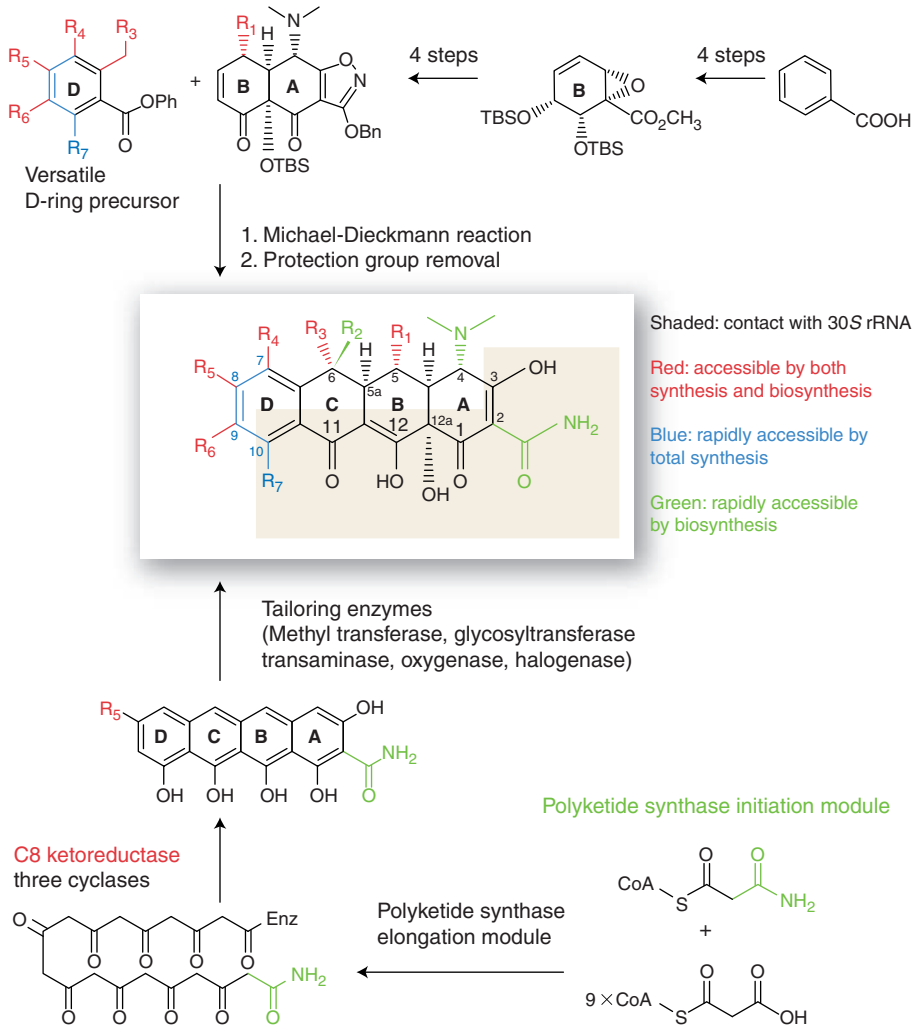

Synthesis and biosynthesis of tetracycline antibiotics. (**Center**) Tetracyclines are composed of four fused rings, designated A, B, C, and D. They bind to 30*S* ribosomal subunits from most bacteria, primarily via contacts at the southern and eastern faces (shaded). In contrast, the northern and western faces (including most of the D ring) are relatively tolerant to modification. (**Top**) The strategy for synthesizing 6-deoxytetracycline analogs reported by Charest *et al.* (*1*) involves preparation of a fully decorated AB-ring precursor, starting from benzoic acid. Various D-ring precursors are stereospecifically coupled to the AB-ring piece via the Michael-Dieckmann reaction to afford tetracycline analogs, including a pharmacologically promising pentacycline. (**Bottom**) In the biosynthetic route to tetracyclines, the tetracycline polyketide synthase uses 10 equivalents of malonyl–coenzyme A to yield an acyclic, enzyme-bound intermediate; the carbon 2 amide is presumably introduced via a separate initiation module. The full-length polyketide backbone is reduced at carbon 8 and cyclized to yield a tetracyclic intermediate, which is then enzymatically tailored to produce tetracycline antibiotics.

tetracycline from the ribosome [such as the TetM protein (*2*)], and another that pumps tetracyclines out of the cell [such as the TetA protein (*3*)]. To conquer resistance, the medicinal chemist must therefore modify the tetracycline to evade recognition by TetM or TetA without adversely affecting evolutionarily optimized interactions between tetracycline and the 30*S* subunit. The synthetic strategy described by Charest *et al.* offers one route toward such modified tetracyclines.

The task has been made much easier by the recent crystal structure of the tetracycline-bound 30*S* subunit (*4*). The structure revealed that the "southern" and "eastern" faces of tetracycline interact extensively with the ribosome, whereas the "northern" and "western" faces point outward (see the figure). There is good evidence suggesting that the latter portions of the antibiotic can be modified to achieve better activity against resistant bacteria. For example, most variations in clinically useful tetracyclines occur on the northern face, and the emerging antibiotic tigecycline (*5*) bears modifications on the western face. Indeed, one of the compounds reported by Charest *et al.*, a pentacyclic analog with a fifth ring fused to the D ring of tetracycline, has promising biological properties (*1*).

Notwithstanding the impressive power of complex-molecule synthesis, in most cases nature makes antibiotics via fundamentally different strategies. As illustrated in the bottom panel of the figure, tetracycline-producing bacteria use polyketide synthases to assemble the complete carbon backbone of tetracycline in an acyclic form; tailoring enzymes then cyclize and decorate the backbone into ABCD-ring antibiotics (*6*). Because of these differences, synthetic and biosynthetic strategies for antibiotic construction have complementary strengths and weaknesses. Synthetic modifications that appear impossible to the synthetic chemist can sometimes be readily achieved via engineered biosynthesis, and vice versa (see the figure). Moreover, at least for the foreseeable future, fermentation is likely to remain a much cheaper route to tetracyclines than de novo chemical synthesis.

There are many possible routes to new tetracyclines. Selective chemical transformations are continually being discovered by synthetic chemists; some of these reactions may yield semisynthetic tetracycline analogs with superior biological properties. Combinatorial expression of enzymes from different tetracycline biosynthesis pathways could yield novel tetracyclines. Designer polyketides could also be generated by rationally modifying the initiation module in the biosynthetic route, or through the use of glycosyl transferases from other biosynthetic pathways. However, the most innovative strategies for engineering new tetracyclines might draw upon synthetic methods to assemble the core ABCD ring structure and biosynthetic strategies to decorate it with appropriate functional groups, or vice versa.

Designer tetracycline antibiotics of the future will benefit from a concerted, judicious application of synthetic and biosynthetic logic, from the initial stages of drug design all the way to large-scale manufacturing. In addition to rejuvenating the waning art of natural product drug development, this approach will lead to a further blurring of the boundaries between chemistry and biology as synthetic sciences.

References

1. M. G. Charest, C. D. Lerner, J. D. Brubaker, D. R. Siegel, A. G. Myers, *Science* **308**, 395 (2005).
2. K. A. Dantley, H. K. Dannelly, V. Burdett, *J. Bacteriol.* **180**, 4089 (1998).
3. N. Tamura, S. Konishi, A. Yamaguchi, *Curr. Opin. Chem. Biol.* **7**, 570 (2003).
4. D. E. Brodersen *et al.*, *Cell* **103**, 1143 (2000).
5. J. McConnell, *Lancet Infect. Dis.* **4**, 717 (2004).
6. H. Petkovic *et al.*, *J. Biol. Chem.* **274**, 32829 (1999).

10.1126/science.1111415

Unveiling the Mechanisms of Cell-Cell Fusion

Elizabeth H. Chen[1]* and Eric N. Olson[2]*

Cell-cell fusion is fundamental to the development and physiology of multicellular organisms, but little is known of its mechanistic underpinnings. Recent studies have revealed that many proteins involved in cell-cell fusion are also required for seemingly unrelated cellular processes such as phagocytosis, cell migration, axon growth, and synaptogenesis. We review advances in understanding cell-cell fusion by contrasting it with virus-cell and intracellular vesicle fusion. We also consider how proteins involved in general aspects of membrane dynamics have been co-opted to control fusion of diverse cell types by coupling with specialized proteins involved in cell-cell recognition, adhesion, and signaling.

The advent of membranes during evolution heralded the appearance of life itself by providing the basic unit of cellular structure and allowing the compartmentalization of metabolites, ions, organelles, and genetic material. Inherent in the organization of phospholipid bilayers is the necessity of maintaining membrane integrity so as to prevent promiscuous membrane fusion. Conversely, the ordered fusion of intracellular membranes is essential for basic cellular functions, and the temporally and spatially regulated fusion of intercellular membranes is required for the formation of multicellular organisms.

Interest in cell-cell fusion was initially stimulated decades ago by the discovery that somatic cells can be induced to fuse by viruses in vitro (*1*). Since then, virus- or chemical-induced cell-cell fusion has become a powerful tool for analysis of gene expression, chromosomal mapping, antibody production, and cancer immunotherapy. The importance of cell-cell fusion during development and disease is underscored by its involvement in a wide range of biological processes, including fertilization; the development of muscle, bone, and placenta; the immune response; tumorigenesis; and aspects of stem cell–mediated tissue regeneration (*2*–*10*). In spite of the diversity of cell types that undergo fusion, the underlying cellular processes, including cell-cell adhesion, alignment, and membrane mixing, are similar irrespective of the cell type. These observations suggest that different cell-cell fusion events may share common mechanisms.

Despite the importance of cell-cell fusion in the development and physiology of multicellular organisms, little is known about the mechanisms underlying this process. How do cells destined to do so recognize and fuse with each other? What determines the specificity of different cell-cell fusion events? What are the minimal requirements for two cells to fuse? Is there a specific set of membrane proteins dedicated to the process of cell-cell fusion, or do the effectors of the process also perform other cellular functions? Does cell-cell fusion involve the same types of mechanisms as other membrane fusion events, such as intracellular vesicle fusion and virus-cell fusion? In this Review, we discuss recent insights into the process of cell-cell fusion. We propose that this type of membrane fusion employs mechanisms distinct from those involved in other membrane fusion events and that the biochemical machinery for cell-cell fusion plays multiple roles in the control of membrane dynamics and cytoskeletal organization as a consequence of its coupling to different upstream and downstream effectors.

Dependence of Virus Cell and Intracellular Vesicle Fusion on α-Helical Bundles

To understand the mechanisms for cell-cell fusion, it is instructive to consider virus-cell fusion and intracellular vesicle fusion, which have been extensively studied. Enveloped viruses use transmembrane viral proteins to mediate fusion with host cell membranes (*11*–*14*). Class I viral fusion proteins, such as the influenza hemagglutinin (HA) and human immunodeficiency virus type 1 (HIV-1) envelope protein (Env), contain a hydrophobic fusion peptide that is normally buried within the molecule. In response to the low pH environment in the endosome (for HA) or binding to its receptor at the cell surface (for Env), both proteins are proteolytically cleaved such that their hydrophobic fusion peptide is exposed and inserted into the target membranes (*11*, *13*, *15*). Concomitantly, the fusion protein undergoes a conformational change in which two well-separated α-helices fold upon each other to form a hairpin-like α-helical bundle, thereby bringing the viral and cell membranes into close proximity and allowing for membrane fusion (*11*–*13*) (Fig. 1A). Class II viral fusion proteins use a different mechanism, which we will discuss later.

Intracellular vesicle fusion that occurs in the secretory and endocytic pathways depends on a similar α-helical bundle structure to bring membranes together (*11*–*13*). After recognition of vesicle and target membranes by the Rab guanosine triphosphatases (GTPases) and their effectors, the SNARE family of membrane proteins, initiates membrane juxtaposition and fusion in a manner similar to class I viral fusion proteins (*12*, *13*). Specifically, vesicle-anchored v-SNAREs and target-anchored t-SNARES interact to form a bundle of α helices (the SNAREpin) that brings apposing membranes together and promotes their fusion (*16*) (Fig. 1B).

The observation that intracellular protein SNAREs use similar α-helical bundles as class I viral fusion proteins raises the question of whether such structural intermediates could be a common feature of all cellular fusogens, including those mediating cell-cell fusion. Indeed, although dispensable for cell-cell fusion in vivo, flipped SNAREs are capable of inducing cell-cell fusion in cultured cells (*17*), and viral fusogens are potent inducers of cell-cell fusion in vitro and in vivo. However, our analyses of different types of cell-cell fusion events suggest that intercellular fusion might use mechanisms distinct from those underlying other types of membrane fusion events.

An Overview of Cell-Cell Fusion

Cell-cell fusion is a widespread phenomenon in organisms ranging from yeast to humans. A number of cell-cell fusion events have been studied in varying detail, including yeast mating, epidermal cell fusion in *Caenorhabditis elegans*, myoblast fusion, fertilization, trophoblast fusion in the placenta, macrophage fusion, and stem cell fusion. Although much remains to be learned about the underlying molecular mechanisms, the following sections provide an overview of our current understanding of these cell-cell fusion events.

Yeast fusion. In *Saccharomyces cerevisiae*, the mating of a- and α-type cells involves cell

[1]Department of Molecular Biology and Genetics, Johns Hopkins University School of Medicine, Baltimore, MD 21205, USA. [2]Department of Molecular Biology, University of Texas Southwestern Medical Center, Dallas, TX 75390, USA.

*To whom correspondence should be addressed. E-mail: echen@jhmi.edu (E.H.C.); eric.olson@utsouthwestern.edu (E.N.O.)

cycle arrest, cell wall degradation, and polarized cell growth, followed by membrane juxtaposition and fusion (*18*) (Fig. 2A). Despite extensive genetic screens for mating-defective mutants in yeast, no mutants have been found in which the membrane fusion process is directly disrupted, perhaps partly because of functional redundancy. To circumvent this problem, Heiman and Walter conducted a bioinformatic screen in search of previously uncharacterized pheromone-regulated membrane proteins (Prms), with the assumption that such proteins might serve as fusogens for pheromone-induced yeast fusion. Phenotypic analyses suggest that one of the Prms, Prm1p, might function in membrane fusion, because *prm1* mutant cells show normal membrane juxtaposition without fusion (*19*). However, it is not clear whether Prm1 is the long-sought fusogen for yeast fusion, because only 50% of *prm1* mutant cells are defective in mating (*19*). In addition, Prm1p lacks hydrophobic fusion peptides or coiled-coil domains capable of forming α-helical bundles, which characterize the SNAREs and class I viral fusion proteins. Thus, if Prm1 or a related protein is a fusogen for yeast mating, its molecular mechanisms are likely to be distinct from those employed by SNAREs and class I viral fusogens.

Epidermal cell fusion in C. elegans. The nematode *C. elegans* provides a unique system to study cell-cell fusion, because about a third of its 959 somatic cells fuse to form 44 multinucleated syncytia. Fusion occurs throughout development of the nematode and is required for the formation of multiple organs (*20*, *21*). Among them, the fusion of epidermal cells has been most well characterized (Fig. 2B). Genetic screens for fusion-defective mutants have identified a potential fusion gene named *epithelial fusion failure 1* (*eff-1*) (*22*), which is required for epidermal cell-cell fusion and can induce ectopic fusion in certain other tissues (*23*, *24*). *eff-1* encodes a protein containing a transmembrane domain and an extracellular hydrophobic peptide (EHP) that is required for fusion (*22*, *24*). Unlike viral fusion peptides, which are thought to be involved in driving fusion-pore formation after virus-host binding, the EHP has been shown to be required in the localization of EFF-1 to sites of cell-cell contact before the pore-forming reaction (*24*). The functional difference between the EHP and the viral fusion peptides, together with the lack of coiled-coil domains in EFF-1, suggest that the putative fusogen EFF-1 is likely to use a different mechanism to mediate fusion than that of class I viral fusogens and SNAREs.

Myoblast fusion in Drosophila. Fusion of mononucleated myoblasts to form multinucleated muscle fibers is an essential step in skeletal muscle differentiation. *Drosophila* embryos contain two populations of myoblasts that are destined to fuse: founder cells that serve as ''seeds'' for future muscle fibers and fusion-competent cells that are attracted to and fuse with founder cells (*2*, *3*). Genetic studies in *Drosophila* have identified two classes of proteins that are required for myoblast fusion. One class includes immunoglobulin (Ig) domain–containing transmembrane proteins, such as Dumbfounded (Duf, also known as Kirre), Roughest (Rst, also known as Irrec), Sticks and stones (Sns), and Hibris (Hbs) (*25*–*29*). Although Duf and Rst are required redundantly for myoblast fusion in founder cells, Sns and Hbs are specifically expressed—and in the case of Sns, required—in fusion-competent cells (Fig. 2C). These cell surface receptors are thought to mediate recognition and adhesion of the two types of muscle cells through direct interactions, as demonstrated for Duf and Sns (*30*). Notably, none of these cell surface proteins contains a hydrophobic fusion peptide or coiled-coil domain capable of forming α-helical bundles, as seen in SNAREs and class I viral fusion proteins. A number of intracellular signaling proteins have also been found to control myoblast fusion in *Drosophila*. These include the small GTPases, Drac and ARF6; their guanine nucleotide exchange factors, Myoblast city (Mbc) and Loner; and the adaptor protein Antisocial (Ants, also known as Rols7), which links the fusion receptor Duf to Mbc (*31*–*37*). It is unclear at present whether these intracellular proteins solely function in cytoskeleton remodeling, which is required for extensive alignment of apposing membranes, or if they are also directly involved in destabilization of the lipid bilayers during the fusion process.

Mammalian fertilization. Fertilization is perhaps the most well-known form of cell-cell fusion. As in yeast mating, membrane fusion between sperm and egg occurs after a series of prefusion events, including penetration of the outer layer of the oocyte by sperm, secretion of enzymes by the lysosome-like acrosome in the sperm head, and penetration of the egg's inner layer, the zona pellucida, by the sperm. Only after entry of the sperm into the egg's perivitelline space does fusion occur between the sperm and egg plasma membranes.

Historically, a number of proteins have been hypothesized to mediate membrane fusion during fertilization. Most prominent among these are A Disintegrin and Metalloprotease (ADAM) family transmembrane proteins on the sperm, such as fertilin α, fertilin β, and cyritestin, and integrins on the egg surface (*6*). However, genetic studies in mice have demonstrated that these proteins are dispensable for membrane fusion (*38*, *39*). To date, the only protein that has been shown to be required for sperm-egg fusion is CD9, a tetraspanin family protein on the egg surface containing four transmembrane domains (*6*, *40*) (Fig. 2D). CD9 mutant eggs bind to sperm normally, but are defective in

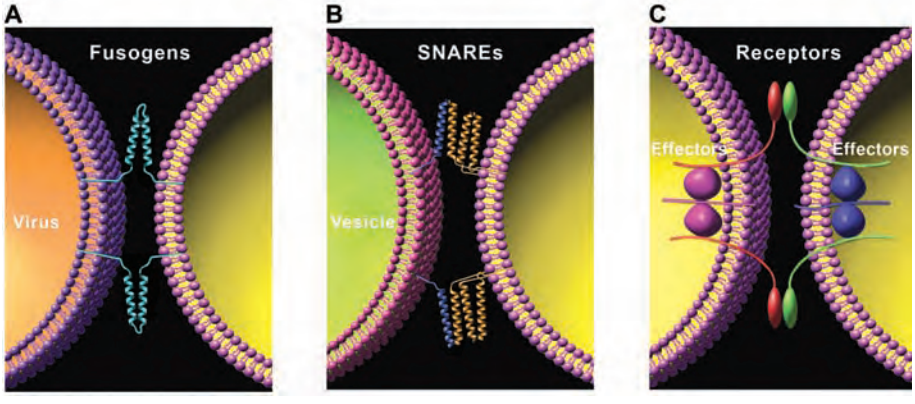

Fig. 1. Models of membrane fusion. (**A**) Enveloped viruses use a single fusion protein to mediate all steps of membrane fusion. This schematic shows the action of the influenza HA upon activation by low pH. The trimeric HA is simplified as a single polypeptide. HA contains a hydrophobic fusion peptide that is inserted into the target membrane. The HA protein forms a hairpin-like structure, in which coiled α helices near the viral membrane fold back and pair with another α helix adjacent to the fusion peptide. Thus, the hairpins bring the viral and cell membranes into close proximity, allowing the initiation of lipid mixing and fusion. (**B**) Fusion between an intracellular vesicle and the target membrane is mediated by SNAREs, which are membrane-embedded receptors localized on the vesicle and target membranes. SNAREs form a core complex that contains a stable coil of four α helices (the SNAREpin). The SNAREpins bring the apposing lipid bilayers together, allowing membrane fusion. (**C**) A two-component system may be used to mediate some cell-cell fusion events. The first component consists of transmembrane receptors (red and green). Their extracellular domains mediate close juxtaposition of the two cell membranes, whereas their cytoplasmic domains organize multiprotein complexes in the two adhering cells. The second component consists of the multiprotein fusion complexes (purple and blue). Protein(s) in the fusion complex (cytoplasmic or membrane proteins) function to destabilize the lipid bilayer, leading to the formation of fusion pores and cytoplasmic mixing.

sperm-egg membrane fusion (*41*–*43*). It remains unclear how CD9, which lacks any hydrophobic fusion peptide or coiled-coil domains, exerts its function during fusion. Because tetraspanin proteins often form multiprotein complexes in the cell membrane (*44*), CD9 could potentially mediate fusion by organizing a multiprotein fusion complex at the site of sperm-egg binding.

Fusion of placenta trophoblasts. In the mammalian placenta, trophoblasts fuse to form a syncytial layer of cells (the syncytiotrophoblast) that functions as a barrier between maternal and fetal blood vessels (*5*). Little is known about the proteins required for trophoblast fusion except for syncytin, a single-pass transmembrane protein that can induce ectopic cell-cell fusion in transfected cells (*45*, *46*) (Fig. 2E). Syncytin is nearly identical to the envelope protein of the human endogenous retrovirus HERV-W, prompting the hypothesis that placental trophoblasts may use a captured viral protein for fusion (*45*). Syncytin functions as a class I fusion protein like HA. However, this mechanism of trophoblast fusion is unlikely to be universal, because syncytin is only present in primates and not in other mammals in which placental trophoblasts also undergo cell fusion to form the layer of syncytiotrophoblasts (*47*).

Macrophage fusion: Osteoclasts and giant cells. Macrophages can differentiate and fuse to form two types of multinucleated cells, osteoclasts and giant cells, that are important for bone resorption and the immune response, respectively (*7*, *8*). Several studies using in vitro cell-cell fusion assays have implicated transmembrane proteins in macrophage fusion (*8*) (Fig. 2F), including CD44, macrophage fusion receptor (MFR), and CD47. Among them, MFR and CD47 both contain Ig domains and act as a receptor-ligand pair on apposing cells to effect macrophage fusion. Thus, MRF and CD47 appear to function in a manner analogous to that of cell surface proteins such as Duf and Sns in *Drosophila* myoblast fusion.

Stem cell fusion. Cell-cell fusion has emerged as an unexpected and complicating mechanism in tissue regeneration by stem cells (*9*, *48*, *49*). Classical experiments demonstrated the potential for genetic reprogramming in heterokaryons under experimental conditions (*50*), but it was not appreciated until recently that this type of cell-cell fusion could occur in vivo (*10*). Circulating hematopoietic stem cells (HSCs) have been shown to fuse with a wide variety of target cells, including cardiac myocytes, hepatocytes, Purkinje cells, and oligodendrocytes, with consequent modification of the gene expression profile of the stem cell (*9*, *48*, *49*) (Fig. 2G). Relatively little is known about the mechanisms of stem cell fusion. It is also unclear whether this is a regulated process or a "random" event that occurs at low frequency or whether it is the HSCs themselves or their descendents that actually fuse with the target cells. Studies of liver regeneration suggest that macrophages derived from HSCs, instead of HSCs themselves, have the capacity to fuse with hepatocytes (*51*–*54*), although these studies cannot formally exclude the possibility of transdetermination of HSCs. If macrophages are indeed the source of hepatocyte fusion partners, it is tempting to speculate that proteins involved in macrophage fusion might also function in stem cell–based fusion, at least in the context of liver regeneration.

Insights from Studies of Cell-Cell Fusion

Cell-cell fusion does not appear to be mediated by α-helical bundles. Despite their seemingly different biological functions, the intracellular fusogen SNAREs and class I viral fusion proteins both use an α-helical bundle structure to promote membrane juxtaposition and fusion. Could other cellular fusogens, such as those governing cell-cell fusion, adopt a similar mechanism to bring lipid bilayers together? So far, this does not appear to be the case. With the exception of syncytin, a retroviral envelope protein that might have been captured by the human genome, none of the cell surface proteins identified so far in the various cell-cell fusion processes resemble SNAREs or class I viral fusion proteins. Although it is formally possible that such proteins are yet to be identified, it seems more likely that cell-cell fusion uses different mechanisms. Fusion of class II viruses with host cells does not involve an α-helical bundle conformation (*55*), which supports the idea that such a conformation is not an absolute requirement for membrane fusion.

An unexpected aspect of *Drosophila* myoblast fusion is that intracellular signaling proteins, which are recruited to the sites of fusion by and function downstream of the cell surface receptors, are required for fusion (*2*, *3*). We speculate that other cell-cell fusion events may involve a similar intracellular signaling input. Such cell-cell fusion events might use a "bipartite" fusion system rather

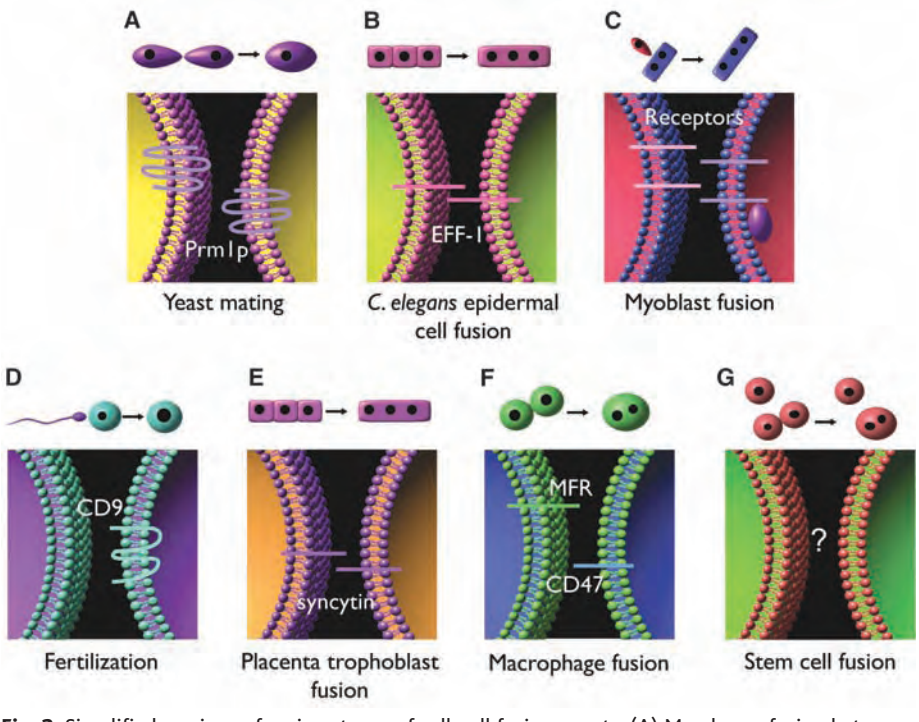

Fig. 2. Simplified versions of various types of cell-cell fusion events. (**A**) Membrane fusion between yeast a and α cells. A five-pass transmembrane protein, Prm1p, functions in both types of cells and is partially required for fusion. (**B**) Epidermal cell fusion in *C. elegans*. A putative single-pass transmembrane protein, EFF-1, is necessary and sufficient for fusion of this type of cell. (**C**) Myoblast fusion in *Drosophila*. Ig domain–containing proteins are localized in founder (purple) and fusion-competent (pink) cells. The purple oval in the founder cell represents the multiprotein complex organized by the fusion receptor. Such a complex has yet to be identified in fusion-competent cells. (**D**) Sperm-egg fusion during mammalian fertilization. A tetraspanin on the egg surface, CD9, is required for the membrane fusion process. (**E**) Trophoblast fusion during syncytiotrophoblast formation in the placenta. Syncytin, the envelope protein of a human retrovirus, is proposed to mediate trophoblast fusion. (**F**) Macrophage fusion to form osteoclasts in the bone or giant cells during immune response. Ig domain–containing proteins are implicated, including a receptor-ligand pair of MFR and CD47. (**G**) Stem cell fusion. Proteins mediating this type of fusion are completely unknown.

than a single fusogen such as viral fusion proteins (Fig. 1C). We propose that fusion receptors such as Duf and Sns not only function in tethering cells together for fusion but also contribute to bringing the apposing membranes into close proximity, in a manner distinct from that of α-helical fusogenic proteins. In a subsequent step, these receptors recruit intracellular proteins such as Ants and Loner to form multiprotein complexes at the sites of fusion. These multiprotein complexes in turn destabilize the lipid bilayer either directly or indirectly by modifying the activity of additional membrane proteins, thus leading to the formation of fusion pores and fusion of the two apposing cells.

The actin cytoskeleton and cell-cell fusion. Several intracellular proteins involved in *Drosophila* myoblast fusion have well-established roles in regulating the actin cytoskeleton. These include Drac, which controls actin polymerization; Mbc, an upstream regulator of Drac; and Kette, a regulator of Wiskott-Aldrich syndrome protein (WASP)–dependent actin cytoskeleton rearrangement (*31*, *36*, *37*, *56*). Constitutively active Drac or a loss of function in *kette* blocks the formation of fusion pores, a late step during myoblast fusion, without affecting early stages of the fusion process (*56*, *57*). These studies raise the issue of the role of the actin cytoskeleton in the formation of fusion pores. The actin cytoskeleton could be involved in transporting essential proteins to sites of fusion, or perhaps it serves as a scaffold to stabilize membrane-membrane interactions. Alternatively, or in addition, the cytoskeleton might directly affect lipid mixing by producing mechanical strain on the lipid bilayer.

We speculate that the actin cytoskeleton could be a general requirement for cell-cell fusion. Furthermore, the cytoskeleton might play a widespread role in membrane fusion events beyond cell-cell fusion. For example, virus-induced cell-cell fusion is blocked when the actin cytoskeleton of the host cells is perturbed by expressing a dominant negative Rac GTPase (*58*). In addition, both the actin- and microtubule-based cytoskeleton are implicated in intracellular vesicle fusion because they participate in transporting vesicles from their sites of synthesis to the sites of membrane fusion (*59*).

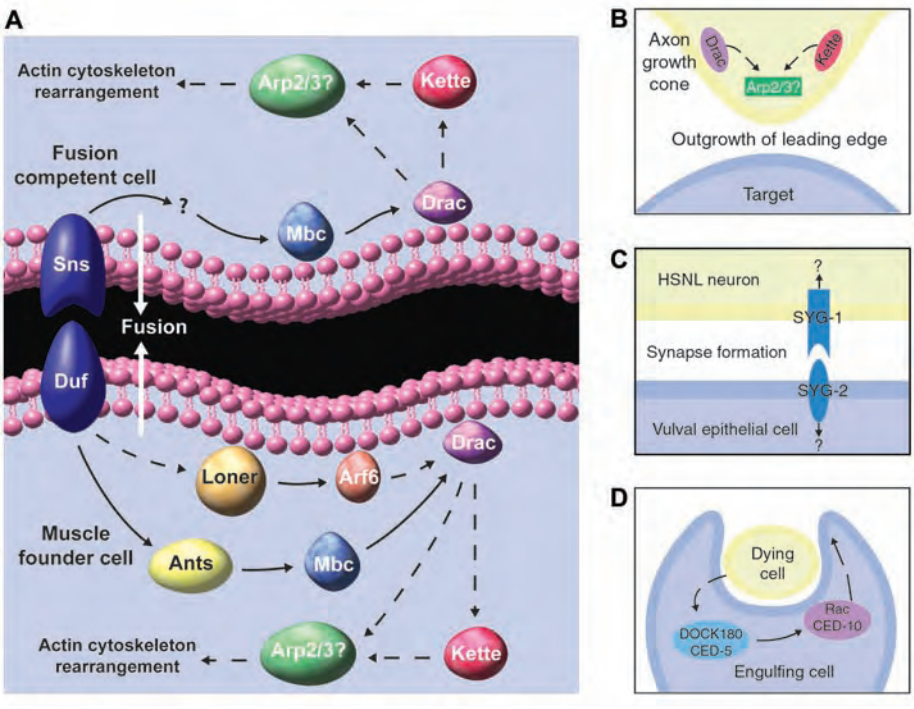

Fig. 3. Components of cell-cell fusion events are implicated in other fusion-independent cellular processes. (**A**) Major components in *Drosophila* myoblast fusion. Transmembrane receptors (dark blue) mediate the juxtaposition of the plasma membranes of a founder cell and a fusion-competent cell. For simplicity, only Duf in the founder cell and Sns in the fusion-competent cell are shown. Two independent signaling pathways, Ants → Mbc → Drac and Loner → ARF6 → Drac, are required to transduce the fusion signal from the membrane receptor to the cytoskeleton. Kette may function downstream or in parallel with Drac to regulate actin cytoskeleton rearrangement, perhaps through the Arp2/3 complex. (**B**) Drac and Kette may function through Arp2/3 to regulate neurite outgrowth and axon pathfinding during nervous system development. (**C**) The *C. elegans* homologs of Duf and Sns, SYG-1 and SYG-2, are required for proper synapse formation between the HSNL neuron and vulval epithelial cells. (**D**) The mammalian and *C. elegans* Mbc and Drac homologs, DOCK180 (CED-5 in *C. elegans*) and Rac (CED-10 in *C. elegans*), are required for phagocytes to engulf dying cells. Solid arrows indicate direct protein interactions.

The specificity and evolution of cell-cell fusion. Studies of various cell-cell fusion processes have identified specialized proteins that are required for specific fusion events. For example, syncytin, a protein involved in trophoblast fusion, differs from EFF-1, the putative fusogen in *C. elegans* epidermal fusion. Furthermore, the function of these fusion proteins is limited to certain species. For example, syncytin is only found in primates and EFF-1 is only present in several closely related nematode species (*22*, *45*, *46*).

The existence of species- and cell type–specific fusion proteins does not exclude a possible involvement of common molecular machinery for fusion. For example, Ig domain–containing proteins are involved in both myoblast and macrophage fusion, suggesting that this type of cell surface protein might have a more general function in multiple fusion events. It is also conceivable that intracellular proteins regulating the actin cytoskeleton might be involved in cell-cell fusion events beyond myoblast fusion.

Cell-cell fusion and other fusion-independent cellular processes. Many components of cell-cell fusion processes have been implicated in other aspects of membrane or cytoskeletal reorganization (Fig. 3). For example, besides their function in myoblast fusion, Drac and Kette are required for axonal growth and guidance by modulating the activity of downstream actin-regulatory proteins (*60*, *61*). The *C. elegans* homologs of Duf and Sns, SYG-1 and SYG-2, are required in certain motor neurons for correct synapse formation (*62*, *63*). Homologs of Mbc and Drac in mammals and *C. elegans* are required for phagocytosis and cell migration, which require extensive cytoskeletal rearrangements (*37*, *64*). Thus, proteins involved in cell-cell fusion are likely to play pleiotropic roles in other cellular processes involving changes in membrane or cytoskeletal structures, with specificity being achieved through the coupling of these proteins to different upstream and downstream effectors. These specific effectors, in turn, determine whether a cell will become part of a syncytium or remain solitary. For example, in cells destined to fuse, the upstream membrane receptors mediate recognition and adhesion of plasma membranes between specific populations of cells, whereas the downstream intracellular proteins transduce fusion signals to the cytoskeleton. The absence of any component in the pathway results in a failure of fusion. Therefore, cell-cell fusion is delicately controlled by a cascade of specific effectors, which ensures the successful fusion between proper partners and protects cells from aberrant fusion.

Cell-cell fusion and human disease. Given the indispensable role of cell-cell fusion in development, it is expected that abnormalities of cell-cell fusion might contribute to certain

human diseases. Indeed, defects in sperm-egg fusion represent a major cause of infertility. Certain muscle diseases, such as centronuclear myopathy and myotonic dystrophy, characterized by minute myofibers, may be due partly to defects in myoblast fusion (*65*, *66*). Furthermore, defects of placental trophoblast fusion result in pregnancy complications such as preeclampsia (*67*), and defects in osteoclast fusion can cause bone abnormalities such as osteopetrosis (*68*).

Although failure of cell-cell fusion can contribute to human pathology, unregulated cell-cell fusion may also promote diseases, especially cancer (*69*). Many tumor cells, for unknown reasons, are particularly fusogenic. Fusion between tumor and normal somatic cells generates hybrid cells that are often more malignant than parental cells, perhaps because of their increased growth rate, resistance to drugs and apoptosis, or ability to metastasize (*70*–*72*). Moreover, these hybrids may facilitate the production of a diversity of malignant cell types (*73*). To some extent, tumor-somatic cell fusion is similar to stem cell fusion, in that both types of fusion result in diverse progeny in various tissues (*9*, *48*, *69*). The analogy between tumor and stem cell fusion is consistent with the hypothesis that tumor cells are of stem cell origin (*74*, *75*).

Therapeutic applications of cell-cell fusion. Perhaps the most well-known application of cell-cell fusion is the production of monoclonal antibodies using hybridomas, the fusion products of antibody-secreting and immortal B cells (*76*). Cell-cell fusion has also been explored to develop more effective cancer immunotherapy. Conventional cancer immunotherapy involves vaccination using dendritic cells that express specific tumor antigens (*77*, *78*). Fusion of tumor cells with intact dendritic cells produces hybrids that express the complete spectrum of tumor-associated antigens. Vaccination with such hybrids is currently being tested as a more effective immunotherapy against cancer (*79*).

The realization that multiple components of the cellular machinery for cell-cell fusion also function in intracellular signaling suggests opportunities for therapeutically modulating the fusion process. Enhancement of cell-cell fusion will bring about increased efficacy of gene therapy for target tissues in vivo. As a hint of things to come, the fusogenic potential of muscle satellite cells has been explored as an approach for cell-based gene delivery to skeletal muscle. For example, intramuscular injection of normal myoblasts into dystrophic mice has been shown to restore dystrophin expression to dystrophin-negative muscles (*80*).

Concluding Remarks

Despite recent advances in our understanding of cell-cell fusion, a central question remains: What is the mechanism underlying plasma membrane merger? The apparent lack of cell-cell fusogens that resemble class I viral fusion proteins and SNAREs indicates the involvement of a distinct mechanism. Although studies of *Drosophila* myoblast fusion suggest a two-component system involving receptor-mediated membrane juxtaposition followed by membrane destabilization, the molecular details of this process are yet to be elucidated. It also remains to be determined whether a universal principle can be extrapolated from the diverse array of cell-cell fusion events currently under investigation. Understanding the basic mechanisms of cell-cell fusion promises to yield insight into related biological processes such as apoptosis, neurogenesis, tumorigenesis, and stem cell biology and, ultimately, to allow the process to be therapeutically manipulated in the setting of human disease.

Note added in proof: An Ig domain–containing transmembrane on sperm, Izumo, has recently been reported to mediate fertilization (*81*), which supports our hypothesis that this type of cell surface protein may have a general function in multiple cell-cell fusion events.

References and Notes

1. Y. Okada, *Exp. Cell Res.* **26**, 98 (1962).
2. S. M. Abmayr, L. Balagopalan, B. J. Galletta, S. J. Hong, *Int. Rev. Cytol.* **225**, 33 (2003).
3. E. H. Chen, E. N. Olson, *Trends Cell Biol.* **14**, 452 (2004).
4. V. Horsley, G. K. Pavlath, *Cells Tissues Organs* **176**, 67 (2004).
5. A. J. Potgens *et al.*, *Placenta* **23** (suppl. A), S107 (2002).
6. P. Primakoff, D. G. Myles, *Science* **296**, 2183 (2002).
7. J. M. Anderson, *Curr. Opin. Hematol.* **7**, 40 (2000).
8. A. Vignery, *Int. J. Exp. Pathol.* **81**, 291 (2000).
9. A. J. Wagers, I. L. Weissman, *Cell* **116**, 639 (2004).
10. J. Pomerantz, H. M. Blau, *Nat. Cell Biol.* **6**, 810 (2004).
11. D. M. Eckert, P. S. Kim, *Annu. Rev. Biochem.* **70**, 777 (2001).
12. R. Blumenthal, M. J. Clague, S. R. Durell, R. M. Epand, *Chem. Rev.* **103**, 53 (2003).
13. R. Jahn, T. Lang, T. C. Sudhof, *Cell* **112**, 519 (2003).
14. L. D. Hernandez, L. R. Hoffman, T. G. Wolfsberg, J. M. White, *Annu. Rev. Cell Dev. Biol.* **12**, 627 (1996).
15. J. J. Skehel, D. C. Wiley, *Annu. Rev. Biochem.* **69**, 531 (2000).
16. T. Weber *et al.*, *Cell* **92**, 759 (1998).
17. C. Hu *et al.*, *Science* **300**, 1745 (2003).
18. J. M. White, M. D. Rose, *Curr. Biol.* **11**, R16 (2001).
19. M. G. Heiman, P. Walter, *J. Cell Biol.* **151**, 719 (2000).
20. G. Shemer, B. Podbilewicz, *Dev. Dyn.* **218**, 30 (2000).
21. G. Shemer, B. Podbilewicz, *Bioessays* **25**, 672 (2003).
22. W. A. Mohler *et al.*, *Dev. Cell* **2**, 355 (2002).
23. G. Shemer *et al.*, *Curr. Biol.* **14**, 1587 (2004).
24. J. J. del Campo *et al.*, *Curr. Biol.* **15**, 413 (2005).
25. M. Ruiz-Gomez, N. Coutts, A. Price, M. V. Taylor, M. Bate, *Cell* **102**, 189 (2000).
26. M. Strunkelnberg *et al.*, *Development* **128**, 4229 (2001).
27. B. A. Bour, M. Chakravarti, J. M. West, S. M. Abmayr, *Genes Dev.* **14**, 1498 (2000).
28. H. A. Dworak, M. A. Charles, L. B. Pellerano, H. Sink, *Development* **128**, 4265 (2001).
29. R. D. Artero, I. Castanon, M. K. Baylies, *Development* **128**, 4251 (2001).
30. B. J. Galletta, M. Chakravarti, R. Banerjee, S. M. Abmayr, *Mech. Dev.* **121**, 1455 (2004).
31. S. Hakeda-Suzuki *et al.*, *Nature* **416**, 438 (2002).
32. E. H. Chen, B. A. Pryce, J. A. Tzeng, G. A. Gonzalez, E. N. Olson, *Cell* **114**, 751 (2003).
33. E. H. Chen, E. N. Olson, *Dev. Cell* **1**, 705 (2001).
34. S. D. Menon, W. Chia, *Dev. Cell* **1**, 671 (2001).
35. A. Rau *et al.*, *Development* **128**, 5061 (2001).
36. M. R. Erickson, B. J. Galletta, S. M. Abmayr, *J. Cell Biol.* **138**, 589 (1997).
37. E. Brugnera *et al.*, *Nat. Cell Biol.* **4**, 574 (2002).
38. Z. Y. He *et al.*, *Dev. Biol.* **254**, 226 (2003).
39. C. Cho, H. Ge, D. Branciforte, P. Primakoff, D. G. Myles, *Dev. Biol.* **222**, 289 (2000).
40. K. Kaji, A. Kudo, *Reproduction* **127**, 423 (2004).
41. F. Le Naour, E. Rubinstein, C. Jasmin, M. Prenant, C. Boucheix, *Science* **287**, 319 (2000).
42. K. Miyado *et al.*, *Science* **287**, 321 (2000).
43. K. Kaji, S. Oda, S. Miyazaki, A. Kudo, *Dev. Biol.* **247**, 327 (2002).
44. J. M. Tarrant, L. Robb, A. B. van Spriel, M. D. Wright, *Trends Immunol.* **24**, 610 (2003).
45. S. Mi *et al.*, *Nature* **403**, 785 (2000).
46. J. L. Blond *et al.*, *J. Virol.* **74**, 3321 (2000).
47. R. Pijnenborg, W. B. Robertson, I. Brosens, G. Dixon, *Placenta* **2**, 71 (1981).
48. F. D. Camargo, S. M. Chambers, M. A. Goodell, *Cell Prolif.* **37**, 55 (2004).
49. K. O'Malley, E. W. Scott, *Exp. Hematol.* **32**, 131 (2004).
50. H. M. Blau, B. T. Blakely, *Semin. Cell Dev. Biol.* **10**, 267 (1999).
51. F. D. Camargo, M. Finegold, M. A. Goodell, *J. Clin. Invest.* **113**, 1266 (2004).
52. H. Willenbring *et al.*, *Nat. Med.* **10**, 744 (2004).
53. G. Q. Daley, *Nat. Med.* **10**, 671 (2004).
54. F. D. Camargo, R. Green, Y. Capetanaki, K. A. Jackson, M. A. Goodell, *Nat. Med.* **9**, 1520 (2003).
55. F. X. Heinz, S. L. Allison, *Curr. Opin. Microbiol.* **4**, 450 (2001).
56. R. H. Schroter *et al.*, *Development* **131**, 4501 (2004).
57. S. K. Doberstein, R. D. Fetter, A. Y. Mehta, C. S. Goodman, *J. Cell Biol.* **136**, 1249 (1997).
58. S. E. Pontow, N. V. Heyden, S. Wei, L. Ratner, *J. Virol.* **78**, 7138 (2004).
59. J. A. Hammer III, X. S. Wu, *Curr. Opin. Cell Biol.* **14**, 69 (2002).
60. T. Hummel, K. Leifker, C. Klambt, *Genes Dev.* **14**, 863 (2000).
61. J. Ng *et al.*, *Nature* **416**, 442 (2002).
62. K. Shen, C. I. Bargmann, *Cell* **112**, 619 (2003).
63. K. Shen, R. D. Fetter, C. I. Bargmann, *Cell* **116**, 869 (2004).
64. P. W. Reddien, H. R. Horvitz, *Annu. Rev. Cell Dev. Biol.* (2004).
65. E. Farkas-Bargeton *et al.*, *J. Neurol. Sci.* **83**, 145 (1988).
66. L. Wockel *et al.*, *Acta Neuropathol. (Berlin)* **95**, 547 (1998).
67. C. W. Redman, I. L. Sargent, *Placenta* **21**, 597 (2000).
68. T. Miyamoto, T. Suda, *Keio J. Med.* **52**, 1 (2003).
69. D. Duelli, Y. Lazebnik, *Cancer Cell* **3**, 445 (2003).
70. F. R. Miller, A. N. Mohamed, D. McEachern, *Cancer Res.* **49**, 4316 (1989).
71. D. M. Duelli, Y. A. Lazebnik, *Nat. Cell Biol.* **2**, 859 (2000).
72. J. M. Pawelek, *Melanoma Res.* **10**, 507 (2000).
73. L. Larizza, V. Schirrmacher, *Cancer Metastas. Rev.* **3**, 193 (1984).
74. D. R. Bell, G. Van Zant, *Oncogene* **23**, 7290 (2004).
75. P. A. Beachy, S. S. Karhadkar, D. M. Berman, *Nature* **432**, 324 (2004).
76. G. Kohler, C. Milstein, *Nature* **256**, 495 (1975).
77. U. Trefzer, P. Walden, *Mol. Biotechnol.* **25**, 63 (2003).
78. J. N. Blattman, P. D. Greenberg, *Science* **305**, 200 (2004).
79. U. Trefzer *et al.*, *Int. J. Cancer* **110**, 730 (2004).
80. T. Partridge, *Neuromuscul. Disord.* **12** (suppl. 1), S3 (2002).
81. N. Inoue *et al.*, *Nature* **434**, 234 (2005).

82. We thank E. Grote, D. Pan, and anonymous reviewers for critical comments on the manuscript; J. Page for editorial assistance; and R. Carre and J. Cabrera for artwork. We apologize to the authors whose original work is not cited because of space limits. Supported by grants from the NIH, the D. W. Reynolds Center for Clinical Cardiovascular Research, and the Robert A. Welch Foundation.

10.1126/science.1104799

A Pair of Shelled Eggs Inside A Female Dinosaur

Tamaki Sato,[1]* Yen-nien Cheng,[2] Xiao-chun Wu,[1]* Darla K. Zelenitsky,[3] Yu-fu Hsiao[4]

Reproductive biology is now an important topic in the study of dinosaur-bird relationships (*1*). Two immature eggs in *Sinosauropteryx* (*2*) and discoveries of paired eggs in maniraptoran nests (*3*–*5*) have been used to suggest that theropod dinosaurs had paired functional oviducts. Occurrences of paired eggs in the nests may also indicate a lack of egg rotation by the adults (*5*). Maniraptoran specimens found atop egg clutches might imply that entire egg clutches were laid in a single sitting (like crocodiles) or laid in multiple sittings (like birds) of the adult female (*4*–*6*). We present here a fossil that tests these ideas.

The specimen is a three-dimensional pelvis that contains a single pair of shelled eggs within its body cavity (Fig. 1). It was identified as an oviraptorosaurian on the basis of the pelvis morphology and a preliminary phylogenetic analysis (supporting online text). Aside from a shift to the left side during fossilization, we believe that the eggs retain their approximate original orientation and position within the oviducts. Compared with the immature eggs of *Sinosauropteryx* (*2*), these eggs are located more caudally in the body cavity and, on the basis of their position relative to the cloacal region, were likely in the uteri at death. The caudal end of the right egg is more pointed than the cranial end of the left egg (Fig. 1D), suggesting a slightly asymmetrical profile of the eggs in life. The left egg has measurable diameters of 175 mm by 78 to 80 mm by 55 mm. The egg shape and surficial ornamentations indicate an affinity to elongatoolithids, and their microscopic structures resemble those of *Macroolithus yaotunensis* (supporting online text).

Two adult oviraptorid specimens have been found atop ring-shaped clutches that contain at least 15 eggs (*6*). Given the relatively large egg size of our specimen, the position of the cloaca (estimated as ventral to the anteriormost caudal vertebra), and the inferred location for shell deposition in the uterus as in modern birds and crocodiles, it is unlikely that this specimen could have had multiple pairs of shelled eggs inside the body at one time. Unless sequential egg formation and shelling was very rapid and/or there was an extremely prolonged period of egg laying, the preservation of only two tightly juxtaposed eggs in the specimen strongly indicates that each of the paired oviducts simultaneously produced a single egg. This supports the theory that maniraptoran dinosaurs retained two functional oviducts like crocodiles but had reduced the number of eggs ovulated to one per oviduct, as in birds.

The pairedness of eggs in some oviraptorosaurian nests was therefore likely due to the oviposition of two eggs nearly simultaneously, rather than the result of egg manipulation by the parent(s). It is also evident that, as in birds, multiple ovipositions would have been required to lay an entire clutch. Furthermore, the slightly pointed end of each egg directing caudally inside the body and toward the periphery in the nests (*4*) suggests that the females came to the centers of the nests to lay neat, multilayered, ring-shaped clutches.

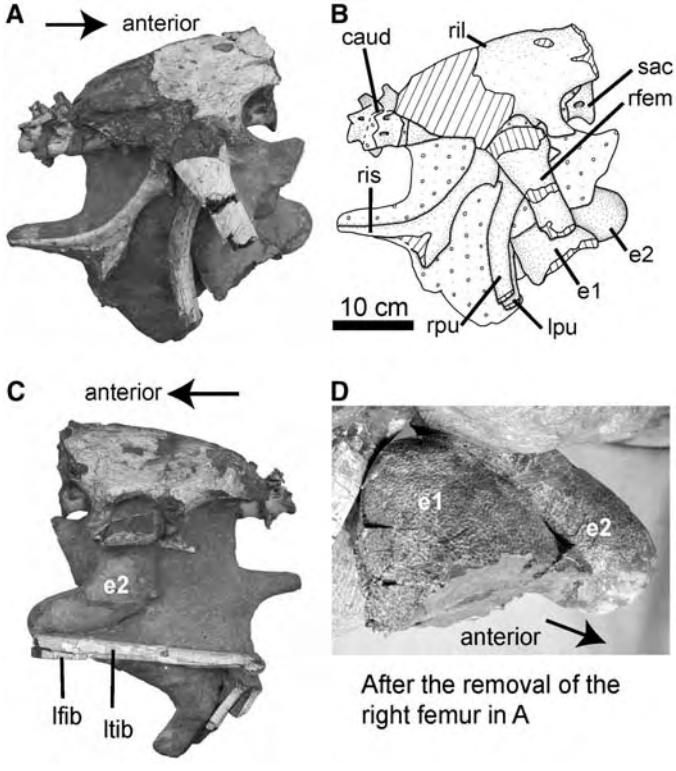

Fig. 1. The oviraptorosaurian specimen at the National Museum of Natural Science in Taiwan (specimen no. NMNS-VPDINO-2002-0901) was excavated from the Upper Cretaceous Nanxiong Formation of the Hongcheng Basin near the city of Ganzhou, in the southern Jiangxi Province, China. It consists of six sacral vertebrae; the first two caudal vertebrae; the ilia, pubes, ischia, and femora; the lower part of the left leg; and a pair of eggs inside the pelvis. The pubes and ischia are slightly disarticulated, but otherwise these bones retain their original anatomical relationships. The eggs are located dorsal to the pubic symphysis, about one egg length anterior to the cloacal region. They are side by side and closely apposed, although the right egg was slightly more ventrally positioned than the left egg. Y.-n.C. and Y.-f.H. supervised the preparation of NMNS-VPDINO-2002-0901, confirming that it is not a composite. (**A** and **B**) Right lateral view. (**C**) Left lateral view. (**D**) A right close-up view of the two eggs. Caud, caudal vertebrae; e, egg; lfib, left fibula; lpu, left pubis; ltib, left tibia; rfem, right femur; ril, right ilium; ris, right ischium; rpu, right pubis; sac, sacral.

References and Notes

1. D. J. Varricchio, F. D. Jackson, in *Feathered Dragons*, P. J. Currie, E. B. Koppelhus, M. A. Shugar, J. L. Wright, Eds. (Indiana Univ. Press, Bloomington, IN, 2004), pp. 215–233.
2. P.-J. Chen, Z.-M. Dong, S.-N. Zhen, *Nature* **391**, 147 (1998).
3. M. A. Norell, J. M. Clark, L. M. Chiappe, D. Dashzeveg, *Nature* **378**, 774 (1995).
4. Z.-M. Dong, P. J. Currie, *Can. J. Earth Sci.* **33**, 631 (1996).
5. D. J. Varricchio, F. Jackson, J. J. Borkowski, J. R. Horner, *Nature* **385**, 247 (1997).
6. J. M. Clark, M. A. Norell, L. M. Chiappe, *Am. Mus. Novit.* **3265**, 1 (1999).
7. We thank M. Norell and C. Mehling of the American Museum of Natural History, New York, for access to the oviraptorid egg nests and R. Holmes of the CMN for reading earlier drafts. T.S., D.K.Z., and X.-C.W. were supported by the Japan Society for the Promotion of Science, Alberta Ingenuity Fund, and the CMN, respectively.

Supporting Online Material

www.sciencemag.org/cgi/content/full/308/5720/375/DC1
SOM Text
Fig. S1
References and Notes

2 February 2005; accepted 4 March 2005
10.1126/science.1110578

[1]Canadian Museum of Nature (CMN), Post Office Box 3443, STN D, Ottawa, Ontario K1P 6P4, Canada. [2]National Museum of Natural Science, 1 Kuan Chien Road, Taichung, Taiwan (ROC). [3]The University of Calgary, Department of Geology and Geophysics, 2500 University Drive Northwest, Calgary, AB T2N 1N4, Canada. [4]Paleowonders Fossil and Mineral Museum, 442 Section 2, Wen-Hwa Road, Banchiao, Taipei, Taiwan (ROC).

*To whom correspondence should be addressed. E-mail: tsato@mus-nature.ca (T.S.); xcwu@mus-nature.ca (X.-c.W.)

Impact of Humans on the Flux of Terrestrial Sediment to the Global Coastal Ocean

James P. M. Syvitski,[1]* Charles J. Vörösmarty,[2] Albert J. Kettner,[1,3] Pamela Green[2]

Here we provide global estimates of the seasonal flux of sediment, on a river-by-river basis, under modern and prehuman conditions. Humans have simultaneously increased the sediment transport by global rivers through soil erosion (by 2.3 ± 0.6 billion metric tons per year), yet reduced the flux of sediment reaching the world's coasts (by 1.4 ± 0.3 billion metric tons per year) because of retention within reservoirs. Over 100 billion metric tons of sediment and 1 to 3 billion metric tons of carbon are now sequestered in reservoirs constructed largely within the past 50 years. African and Asian rivers carry a greatly reduced sediment load; Indonesian rivers deliver much more sediment to coastal areas.

Coastal retreat has major implications for human habitat, because >37% (2.1 billion people in 1994) of the world's population live within 100 km of a coastline, and approximately 44% live within 150 km of a coastline (*1*). Coastal retreat is directly influenced by the reduction of river-supplied sediment (*2*). Thus, a goal of the International Geosphere Biosphere Programme (IGBP) and its core project, Land Ocean Interaction in the Coastal Zone (LOICZ), has been to survey the terrestrial sediment supply to the coast and to analyze human perturbation of this flux (*3*). Changes in sediment supply can greatly influence the benthic environment of coastal estuaries (*4*), coral reefs (*5*), and seagrass communities (*6*). In addition, nutrient fluxes, particularly carbon, are intimately tied to the flux of sediment (*7*), which has implications for coastal fisheries (*8*). Sediment delivery will also affect harbor maintenance and the potential for burial of pollutants (*9*).

Yet even with such environmental importance, <10% of the world's rivers have been monitored for their sediment delivery to the coastal zone or have observational data on them available to researchers (*3*). Of the rivers that have been monitored, most have had their sediment-gauging activities terminated (*3*). To address this paucity of data, we describe a globally consistent method for the estimation of the sediment flux near river mouths. We combine databases and models to determine the prehuman and modern delivery rate of sediment to the coast, including seasonal attributes, on a river-by-river global basis.

Global river discharge. A recent update to the Simulated Topological Network 30 minute (latitude × longitude) (STN-30p) for potential river flow paths (*10*) provides the spatial framework for organizing environmental data into distinct river basins. STN-30p is made up of ~60,000 grid cells at 30′ spatial resolution for the continental land mass. These cells define 6292 river basins with drainage areas >100 km^2. 4464 of these (i.e., those basins that are not covered by the ice sheets of Antarctica, Greenland, and portions of the Canadian Archipelago) have a positive discharge to the ocean or sea and are analyzed in this work. STN-30p catchment areas have a 7.5% absolute error, with a 2% positive bias (*11*).

The University of New Hampshire water balance and transport model (WBM/WTM), based on the STN-30p network, provides a fundamental structure for analyzing sediment flux distribution by river basin, continent, climatic zone, and receiving ocean or sea (*12*). WBM/WTM estimates of discharge are constrained by observed hydrographic data (*11*, *13*). Selected (663) gauging stations from the Global Runoff Data Centre (GRDC) archive were coregistered to the STN-30p network, and these represent 76 Mkm^2 (72%) of the world's actively discharging landmass. The accuracy of GRDC discharge measurements is ~10 to 20%, which is much higher than what

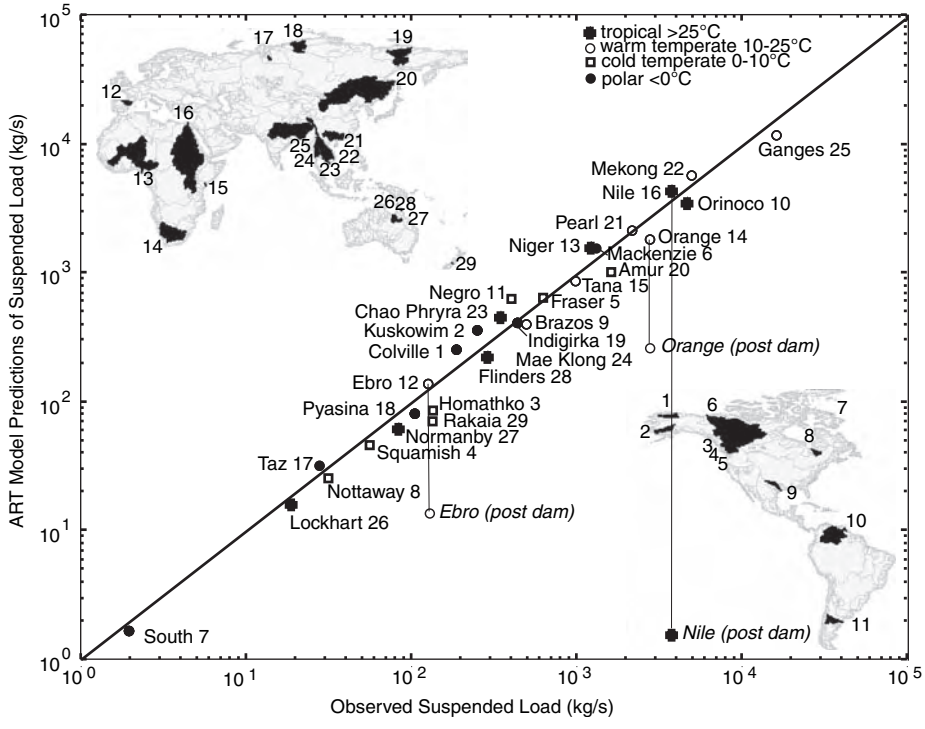

Fig. 1. Comparing observations of sediment loads with ART model predictions (*16*) for selected pristine (largely unregulated) rivers (e.g., South, Colville, Indigirka, Pyasina, Squamish, Kuskowim, Mae Klong, and Orinoco) or rivers observed before major human impacts (e.g., compare the after-dam values of the Ebro, Nile, and Orange with before-dam values). The data are from (*16*). The largest difference between predictions and observations is 63% (Negro). Errors associated with observational data are of the same magnitude as those associated with predictions.

[1]Environmental Computation and Imaging Facility, Institute of Arctic and Alpine Research (INSTAAR), University of Colorado, Boulder, CO 80309–0450, USA. [2]Water Systems Analysis Group, Institute for the Study of Earth, Oceans, and Space, University of New Hampshire, Durham, NH 03824, USA. [3]Applied Earth Sciences, Delft University of Technology, Delft, Netherlands.

*To whom correspondence should be addressed. E-mail: james.syvitski@colorado.edu

can be achieved from measuring precipitation (*14*). Differences between station data and simulated WBM/WTM discharge estimates derived from modern climatology were used to develop correction factors and then revised to account for human-induced losses of water within basins caused by interbasin water diversions or irrigation losses to the atmosphere. These factors are estimated to be 6% of the global discharge total of 40,000 km^3/year (*15*). The resulting composite discharge field is a mix of observed discharge and WBM/WTM simulations where observations are not available, at a 0.5° × 0.5° resolution (latitude × longitude) for monthly climatology.

Global prehuman sediment flux. To predict the long-term fluvial discharge of sediment to the world's coastal zone, we used a drainage basin flux model (DBFM), which is based on relief, drainage area, or averaged discharge, and basin-distributed temperature (*16*). Unique solutions for each of the major climate regions (polar, temperate, and tropic) predict the flux of suspended sediment to within the uncertainties associated with global observations. Observational uncertainties can be large and may range from a factor of 2 for estimates for well-monitored rivers to an order of magnitude for poorly monitored rivers if important transport events are not captured (*16*, *17*). Measured loads may also be biased if observations fall largely within a single climate period; variations in loads between wet and dry intervals of the Pacific/North American climate pattern may vary by a factor of 5 (*18*).

To determine the prehuman sediment load of global rivers, we used the Area Relief Temperature sediment delivery model (ART) version of the INSTAAR-DBFM model (*12*, *16*). The use of the ART model as an estimator of prehuman global sediment loads is based on the following considerations. The model was trained on a global database of 340 rivers that cover 70% of the hydrologically active landmass, a majority of which are either in pristine form, or whose sediment loads were measured before the dominating impact of humans (before sediment sequestering in reservoirs, or increased sediment production from disturbance). Rivers in the database that showed large impact from human activities always fell off the line of regression between observation and prediction (*16*). On the basis of a smaller database of 145 major rivers (*19*), which were monitored across the 20th century, 48% of the rivers showed little change in their historical sediment loads, 47% showed decreasing loads caused by impoundments, and 5% showed increased sediment loads caused by disturbance. Walling and Fan (*19*) note that rivers showing little change in flux may "point to a lack of environmental change within the associated drainage basin, or at least a lack of sensitivity to ongoing changes, [or] … are buffered by the longer-term storage and remobilization of sediment within the upstream basin, associated with a relatively low sediment delivery ratio." Reductions could indicate deposition behind dams.

To test the appropriateness of using the ART model as an estimator of prehuman sediment flux, six to seven rivers from each climatic zone (polar, <0°C; cold temperate, 0° to 10°C; warm temperate, 10° to 25°C; and tropical, >25°C) were selected to be representative (small to large area, low to high relief)

Table 1. Predictions about the seasonal flux of sediment to the world's coastal zone under modern (Anthropocene) and prehuman conditions. Area, hydrologic-active drainage area with runoff >3 mm/year (global uncertainty ±7.5%) (*11*). Discharge, 35-year mean using the GRDC-WBM/WTM method of observations and predictions to determine composite runoff (global uncertainty ±15%) (*14*). Prehuman load Qs (sediment discharge), ART model predictions of fluvial long-term suspended sediment load (global uncertainty ±25%) (Fig. 1). Modern load Qs, observed suspended sediment loads where available (70% of global drainage) and QRT model predictions for the remaining 30% of world drainage, with sediment retention in large reservoirs taken into account (global uncertainty ±15%). Load retained in reservoirs, sediment flux trapped behind large reservoirs as percent of modern flux (uncertainties are ±30% of stated value). Trapping in small reservoirs increases by another 30% (global trapping of 20% would increase to 26% with small reservoirs). DJF, December January February; MAM, March April May; JJA, June July August; SON, September October November.

	Area (Mkm^2)	Discharge (km^3/year)	Prehuman load Qs (MT/year)	Modern suspended sediment load Qs					Load retained in reservoirs
				Annual (MT/year)	Seasonal percentages				
					DJF	MAM	JJA	SON	
Landmass									
Africa	20	3,800	1,310 ± 250	800 ± 100	30%	28%	22%	20%	25%
Asia	31	9,810	5,450 ± 1,300	4,740 ± 800	8%	12%	49%	31%	31%
Australasia	4	610	420 ± 100	390 ± 40	26%	27%	26%	21%	8%
Europe	10	2,680	920 ± 210	680 ± 90	29%	40%	18%	13%	12%
Indonesia	3	4,260	900 ± 340	1,630 ± 300	31%	28%	19%	21%	1%
North America	21	5,820	2,350 ± 610	1,910 ± 250	15%	24%	33%	28%	13%
Ocean islands	0.01	20	4 ± 1	8 ± 3	25%	13%	38%	25%	0%
South America	17	11,540	2,680 ± 690	2,450 ± 310	21%	32%	29%	18%	13%
Ocean basin									
Arctic Ocean	17	3,570	580 ± 120	420 ± 60	2%	20%	63%	15%	5%
Atlantic Ocean	42	18,480	3,850 ± 800	3,410 ± 420	20%	30%	27%	23%	14%
Indian Ocean	15	5,060	3,810 ± 1,020	3,290 ± 410	12%	12%	46%	30%	15%
Inland seas (endorheic)	5	400	470 ± 180	140 ± 30	13%	51%	28%	8%	30%
Mediterranean and Black Seas	8	710	890 ± 280	480 ± 60	43%	42%	9%	7%	30%
Pacific Ocean	18	10,320	4,430 ± 1,100	4,870 ± 910	18%	23%	33%	26%	26%
Climate zone									
Tropical (>25°C)	17	7,110	1,690 ± 480	2,220 ± 360	22%	17%	29%	32%	16%
Warm temperate (10–25°C)	47	21,110	9,070 ± 2,600	8,030 ± 1,250	18%	22%	35%	25%	15%
Cold temperate (0–10°C)	17	4,760	1,940 ± 250	1,460 ± 160	17%	35%	30%	19%	47%
Polar (<0°C)	24	5,560	1,330 ± 170	900 ± 120	2%	24%	58%	17%	6%
Elevation class									
High mountain (>5000 m)	21	12,500	5,120 ± 1,600	4,100 ± 740	11%	18%	44%	27%	31%
Mountain (3000–5000 m)	30	6,420	2,970 ± 610	2,190 ± 340	20%	28%	31%	21%	22%
Low mountain (1000–3000 m)	36	12,790	4,670 ± 1,030	4,800 ± 630	20%	23%	31%	25%	12%
Upland (500–1000 m)	10	3,670	910 ± 180	1,060 ± 110	24%	24%	28%	23%	4%
Lowland (100–500 m)	8	2,560	330 ± 70	360 ± 50	21%	34%	26%	19%	2%
Coastal plain (<100 m)	1	600	30 ± 10	100 ± 20	27%	40%	20%	13%	0%
Global	106	38,540	14,030	12,610	18%	23%	35%	25%	20%

and be either pristine (largely unregulated) or have observations collected before a major human disturbance (Fig. 1); for most rivers, the anthropogenic footprint increases sharply after World War II (*19*). The ART model shows no systematic bias and provides flux predictions within ±25% for these pristine or once-pristine rivers. Because the ART model, as applied here, does not take into account variability in geology, the model is not a good estimator everywhere. However, the ensemble regional estimates of landscape erosion before human influence should be reasonable.

Table 1 provides the prehuman fluxes of suspended sediment as differentiated by landmass, ocean basin or sea, climate zone, and elevation class. The global flux of sediment is 14 billion metric tons (BT, where 1 BT = 1 Tg) per year or, when a global estimate of bedload is included (*16*), 15.5 BT/year. Asia is the largest producer of fluvial sediment, followed by the Americas. The highest sediment yield (sediment load divided by drainage area) is from Indonesia and Oceania, both of which receive the most runoff (discharge divided by area). The lowest sediment yield is from the polar terrain draining into the Arctic Ocean. Warm temperate regions have the highest sediment yield as compared with other climates, and they account for nearly two-thirds of global sediment delivery. Close to 60% of global sediment delivery to the coastal zone is derived from basins draining high mountains (altitude >3000 m).

Global modern sediment flux. With the increase in human activities, much has changed in terms of sediment delivery, with variances in both directions (*19*, *20*). Changes in surface runoff affect the transport agent of the fluvial load and include aquifer mining, surface water diversion, volume changes of inland lakes, desertification, wetland drainage, soil reservoir storage, deforestation, and dam building (*15*). Although these changes are almost in balance, with 200 $km^3\ year^{-1}$ in increased runoff balanced by water retention behind artificial impoundments of 170 $km^3\ year^{-1}$, the global pattern shows large regional differences (*15*). Reservoir operations also influence the timing of runoff; for example, there is winter release for hydroelectric power generation and summer release for agricultural purposes, in contrast with the more normal spring and fall wet periods in the temperate regions of the world. To address these contemporary issues, we used the GRDC–WBM/WTM composite discharge fields that define the modern Anthropocene world (that is, the period after the Industrial Revolution).

In addition to human impacts on global runoff, there are many anthropogenic influences on global sediment yield, including urbanization, deforestation, agricultural practices, mining, and the retention of sediment by reservoirs. These changes can affect both small river systems, where human activities can overwhelm pristine conditions, and large systems such as the Mississippi, Colorado, Yellow, and Nile Rivers (*3*, *19*, *20*). The magnitude of the composite anthropogenic effect is a moving target. For example, historic land use and sediment discharge response have come full circle for the eastern seaboard of the United States, where peak fluxes occurred along with 18th-century deforestation but have returned to background conditions through reservoir construction (*21*).

To model the Anthropocene period, we merged observations (from the years 1960 to 1995) of sediment loads of rivers that drain 70% of the land surface and predictions from the Discharge Relief Temperature sediment delivery model (QRT) (*16*) for basins for which observations are missing (*12*). The QRT model is similar to the ART model in development, bias, and accuracy and also could be considered to represent pre-Anthropocene values. However, the QRT model uses discharge rather than basin area and is thus able to incorporate changes in runoff caused by humans. The QRT model also accounts for trapping of sediment in reservoirs (*22*). The load database includes observed values of sediment load both before and after damming (see Fig. 1 for reservoir influence on the Ebro, Orange, and Nile Rivers) and estimates of sediment trapping from both large and small reservoirs for the rivers ungauged for sediment flux (*22*).

Figure 2 shows the human impact on the natural sediment load estimates for 217 rivers with good observational data (before/after damming). When before-dam values are examined, the analysis indicates that the rivers are globally getting dirtier and would otherwise move more sediment to the coast if not for the impact of reservoirs. Two curves excluding the impact of reservoirs are provided: one with and one without Yellow River (Huang He) loads. The Yellow is an example of a river whose sediment load is a moving target. In the period from 1950 to 1977, the Yellow River had a load of 1.6 BT/year, which was largely related to poor farming practices on the Loess Plateau (*23*). Since the 1980s, the sediment load of the Yellow has dropped to <50% of this earlier value because of a reduced hinterland precipitation, increased water abstraction, and improved sediment control practices in the Loess region (*19*). Other curves in Fig. 2 show the impact of sediment impoundment behind reservoirs. One curve demonstrates the basin-wide trapping of suspended sediment flux by the large (> 0.5 km^3 maximum storage) reservoirs that account for about 70% of the impoundment storage volume filed with the International Commission on World Registry of Dams (*22*). Another curve highlights the impact of the millions of smaller reservoirs that have much lower trapping efficiencies because of their size but still greatly decrease the flux of sediment to the coast because of their number.

The global modern sediment flux is calculated to be 12.6 BT/year, or 10% less than the pre-Anthropocene load (Table 1). Given that large reservoirs trap 20% of the global sediment flux and small reservoirs trap another 6% (Table 1), then in a modern world without reservoirs, the global annual flux would be [(0.26 × 14 BT) + 12.6 BT] = 16.2 BT of suspended sediment, or 17.8 BT when bedload is included. This value is smaller than the 20 BT/year estimated by Milliman and Syvitski

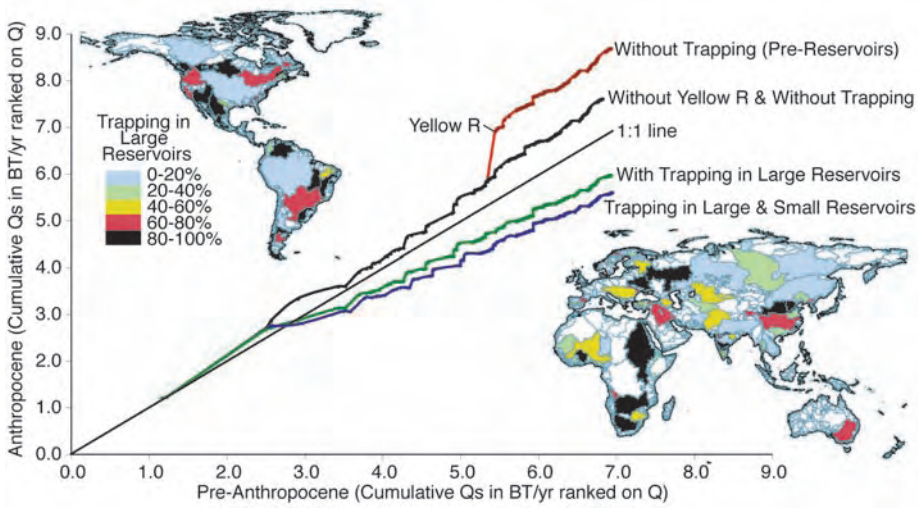

Fig. 2. Comparison between pre-Anthropocene (Fig. 1) and modern sediment loads, using 217 global rivers with good observational before- and after-dam data. Data are presented as cumulative curves ranked by decreasing river discharge (e.g., the first value to the left is the Amazon). 1:1 line represents no influence by humans. Two curves (with and without the Yellow River) had trapping by reservoirs removed and represent the increased sediment yield caused by human activity (e.g., deforestation). Two other curves show the impact of sediment sequestering in large or small reservoirs. Inserts include the global geography of basinwide trapping of sediment by large reservoirs (*22*).

(*23*), who surveyed a larger landmass in their analysis (the glaciated Arctic) and did not undertake a basin-by-basin upscaling analysis.

Africa and Asia see the largest reduction in sediment flux to the coast (Table 1 and Fig. 3) in rivers such as the Nile, Orange, Niger, and Zambezi in Africa and the Yangtze, Indus, and Yellow in Asia. Inland seas and the Mediterranean and the Black Seas, are the bodies of water most affected by reservoirs (Table 1) (*2*). The cold temperate zone encompasses the industrialized countries, where power consumption is highest, and host reservoirs that trap 47% of the regional sediment flux. As expected, mountain-draining rivers show decreased sediment fluxes on average, caused by the proliferation of impoundments (Table 1), in contrast to nonmountainous drainage basins, where sediment flux has increased (Table 1 and Fig. 3) (*24*). The tropics in general, and Indonesia in particular, are the regions most influenced by increased sediment loads (Table 1 and Fig. 3), largely because of deforestation (*25*).

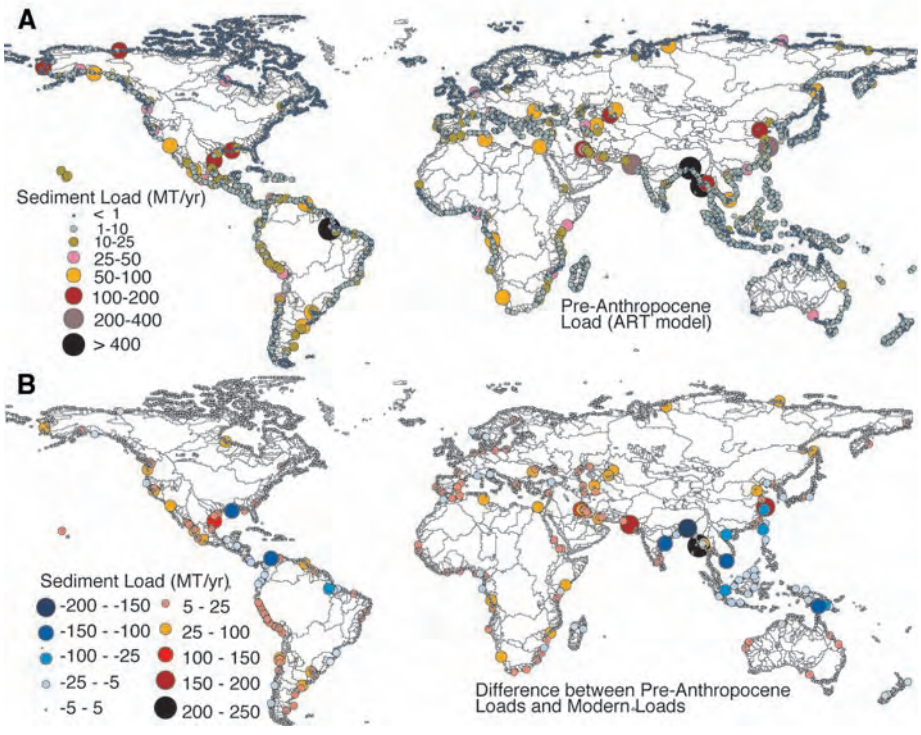

Fig. 3. (**A**) Global distribution of prehuman sediment flux, based on ART model (*12*) predictions (Fig. 1). (**B**) Differences between prehuman and modern sediment load [observations merged with QRT model predictions (*12*) accounting for anthropogenic impacts (*22*)] (Fig. 2).

Global modern seasonal sediment flux. To predict sediment discharge at the dynamic (daily) level, Morehead *et al*. (*17*) recast the classic rating curve to account for interday and interannual variability. Their PSI model successfully captures the behavior of both large and small rivers, such as the ice-melt–dominated Kliniklini River, British Columbia, Canada (*26*); the snowmelt Liard River, northern Canada (*27*); the rain-dominated Eel River, California, USA (*28*); the cyclone-dominated Lanyang River, Taiwan (*29*); and the agricultural Po River, Italy (*30*).

To apply the PSI model (*12*) to global rivers, we use the Anthropocene values of monthly discharge from the GRDC–WBM/WTM time series (1960 to 1995) and the merged observations/QRT simulations of long-term sediment load (Fig. 3). Figure 4 shows details of the result when applied to three river types. Monthly averages of the modeled discharge compare well with measured values and lie within the observed interannual variability. The Po is an exception and highlights the coarseness of the STN-30p grid, which is not able to separate two adjoining river basins (the Po and the Adige) (Fig. 4A, note 1). As a consequence, the modeled discharge is larger than observations for the Po alone. Modeled monthly averages of suspended load compare well for many rivers (e.g., the Fraser) (Fig. 4, center row) but show deviations for strongly influenced rivers. For example: (i) For the Mississippi, the modeled load is overpredicted

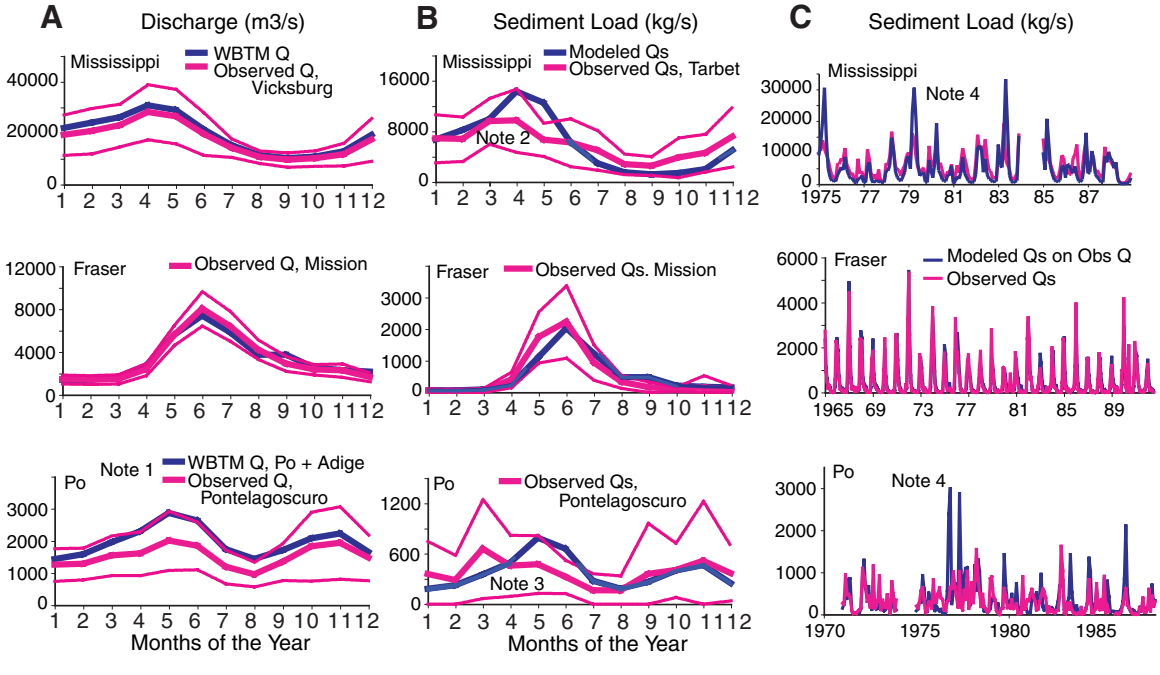

Fig. 4. Observed and modeled monthly discharge and sediment load for three river types that highlight model capabilities and problems (see text for discussion of notes). The horizontal panels represent three rivers: (Top) The 3,220,000 km^2 Mississippi, USA; (middle) the 220,000 km^2 Fraser, Canada; (bottom) the 77,000 km^2 Po, Italy. (**A**) Observed water discharge with 35-year mean ± 1 SD and the composite WBTM discharge values (*12*). (**B**) Observed sediment discharge with 35-year mean ± 1 SD and QRT-PSI model predictions (*12*). (**C**) Time series of observed monthly sediment load and QRT-PSI predictions (*12*).

in the spring and underpredicted in the fall, because the full impact of the basin's 65,000 reservoirs is not adequately captured (Fig. 4B, note 2). (ii) For the Po, the modeled load does not capture the two-dimensional effect of different water sources (for example, relatively clean water released from large Alpine reservoirs during winter months compared with the unfiltered Apennine load) (Fig. 4B, note 3). These variances are clearly seen on the time series of sediment discharge (Fig. 4C, note 4). Seasonal averages were therefore calculated to reduce these within-month variances.

To calculate the global seasonal sediment load, we applied the composite observation/WBM/WTM-QRT PSI model to produce global monthly averages of sediment loads (*12*). The monthly values are summed across March to May, June to August, September to November, and December to February, in order to produce the seasonal values (Table 1 and Fig. 5). The influence of the geographic asymmetry of the world's landmass is amplified by the patterns of the monsoonal discharge (i.e., December to April in the southern tropics versus June to October in the northern tropics), temperate discharge (winter/spring rain and snowmelt), and arctic discharge (summer rain mixed with snow and ice melt) (Fig. 5). Table 1 shows which coasts are dominated by highly seasonal fluxes of sediment and which receive more constant, albeit episodic, fluxes of material. Rivers affected by monsoons are highly seasonal in their sediment fluxes (e.g., in Indonesia and Asia). Figure 5 also depicts the east coast of the Americas, where flux patterns show similarity to global seasonal patterns but also deviations that reflect the size distribution of drainage basins relative to mountain chains and climate zones. As expected, the Arctic Ocean, polar region, and rivers draining high mountains show the largest seasonality in their sediment flux (Table 1).

Summary. This study attempts to predict the global flux of sediment on a river-by-river basis (4462 rivers >100 km^2) under modern conditions and before human influence. The method allows global hot spots to be located on a 0.5° grid of the global coast. These hot spots of high or modified sediment flux should allow coupled, dynamic, ocean-land-atmosphere models to be developed. Humans are simultaneously increasing the river transport of sediment through soil erosion activities and decreasing this flux to the coastal zone through sediment retention in reservoirs. The net result is a global reduction in sediment flux by about 1.4 BT/year over prehuman loads. This impact on coastal erosion will be further accelerated as the sea level rises, which is anticipated because of human-induced climate change (*31*). Given the modern levels of fluvial sediment loads, over 100 BT of sediment, including carbon (~1 to 3%), have been sequestered behind human-made reservoirs. Regions with more limited reservoir construction, such as Indonesia, see much of the sediment production and transported carbon buried on the surrounding continental margins. The seasonal pattern in the global delivery of sediment to the coast is displayed here and should be a valuable aid to those investigating the dynamics of nutrient fluxes to the coast and to those monitoring coastal fisheries, coral reefs, and seagrass communities.

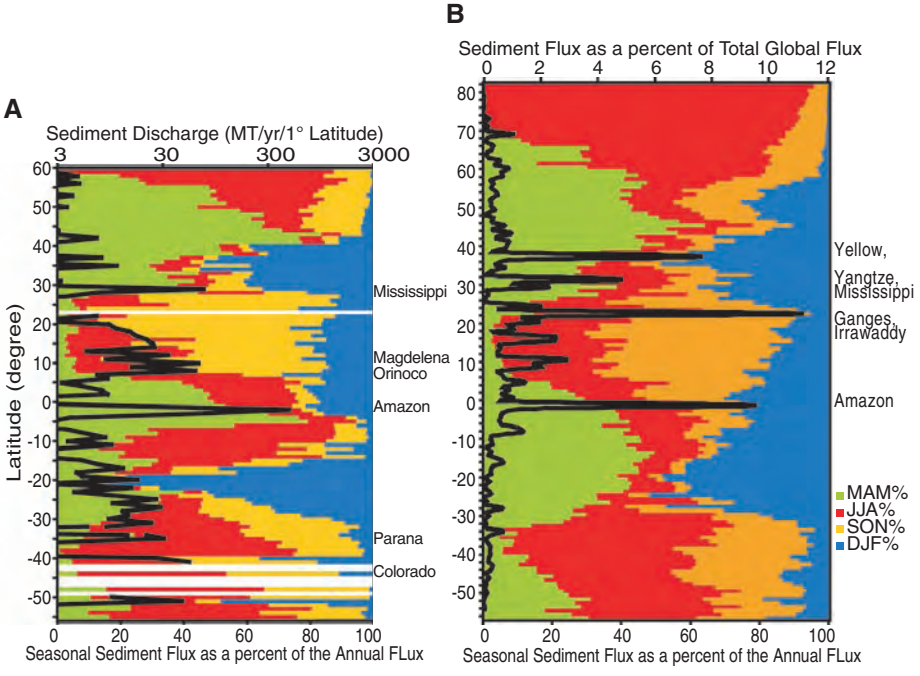

Fig. 5. Modern seasonal sediment load for global rivers. (**A**) Seasonal flux as percent of annual flux for rivers draining from the Americas into the Atlantic Ocean. Green, MAM; Red, JJA; Yellow, SON; Blue, DJF. Superimposed is the annual flux averaged across 1° of latitude, with major rivers that contribute to hot spots of sediment discharge. (**B**) Seasonal flux to the world's coastal zone, as percent of annual flux. Superimposed is the annual flux as percent of global total, averaged across 1° of latitude, with major rivers that contribute to hot spots of sediment discharge.

References and Notes

1. J. E. Cohen *et al.*, *Science* **278**, 1209 (1997).
2. C. Liquete, M. Canals, P. Arnau, R. Urgeles, X. Durrieu de Madron, *Oceanography* **17**, 70 (2004).
3. J. P. M. Syvitski, *Global Planet. Change* **39**, 1 (2003).
4. E. Wolanski, S. Spagnol, *Reg. Environ. Change* **1**, 152 (2000).
5. C. J. McLaughlin, C. A. Smith, R. W. Buddemeier, J. D. Bartley, B. A. Maxwell, *Global Planet. Change* **39**, 191 (2003).
6. J. D. Restropo, P. Zapata, J. M. Diaz, J. Garzon-Ferreira, C. B. Garcia, *Global Planet. Change*, in press.
7. S. V. Smith, W. H. Renwick, R. W. Buddemeier, C. J. Crossland, *Global Biogeochem. Cycles* **15**, 697 (2001).
8. G. Marmulla, Ed., *Dams, Fish and Fisheries, Opportunities, Challenges and Conflict Resolution. FAO Fisheries Tech. Paper* 419 [Food and Agriculture Organization (FAO) of the United Nations, Rome, 2001].
9. J. P. M. Syvitski, D. C. Burrell, J. M. Skei, *Fjords: Processes & Products* (Springer, New York, 1987).
10. C. J. Vörösmarty, B. M. Fekete, M. Meybeck, R. Lammers, *Global Biogeochem. Cycles* **14**, 599 (2000).
11. B. M. Fekete, C. J. Vörösmarty, W. Grabs, *Global, Composite Runoff Fields Based on Observed River Discharge and Simulated Water Balances* (Report No. 22, GRDC, Koblenz, Germany, ed. 2, 1999).
12. Materials and methods are available as supporting material on *Science* Online.
13. The World Meteorological Organization GRDC archive is available online at http://grdc.bafg.de.
14. S. Hagemann, L. Dümenil, *Clim. Dyn.* **14**, 17 (1998).
15. C. J. Vörösmarty, D. Sahagian, *Bioscience* **50**, 753 (2000).
16. J. P. M. Syvitski, S. D. Peckham, R. D. Hilberman, T. Mulder, *Sediment. Geol.* **162**, 5 (2003), and erratum, *Sediment. Geol.* **164**, 345 (2004).
17. M. D. Morehead, J. P. M. Syvitski, E. W. H. Hutton, S. D. Peckham, *Global Planet. Change* **39**, 95 (2003).
18. D. L. Inman, S. A. Jenkins, *J. Geol.* **107**, 251 (1999).
19. D. E. Walling, D. Fan, *Global Planet. Change* **39**, 111 (2003).
20. J. A. Dearing, R. T. Jones, *Global Planet. Change* **39**, 147 (2003).
21. G. B. Pasternak, G. S. Brush, W. B. Hilgartner, *Earth Surf. Processes Landforms* **26**, 409 (2001).
22. C. J. Vorosmarty *et al.*, *Global Planet. Change* **39**, 169 (2003).
23. J. D. Milliman, J. P. M. Syvitski, *J. Geol.* **100**, 525 (1992).
24. I. Douglas, in *The Earth as Transformed by Human Action*, B. L. Turner *et al.*, Eds. (Cambridge Univ. Press, Cambridge, 1993), pp. 215–234.
25. D. Hu, Y. Saito, S. Kempe, in *Asian Change in the Context of Global Climate Change: Impact of Natural and Anthropogenic Changes in Asia on Global Biogeochemical Cycles*, J. N. Galloway, J. M. Melillo, Eds. (IGBP Publication Series 3, Cambridge Univ. Press, Cambridge, 2001), pp. 245–270.
26. M. D. Morehead, J. P. M. Syvitski, E. W. H. Hutton, *Global Planet. Change* **28**, 107 (2001).
27. J. P. M. Syvitski, *Polar Res.* **21**, 323 (2002).
28. J. P. M. Syvitski, M. D. Morehead, *Mar. Geol.* **154**, 13 (1999).
29. J. P. M. Syvitski, A. J. Kettner, S. D. Peckham, S.-J. Kao, *J. Coastal Res.*, in press.
30. J. P. M. Syvitski, A. J. Kettner, A. Correggiari, B. W. Nelson, *Mar. Geol.*, in press.
31. J. P. M. Syvitski *et al.*, *LOICZ: Coastal Change and the Anthopocene*, C. Crossland, Ed. (Springer, New York, in press).

32. We thank the Office of Naval Research and NASA (IDS/NNG04GH75G) for financially supporting this investigation and IGBP, LOICZ, and Global Water System Project scientists for supporting workshops and discussions that led to this analysis.

Supporting Online Material

www.sciencemag.org/cgi/content/full/308/5720/376/DC1
Materials and Methods
References

6 January 2005; accepted 17 March 2005
10.1126/science.1109454

An Epidermal Barrier Wound Repair Pathway in *Drosophila* Is Mediated by *grainy head*

Kimberly A. Mace,* Joseph C. Pearson, William McGinnis†

We used wounded *Drosophila* embryos to define an evolutionarily conserved pathway for repairing the epidermal surface barrier. This pathway includes a wound response enhancer from the *Ddc* gene that requires *grainy head* (*grh*) function and binding sites for the Grh transcription factor. At the signaling level, tyrosine kinase and extracellular signal–regulated kinase (ERK) activities are induced in epidermal cells near wounds, and activated ERK is required for a robust wound response. The conservation of this Grh-dependent pathway suggests that the repair of insect cuticle and mammal skin is controlled by an ancient, shared control system for constructing and healing the animal body surface barrier.

Animals have evolved biological armor, an epidermally derived integument, to protect their bodies from physical injury and dehydration and have evolved control pathways to regenerate this barrier after wounding. A key component of this barrier in mammals is the stratum corneum of the skin, and a key component of the barrier in insects is the cuticle. In invertebrates, the immediate barrier response to wounding involves the formation of a temporary plug at wound sites, along with the activation of melanization and cross-linking enzymes that encapsulate invading microbes and help seal wound openings (*1*–*3*). In vertebrates, the immediate humoral response to vascular wounding results in the activation of proteases leading to the formation of a fibrin clot to help seal wound openings (*4*).

In both invertebrates and vertebrates, introducing infectious microbes through wounds results in the induction of the innate immune pathways (*5*). In two branches of these pathways, Toll-family transmembrane receptors or Imd-dependent signals trigger a signaling cascade that allows transcription factors from the NF-κB family to enter the nucleus, where they directly activate the transcription of genes that provide a first line of defense against pathogens (*5*–*7*).

Another response to epithelial wounds is mediated by wound healing pathways that re-epithelialize the breach (*8*). Genes that are required for regenerating the epithelial sheet after laser-induced or mechanically induced wounds in the *Drosophila* epidermis include those encoding Rho, Cdc42, and Jun N-terminal kinase (JNK) (*3*, *9*, *10*). Additional *Drosophila* genes have been implicated in the process of epithelial repair by means of their requirement for epidermal dorsal closure during late embryogenesis. These include genes encoding the *Drosophila* Jun and Fos transcription factors as well as Dpp, Ras, and Puckered (*11*, *12*). Homologs of most of these proteins, in addition to many others, are associated with the process of epithelial regeneration in vertebrates (*8*, *11*, *13*, *14*).

By comparison, the genetic pathways that respond to aseptic breaks in the barrier integument and provide for its regeneration are poorly understood. Although the integuments of both mammals and insects depend on a dense, highly cross-linked matrix of proteins and other macromolecules, heretofore there has been no reason to suspect common genetic control pathways in the repair of mammal skin and insect cuticle.

Ectopic sclerites in *Hox* or *spen* mutants correlate with loss of epidermal integrity. *Drosophila* embryos that lack all *Hox* gene function in a body region, or that are mutant for the *Hox*-interacting gene *spen*, develop ectopic sclerites (hard, melanized cuticular structures) in the trunk of first instar larvae (*15*–*18*). These sclerites were proposed to be ectopic head skeleton, but we observed that the sclerites in these mutant larvae often looked like the cuticular scar tissue that often surrounds the healed hole generated by a sterile needle in late-stage embryos (Fig. 1, B to D).

We therefore tested whether the sclerites observed in *spen* or *Scr Antp* double-mutant larvae were associated with breaks in the epidermal integument. To assay this, we injected rhodamine-labeled dextran into the perivitelline space of stage 17 wild-type, *spen* mutant, and *Scr Antp* mutant embryos. As a positive control, we injected rhodamine-dextran directly into the body cavity of a wild-type embryo (Fig. 1H). We observed that the fluorescent dye penetrated the body cavity of *spen* mutant (Fig. 1F) and *Scr Antp* double-mutant (Fig. 1G) embryos but not control wild-type embryos (Fig. 1E). We conclude that there are localized failures of epidermal integrity in late-stage embryos that lack the function of *spen* or both *Scr* and *Antp*.

Sclerotization genes are rapidly activated near aseptic wound sites in late embryos. Next, we tested whether two genes required for normal cuticular sclerotization were activated in the wound regions that developed scars. The genes were *Ddc*, which encodes dopa decarboxylase, and *pale* (*ple*), which encodes tyrosine hydroxylase. These proteins contribute to the formation of the larval and adult cuticular skeleton in epithelial cells through the production of catecholamines that are converted to quinones by phenol oxidases (*19*). The reactive quinones then cross-link protein polymers and chitin polymers to generate the largely impermeable integument of insects (*20*). First instar larvae that are doubly mutant for *Ddc* and *ple* have almost no melanization and sclerotization of the head skeleton (Fig. 2, A and B). A key

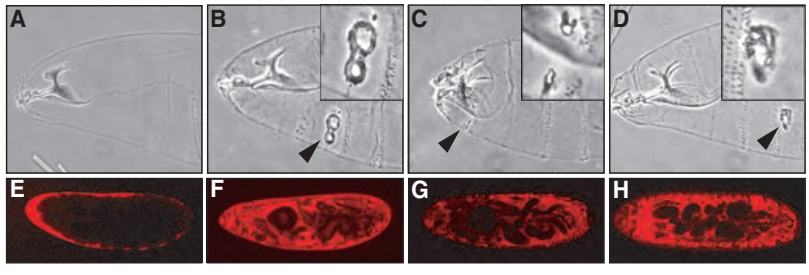

Fig. 1. *spen* mutants and *Scr Antp* double mutants have defective epidermal integrity. Cuticle preparations showing the position of normal and ectopic sclerites in (**A**) a wild-type embryo, (**B**) a *spen* mutant embryo, (**C**) a *Scr Antp* double-mutant embryo, and (**D**) an aseptically injured wild-type embryo. Insets are enlargements of sclerites indicated by the arrowheads. At 17 to 19 hours after egg lay, rhodamine-dextran was injected into the perivitelline space of (**E**) wild-type embryos, (**F**) *spen* mutant embryos, or (**G**) *Scr Antp* double-mutant embryos; or (**H**) directly through the epidermal layer of wild-type embryos. Red stain in the body cavity indicates the presence of breaks in the epidermis.

Section of Cell and Developmental Biology, Division of Biology, University of California, San Diego, La Jolla, CA 92093, USA.

*Present address: Surgical Research Laboratory, University of California, San Francisco, CA 94143–1302, USA.

†To whom correspondence should be addressed. E-mail: wmcginnis@ucsd.edu

regulatory step in the localized deposition of hard, dark cuticle is exerted at the transcriptional level of these genes, given that the hard skeleton–producing cells of the late embryo and early larva accumulate abundant *Ddc* and *ple* transcripts (Fig. 2, C and D).

In aseptically wounded late embryos, transcripts from both *Ddc* and *ple* accumulate to high levels in the epidermal cells near the wound site (Fig. 2, E and F). Transcripts from these genes can be detected within 30 min after injury (*21*), suggesting that these genes are direct targets of a wound-induced signal transduction pathway. Transcription of *Ddc* and *ple* is also abundant in the defective epidermal regions that develop sclerotic scar tissue in *spen* mutants and *Scr Antp* double mutants (Fig. 2, G to J). Control in situ hybridizations were done to eliminate the possibility that the increased *Ddc* and *ple* signals at wound sites were an accessibility artifact in late embryos (*21*).

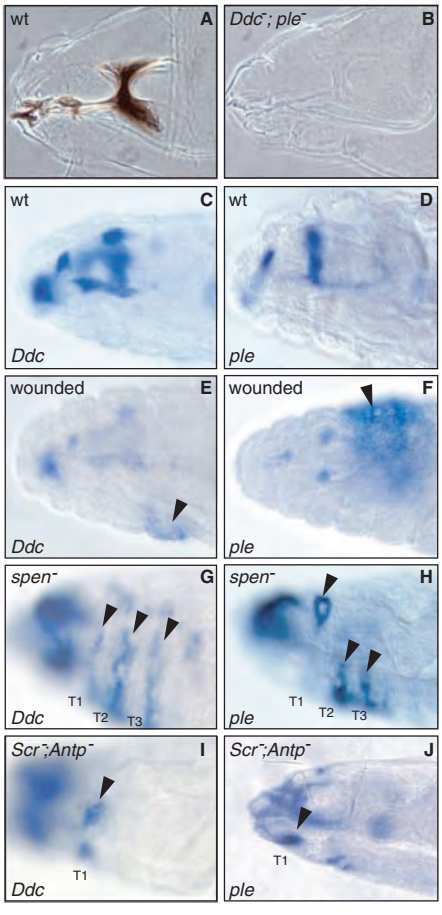

Fig. 2. *Ddc* and *ple* are transcriptionally activated where sclerotized structures develop. Cuticle preparations are shown for (**A**) wild-type (wt) first instar larva and (**B**) *Ddc; ple* double-mutant larva. The rest of the panels show localization of *Ddc* and *ple* RNA with in situ hybridization (*21*) in wild-type embryos (**C** and **D**), aseptically wounded wild-type embryos (**E** and **F**), *spen* mutant embryos (**G** and **H**), and *Scr Antp* double-mutant embryos (**I** and **J**). Arrowheads show ectopic *Ddc* or *ple* transcripts surrounding puncture wounds or epidermal breaks in stage 17 embryos. T1, T2, and T3 mark the first, second, and third thoracic segments, respectively.

A wound response regulatory element upstream of the *Ddc* transcriptional start. To dissect transcriptional regulatory inputs involved in the activation of epidermal wound response genes, we first analyzed the regulatory regions of *Ddc* (*22*, *23*). We began by testing the expression pattern provided by a 7.5-kb segment of DNA that included a hemagglutinin-tagged *Ddc* protein coding sequence (Fig. 3A). This 7.5-kb region provides the normal *Ddc* expression pattern during embryogenesis (Fig. 3B shows the head skeletal pattern) and is also activated near wound sites in late-embryonic epidermal cells (Fig. 3, C and D).

Deletion analyses of lacZ and/or green fluorescent protein (GFP) reporter constructs fused to the *hsp70* basal promoter show that sequences between –1.4 kb to the *Ddc* transcription start are sufficient for a wound response, but sequences from –381 base pairs (bp) to the transcription start are not (Fig. 3, A, E, and F). The –1.4-kb *Ddc*-GFP reporter is activated over many cell diameters near wound sites (Fig. 3G), and the extent of activation increases with larger wounds and longer incubations after injury. The graded nature of the response (Fig. 3G) suggests that a signal is produced at the injury boundaries that activates the wound response enhancer in a dose-dependent fashion in nearby epidermal cells. We also tested the –1.4-kb *Ddc*-GFP reporter (Fig. 3A) in *Scr Antp* double-mutant embryos and found that the wound response reporter is activated in regions where cuticular scars develop (Fig. 3H). Similar results were obtained in *spen* mutants.

Response of the –1.4-kb *Ddc* wound response enhancer in mutants for the NF-κB and AP-1 pathways. To determine whether the aseptic wound response pathway (as defined by the *Ddc* wound response enhancer) and the infectious wound response pathways overlapped, we tested for activation of the –1.4-kb *Ddc*-GFP wound response reporter after aseptic wounding of zygotic mutants of the innate immunity signaling pathway genes *Toll*, *tube*, *imd*, and *18-wheeler* as well as in zygotic mutants of the innate immunity transcription factor genes *rel*, *Dif*, and *Dl* (*Dl* and *Dif* were tested as a double-mutant combination). In all of these mutant backgrounds, the –1.4-kb *Ddc*-GFP reporter was activated near wounds, as it was in wild-type embryos. We also tested *Toll* maternal/zygotic

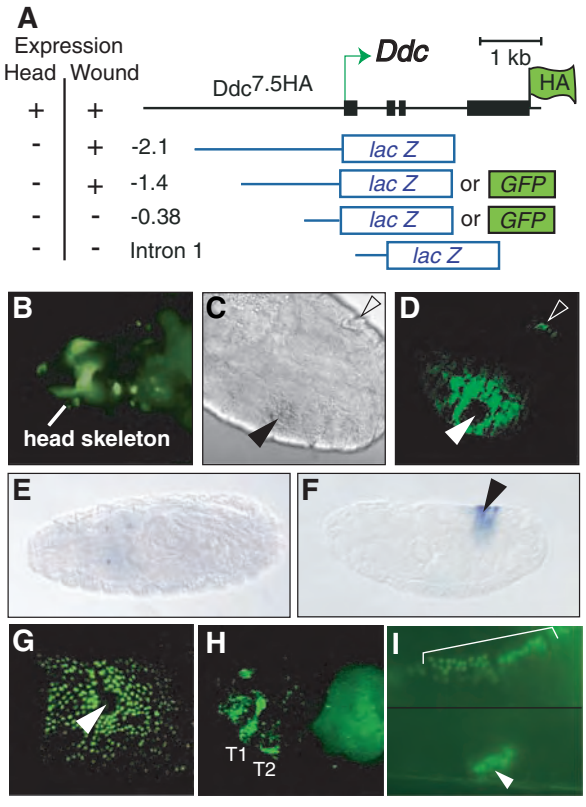

Fig. 3. The region between –1.4 and –0.38 kb of the *Ddc* transcription start site functions as a wound response enhancer. (**A**) Diagram of the *Ddc* locus and the reporter constructs used to identify embryonic transcriptional activation functions. A summary of the expression patterns seen with each *Ddc* regulatory construct is shown to the left of each construct: +, expression; –, no expression. (**B**) Immunofluorescent detection of the hemagglutinin (HA) tag in an embryo carrying the $Ddc^{7.5HA}$ transgene showing normal *Ddc* head skeleton expression (*21*). (**C**) Nomarski image of an aseptically wounded stage 17 $Ddc^{7.5HA}$ embryo. Black and open arrowheads indicate entry and exit wounds, respectively. (**D**) Anti-HA stain of the embryo in (C), showing wound response activation of the $Ddc^{7.5HA}$ transgene. (**E**) Unwounded embryo carrying the –1.4-kb *Ddc-lacZ* reporter, hybridized to detect *lacZ* transcripts (*21*). (**F**) Aseptically wounded embryo carrying the –1.4-kb *Ddc-lacZ* reporter, hybridized to detect *lacZ* transcripts. Black arrowhead, entry wound. (**G**) Closeup of an aseptically wounded embryo carrying the –1.4-kb *Ddc*-GFP reporter (*21*), showing GFP expression in a gradient surrounding the entry wound (white arrowhead). (**H**) *Scr Antp* mutant embryo carrying the –1.4-kb *Ddc*-GFP reporter, showing GFP expression in the first and second thoracic segments (T1 and T2). (**I**) JNK mutant *bsk* with –1.4-kb *Ddc*-GFP reporter; bracket denotes arrested dorsal leading edge of epidermis. Jun mutant *Jra* and Fos mutant *kay* with the same wound reporter show identical staining pattern as *bsk* mutants (*24*).

mutants and *tube* maternal/zygotic mutants, and we observed activation of the wound response reporter at the breaks in the epidermal integument that occur in these mutants. Additional evidence that the *Toll* and *imd* pathways are not required to activate the *Ddc* wound response enhancer is reported in the supporting online material (*21*).

Previous studies have indicated that the JNK pathway is required for the process of wound healing in embryos and adults (*9*–*12*). We found that the –1.4-kb *Ddc*-GFP wound response reporter is still activated at aseptic wound sites of zygotic mutants in either *Drosophila* JNK (Fig. 3I), Jun, or Fos (*24*) and is also activated in cells at and near the dorsal epidermal leading edge "wound boundaries" (brackets in Fig. 3I) that form when dorsal closure fails in these mutant backgrounds. The wound response reporter is not activated in dorsal epidermal leading edge cells in wild-type embryos. We conclude that the zygotic functions of JNK, Jun, and Fos are dispensable for the activation of the –1.4-kb *Ddc* wound response reporter, even in the cells where the zygotic functions of these genes are required for the migration and sealing of epithelial cell sheets during dorsal closure.

***grainy head* is required for activation of the *Ddc* wound response enhancer.** The *Drosophila grainy head* (*grh*) gene encodes two major transcription factor isoforms (Grh-N and Grh-O). Grh-N is expressed in regions of the central nervous system, whereas Grh-O is expressed in barrier epithelia such as the embryonic epidermis, the foregut, the hindgut, and the tracheal system (*25*, *26*). Zygotic mutants in *grh* die at the embryonic/larval transition with weak epidermal cuticle, malformed head skeletons that are composed of discontinuous grainy sclerites, and abnormal tracheal trunks (*26*–*29*). Clones of *grh* mutant cells in the adult epidermis have defects in pigmentation, cell polarity, and epidermal hair differentiation (*30*).

The similarity of the *grh* mutant phenotype to *Ddc* and *ple* mutants prompted us to test whether *grh* function is required for activation of –1.4-kb *Ddc* wound response element, which has two evolutionarily conserved Grh binding sites (Fig. 4A). In aseptically wounded *grh* mutant embryos, the –1.4-kb *Ddc* wound response reporter is at most weakly activated in a few cells immediately adjacent to the wound border (Fig. 4B). This is consistent with the abnormal wound healing in *grh* mutant larval cuticle (Fig. 4, E and F). When compared with wild-type wounds, the *grh* mutant wound sites are deficient in normal cuticle regeneration, as well as in displacement of the melanized plug that forms immediately after wounding (*3*). A similar phenotype is seen in wounded *Ddc* mutants, although the remaining plug is less melanized (Fig. 4G).

Grh and CREB/AP-1–like consensus binding sites are required for the function of *Ddc* wound response enhancers. The −1.4-kb *Ddc* wound response enhancer has consensus transcription factor binding sites for Grh, NF-κB/Rel proteins, adenosine 3′,5′-monophosphate response element–binding protein (CREB)–A proteins, and AP-1–like/basic-leucine zipper proteins (Fig. 4A), which we believed were candidate sites required for the function of the wound response enhancer. Transgenic embryos for the –1.4-kb *Ddc*-GFP reporter with point mutations in the six consensus sites for NF-κB family proteins (fig. S1) showed normal wound-induced activation (*24*), whereas a similar reporter with point mutations in the single CREB-A and the three AP-1–like consensus sites showed a marked reduction in wound-induced activation compared with wild-type reporter controls (Fig. 4C).

Further deletion analyses define a minimal *Ddc* epidermal wound response element from –472 bp to the start of transcription, in which sequences from –472 to –381 bp are required for wound response function (Fig. 4, A and D). The –0.47-kb *Ddc* wound response element from *D. melanogaster* has only five blocks of marked sequence conservation (a perfect match of 6 bp or greater; fig. S1) with a *D. virilis Ddc* promoter proximal fragment from base pairs –392 to +13, which provides a wound response when attached to reporter genes in *D. melanogaster* embryos (Fig. 4, A and H). The blocks of sequence conservation are each 12 to 13 bp and they include one Grh site, one AP-1 consensus site, one ETS consensus site, a GGGGGATT motif (which overlaps with one of the NF-κB consensus sites), and the TATA box region (fig. S1). In *D. melanogaster*, the conserved GGGGGATT motif, AP-1–like site, and ETS site are all within the interval of –472 to –381 bp that is required for wound response function. The conserved Grh site, which is closer to the promoter, is required for the –472-bp element function, given that its mutation abolished wound response reporter activation (Fig. 4, A and I).

To identify potential wound response enhancers at the *D. melanogaster ple* gene, we scanned the sequences from 10 kb upstream to 10 kb downstream of the *ple* transcription start for clusters of evolutionarily conserved Grh, AP-1, ETS, and GGGGGATT sites and selected two regions. One is a 3.0-kb DNA fragment beginning 2.9 kb upstream of the *ple* transcription start, which contains two Grh sites, two AP-1 sites, four ETS sites, and three GGGGGATT sites (fig. S2). The second is a 995-bp fragment just upstream of the *ple* transcription start, which conserves one Grh, one AP-1, and three ETS sites but no GGGGGATT motif (fig. S3). We tested both fragments in red fluorescent protein (DsRed) reporter constructs (*31*) and

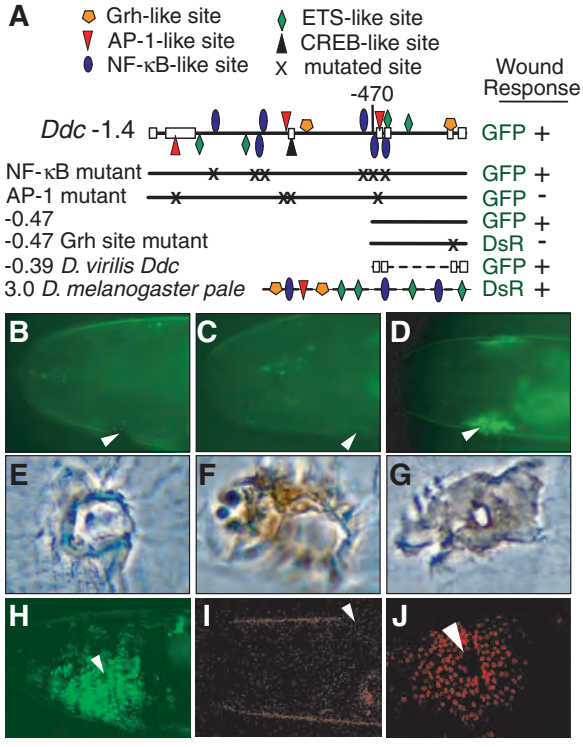

Fig. 4. Analysis of *Ddc* and *ple* wound response enhancers. (**A**) Schematic of *Ddc* and *ple* reporter constructs. Sequence blocks conserved between *D. melanogaster*, *D. pseudoobscura*, and *D. virilis* (figs. S1 and S2) are indicated by white blocks on construct –1.4, as are consensus Grh (orange pentagons), CREB (black triangle), AP-1–like (red triangles), NF-κB (blue ovals), and ETS sites (green diamonds). Mutated consensus sites are indicated by X's on the pertinent constructs, and a summary of the reporter response to aseptic wounding is shown in the column to the right of the construct. (**B** to **D**) GFP reporter expression patterns after aseptic wounding (arrowheads indicate wound sites) of stage 17 embryos with the following genotypes: (B) *grh* mutant with the –1.4-kb *Ddc*-GFP construct; (C) wild-type embryo with the –1.4 kb $^{mutAP\text{-}1\text{-}like}$*Ddc*-GFP construct, which has one CREB and three AP-1 consensus sites mutated (*21*); and (D) wild-type embryo with the –0.47-kb *Ddc*-GFP construct, the smallest sequence sufficient for a wound response. (**E** to **G**) Cuticle surrounding wound sites in representative early first instar larvae after wounding with a sterile micropipette at embryonic stage 17 (*21*) (E) wild-type embryo, (F) *grh* mutant, (G) *Ddc* mutant (*21*). (**H**) Wild-type embryo with the *D. virilis* –392-bp *Ddc*-GFP wound response enhancer (fig. S1). (**I**) Wild-type embryo with the –0.47-kb *Ddc*-GFP construct in which the Grh binding site is mutated (fig. S1). (**J**) Wild-type embryo with the *ple* 3.0-kb wound response enhancer (fig. S2).

found that the 3.0-kb *ple* fragment robustly activates reporter expression around aseptic wounds (Fig. 4, A and J), whereas the 995-bp fragment shows a very weak and slow response (*24*).

Activation of ERK-MAP kinase is required for robust wound enhancer function. The involvement of mitogen-activated protein (MAP) kinases in epithelial injury response (*32*) prompted us to test for receptor tyrosine kinase or MAP kinase activation in cells that induce wound response enhancers. Using antibodies directed against phosphotyrosine (p-Tyr), we found an increase in p-Tyr staining in the cells near aseptic wounds (Fig. 5B), as well as in the wounded thorax of *spen* mutants (Fig. 5C), when compared with controls (Fig. 5A). This increase in p-Tyr correlates well with cells that activate the –1.4-kb *Ddc*-GFP wound response construct (green), although at the times we could test for both (2 hours postwounding), some cells showed activation of the wound response enhancer without a detectable increase in p-Tyr.

To assay MAP kinase pathway activation near embryonic wound sites, we used antibodies that detect the active, dually phosphorylated form of ERK (dpERK). As shown in Fig. 5, D to F, there is an increase in activated ERK surrounding embryonic wound sites. ERK activation is detected within 30 min after aseptic injury, with a variable extent of activation. In *grh* mutant embryos, increased dpERK staining was still detected at wound sites (Fig. 5G), suggesting that dpERK is upstream of, or acting in parallel to, Grh in the barrier wound response pathway. Control antibody stains (*21*) were done to eliminate the possibility that the increased pTyr and dpERK staining at wound sites was an accessibility artifact.

Mutant alleles that eliminate ERK function in embryos but still develop into first instar larvae are not currently available. To test whether activated ERK is required for the wound response, we injected PD98059, a MAP kinase kinase (MEK) inhibitor that reduces the phosphorylation and activation of the ERK-MAP kinase (*21*), into the perivitelline space of late-stage embryos carrying the –1.4-kb *Ddc*-GFP wound response reporter. After a 45-min incubation, the embryos were aseptically wounded, and 4 hours later they were assayed for activation of the wound response reporter (*21*). Compared with controls (Fig. 5H), the activation of the *Ddc* wound response reporter was less frequent and at lower levels (*21*) in the PD98059-treated embryos (Fig. 5I).

Discussion. We provide evidence for a wound response pathway that senses aseptic breaks in the barrier epidermis of *Drosophila* embryos. A minimal 472-bp *Ddc* wound response enhancer requires a Grh protein binding site and the function of the *grh* gene, and all of the naturally evolved *Drosophila Ddc* or *ple* wound response enhancers we tested contain evolutionarily conserved consensus binding sites for Grh, ETS, and AP-1 transcription factors, as well as GGGGGATT sequence motifs (Fig. 5J and figs. S1 and S2) (*21*). Robust induction of *Ddc* wound response reporters also requires activated ERK kinase, which may transduce the wound signal to Grh, given that Grh protein can be phosphorylated by ERK in vitro (*33*). The signaling pathway components that lead to activation of the Grh-mediated wound response need further investigation, because the molecules that sense breaks in the epithelial integument and transmit this information to the *Ddc* wound enhancer in adjacent cells are still unknown.

A major biological role of the Grh-mediated activation of *Ddc* and *ple* near *Drosophila* wounds is apparently to provide the abundant cross-linking molecules that repair and replace the cuticular barrier. This integument repair process is apparently often too vigorous at the borders of cuticular wound sites, resulting in scars (Fig. 1). Larvae that do not rapidly repair the integument as a result of the absence of phenol oxidase in the cuticle and epidermis (*3*, *34*) die rapidly from blood loss (*3*).

The expression patterns and functions of structural orthologs of the *grh* gene in other species are consistent with the evolutionary conservation of this barrier wound response pathway. The *C. elegans* genome encodes an ortholog of the *Drosophila* Grh protein called Ce-GRH-1 (*35*). Depletion of Ce-GRH-1 function with RNA interference results in larvae with fragile epidermal cuticle, similar to the larval cuticle phenotype of *Drosophila grh* mutants. There are three mouse orthologs of *grh*, which are expressed abundantly in developing epithelial cells (*36*–*39*). Interestingly, in a study complementary to ours, a mutation in one of the mouse *grh* orthologs, *Grainy head–like 3* (*Grhl-3*), results in embryos with defective epidermal wound repair (*40*). Grhl-3 function is also required in developing embryos for the epidermal expression of *Transglutaminase 1*, which is required for epidermal protein barrier cross-linking, similar to *Ddc* and *ple* in flies. Thus, although *grh* orthologs are required for a diverse set of functions in animal epithelial cells, one evolutionarily conserved function in mice and flies is a *grh* requirement for transcriptional activation of epidermal barrier cross-linking genes, and the regeneration of an epidermally derived barrier after wounding. The ability to study a conserved barrier wound response pathway with *Drosophila* genetics may provide new insight into wound healing pathways in mammals.

Our evidence indicates that activation of the *Drosophila Ddc* wound response enhancer does not require the zygotic functions of either the signaling proteins and transcription factors that mediate the response to septic injury, or the JNK pathway that mediates re-epithelialization of wounds. However, our current assays of embryonic wound response enhancers are only

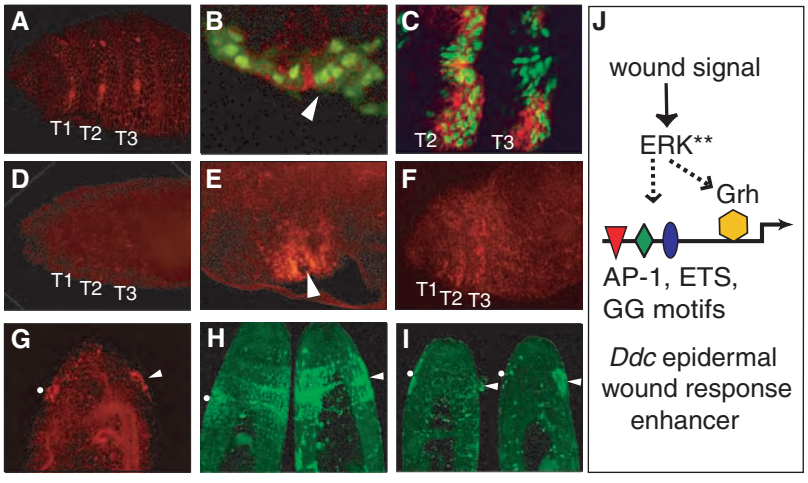

Fig. 5. Phosphotyrosine and diphospho-ERK (dpERK) concentrations are increased surrounding wound sites in wild-type or *spen* mutant embryos. Anti–p-Tyr staining (red) in (**A**) unwounded wild-type embryos carrying the –1.4-kb *Ddc*-GFP construct, (**B**) aseptically wounded embryos with the –1.4-kb *Ddc*-GFP construct (green, wound response enhancer expression), and (**C**) *spen* mutant embryos with the –1.4-kb *Ddc*-GFP construct. Anti-dpERK staining in (**D**) unwounded wild-type embryo, (**E**) aseptically wounded wild-type embryo, and (**F**) *spen* mutant embryo. (**G**) *grh* mutant embryo, wounded and stained for dpERK. (**H**) Two wounded embryos with the –0.47-kb *Ddc*-GFP construct that were treated only with 1% dimethyl sulfoxide. (**I**) Two wounded embryos with the –0.47-kb *Ddc*-GFP construct, treated with 100 μM PD98059 (MEK inhibitor) in 1% dimethyl sulfoxide (*21*). T1, T2, and T3, thoracic segments; white arrowheads, aseptic entry wounds; white dots, exit wounds. (**J**) Model of the epidermal barrier wound response pathway in *Drosophila* epidermal cells. A wound signal (unknown) activates ERK, which may signal through modification of Grh or another required factor (dotted lines). Evidence from mutagenesis and evolutionary comparison indicates that sequence motifs TGANTCA (AP-1), CMGGAW (ETS), and GGGGGATT (GG) are also important for barrier wound response enhancers.

qualitative, and it is still possible that these pathways have a quantitative influence on the epidermal barrier wound response.

References and Notes

1. A. J. Nappi, E. Ottaviani, *Bioessays* **22**, 469 (2000).
2. H. G. Boman, D. Hultmark, *Annu. Rev. Microbiol.* **41**, 103 (1987).
3. M. J. Galko, M. A. Krasnow, *PLoS Biol.* **2**, E239 (2004).
4. P. N. Walsh, S. S. Ahmad, *Essays Biochem.* **38**, 95 (2002).
5. J. A. Hoffmann, J. M. Reichhart, *Nat. Immunol.* **3**, 121 (2002).
6. S. Thoma-Uszynski *et al.*, *Science* **291**, 1544 (2001).
7. N. Silverman, T. Maniatis, *Genes Dev.* **15**, 2321 (2001).
8. P. Martin, *Science* **276**, 75 (1997).
9. W. Wood *et al.*, *Nat. Cell Biol.* **4**, 907 (2002).
10. M. Ramet, R. Lanot, D. Zachary, P. Manfruelli, *Dev. Biol.* **241**, 145 (2002).
11. A. Jacinto, A. Martinez-Arias, P. Martin, *Nat. Cell Biol.* **3**, E117 (2001).
12. L. Kockel, J. G. Homsy, D. Bohmann, *Oncogene* **20**, 2347 (2001).
13. S. Werner, R. Grose, *Physiol. Rev.* **83**, 835 (2003).
14. G. Li *et al.*, *Dev. Cell* **4**, 865 (2003).
15. E. B. Lewis, *Nature* **276**, 565 (1978).
16. G. Struhl, *J. Embryol. Exp. Morphol.* **76**, 297 (1983).
17. A. Macias, G. Morata, *EMBO J.* **15**, 334 (1996).
18. E. L. Wiellette *et al.*, *Development* **126**, 5373 (1999).
19. T. R. Wright, *J. Hered.* **87**, 175 (1996).
20. J. Schaefer *et al.*, *Science* **235**, 1200 (1987).
21. Materials and methods are available as supporting material on *Science* Online.
22. S. B. Scholnick, S. J. Bray, B. A. Morgan, C. A. McCormick, J. Hirsh, *Science* **234**, 998 (1986).
23. L. Chen *et al.*, *MOD* **114**, 95 (2002).
24. K. A. Mace, J. C. Pearson, W. McGinnis, data not shown.
25. S. J. Bray, F. C. Kafatos, *Genes Dev.* **5**, 1672 (1991).
26. A. E. Uv, E. J. Harrison, S. J. Bray, *Mol. Cell. Biol.* **17**, 6727 (1997).
27. C. Nusslein-Volhard, E. Wieschaus, H. Kluding, *Rouxs Arch. Dev. Biol.* **193**, 267 (1984).
28. S. Ostrowski, H. A. Dierick, A. Bejsovec, *Genetics* **161**, 171 (2002).
29. J. Hemphala, A. Uv, R. Cantera, S. Bray, C. Samakovlis, *Development* **130**, 249 (2003).
30. H. Lee, P. N. Adler, *Mech. Dev.* **121**, 37 (2004).
31. S. Barolo, B. Castro, J. W. Posakony, *Biotechniques* **36**, 436 (2004).
32. B. K. Dieckgraefe, D. M. Weems, *Am. J. Physiol.* **276**, G322 (1999).
33. G. J. Liaw *et al.*, *Genes Dev.* **9**, 3163 (1995).
34. M. Ashida, P. T. Brey, *Proc. Natl. Acad. Sci. U.S.A.* **92**, 10698 (1995).
35. K. Venkatesan, H. R. McManus, C. C. Mello, T. F. Smith, U. Hansen, *Nucleic Acids Res.* **31**, 4304 (2003).
36. T. Wilanowski *et al.*, *Mech. Dev.* **114**, 37 (2002).
37. S. B. Ting *et al.*, *Biochem. J.* **370**, 953 (2003).
38. E. I. Kudryavtseva *et al.*, *Dev. Dyn.* **226**, 604 (2003).
39. S. B. Ting *et al.*, *Nat. Med.* **9**, 1513 (2003).
40. S. B. Ting *et al.*, *Science* **308**, 411 (2005).

41. We thank S. Jane for communication of unpublished results, A. Tugores for the *Ddc* genomic clone, O. Drivenes for enhancer stains, and M. Ronshaugen for rhodamine-dextran injections and manuscript suggestions. L. Chen, R. Hodgetts, S. Barolo, J. Posakony, S. Wasserman, and T. Ip provided materials, and D. Kosman helped with confocal microscopy. W.M. is funded by R01HD28315, and J.C.P. is funded by T32GM07240.

Supporting Online Material

www.sciencemag.org/cgi/content/full/308/5720/381/DC1
Materials and Methods
Figs. S1 to S3
References and Notes

16 November 2004; accepted 26 January 2005
10.1126/science.1107573

Complement Factor H Polymorphism in Age-Related Macular Degeneration

Robert J. Klein,[1] Caroline Zeiss,[2]* Emily Y. Chew,[3]* Jen-Yue Tsai,[4]* Richard S. Sackler,[1] Chad Haynes,[1] Alice K. Henning,[5] John Paul SanGiovanni,[3] Shrikant M. Mane,[6] Susan T. Mayne,[7] Michael B. Bracken,[7] Frederick L. Ferris,[3] Jurg Ott,[1] Colin Barnstable,[2] Josephine Hoh[7]†

Age-related macular degeneration (AMD) is a major cause of blindness in the elderly. We report a genome-wide screen of 96 cases and 50 controls for polymorphisms associated with AMD. Among 116,204 single-nucleotide polymorphisms genotyped, an intronic and common variant in the complement factor H gene (*CFH*) is strongly associated with AMD (nominal *P* value $<10^{-7}$). In individuals homozygous for the risk allele, the likelihood of AMD is increased by a factor of 7.4 (95% confidence interval 2.9 to 19). Resequencing revealed a polymorphism in linkage disequilibrium with the risk allele representing a tyrosine-histidine change at amino acid 402. This polymorphism is in a region of CFH that binds heparin and C-reactive protein. The *CFH* gene is located on chromosome 1 in a region repeatedly linked to AMD in family-based studies.

Age-related macular degeneration (AMD) is the leading cause of blindness in the developed world. Its incidence is increasing as the elderly population expands (*1*). AMD is characterized by progressive destruction of the retina's central region (macula), causing central field visual loss (*2*). A key feature of AMD is the formation of extracellular deposits called drusen concentrated in and around the macula behind the retina between the retinal pigment epithelium (RPE) and the choroid. To date, no therapy for this disease has proven to be broadly effective. Several risk factors have been linked to AMD, including age, smoking, and family history (*3*). Candidate-gene studies have not found any genetic differences that can account for a large proportion of the overall prevalence (*2*). Family-based whole-genome linkage scans have identified chromosomal regions that show evidence of linkage to AMD (*4*–*8*), but the linkage areas have not been resolved to any causative mutations.

Like many other chronic diseases, AMD is caused by a combination of genetic and environmental risk factors. Linkage studies are not as powerful as association studies for the identification of genes contributing to the risk for common, complex diseases (*9*). However, linkage studies have the advantage of searching the whole genome in an unbiased manner without presupposing the involvement of particular genes. Searching the whole genome in an association study requires typing 100,000 or more single-nucleotide polymorphisms (SNPs) (*10*). Because of these technical demands, only one whole-genome association study, on susceptibility to myocardial infarction, has been published to date (*11*).

Study design. We report a whole-genome case-control association study for genes involved in AMD. To maximize the chance of success, we chose clearly defined phenotypes for cases and controls. Case individuals exhibited at least some large drusen in a quantitative photographic assessment combined with evidence of sight-threatening AMD (geographic atrophy or neovascular AMD). Control individuals had either no or only a few small drusen. We analyzed our data using a statistically conservative approach to correct for the large number of SNPs tested, thereby guaranteeing that the probability of a false positive is no greater than our reported *P* values.

We used a subset of individuals who participated in the Age-Related Eye Disease Study (AREDS) (*12*). From the AREDS

[1]Laboratory of Statistical Genetics, Rockefeller University, 1230 York Avenue, New York, NY 10021, USA. [2]Department of Ophthalmology and Visual Science, Yale University School of Medicine, 330 Cedar Street, New Haven, CT 06520, USA. [3]National Eye Institute, Building 10, CRC, 10 Center Drive, Bethesda, MD 20892–1204, USA. [4]Biological Imaging Core, National Eye Institute, 9000 Rockville Pike, Bethesda, MD 20892, USA. [5]The EMMES Corporation, 401 North Washington Street, Suite 700, Rockville MD 20850, USA. [6]W. M. Keck Facility, Yale University, 300 George Street, Suite 201, New Haven, CT 06511, USA. [7]Department of Epidemiology and Public Health, Yale University School of Medicine, 60 College Street, New Haven, CT 06520, USA.

*These authors contributed equally to this work.
†To whom correspondence should be addressed. E-mail: josephine.hoh@yale.edu

sample, we identified 96 case subjects and 50 control subjects as described (*13*). Because there can be many precursors to the development of either geographic atrophy or choroidal neovascularization, we purposely selected the group of study participants who had both large drusen and sight-threatening AMD as cases. All individuals identified themselves as "white, not of Hispanic origin." To the extent possible, we kept the proportions of males/females and smokers/nonsmokers the same in cases and controls. Controls were purposely chosen to be older than the cases to increase the probability that they would remain without AMD (table S1).

All 146 individuals were genotyped as described (*13*). A summary of genotyping quality can be found in table S2. Of the 116,204 SNPs genotyped, 105,980 both were informative and passed our quality-control checks. We then proceeded to analyze the 103,611 of these SNPs that lie on the 22 autosomal chromosomes.

Single-marker associations. For each SNP, we tested for allelic association with disease status. To account for multiple testing, we used the Bonferroni correction and considered significant only those SNPs for which $P < 0.05/103{,}611 = 4.8 \times 10^{-7}$. This correction is known to be conservative and thus "overcorrected" the raw P values (*14*). Of the autosomal SNPs, only two, rs380390 and rs10272438, are significantly associated with disease status (Bonferroni-corrected $P = 0.0043$ and $P = 0.0080$, respectively) (Fig. 1A).

One criticism of case-control association studies such as ours is that population stratification can result in false-positive results. If the cases and controls are drawn from populations of different ancestry, with different allele frequencies, we might detect these population differences instead of loci associated with the disease. All individuals in this study self-identify their ethnicity as non-Hispanic white, and all of the case and control individuals are drawn from the same AREDS population. There was some differential recruiting of cases from office practices and recruiting of controls from radio and newspaper advertising (*3*). Finding two SNPs out of >100,000 implied the absence of genetic stratification, but we nonetheless used genomic control methods to control for this possibility (*15*). We consistently found that the significance of the tests was not inflated and that, therefore, these two SNPs are significantly associated with disease.

SNP rs380390 was successfully genotyped in all individuals. In 21 individuals, no genotype was determined for SNP rs10272438, and it appears to be excessively out of Hardy-Weinberg equilibrium (HWE $\chi^2 = 36$), indicating possible genotyping errors. Missing genotypes were determined by resequencing (*16*). After inclusion of these additional genotypes, the association was no longer significant after Bonferroni correction. Furthermore, the SNP with the third-lowest P value, rs1329428 (Bonferroni-corrected $P = 0.14$), is located 1.8 kb telomeric to rs380390. The genotype frequencies at these two neighboring loci vary between the case and control populations (Fig. 1B). Homozygotes for the C allele of rs380390 and the C allele at rs1329428 have an increased risk of developing AMD (Table 1). The risk conferred by these genotypes accounts for approximately 45% (rs380390) to 61% (rs1329428) of the total population risk (Table 1). We therefore focused on these two SNPs.

Risk haplotype. These two SNPs lie in an intron of the gene for complement factor H (*CFH*), located on chromosome 1q31 (GenBank accession NM_000186). Because both SNPs are noncoding and neither appears to alter a conserved sequence, we explored whether the two SNPs are in linkage disequilibrium with a functional polymorphism. Analysis of linkage disequilibrium throughout this chromosomal region (Fig. 2A) revealed that the two SNPs lie in a 500-kb region of high linkage disequilibrium. Because this region is longer than typically observed blocks of high linkage disequilibrium (*17*) and there are long stretches in this region where there are no SNPs in our data set (Fig. 2B), we referred to other data sources with denser SNP coverage to narrow the region.

We used data from the International HapMap project to look at patterns of linkage disequilibrium in a population of residents of Utah with ancestry from northern and western

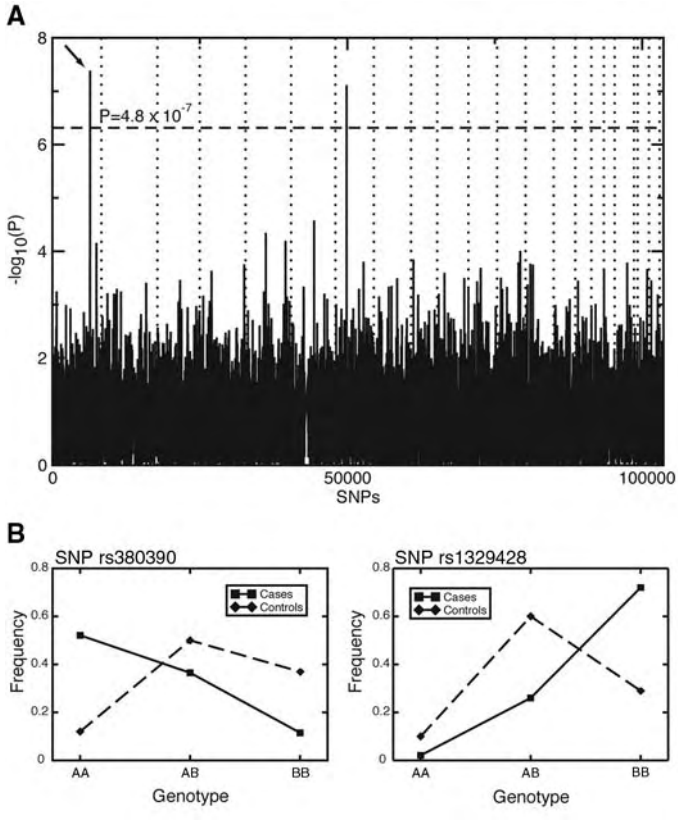

Fig. 1. (**A**) P values of genome-wide association scan for genes that affect the risk of developing AMD. $-\log_{10}(p)$ is plotted for each SNP in chromosomal order. The spacing between SNPs on the plot is uniform and does not reflect distances between SNPs on the chromosomes. The dotted horizontal line shows the cutoff for $P = 0.05$ after Bonferroni correction. The vertical dotted lines show chromosomal boundaries. The arrow indicates the peak for SNP rs380390, the most significant association, which was studied further. (**B**) Variation in genotype frequencies between cases and controls.

Table 1. Odds ratios and population attributable risks (PARs) for AMD. The dominant odds ratio and PAR compare the likelihood of AMD in individuals with at least one copy of the risk allele versus individuals with no copy of the risk allele. The recessive odds ratio and PAR compare the likelihood of AMD in individuals with two copies of the risk allele versus individuals with no more than one copy of the risk allele. The population frequencies for the risk genotypes are taken from the CEU HapMap population (CEPH collection of Utah residents of northern and western European ancestry).

Attribute	rs380390 (C/G)	rs1329428 (C/T)
Risk allele	C	C
Allelic association χ^2 nominal P value	4.1×10^{-8}	1.4×10^{-6}
Odds ratio (dominant) (95% CI)	4.6 (2.0–11)	4.7 (1.0–22)
PAR (95% CI)	70% (42–84%)	80% (0–96%)
Frequency in HapMap CEU	0.70	0.82
Odds ratio (recessive) (95% CI)	7.4 (2.9–19)	6.2 (2.9–13)
PAR (95% CI)	46% (31–57%)	61% (43–73%)
Frequency in HapMap CEU	0.23	0.41

Europe [the Centre d'Étude du Polymorphisme Humain (CEPH) sample] (*18*). In the 500-kb region of interest, there were only 19 SNPs in our data set as compared with 152 SNPs in the HapMap data set. Using a standard definition of linkage-disequilibrium blocks (*17*), we found that the two associated SNPs lie in a block that is 41 kb long and entirely contained within the *CFH* gene (Fig. 2C).

Six SNPs from our data set were in this 41-kb region. These SNPs form four predominant haplotypes, each with a frequency greater than 1% (table S3). Combined, these four haplotypes represent 99% of the chromosomes in this study. Reconstructing inferred haplotypes and building a phylogenetic tree allowed assessment of the evolutionary relationship between haplotypes (Fig. 2D). Using inferred haplotypes for each individual, we computed the odds ratio of the risk for disease in a nested cladistic framework under both dominant and recessive models (*19*). The highest risk was conferred by haplotype N1, which is the only haplotype containing the risk allele at SNP rs380390. Being heterozygous for this haplotype increases the likelihood for AMD by a factor of 4.6 [95% confidence interval (CI) 2.0 to 11] in our sample population. Being homozygous for this haplotype increases the likelihood for AMD by a factor of 7.4 (95% CI 3.0 to 19) in our sample population. Therefore, we expected to find the functionally relevant polymorphism in the context of haplotype N1. Most likely, this polymorphism would occur somewhere in the *CFH* gene, because the 41-kb haplotype block is entirely within *CFH*.

From markers to candidate functional polymorphism. To identify the polymorphism underlying susceptibility to AMD, we chose 96 individuals for exonic resequencing, including the exon/intron junctions. We sequenced all *CFH* exons, including those outside of the 41-kb block, as well as the region of SNP rs380390 as a control. SNP rs380390 was successfully resequenced in 93 individuals; the genotype derived from resequencing matched the original genotype in all cases. We identified a total of 50 polymorphisms; 17 of these have a minor-allele frequency of at least 5% (table S4). Of these 17, three represent nonsynonymous polymorphisms. We found a polymorphism in exon 9 of *CFH* (rs1061170) that is located 2 kb upstream of the 41-kb haplotype block, represents a tyrosine-histidine change, and is the polymorphism most strongly associated with AMD among the nonsynonymous SNPs we found. Adding this

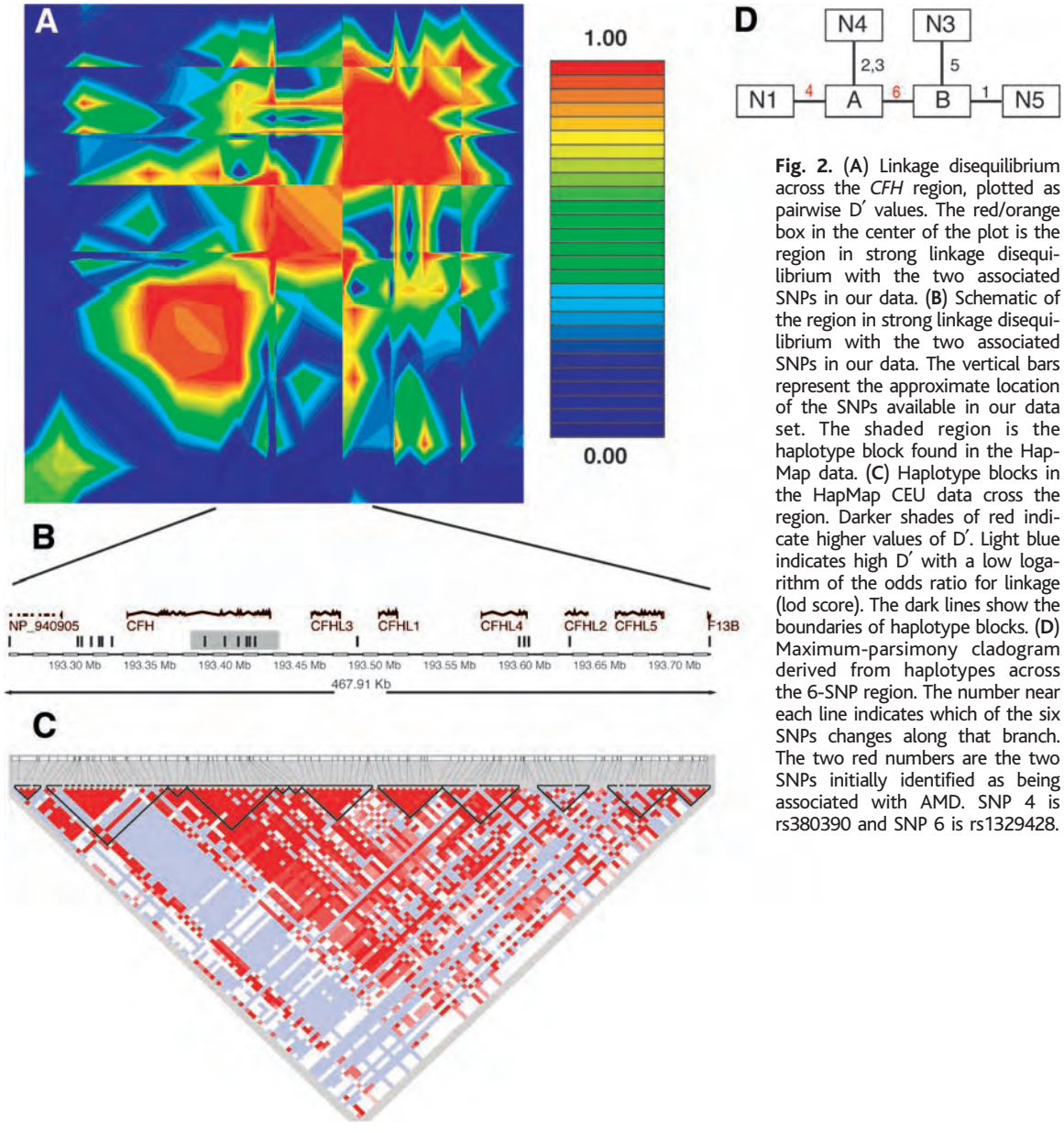

Fig. 2. (**A**) Linkage disequilibrium across the *CFH* region, plotted as pairwise D′ values. The red/orange box in the center of the plot is the region in strong linkage disequilibrium with the two associated SNPs in our data. (**B**) Schematic of the region in strong linkage disequilibrium with the two associated SNPs in our data. The vertical bars represent the approximate location of the SNPs available in our data set. The shaded region is the haplotype block found in the HapMap data. (**C**) Haplotype blocks in the HapMap CEU data cross the region. Darker shades of red indicate higher values of D′. Light blue indicates high D′ with a low logarithm of the odds ratio for linkage (lod score). The dark lines show the boundaries of haplotype blocks. (**D**) Maximum-parsimony cladogram derived from haplotypes across the 6-SNP region. The number near each line indicates which of the six SNPs changes along that branch. The two red numbers are the two SNPs initially identified as being associated with AMD. SNP 4 is rs380390 and SNP 6 is rs1329428.

SNP to the haplotype analysis reveals that 97% of the chromosomes with the highest risk haplotype (N1) also have the risk allele (His).

Human complement factor H. Several lines of evidence support the hypothesis that sequence polymorphisms in *CFH* can lead to AMD. First, the gene for *CFH* is located on chromosome 1q31, a region that had been implicated in AMD by six independent linkage scans (*4*–*8*, *20*). Although one study concluded that mutations in a different gene in this region (*HEMICENTIN-1*) were responsible for AMD (*20*), mutations in *HEMICENTIN-1* have not been found to be generally associated with AMD in three separate, independent studies (*7*, *21*, *22*).

CFH is a key regulator of the complement system of innate immunity (*23*). The complement system protects against infection and attacks diseased and dysplastic cells and normally spares healthy cells. When C3 convertase is activated, it leads to the production of C3a and C3b and then to the terminal C5b-9 complex. CFH on cells and in circulation regulates complement activity by inhibiting the activation of C3 to C3a and C3b and by inactivating existing C3b.

Various components of the complement cascade, including the C5b-9 complex, have been identified in the drusen of patients with AMD (*24*, *25*). We also examined the eyes of four patients with AMD to look for the presence of C5b-9 (fig. S1). Deposition of activated complement C5b-9 was noted in Bruch's membrane, in the intercapillary pillars, and within drusen. The observation of complement components in drusen in both humans (*24*, *25*) and mice (*26*) has led to the hypothesis that AMD results from an aberrant inflammatory process that includes inappropriate complement activation (*27*).

Both age and smoking, two important risk factors for AMD, influence plasma levels of complement factor H (*28*). *CFH* sequences have been observed in an expressed sequence tag library derived from human RPE and choroid (*29*). We confirmed by immunofluorescence experiments that CFH is present in this region of the eye (Fig. 3). Strong staining was observed in choroid vessels (retinal blood vessels) and in an area bordering the RPE. Drusen of similar composition to that found in AMD are found in the eyes of patients with membranoproliferative glomerulonephritis type II (MPGNII), a kidney disease (*30*); CFH deficiency can cause MPGNII (*23*). Our immunostaining experiments (Fig. 3 and fig. S1) suggest that in AMD, the risk variant of CFH may give rise to complement deposition in choroidal capillaries (more severe) and choroidal vessels (less severe), with subsequent leakage of plasma proteins into Bruch's membrane. Nutritional supplementation with zinc slows down the progression of AMD; biochemical studies have shown that CFH function is sensitive to zinc concentration (*12*, *31*).

We identified a tyrosine-histidine polymorphism in which the histidine variant almost always occurs in the context of the AMD risk haplotype. This polymorphism is located in a region of CFH that binds to both heparin and C-reactive protein (CRP) (*23*). It has been previously suggested that this binding could be altered by the replacement of a neutral tyrosine with a positively charged histidine (*23*). Elevated serum levels of CRP have been shown to be associated with AMD (*32*). Further work to establish the causal role of the tyrosine-histidine polymorphism in AMD is warranted.

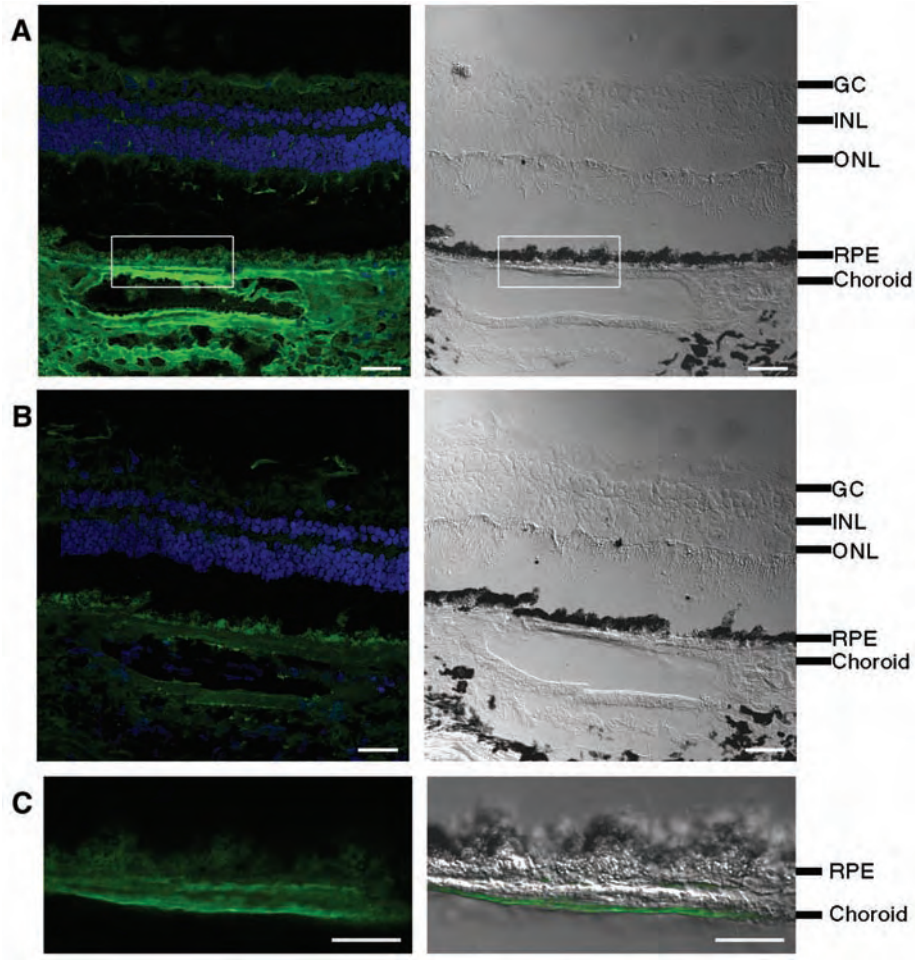

Fig. 3. Immunofluorescence localization of CFH protein in human retina. Neighboring human retina sections are stained with (**A**) antibody to CFH or (**B**) antibody to CFH preabsorbed with CFH as negative control. (**C**) High-magnification view of the boxed area in (A). For (A), (B), and (C), left panels are the fluorescence images, with CFH labeling in green and DAPI (4′,6′-diamidino-2-phenylindole)–stained nuclei in blue; right panels are differential interference contrast (DIC) images showing the tissue morphology. In (C), the CFH signal is superimposed onto the DIC image. Labeling of CFH is intense in choroid, including blood vessels and areas bordering RPE [(A) and (C)]; this CFH signal is competed away by purified CFH protein (B), which demonstrates the labeling specificity. The fluorescence signal from RPE arises from lipofuscin autofluorescence, which cannot be competed away with CFH protein [(A) and (B)]. The black spots in DIC images correspond to melanin granules in RPE and choroids. The cell layers are indicated: GC, ganglion cells; INL, inner nuclear layer; ONL, outer nuclear layer; RPE, retinal pigment epithelium. Scale bars: 40 μm in (A) and (B), 20 μm in (C).

References and Notes

1. D. S. Friedman *et al.*, *Arch. Ophthalmol.* **122**, 564 (2004).
2. J. Tuo, C. M. Bojanowski, C. C. Chan, *Prog. Retinal Eye Res.* **23**, 229 (2004).
3. AREDS Research Group, *Ophthalmology* **107**, 2224 (2000).
4. J. Majewski *et al.*, *Am. J. Hum. Genet.* **73**, 540 (2003).
5. J. M. Seddon, S. L. Santangelo, K. Book, S. Chong, J. Cote, *Am. J. Hum. Genet.* **73**, 780 (2003).
6. D. E. Weeks *et al.*, *Am. J. Hum. Genet.* **75**, 174 (2004).
7. G. R. Abecasis *et al.*, *Am. J. Hum. Genet.* **74**, 482 (2004).
8. S. K. Iyengar *et al.*, *Am. J. Hum. Genet.* **74**, 20 (2004).
9. N. Risch, K. Merikangas, *Science* **273**, 1516 (1996).
10. D. Botstein, N. Risch, *Nat. Genet.* **33** (suppl.), 228 (2003).
11. K. Ozaki *et al.*, *Nat. Genet.* **32**, 650 (2002).
12. AREDS Research Group, *Arch. Ophthalmol.* **119**, 1417 (2001).
13. Materials and methods are available as supporting material on *Science* Online.
14. L. M. McIntyre, E. R. Martin, K. L. Simonsen, N. L. Kaplan, *Genet. Epidemiol.* **19**, 18 (2000).
15. B. Devlin, S. A. Bacanu, K. Roeder, *Nat. Genet.* **36**, 1129 (2004).
16. Klein *et al.*, data not shown.
17. S. B. Gabriel *et al.*, *Science* **296**, 2225 (2002).

18. The International HapMap Consortium, *Nature* **426**, 789 (2003).
19. A. R. Templeton, E. Boerwinkle, C. F. Sing, *Genetics* **117**, 343 (1987).
20. D. W. Schultz *et al.*, *Hum. Mol. Genet.* **12**, 3315 (2003).
21. M. Hayashi *et al.*, *Ophthalmic Genet.* **25**, 111 (2004).
22. G. J. McKay *et al.*, *Mol. Vis.* **10**, 682 (2004).
23. S. Rodríguez de Cordoba, J. Esparza-Gordillo, E. Goicoechea de Jorge, M. Lopez-Trascasa, P. Sanchez-Corral, *Mol. Immunol.* **41**, 355 (2004).
24. L. V. Johnson, W. P. Leitner, M. K. Staples, D. H. Anderson, *Exp. Eye Res.* **73**, 887 (2001).
25. R. F. Mullins, S. R. Russell, D. H. Anderson, G. S. Hageman, *FASEB J.* **14**, 835 (2000).
26. J. Ambati *et al.*, *Nat. Med.* **9**, 1390 (2003).
27. G. S. Hageman *et al.*, *Prog. Retinal Eye Res.* **20**, 705 (2001).
28. J. Esparza-Gordillo *et al.*, *Immunogenetics* **56**, 77 (2004).
29. G. Wistow *et al.*, *Mol. Vis.* **8**, 205 (2002).
30. R. F. Mullins, N. Aptsiauri, G. S. Hageman, *Eye* **15**, 390 (2001).
31. A. M. Blom, L. Kask, B. Ramesh, A. Hillarp, *Arch. Biochem. Biophys.* **418**, 108 (2003).
32. J. M. Seddon, G. Gensler, R. C. Milton, M. L. Klein, N. Rifai, *JAMA* **291**, 704 (2004).
33. The Raymond and Beverly Sackler Fund for Arts and Sciences' generous support made this project possible. We thank Raymond Sackler, J. Sackler, and E. Vosburg for their input and encouragement. We also thank AREDS participants and investigators; G. Gensler, T. Clemons, and A. Lindblad for work on the AREDS Genetic Repository; S. Westman and A. Evan for assistance with the microarrays; R. Fariss for the human retinal sections and advice on confocal microscopy; E. Johnson for assistance with immunostaining; and J. Majewski for constructive comments on the manuscript. Partially funded by NIH-K25HG000060 and NIH-R01EY015771 (J.H.), Macula Vision Research Foundation and the David Woods Kemper Memorial Foundation (C.B.), NIH-R01MH44292 (J.O.), and NIH-K01RR16090 and Yale Pepper Center for Study of Diseases in Aging (C.Z.). This work also benefited from the International HapMap Consortium making their data available prior to publication.

Supporting Online Material
www.sciencemag.org/cgi/content/full/1109557/DC1
Materials and Methods
Fig. S1
Tables S1 to S5
References

10 January 2005; accepted 22 February 2005
Published online 10 March 2005;
10.1126/science.1109557
Include this information when citing this paper.

REPORTS

Quantum Phase Transition of a Magnet in a Spin Bath

H. M. Rønnow,[1,2,3]* R. Parthasarathy,[2] J. Jensen,[4] G. Aeppli,[5] T. F. Rosenbaum,[2] D. F. McMorrow[3,4,6]

The excitation spectrum of a model magnetic system, $LiHoF_4$, was studied with the use of neutron spectroscopy as the system was tuned to its quantum critical point by an applied magnetic field. The electronic mode softening expected for a quantum phase transition was forestalled by hyperfine coupling to the nuclear spins. We found that interactions with the nuclear spin bath controlled the length scale over which the excitations could be entangled. This generic result places a limit on our ability to observe intrinsic electronic quantum criticality.

The preparation and preservation of entangled quantum states is particularly relevant for the development of quantum computers, where interacting quantum bits (qubits) must produce states sufficiently long lived for meaningful manipulation. The state lifetime, typically referred to as decoherence time, is derived from coupling to the background environment. For solid-state quantum computing schemes, the qubits are typically electron spins, and they couple to two generic background environments (*1*). The oscillator bath—that is, delocalized environmental modes (*2*) such as thermal vibrations coupled via magnetoelastic terms to the spins—can be escaped by lowering the temperature to a point where the lattice is essentially frozen. Coupling to local degrees of freedom, such as nuclear magnetic moments that form a spin bath, may prove more difficult to avoid, because all spin-based candidate materials for quantum computation have at least one naturally occurring isotope that carries nuclear spin.

Experimental work in this area has been largely restricted to the relaxation of single, weakly interacting magnetic moments such as those on large molecules (*3*); much less is known about spins as they might interact in a real quantum computer. In this regard, the insight that quantum phase transitions (QPTs) (*4*) are a good arena for looking at fundamental quantum properties of strongly interacting spins turns out to be valuable, as it has already been for explorations of entanglement. In particular, we show that coupling to a nuclear spin bath limits the distance over which quantum mechanical mixing affects the electron spin dynamics.

QPTs are transitions between different ground states driven not by thermal fluctuations but by quantum fluctuations controlled by a parameter such as doping, pressure, or magnetic field (*5*, *6*). Much of the interest in QPTs stems from their importance for understanding materials with unconventional properties, such as heavy fermion systems and high-temperature superconductors. However, these materials are rather complex and do not easily lend themselves to a universal understanding of QPTs. To this end, it is desirable to identify quantum critical systems with a well-defined and solvable Hamiltonian and with a precisely controllable tuning parameter. One very simple model displaying a QPT is the Ising ferromagnet in a transverse magnetic field (*5*, *7*–*9*) with the Hamiltonian

$$\mathcal{H} = -\sum_{ij} \mathcal{J}_{ij}\, \sigma_i^z \cdot \sigma_j^z - \Gamma \sum_i \sigma_i^x \qquad (1)$$

where $\mathcal{J}_{ij}$ is the coupling between the spins on sites i and j represented by the Pauli matrices σ^z with eigenvalues ±1. In the absence of a magnetic field, the system orders ferromagnetically below a critical temperature T_c. The transverse-field Γ mixes the two states and leads to destruction of long-range order in a QPT at a critical field Γ_c, even at zero temperature. In the ferromagnetic state at zero field and temperature, the excitation spectrum is momentum independent and is centered at the energy $4\sum_j J_{ij}$ associated with single-spin reversal. Upon application of a magnetic field, however, the excitations acquire a dispersion, softening to zero at the zone center $q = 0$ when the QPT is reached.

We investigated the excitation spectrum around the QPT in $LiHoF_4$, which is an excellent physical realization of the transverse-field Ising model, with an added term accounting for the hyperfine coupling between electronic and nuclear moments (*10*–*12*). The dilution series $LiHo_xY_{1-x}F_4$ is the host for a wide variety of collective quantum effects, ranging from tunneling of single moments and domain walls to quantum annealing, entanglement, and Rabi oscillations (*13*–*17*). These intriguing properties rely largely on the ability of a transverse field, whether applied externally or generated internally by the off-diagonal part of the magnetic dipolar interaction, to mix two degenerate crystal field states of each Ho ion.

[1]Laboratory for Neutron Scattering, ETH-Zürich and Paul Scherrer Institut, 5232 Villigen, Switzerland. [2]James Franck Institute and Department of Physics, University of Chicago, Chicago, IL 60637, USA. [3]Risø National Laboratory, DK-4000 Roskilde, Denmark. [4]Ørsted Laboratory, Niels Bohr Institute fAPG, Universitetsparken 5, 2100 Copenhagen, Denmark. [5]London Centre for Nanotechnology and Department of Physics and Astronomy, University College London, London WC1E 6BT, UK. [6]ISIS, Rutherford Appleton Laboratory, Chilton, Didcot OX11 0QX, UK.

*To whom correspondence should be addressed. E-mail: henrik.ronnow@psi.ch

The Ho ions in $LiHoF_4$ are placed on a tetragonal Scheelite lattice with parameters $a = 5.175$ Å and $c = 10.75$ Å. The crystal-field ground state is a $\Gamma_{3,4}$ doublet with only a c component to the angular momentum and hence can be represented by the $\sigma^z = \pm 1$ Ising states. A transverse field in the a-b plane mixes the higher lying states with the ground state; this produces a splitting of the doublet, equivalent to an effective Ising model field. The phase diagram of $LiHoF_4$ (Fig. 1A) was determined earlier by susceptibility measurements (*10*) and displays a zero-field T_c of 1.53 K and a critical field of $H_c = 49.5$ kOe in the zero temperature limit. The same measurements confirmed the strong Ising anisotropy, with longitudinal and transverse g factors differing by a factor of 18 (*10*). The sudden increase in H_c below 400 mK was explained by alignment of the Ho nuclear moments through the hyperfine coupling. Corrections to phase diagrams as a result of hyperfine couplings have a long history (*18*) and were noted for the Li*RE*F_4 (*RE* = rare earth) series, of which $LiHoF_4$ is a member, more than 20 years ago (*19*). What is new here is that the application of a transverse field and the use of high-resolution neutron scattering spectroscopy allow us to carefully study the dynamics as we tune through the quantum critical point (QCP).

We measured the magnetic excitation spectrum of $LiHoF_4$ with the use of the TAS7 neutron spectrometer at Risø National Laboratory, with an energy resolution (full width at half maximum) of 0.06 to 0.18 meV (*20*). The transverse field was aligned to better than 0.35°, and the sample was cooled in a dilution refrigerator. At the base temperature of 0.31 K, giving a critical field of 42.4 kOe, the excitation spectrum was mapped out below, at, and above the critical field (Fig. 2). For all fields, a single excitation branch disperses upward from a minimum gap at (2,0,0) toward (1,0,0). From (1,0,0) to (1,0,1), the mode shows little dispersion but appears to broaden. The discontinuity on approaching $(1,0,1-\varepsilon)$ and $(1+\varepsilon,0,1)$ as $\varepsilon \rightarrow 0$ reflects the anisotropy and long-range nature of the magnetic dipole coupling. However, the most important observation is that the (2,0,0) energy, which is always lower than the calculated single-ion energy (~0.39 meV at 42.4 kOe), shrinks upon increasing the field from 36 to 42.4 kOe and then hardens again at 60 kOe. At this qualitative level, what we see agrees with the mode softening predicted for the simple Ising model in a transverse field. However, it appears that the mode softening is incomplete. At the critical field of 42.4 kOe, the mode retains a finite energy of 0.24 ± 0.01 meV. This result is apparent in Fig. 1B, which shows the gap energy as a function of the external field.

To obtain a quantitative understanding of our experiments, we consider the full rare-earth Hamiltonian, which closely resembles that of

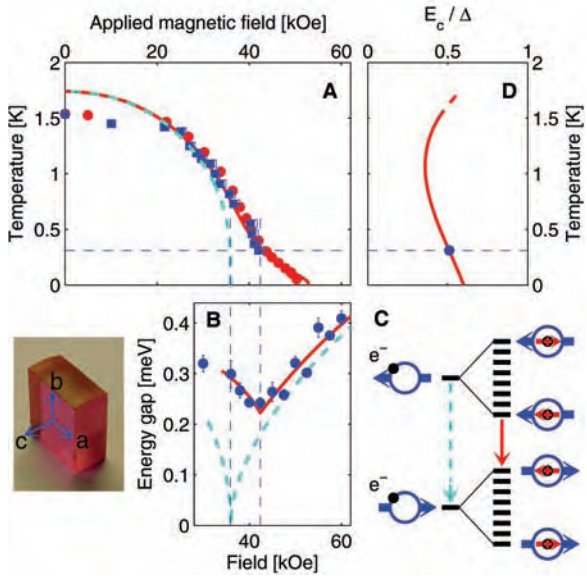

Fig. 1. (**A**) Phase diagram of $LiHoF_4$ as a function of transverse magnetic field and temperature from susceptibility (*10*) (circles) and neutron scattering (squares) measurements. Lines are 1/z calculations with (solid) and without (dashed) hyperfine interaction. Horizontal dashed guide marks the temperature 0.31 K at which inelastic neutron measurements were performed. (**B**) Field dependence of the lowest excitation energy in $LiHoF_4$ measured at $Q = (1+\varepsilon,0,1)$. Lines are calculated energies scaled by $Z = 1.15$ with (solid) and without (dashed) hyperfine coupling. The dashed vertical guides show how in either case the minimum energy occurs at the field of the transition [compare with (A)]. (**C**) Schematic of electronic (blue) and nuclear (red) levels as the transverse field is lowered toward the QCP. Neglecting the nuclear spins, the electronic transition (light blue arrow) would soften all the way to zero energy. Hyperfine coupling creates a nondegenerate multiplet around each electronic state. The QCP now occurs when the excited-state multiplet through level repulsion squeezes the collective mode of the ground-state multiplet to zero energy, hence forestalling complete softening of the electronic mode. Of course, the true ground and excited states are collective modes of many Ho ions and should be classified in momentum space. (**D**) Calculated ratio of the minimum excitation energy E_c to the single-ion splitting Δ at the critical field as a function of temperature. This measures how far the electronic system is from the coherent limit, for which $E_c/\Delta = 0$.

HoF_3 (*21*, *22*). Each Ho ion is subject to the crystal field, the Zeeman coupling, and the hyperfine coupling. The interaction between moments is dominated by the long-range dipole coupling, with a small nearest neighbor exchange interaction J_{12}:

$$\mathcal{H} = \sum_i \left[\mathcal{H}_{CF}(\mathbf{J}_i) + A\mathbf{J}_i \cdot \mathbf{I}_i - g\mu_B \mathbf{J}_i \cdot \mathbf{H}\right] - \frac{1}{2}\sum_{ij}\sum_{\alpha\beta} \mathcal{J}_D D_{\alpha\beta}(ij) J_{i\alpha} J_{j\beta} - \frac{1}{2}\sum_{ij}^{n.n.} \mathcal{J}_{12}\, \mathbf{J}_i \cdot \mathbf{J}_j \qquad (2)$$

where $\mathbf{J}$ and $\mathbf{I}$ are the electronic and nuclear moments, respectively, and for $^{165}Ho^{3+}$ $J = 8$ and $I = 7/2$. Hyperfine resonance (*23*) and heat capacity measurements (*24*) show the hyperfine coupling parameter $A = 3.36$ μeV as for the isolated ion, with negligible nuclear-quadrupole coupling. The Zeeman term is reduced by the demagnetization field. The normalized dipole tensor $D_{\alpha\beta}(ij)$ is directly calculable, and the dipole coupling strength J_D is simply fixed by lattice constants and the magnetic moments of the ions at $J_D = (g\mu_B)^2 N = 1.1654$ μeV, where μ_B is the Bohr magneton. This leaves as free parameters various numbers appearing in the crystal-field Hamiltonian H_{CF} and the exchange constant J_{12}. The former are determined (*25*) largely from electron spin resonance for dilute Ho atoms substituted for Y in $LiYF_4$, whereas the latter is constrained by the phase diagram determined earlier (*10*) (Fig. 1A). We have used an effective medium theory (*9*) previously applied to HoF_3 (*26*) to fit the phase diagram, and we conclude that a good overall description—except for a modest (14%) overestimate of the zero-field transition temperature—is obtained for $J_{12} = -0.1$ μeV. On the basis of quantum Monte Carlo simulation data, others (*27*) have also concluded that J_{12} is substantially smaller than J_D.

Having established a good parameterization of the Hamiltonian, we model the dynamics, where expansion to order 1/z (where z is the number of nearest neighbors of an ion in the lattice) leads to an energy-dependent renormalization $[1 + \Sigma(\omega)]^{-1}$ (on the order of 10%) of the dynamic susceptibility calculated in the random phase approximation, with the self energy $\Sigma(\omega)$ evaluated as described in (*26*). For the three fields investigated in detail, the dispersion measured by neutron scattering is closely reproduced throughout the Brillouin zone. As indicated by the solid lines in Fig. 2, the agreement becomes excellent if the calculated excitation energies are multiplied by a renormalization factor $Z = 1.15$. The point is not that the calculation is imperfect but rather that it matches the data as closely as it does. Indeed, it also predicts a weak mode splitting of about 0.08 meV at $(1,0,1-\varepsilon)$, consistent with the increased width in the measurements. The agreement for the discontinuous jump between $(1,0,1-\varepsilon)$ and $(1+\varepsilon,0,1)$ as a result of the long-range nature of the dipole coupling shows that this is indeed the dominant coupling.

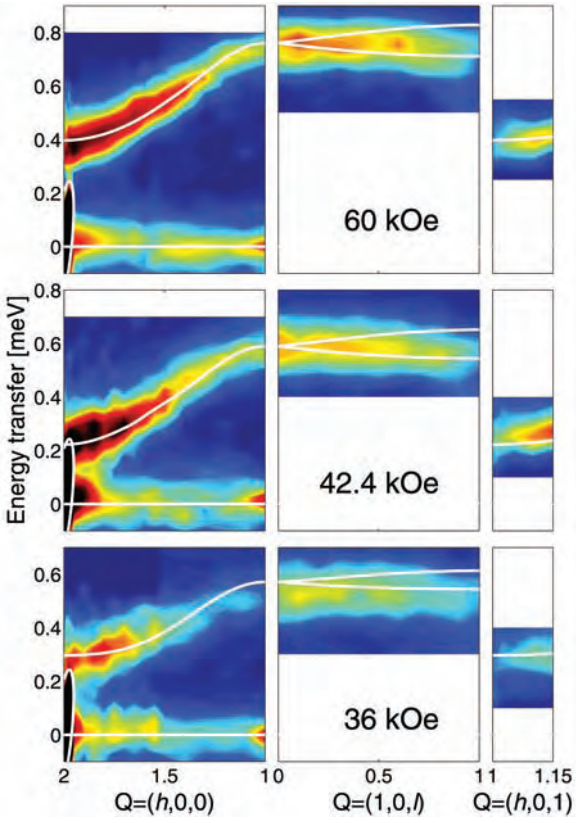

Fig. 2. Pseudocolor representation of the inelastic neutron scattering intensity for $LiHoF_4$ at T = 0.31 K observed along the reciprocal space trace (2,0,0) → (1,0,0) → (1,0,1) → (1.15,0,1). White lines show the 1/z calculation for the excitation energies as described in the text. White ellipses around the (2,0,0) Bragg peak indicate 5 times the resolution tail (full width at half maximum).

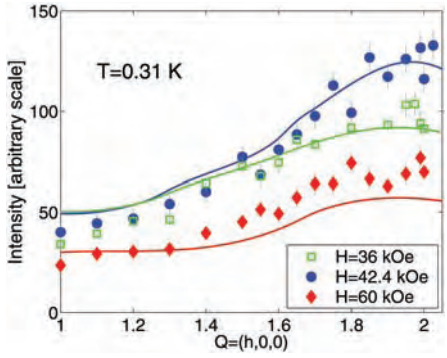

Fig. 3. Measured intensities of the excitations along Q = (h,0,0) at the same values of the field as in Fig. 2. Lines are calculated with geometric and resolution corrections applied to allow comparison to the neutron data.

The simple origin of the incomplete softening and enhanced critical field (Fig. 1, B and C) is easiest to understand if we start from the polarized paramagnetic state above H_c, where the experiment, the purely electronic calculation, and the theory including the hyperfine coupling all coincide. At high fields, the only effect of the hyperfine term is to split both the ground state and the electronic excitation modes into multiplets that are simply the direct products of the electronic and nuclear levels, with a total span of $2A\langle J\rangle I \approx 0.1$ meV (Fig. 1C). Upon lowering the field, the electronic mode softens and would reach zero energy at H_c^0 = 36 kOe in the absence of hyperfine coupling. The hyperfine coupling, however, already mixes the original ground and excited (soft mode) states above H_c. As this happens, the formation of a composite spin from mixed nuclear and electronic contributions immediately stabilizes ordering along the c axis of the crystal. In other words, the hyperfine coupling shunts the electronic mode, raising the critical field to the observed H_c = 42.4 kOe, where the mode reaches a nonzero minimum. This process is accompanied by transfer of intensity from the magnetic excitation of electronic origin to soft modes of much lower energy (in the 10-μeV range) that have an entangled nuclear/electronic character. Cooling to very low temperatures would reveal these modes as propagating and softening to zero at the QCP, but at the temperatures reachable in our measurements there is thermalization, dephasing the composite modes to yield the strong quasi-elastic scattering appearing around Q = (2,0,0) and zero energy at the critical field, as in Fig. 2.

The intensities of the excitations are simply proportional to the matrix elements $|\langle f|\sum_j \exp(iQ \cdot R_j)J_j^+|0\rangle|^2$, and therefore provide a direct measure of the wave functions via the interference effects implicit in the spatial Fourier transform of J_j. Figure 3 shows intensities recorded along (h,0,0) for the three fields 36, 42.4, and 60 kOe. They follow a momentum dependence characterized by a broad peak near (2,0,0), which is well described by our theory. In the absence of hyperfine interactions, the intensity at H_c^0 would diverge as q approaches (2,0,0), reflecting that the real-space dynamical coherence length ξ_c of the excited state grows to infinity. The finite width of the peak observed at H_c corresponds in real space to a distance on the order of the interholmium spacing; because the hyperfine interactions forestall the softening of the electronic mode, the implication is that these interactions also limit the distance over which the electronic wave functions can be entangled (*4*). Thus, Fig. 3 is a direct demonstration of the limitation of quantum coherence in space via coupling to a nuclear spin bath. ξ_c is obtained from a sum over matrix elements connecting the ground state to a particular set of excited states, whereas the thermodynamic correlation length ξ_t is derived from the equal time correlation function $S(r)$, which is the sum over all final states. ξ_t diverges at second-order transitions such as those in $LiHoF_4$, where the quasielastic component seen in our data dominates the long-distance behavior of $S(r)$ at $T_c(H)$. It is the electronic mode, and hence ξ_c, that dictates to what extent $LiHoF_4$ can be characterized and potentially exploited as a realization of the ideal transverse-field Ising model.

Beyond providing a quantitative understanding of the excitations near the QCP of a model experimental system, we obtain new insight by bringing together the older knowledge from rare-earth magnetism and the contemporary ideas of entanglement, qubits, and decoherence. Although the notion of the spin bath was developed to address decoherence in localized magnetic clusters and molecules (*1*), our work discloses its importance for QPTs. In particular, we establish that the spin bath is a generic feature that will limit our ability to observe intrinsic electronic quantum criticality. This may not matter much for transition metal oxides with very large exchange constants, but it could matter for rare earth and actinide intermetallic compounds, which show currently unexplained crossovers to novel behaviors at low (<1 K) temperatures [see, e.g., (*28*)].

For magnetic clusters, decoherence can be minimized in a window between the oscillator bath–dominated high-temperature regions and the spin bath–dominated low-temperature regions (*29*). Our calculations suggest that the dense quantum critical magnet shows analogous behavior. Here the interacting electron spins themselves constitute the oscillator bath, and the extent to which the magnetic excitation softens at $T_c(H)$, as measured by the ratio of the zone center energy E_c to the field-induced single-ion splitting Δ (Fig. 1D), gauges the electronic decoherence. E_c/Δ achieves its minimum not at T = 0 but rather at an intermediate temperature $T \approx 1$ K, exactly where the phase boundary in Fig. 1A begins to be affected by the nuclear hyperfine interactions.

References and Notes

1. N. V. Prokof'ev, P. C. E. Stamp, *Rep. Prog. Phys.* **63**, 669 (2000).
2. R. P. Feynman, F. L. Vernon, *Ann. Phys.* **24**, 118 (1963).
3. W. Wernsdorfer, S. Bhaduri, R. Tiron, D. N. Hendrickson, G. Christou, *Phys. Rev. Lett.* **89**, 197201 (2002).
4. A. Osterloh, L. Amico, G. Falci, R. Fazio, *Nature* **416**, 608 (2002).
5. S. Sachdev, *Phys. World* **12**, 33 (1999).
6. S. Sachdev, *Quantum Phase Transitions* (Cambridge Univ. Press, Cambridge, 1999).
7. P. G. de Gennes, *Solid State Commun.* **1**, 132 (1963).
8. R. J. Elliott, P. Pfeuty, C. Wood, *Phys. Rev. Lett.* **25**, 443 (1970).
9. R. B. Stinchcombe, *J. Phys. C* **6**, 2459 and 2484 (1973).
10. D. Bitko, T. F. Rosenbaum, G. Aeppli, *Phys. Rev. Lett.* **77**, 940 (1997).
11. T. F. Rosenbaum *et al.*, *J. Appl. Phys.* **70**, 5946 (1991).
12. D. Bitko, thesis, University of Chicago (1997).
13. R. Giraud *et al.*, *Phys. Rev. Lett.* **87**, 057203 (2001).
14. J. Brooke, D. Bitko, T. F. Rosenbaum, G. Aeppli, *Science* **284**, 779 (1999).
15. J. Brooke, T. F. Rosenbaum, G. Aeppli, *Nature* **413**, 610 (2001).
16. S. Ghosh, R. Parthasarathy, T. F. Rosenbaum, G. Aeppli, *Science* **296**, 2195 (2002).
17. S. Ghosh *et al.*, *Nature* **425**, 48 (2003).
18. K. Andres, *Phys. Rev. B* **7**, 4295 (1973).
19. R. W. Youngblood, G. Aeppli, J. D. Axe, J. A. Griffin, *Phys. Rev. Lett.* **49**, 1724 (1982).
20. H. M. Rønnow, thesis, Risø National Laboratory, Denmark (2000).
21. M. J. M. Leask *et al.*, *J. Phys. C* **6**, 505 (1994).
22. A. P. Ramirez, J. Jensen, *J. Phys. C* **6**, L215 (1994).
23. J. Magariño, J. Tuchendler, P. Beauvillain, I. Laursen, *Phys. Rev. B* **21**, 18 (1980).
24. G. Mennenga, L. J. de Jongh, W. J. Huiskamp, *J. Magn. Magn. Mater.* **44**, 59 (1984).
25. H. M. Rønnow *et al.*, in preparation.
26. J. Jensen, *Phys. Rev. B* **49**, 11833 (1994).
27. P. B. Chakraborty, P. Henelius, H. Kjønsberg, A. W. Sandvik, S. M. Girvin, *Phys. Rev. B* **70**, 144411 (2004).
28. P. Gegenwart *et al.*, *Phys. Rev. Lett.* **89**, 056402 (2002).
29. P. C. E. Stamp, I. S. Tupitsyn, *Phys. Rev. B* **69**, 014401 (2004).

30. We thank G. McIntyre for his expert assistance during complementary measurements on the D10 diffractometer at the Institut Laue Langevin, Grenoble, France. Work at the University of Chicago was supported by NSF Materials Research Science and Engineering Centers grant DMR-0213745. Work in London was supported by the Wolfson–Royal Society Research Merit Award Program and the Basic Technologies program of the UK Research Councils.

6 December 2004; accepted 23 February 2005
10.1126/science.1108317

Atomic-Scale Visualization of Inertial Dynamics

A. M. Lindenberg,[1] J. Larsson,[2] K. Sokolowski-Tinten,[3] K. J. Gaffney,[1] C. Blome,[4] O. Synnergren,[2] J. Sheppard,[5] C. Caleman,[6] A. G. MacPhee,[7] D. Weinstein,[7] D. P. Lowney,[7] T. K. Allison,[7] T. Matthews,[7] R. W. Falcone,[7] A. L. Cavalieri,[8] D. M. Fritz,[8] S. H. Lee,[8] P. H. Bucksbaum,[8] D. A. Reis,[8] J. Rudati,[9] P. H. Fuoss,[10] C. C. Kao,[11] D. P. Siddons,[11] R. Pahl,[12] J. Als-Nielsen,[13] S. Duesterer,[4] R. Ischebeck,[4] H. Schlarb,[4] H. Schulte-Schrepping,[4] Th. Tschentscher,[4] J. Schneider,[4] D. von der Linde,[14] O. Hignette,[15] F. Sette,[15] H. N. Chapman,[16] R. W. Lee,[16] T. N. Hansen,[2] S. Techert,[17] J. S. Wark,[5] M. Bergh,[6] G. Huldt,[6] D. van der Spoel,[6] N. Timneanu,[6] J. Hajdu,[6] R. A. Akre,[18] E. Bong,[18] P. Krejcik,[18] J. Arthur,[1] S. Brennan,[1] K. Luening,[1] J. B. Hastings[1]

The motion of atoms on interatomic potential energy surfaces is fundamental to the dynamics of liquids and solids. An accelerator-based source of femtosecond x-ray pulses allowed us to follow directly atomic displacements on an optically modified energy landscape, leading eventually to the transition from crystalline solid to disordered liquid. We show that, to first order in time, the dynamics are inertial, and we place constraints on the shape and curvature of the transition-state potential energy surface. Our measurements point toward analogies between this nonequilibrium phase transition and the short-time dynamics intrinsic to equilibrium liquids.

In a crystal at room temperature, vibrational excitations, or phonons, only slightly perturb the crystalline order. In contrast, liquids explore a wide range of configurations set by the topology of a complex and time-dependent potential energy surface (*1*, *2*). By using light to trigger changes in this energy landscape, well-defined initial and final states can be generated to which a full range of time-resolved techniques may be applied. In particular, light-induced structural transitions between the crystalline and liquid states of matter may act as simple models for dynamics intrinsic to the liquid state or to transition states in general (*3*).

In this context, a new class of nonthermal processes governing the ultrafast solid-liquid melting transition has recently emerged, supported by time-resolved optical (*4*–*7*) and x-ray (*8*–*10*) experiments and with technological applications ranging from micromachining to eye surgery (*11*). Intense femtosecond excitation of semiconductor materials results in the excitation of a dense electron-hole plasma, with accompanying dramatic changes in the interatomic potential (*12*–*14*). At sufficiently high levels of excitation, it is thought that this process leads to disordering of the crystalline lattice on time scales faster than the time scale for thermal equilibration [often known as the electron-phonon coupling time, on the order of a few picoseconds (*15*)]. In a pioneering study, Rousse *et al.* (*9*) determined that the structure of indium antimonide (InSb) changes on sub-picosecond time scales, but the mechanism by which this occurs and the microscopic pathways the atoms follow have remained elusive, in part because of uncertainties in the pulse duration of laser-plasma sources and signal-to-noise limitations.

Research and development efforts leading toward the Linac Coherent Light Source (LCLS) free-electron laser have facilitated the construction of a new accelerator-based x-ray source, the Sub-Picosecond Pulse Source (SPPS), which uses the same linac-based acceleration and electron bunch compression schemes to be used at future free-electron lasers (*16*, *17*). In order to produce femtosecond x-ray bursts, electron bunches at the Stanford Linear Accelerator Center (SLAC) are chirped and then sent through a series of energy-dispersive magnetic chicanes to create 80-fs electron pulses. These pulses are then transported through an undulator to create sub-100-femtosecond x-ray pulses (*18*). In order to overcome the intrinsic jitter between x-rays and a Ti:sapphire-based femtosecond laser

[1]Stanford Synchrotron Radiation Laboratory/Stanford Linear Accelerator Center (SLAC), Menlo Park, CA 94025, USA. [2]Department of Physics, Lund Institute of Technology, Post Office Box 118, S-22100, Lund, Sweden. [3]Institut für Optik und Quantenelektronik, Friedrich-Schiller Universität Jena, Max-Wien-Platz 1, 07743 Jena, Germany. [4]Deutsches Elektronen-Synchrotron DESY, Notkestrasse 85, 22607 Hamburg, Germany. [5]Department of Physics, Clarendon Laboratory, Parks Road, University of Oxford, Oxford OX1 3PU, UK. [6]Department of Cell and Molecular Biology, Biomedical Centre, Uppsala University, SE-75124 Uppsala, Sweden. [7]Department of Physics, University of California, Berkeley, CA 94720, USA. [8]FOCUS (Frontiers in Optical Coherent and Ultrafast Science) Center, Department of Physics and Applied Physics Program, University of Michigan, Ann Arbor, MI 48109, USA. [9]Advanced Photon Source, [10]Materials Science Division, Argonne National Laboratory, Argonne, IL 60439, USA. [11]National Synchrotron Light Source, Brookhaven National Laboratory, Upton, NY 11973, USA. [12]Consortium for Advanced Radiation Sources, University of Chicago, Chicago, IL 60637, USA. [13]Niels Bohr Institute, Copenhagen University, 2100 Copenhagen Ø, Denmark. [14]Institut für Experimentelle Physik, Universität Duisburg-Essen, D-45117 Essen, Germany. [15]European Synchrotron Radiation Facility, 38043 Grenoble Cedex 9, France. [16]Physics Department, Lawrence Livermore National Laboratory, Livermore, CA 94550, USA. [17]Max Plank Institute for Biophysical Chemistry, Am Faßberg 11, 37077 Göttingen, Germany. [18]SLAC, Menlo Park, CA 94025, USA.

system, pump-probe measurements using an InSb sample were conducted in a cross-beam geometry (*19*, *20*) with the optical pump pulse incident at an angle with respect to the x-ray probe pulse. In this way, a temporal sweep is created along the crystal surface that transforms temporal information into spatial information as a result of the difference in propagation times across the sample surface. By imaging the diffracted x-ray spot with a charge-coupled device (CCD) camera, we obtained the complete time history around $t = 0$ in a single shot.

Typical single-shot images are shown in Fig. 1. The top image shows x-rays diffracted from the unperturbed sample. The bottom image is obtained when the pump and probe pulses overlap in space and time on the sample. The sharp edge in the bottom image indicates time zero. To the left of this edge, x-rays scatter from the unperturbed sample before the optical excitation pulse arrives. To the right, x-rays probe the optically induced liquid state, resulting in a strong decrease in the diffracted intensity. Our temporal resolution is set by the pulse duration of the x-ray probe and the accuracy with which we can image the surface topography; we estimated this to be ≤130 fs for the (111) reflection and ≤80 fs for the (220) reflection by imaging the sharp edge of a razor blade placed on the sample surface.

The measured time-dependent intensity values, $I(Q,t)$ (where Q is the reciprocal lattice vector for the reflection probed), for both the (111) and (220) reflections were averaged over 10 single-shot images (Fig. 2) (*21*). The x-ray incidence angle was kept constant at 0.4° for both reflections by rotating an asymmetrically cut crystal about its surface normal (the same crystal is used for both reflections). In this way, the x-ray probe depth was fixed at 50 nm (comparable to the laser excitation depth), and the laser spot size was unchanged when switching between different x-ray reflections. Thus, the experiments probed the dynamical behavior for the two reflections under identical conditions. Figure 2 shows (111) and (220) data fit to both exponential and Gaussian decays.

We observe first that, for times after excitation, the diffracted intensity is nonexponential and well-fit by a Gaussian with peak centered at the excitation time. Moreover, the (220) reflection decays with a time constant qualitatively faster than that for the (111). The times for the intensity to fall from 90% to 10% of its initial value for the (111) and (220) reflections are 430 and 280 fs, respectively, with ratio $\tau_{111}/\tau_{220} = 1.5 \pm 0.2$. This value is equal (within experimental error) to the ratio of the magnitude of the reciprocal lattice vectors for the two reflections ($\sqrt{8/3}$).

This inverse Q-dependent scaling and Gaussian time dependence strongly implies statistical atomic motion and suggests that the data can be described with use of a time-dependent Debye-Waller (DW) model, which relates the time-dependent decrease in scattered intensity to a time-dependent root mean square (RMS) displacement:

$$I(Q,t) = e^{-2W} = e^{-Q^2\langle u^2(t)\rangle/3} \qquad (1)$$

Here, W is the standard DW factor and $\langle u^2(t)\rangle$ is the time-dependent mean-square displacement of the photoexcited atoms averaged spatially over the sample. This model makes physical sense if the disordering process can be described as an effective amplification of the RMS displacements characteristic of a room temperature thermal distribution, preserving $\langle u\rangle = 0$. The time-averaged assumption that is usually made in the derivation of the DW factor may then be replaced by a spatial average over all excited atoms (*22*). A time-dependent increase in the RMS displacement is indeed what one would expect given the strong optically induced modification of the potential surface. After an impulsive softening of the interatomic potential and for short times afterward (to first order in time), the atoms continue to move with velocities set by initial conditions, i.e., inertially, following Newton's Third Law. To first order in time, with $\langle u^2(t)\rangle^{1/2} = v_{rms}t$, the time-resolved diffracted intensity $I(Q,t)$ is then expected to decay as $I(t) \sim e^{-Q^2 v_{rms}^2 t^2/3}$, i.e., Gaussian in both Q and t with a time constant that varies inversely with Q, exactly as observed.

The validity of this model was checked in three different ways: (i) comparison of the extracted RMS displacements for the (111) and (220) reflections, (ii) comparison of the

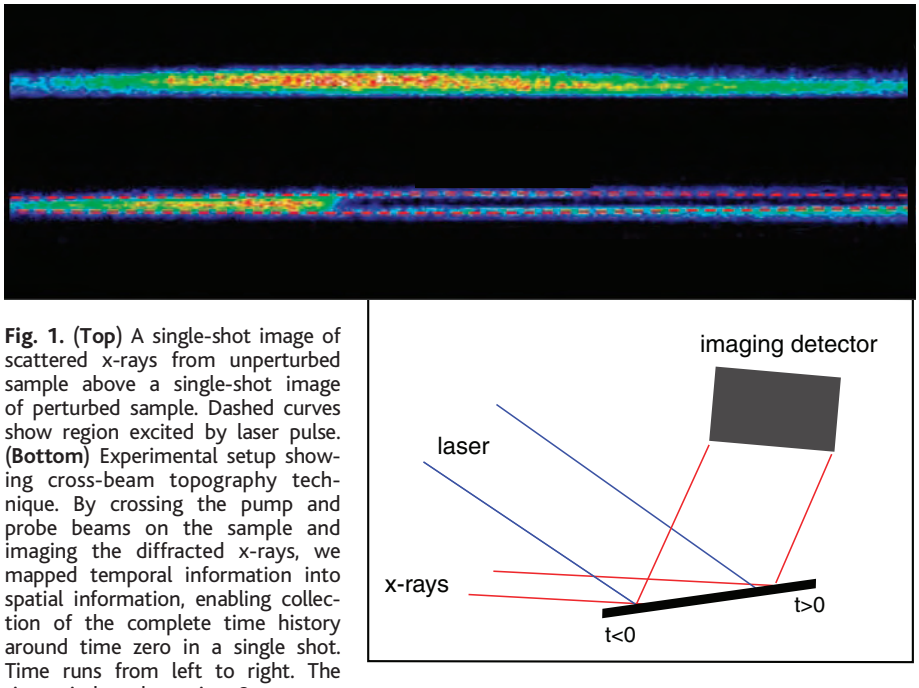

Fig. 1. (**Top**) A single-shot image of scattered x-rays from unperturbed sample above a single-shot image of perturbed sample. Dashed curves show region excited by laser pulse. (**Bottom**) Experimental setup showing cross-beam topography technique. By crossing the pump and probe beams on the sample and imaging the diffracted x-rays, we mapped temporal information into spatial information, enabling collection of the complete time history around time zero in a single shot. Time runs from left to right. The time window shown is ~8 ps.

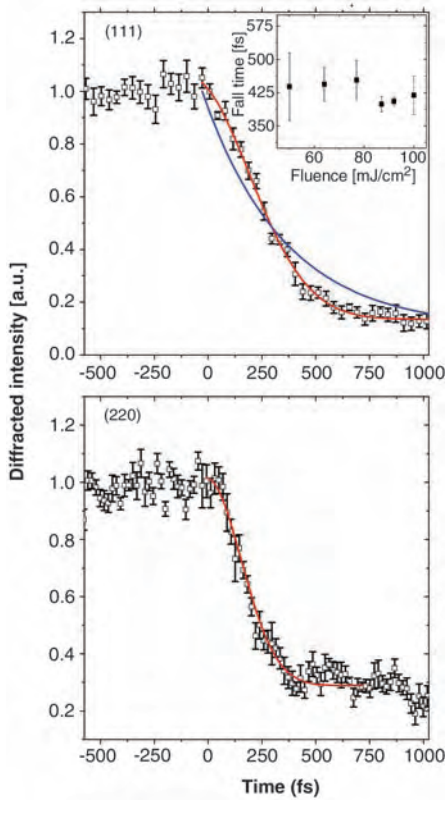

Fig. 2. Time-dependent diffracted intensity for (111) (**top**) and (220) (**bottom**) reflections, measured under identical excitation conditions. Red curves are Gaussian fits to the data, corresponding to 10 to 90% fall times of 430 fs and 280 fs. Blue curve is an exponential fit. (Inset) Fluence dependence of 10 to 90 time constants for (111) data. Error bars reflect the standard deviation of the mean, determined from the scatter in the individual measurements.

measured velocity of the atoms to room temperature excitations, and (iii) fluence dependence of the time-constants of the decay of the diffracted intensity. Extracted RMS displacements for the (111) and the (220) reflections are shown in Fig. 3, obtained by using Eq. 1 to invert the raw $I(Q,t)$ data. For short times, the two curves overlap well, indicating an initial isotropic-disordering process, independent of reciprocal lattice vector. (At long times, different final displacements derived from the two reflections may imply an anisotropy in the disordering process and/or a breakdown in the DW model; however, uncertainty in the effective laser penetration depth makes this conclusion uncertain.)

Second, for short times, we observe that the RMS displacements are linear in time, with a slope (corresponding to a velocity) of 2.3 Å/ps. This value is in good agreement with room temperature RMS velocities in InSb [$(3k_bT/M)^{1/2}$ = 2.5 Å/ps, where M is the average mass of InSb and T = 300 K (*23*)]. Lastly, the Fig. 2 inset shows the fluence dependence of the time constants for the (111) reflection. There is little variation with fluence (a similar result is obtained for the 220 reflection). Thus, as might be expected for short times, it is difficult to tell the difference between a flat potential (corresponding to a free particle) and a motion driven by a softened phonon with an imaginary frequency (corresponding to a saddle point on the potential energy surface). From our data, we can place both an upper and lower bound on the extent of the softening of the potential surface. At very large softenings, we expect to observe acceleration of the atoms as they fall down the potential energy surface. Because we observe that the dynamics remain inertial for at least 250 fs, it can be shown (neglecting anharmonicities in the potential) that this requires a negative curvature ≤1 eV/Å^2. Similarly, that we observe displacements on the order of 1 Å from the equilibrium position implies a maximum positive curvature (corresponding to a real frequency) of ~0.1 eV/Å^2, which represents a dramatic change in the interatomic potential. Figure 4 illustrates the changes in the interatomic potential and atomic-scale displacements calculated on the basis of this model. The implication is then of a transition state in which the interatomic potential is softened enough that the atoms initially move freely with large amplitude along an effectively barrierless potential energy surface with initial conditions set by room-temperature thermodynamic velocities. This simple model fits all of our data at short times with no adjustable parameters.

The dynamics we observe during the ultrafast transition of a crystalline solid into a liquid show similarity with the intrinsic short time dynamics observed in equilibrium liquids from frequency-domain inelastic neutron scattering and molecular dynamics simulations (*24*, *25*). Indeed, one may show (*26*) that the RMS displacement of an atom in the liquid state obeys

$$u^2(t) = \frac{3k_BT}{M}t^2 - \frac{k_bT}{4M}\Omega^2t^4 \qquad (2)$$

where Ω is a collision frequency. To first order in time, the dynamics are inertial, with atoms moving at their thermal velocities along a potential landscape characteristic of the instantaneous atomic positions. Our results thus indicate that, at short times, the ultrafast solid-liquid transition may be viewed as representative of the short time-scale structural rearrangements intrinsic to the liquid state. At longer times, atoms begin to collide and a transition to a diffusive regime occurs. Although we resolve an inertially driven divergence of the mean square displacements [typically associated with solid-liquid transitions (*27*) but here observed before any heat is transferred to the lattice], we do not observe clear evidence of diffusive dynamics. This would manifest itself in the tail of the decay in the diffracted intensity as an exponential rather than a Gaussian time response (with $u \sim t^{1/2}$ one obtains this result). Thus, during the first few hundred femtoseconds, although the lattice displacements correspond to a large fraction of the interatomic distances and the strong covalent bonds characteristic of the crystalline state are broken or strongly modified, the average displacement $\langle u(t) \rangle$ from the equilibrium lattice sites is still zero, reflective of the initial crystalline state. In this respect, for the first few hundred femtoseconds, the state of the system is intermediate between that of a solid and that of a liquid.

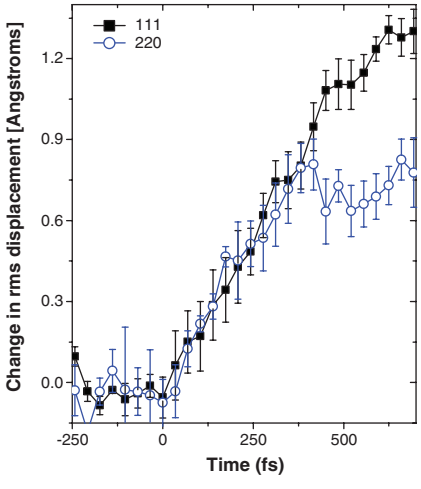

Fig. 3. The change in the RMS displacement $\sqrt{\delta u^2(t)}$ extracted from the time-dependent diffracted intensity with use of the DW model. For short times, the measured displacements agree well for both x-ray reflections, validating the model. The slope corresponds to a velocity in good agreement with the room-temperature RMS velocity in InSb.

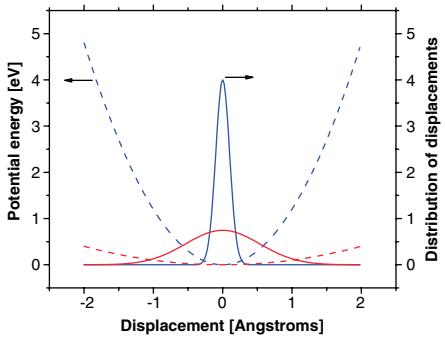

Fig. 4. One-dimensional illustration of changes in the interatomic potential (dashed) and distribution of atomic displacements (solid) from the equilibrium state. Blue curves refer to the unperturbed state, and red curves refer to t = 200 fs after excitation. At equilibrium and at room temperature in InSb, RMS displacements are ~0.1 Å (*29*). The interatomic potential for this case is calculated by using equipartition and an assumption of one-dimensional simple harmonic behavior. At t = 200 fs, we measure RMS displacements ~ 0.5 Å corresponding to a substantial fraction of the interatomic spacing. The softened potential shown (dashed red) corresponds to the minimum softening required (0.1 eV/Å^2) to be consistent with our experimental results.

References and Notes

1. F. H. Stillinger, T. A. Weber, *Phys. Rev. A.* **25**, 978 (1982).
2. R. Stratt, *Accts. Chem. Res.* **28**, 201 (1995).
3. B. J. Siwick *et al.*, *Science* **302**, 1382 (2003).
4. C. Shank, R. Yen, C. Hirlimann, *Phys. Rev. Lett.* **51**, 900 (1983).
5. I. Shumay, U. Hofer, *Phys. Rev. B* **53**, 15878 (1996).
6. K. Sokolowski-Tinten, J. Bialkowski, D. von der Linde, *Phys. Rev. B* **51**, 14186 (1995).
7. S. Sundaram, E. Mazur, *Nat. Mater.* **1**, 217 (2002).
8. C. Siders *et al.*, *Science* **286**, 1340 (1999).
9. A. Rousse *et al.*, *Nature* **410**, 65 (2001).
10. K. Sokolowski-Tinten *et al.*, *Phys. Rev. Lett.* **87**, 225701 (2001).
11. X. Lui, D. Du, G. Mourou, *IEEE J. Quantum Electron.* **33**, 1706 (1997).
12. P. Stampfli, K. Bennemann, *Phys. Rev. B* **49**, 7299 (1994).
13. T. Dumitrica, A. Burzo, Y. Dou, R. Allen, *Phys. Status Solidi B* **241**, 2331 (2004).
14. H. O. Jeschke *et al.*, *Appl. Surf. Sci.* **197**, 839 (2002).
15. A. H. Chin *et al.*, *Phys. Rev. Lett.* **83**, 336 (1999).
16. P. Krejcik *et al.*, in *Proceedings of the 2003 Particle Accelerator Conference*, IEEE, Portland, OR, 12 to 16 May 2003, J. Chew, P. Lucas, S. Webber, Eds. (IEEE, Piscataway, NJ, 2003), p. 423.
17. R. Service, *Science* **298**, 1356 (2002).
18. Measurements of electron bunch length and energy spread as they evolve through the SLAC linac are in good agreement with the particle tracking codes used to predict 80-fs bunches. Measurements by interferometric autocorrelation of the coherent transition radiation from the electron bunches are also consistent with 80-fs electron bunches. These independent measurements provide strong evidence that our estimates of the x-ray pulse duration as well as the pulse shape at optimal compression are accurate.
19. O. Synnergren *et al.*, *Appl. Phys. Lett.* **80**, 3727 (2002).
20. R. Neutze, J. Hajdu, *Proc. Natl. Acad. Sci. U.S.A.* **94**, 5651 (1997).
21. The measured time constants are in good agreement with the average of the time constants extracted from each image. By comparing our measurements with independent measurements of the electron-bunch arrival time, we estimate that the relative timing of laser and x-rays from shot to shot can be determined to better than 60 fs by spatially recording the midpoint of the sudden drop in diffracted intensity (*28*).

22. P. Liu, P. Okamoto, N. Zaluzec, M. Meshii, *Phys. Rev. B* **60**, 800 (1999).
23. G. L. Squires, *Introduction to the Theory of Thermal Neutron Scattering* (Cambridge Univ. Press, Cambridge, 1978).
24. B. Dasannacharya, K. Rao, *Phys. Rev.* **137**, A417 (1965).
25. A. Paskin, A. Rahman, *Phys. Rev. Lett.* **16**, 300 (1966).
26. U. Balucani, M. Zoppi, *Dynamics of the Liquid State* (Clarendon Press, Oxford, 1994).
27. F. Lindemann, *Phys. Z.* **11**, 609 (1910).
28. A. Cavalieri *et al.*, *Phys. Res. Lett.*, in press.
29. J. F. Vetelino, S. P. Gaur, S. S. Mitra, *Phys. Rev. B* **5**, 2360 (1972).
30. Portions of this research were supported by the U.S. Department of Energy, Office of Basic Energy Science, through direct support for the SPPS and individual investigators and through the Stanford Synchrotron Radiation Laboratory, a national user facility operated by Stanford University. Additional support for the construction of SPPS was provided in part by Uppsala University and the Swedish Research Council. K.S.-T., D.V.D.L., and S.T. gratefully acknowledge financial support by the Deutsche Forschungsgemeinschaft. J.L., O.S., T.N.H., K.S.-T., and D.V.D.L. acknowledge the support of the European Commission through the FAMTO, X-RAY FEL PUMP-PROBE, and XPOSE projects. J.L. acknowledges the support from Wallenberg Research Link and the Swedish Foundation for Strategic Research. R.W.F. acknowledges support from the U.S. Department of Energy through the High Energy Density Science Grants Program and through a collaboration with Chemistry and Materials Science at Lawrence Livermore National Laboratory. A.M.L. thanks D. Moncton for useful conversations.

Supporting Online Material
www.sciencemag.org/cgi/content/full/308/5720/392/DC1
Materials and Methods
Figs. S1 and S2

29 November 2004; accepted 22 February 2005
10.1126/science.1107996

A Convergent Enantioselective Route to Structurally Diverse 6-Deoxytetracycline Antibiotics

Mark G. Charest, Christian D. Lerner, Jason D. Brubaker, Dionicio R. Siegel, Andrew G. Myers*

Complex antibiotics based on natural products are almost invariably prepared by semisynthesis, or chemical transformation of the isolated natural products. This approach greatly limits the range of accessible structures that might be studied as new antibiotic candidates. Here we report a short and enantioselective synthetic route to a diverse range of 6-deoxytetracycline antibiotics. The common feature of this class is a scaffold of four linearly fused rings, labeled A through D. We targeted not a single compound but a group of structures with the D ring as a site of structural variability. A late-stage, diastereoselective C-ring construction was used to couple structurally varied D-ring precursors with an AB precursor containing much of the essential functionality for binding to the bacterial ribosome. Five derivatives were synthesized from benzoic acid in yields ranging from 5 to 7% over 14 to 15 steps, and a sixth, (–)-doxycycline, was synthesized in 8.3% yield over 18 steps.

The limitations of chemical synthesis frequently present a substantial obstacle to the development and discovery of new antibiotics and of pharmaceutical agents in general. The problem is nowhere more evident than among the structurally complex natural products tetracycline (**1**) and erythromycin. Both agents have proven highly effective in treating a wide range of bacterial infections, but decades of clinical use have led to the emergence of widespread bacterial resistance and, as a result, a need for the development of new antibiotics (*1*–*3*). The approach to the synthesis of varied structures in these classes has changed little in more than 50 years of research and is largely restricted to a process of semisynthesis, whereby the natural product is isolated and then modified, although approaches based on modified biosynthetic pathways are under development (*4*–*6*).

The tetracycline class of molecules is characterized by a carbon skeleton composed of four linearly fused six-membered carbon rings, conventionally labeled A through D (Fig. 1A). Among the derivatives accessed by semisynthesis, those with the hydroxyl group removed from carbon 6 of the C ring have shown particular clinical promise. These 6-deoxytetracyclines are considerably more resistant to degradation than their 6-hydroxy counterparts, and they show equal or greater potencies in antibacterial assays (*7*, *8*). The clinical efficacy of 6-deoxytetracyclines such as doxycycline (**2**) and minocycline (**3**) argues for a broad evaluation of 6-deoxytetracyclines. Unfortunately, the elaboration of natural tetracyclines is greatly limiting in terms of scope, and a general synthetic route to diverse tetracyclines has been elusive.

Here we report a short and efficient route for the synthesis of enantiomerically pure members of the 6-deoxytetracyclines from benzoic acid. The route we describe allows for the synthesis of 6-deoxytetracyclines (both with and without a hydroxyl group at C5) by a late-stage coupling reaction of the AB precursors **4** or **5** (Figs. 1B and 2) and provides access to a wide range of 6-deoxytetracyclines with modified D rings, as illustrated by the preparation of (–)-doxycycline (**2**), (–)-6-deoxytetracycline (**6**), the D-ring heterocyclic derivatives **7** and **8**, 10-deoxysancycline (**9**), and the pentacycline derivative **10** (see Fig. 3 for structures). The advantage of the late-stage

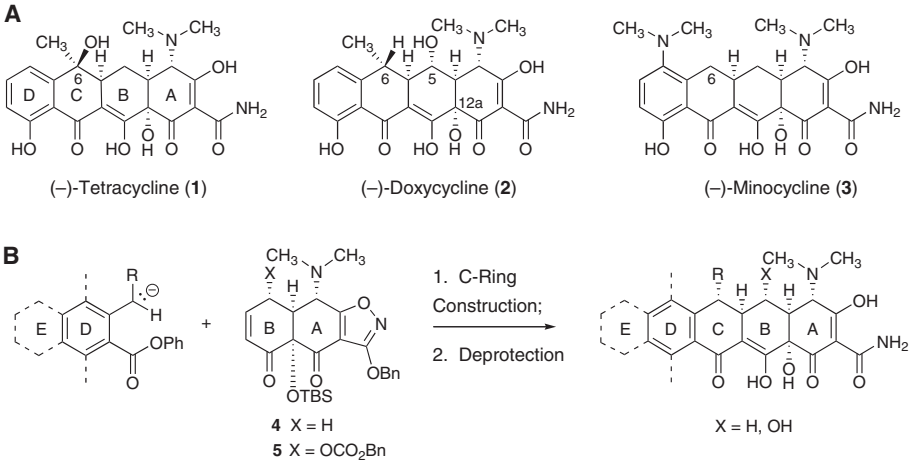

Fig. 1. (**A**) Chemical structures of tetracycline antibiotics. (–)-Tetracycline (**1**) was first produced semisynthetically, by hydrogenolysis of the fermentation product aureomycin (7-chlorotetracycline), but later was discovered to be a natural product and is now produced by fermentation (*8*). (–)-Doxycycline (**2**) and minocycline (**3**) are clinically important non-natural antibiotics and are both manufactured by multistep chemical transformations of fermentation products (semisynthesis) (*8*). (**B**) A generalized Michael-Dieckmann reaction sequence that forms the C ring of tetracyclines from the coupling of structurally varied carbanionic D-ring precursors with either of the AB precursors **4** or **5**.

Department of Chemistry and Chemical Biology, Harvard University, Cambridge, MA 02138, USA.

*To whom correspondence should be addressed. E-mail: myers@chemistry.harvard.edu

C-ring construction that we report [AB + D → ABCD (Fig. 1B)] is that much of the polar functionality known to play a role in the binding of tetracyclines to the bacterial ribosome lies within the AB fragment (*9*, *10*). At the same time, wide structural variation on or near the D ring has been cited as a means to overcome bacterial resistance. For example, the advanced clinical candidate tigecycline (*11*), which bears a substituted D ring, is reported to be one of the most promising new antibiotics under evaluation by the U.S. Food and Drug Administration (*12*).

Previous approaches to the synthesis of the tetracycline antibiotics have proceeded by stepwise assembly of the ABCD ring system, beginning with D or CD precursors, and are typically low-yielding. Examples are the Woodward synthesis of (±)-6-deoxy-6-demethyltetracycline (sancycline, 25 steps, ~0.002% yield) (*13*); the Shemyakin synthesis of (±)-12a-deoxy-5a,6-anhydrotetracycline (*14*); and the Muxfeldt synthesis of (±)-5-oxytetracycline (terramycin, 22 steps, 0.06% yield) (*15*); as well as the synthesis of (–)-tetracycline itself from the A-ring precursor D-glucosamine (34 steps, 0.002% yield) (*16*). The most efficient construction of the tetracycline ring system thus far is the synthesis of (±)-12a-deoxytetracycline by the Stork laboratory (16 steps, 18 to 25% yield) (*17*). In this case, however, the absence of a hydroxyl group at a fusion point of the A and B rings (C12a) is associated with greatly reduced antimicrobial activity (*18*), and late-stage introduction of this group has not been practical (*13*–*17*). We therefore introduced the C12a hydroxyl group in the first step of our sequence (Fig. 2) and used the stereogenic center produced in that step to elaborate all others in the target molecule.

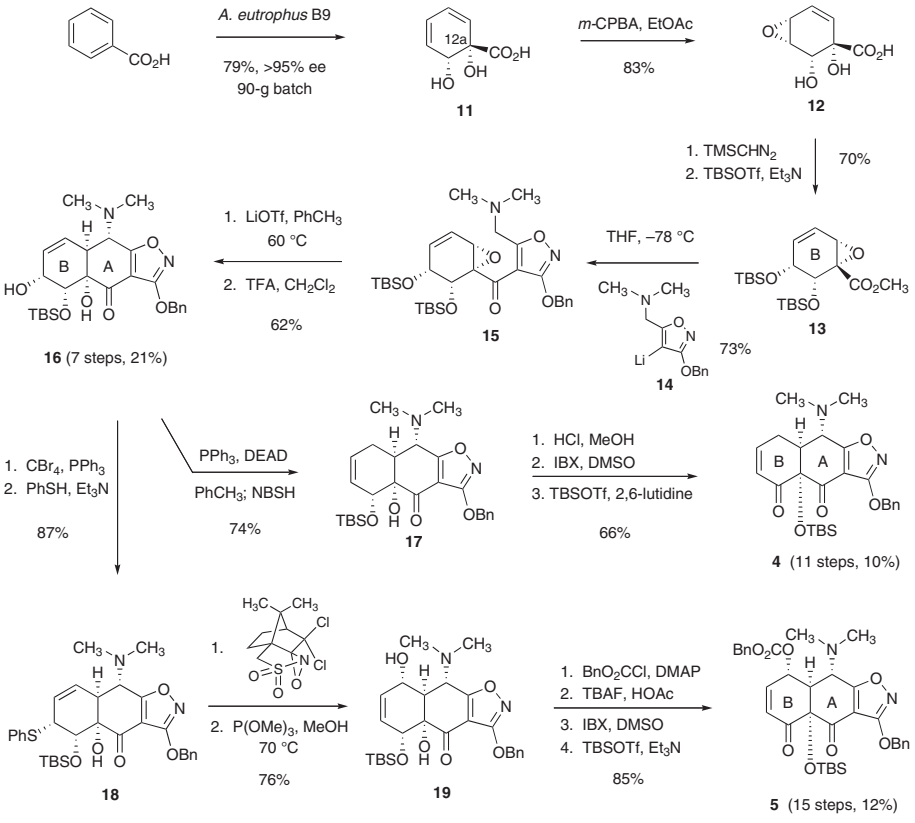

Fig. 2. Benzoic acid is transformed in seven steps to the key bicyclic intermediate **16**. This product is then used to prepare the AB precursor enone **4** by the four-step sequence shown or to enone **5**, the AB precursor to 6-deoxy-5-hydroxytetracycline derivatives, by the eight-step sequence shown.

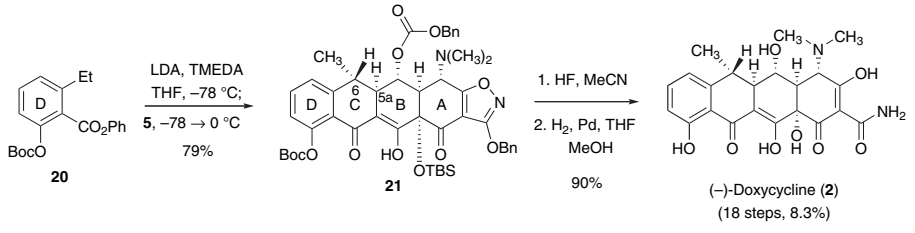

Scheme 1.

Our synthesis (Fig. 2) was initiated by whole-cell microbial dihydroxylation of benzoic acid (which would become the B ring of the targeted 6-deoxytetracyclines) using a mutant strain of *Alcaligenes eutrophus* (*19*, *20*), producing the diol **11** with >95% enantiomeric excess in 79% yield (a 90-g batch, ~13 g/liter). Hydroxyl-directed epoxidation of the microcrystalline product (**11**, *m*-chloroperbenzoic acid) provided the α-oriented epoxide **12** in 83% yield; esterification of this product with trimethylsilyldiazomethane, followed by bis-silylation and concomitant epoxide isomerization in the presence of *tert*-butyldimethylsilyl triflate (three equivalents), afforded the epoxy ester **13** in 70% yield (*20*).

In constructing the A ring, we protected the vinylogous carbamic acid function (the right side of the final A ring as drawn) as a 5-benzyloxyisoxazole group, developed by Stork and Haggedorn for that purpose (*21*). 3-Benzyloxy-5-dimethylaminomethylisoxazole, prepared on the mole scale by a simple four-step sequence from glyoxylic acid (*22*, *23*), was deprotonated at C4 with *n*-butyllithium, and the resulting organolithium reagent (**14**) was then added to the epoxy ester **13**, forming the ketone **15** (73%). In a key step of the synthesis, closure of the A ring was achieved by warming of the ketone **15** with lithium triflate (5 mole %) at 60°C, followed by selective removal of the allylic silyl ether of the rearranged product by means of trifluoroacetic acid. The tricyclic AB precursor **16** was isolated in 62% yield after purification by flash-column chromatography. We believe that the transformation of **15** to **16** involves initial S_N-prime opening of the allylic epoxide by the *N*,*N*-dimethylamino group, followed by ylide formation and [2,3]-sigmatropic rearrangement, a process that is reminiscent of the Sommelet-Hauser rearrangement (*24*). Compound **16** possesses the requisite cis stereochemistry of the AB fusion, as well as an α-oriented *N*,*N*-dimethylamino substituent (confirmed by x-ray crystallographic analysis of a derivative), and serves as a common intermediate for the synthesis of both the AB precursor enone **4** (four steps, 49% yield) and the AB precursor to 5-α-hydroxy-6-deoxytetracyclines, enone **5** (eight steps, 56% yield), as detailed below.

Conversion of intermediate **16** to enone **4** first required migration of the B-ring double bond, with concurrent reduction of the hydroxyl group. This reductive transposition (*25*) was achieved using triphenylphosphine, diethyl azodicarboxylate, and *o*-nitrobenzenesulfonyl hydrazide (added last, in a procedural variant), affording the transposed cycloalkene **17** in 74% yield. Hydrolysis of the silyl ether protective group within **17** (using HCl and methanol), oxidation of the resulting allylic alcohol (using *o*-iodoxybenzoic acid in dimethylsulfoxide) (*26*), and protection of the remaining (tertiary) carbinol with *tert*-butyldimethylsilyl trifluoro-

methanesulfonate and 2,6-lutidine (*27*) then provided the enone **4** in 66% yield (three steps) after flash-column chromatography.

By a somewhat longer but slightly more efficient sequence, the intermediate **16** could also be transformed into the enone **5**, the AB precursor to 5-α-hydroxy-6-deoxytetracyclines (Fig. 2). This sequence began with the replacement of the secondary hydroxyl group of **16** with a thiophenyl group to form **18**, with net stereochemical retention. Next, diastereoselective sulfoxidation with a chiral oxidant (*28*) (99:1 selectivity) and Mislow-Evans rearrangement (*29*) produced the allylic alcohol **19** in 66% yield over the four steps. High diastereoselectivity in the sulfoxidation step was essential, because only one diastereomer (the major isomer under the conditions specified, stereochemistry not determined) underwent efficient thermal rearrangement. After protection of the allylic alcohol **19** by means of benzyl chloroformate, a sequence nearly identical to the final three steps of the synthesis of **4** was employed to transform the resulting benzyl carbonate into the enone **5** in 85% yield (56% net yield over the eight steps from **16**).

From these precursors, 6-deoxytetracyclines were assembled with all requisite functionality and stereochemistry in a single operation. Enones **4** or **5** were coupled with a range of different carbanionic D-ring precursors in a Michael-Dieckmann reaction sequence (*30*) that forms two carbon-carbon bonds and the C ring of the 6-deoxytetracyclines (Figs. 1B and 3). The process is perhaps best illustrated in detail by the three-step synthesis of (–)-doxycycline from the AB precursor **5** (Scheme 1). The D-ring precursor in this case (**20**) was synthesized in 42% yield over five steps from anisic acid. Deprotonation of **20** (4.5 equivalents) at the benzylic position (C6 in the product) was achieved with lithium diisopropyl amide in the presence of *N*,*N*,*N*′,*N*′-tetramethylethylenediamine in tetrahydrofuran at –78°C. The enone **5** was then added to the solution and the temperature was raised to 0°C. The tetracyclic coupling product **21** was isolated as a single diastereomer in 79% yield after purification by reverse-phase high-performance liquid chromatography (RP-HPLC). Removal of the protective groups (90% yield over two steps) and purification by RP-HPLC afforded (–)-doxycycline hydrochloride in 8.3% net yield over 18 steps from benzoic acid.

A remarkable feature of the convergent coupling reaction that produces the tetracyclic product **21** is its stereoselectivity. Although, in theory, four diastereomeric products can be formed by stereochemical variation of carbons 5a and 6 (the former being a BC fusion point), only one emerged in significant yield, and it matched the configuration (5a*R*, 6*R*) of the known biologically active 6-deoxytetracyclines. A minor diastereomeric impurity, believed to be 6-epi-**21**, was also isolated in separate RP-HPLC fractions (<7% yield). Michael-Dieckmann cyclization sequences (*30*) and condensations of *o*-toluate anions in particular (*31*–*33*) are extensively precedented in synthesis but not with the high degree of diastereoselectivity seen here.

Phenyl ester activation in toluate condensations is also precedented, though in a system that forms a fully aromatized cyclization product (*34*). We observed that the presence of the phenyl ester group of the D-ring precursor **20** was essential for successful cyclization to occur. Anions derived from D-ring

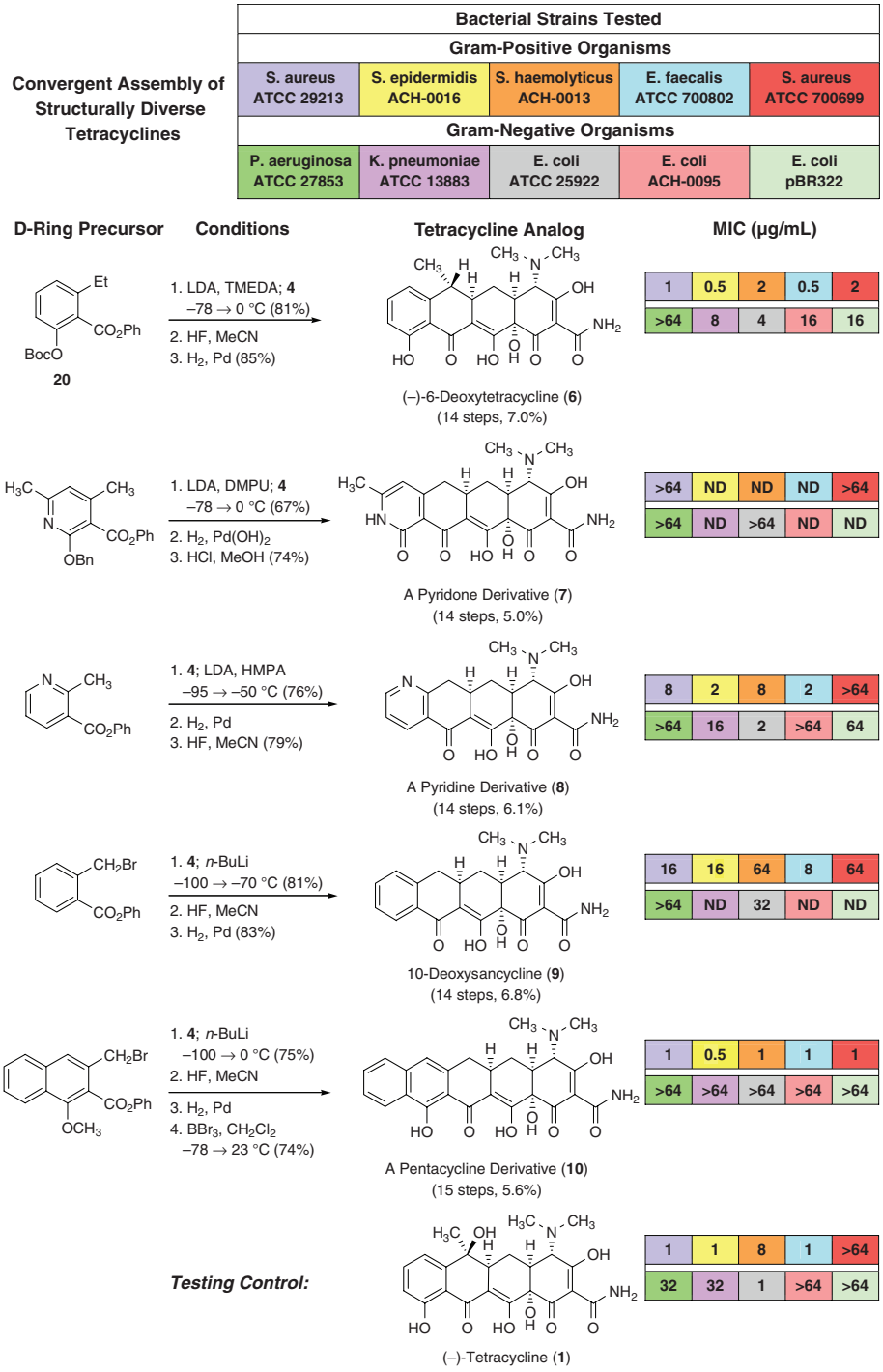

Fig. 3. Synthesis of structurally diverse 6-deoxytetracyclines by coupling of structurally diverse D-ring precursors and AB precursors **4** or **5**. The number of steps and overall yields from benzoic acid are shown in parentheses below each structure synthesized. Shown also are MIC values (in μg/ml) for whole-cell antibacterial testing of each analog against five Gram-positive and five Gram-negative microorganisms. Corresponding MICs for tetracycline (**1**), a testing control, appear at the bottom.

precursors containing simple alkyl esters underwent Michael addition, but the resulting adducts did not cyclize. Perhaps even more remarkable than the condensation that produces **21** is the parallel transformation of **20** with the enone **4** (Fig. 3, entry 1), which forms (–)-6-deoxytetracycline (**6**) in protected form with >20:1 diastereoselectivity, in 81% yield after purification by RP-HPLC (diastereomerically pure, a minor diastereomer, epimeric at C6, was also isolated separately). It appears that additions to **4** and **5** proceed almost exclusively by addition to one face of each enone (the top face as drawn in Fig. 1B), producing C5a stereochemistry corresponding to that of natural tetracyclines, although why this should be the case is not obvious.

Efficient and stereoselective condensations were not restricted to the *o*-toluate anion derived from the D-ring substrate **20**. In all, we prepared six 6-deoxytetracycline variants (Fig. 3). In each case, it was necessary to optimize the specific conditions for *o*-toluate anion generation and trapping. For the synthesis of products **8**, **9**, and **10** (Fig. 3), anion generation was best conducted in situ, in the presence of the enone **4**, either by selective deprotonation (**8**) or by lithium-halogen exchange (**9** and **10**). A number of potentially competing nonproductive reaction sequences might have intervened during in situ anion generation (such as enolization of **4**); the observed efficiencies of the transformations are surprising in light of this. It is also noteworthy that in situ anion generation permits the use of *o*-toluates lacking an *o*-alkoxy substituent (such as used in the synthesis of **8** and **9**), substrates that are known to be problematic from prior studies (*35*). Also, lithium-halogen exchange reactions of benzylic halides (such as used in the synthesis of **9** and **10**) had previously been considered impracticable (*36*, *37*).

The efficiencies of the synthetic sequences we report have allowed for the preparation of sufficient quantities of each tetracycline analog for antibacterial testing, using standard serial-dilution techniques (in 5- to 20-mg amounts). Minimum inhibitory concentrations (MICs) were determined for each analog in whole-cell antimicrobial assays using five Gram-positive and five Gram-negative organisms (Fig. 3). Thus far, the pentacycline derivative **10** has shown the most promising antibacterial properties, with activity equal to or greater than tetracycline in each of the Gram-positive strains examined, including strains with resistance to tetracycline, methicillin, and vancomycin. Although this finding is noteworthy, it is very likely that antibiotics with even greater potencies and/or improved pharmacological properties will emerge with further exploration of the complex chemical space now made accessible by the versatile synthetic route described.

References and Notes

1. C. Walsh, *Antibiotics: Actions, Origins, Resistance* (American Society for Microbiology Press, Washington, DC, 2003).
2. S. G. B. Amyes, *Magic Bullets, Lost Horizons: the Rise and Fall of Antibiotics* (Taylor and Francis, New York, 2001).
3. M. Leeb, *Nature* **431**, 892 (2004).
4. W. R. Strohl, *Metab. Eng.* **3**, 4 (2001).
5. D. E. Cane, C. T. Walsh, C. Khosla, *Science* **282**, 63 (1998).
6. L. Katz, *Chem. Rev.* **97**, 2557 (1997).
7. C. R. Stephens *et al.*, *J. Am. Chem. Soc.* **85**, 2643 (1963).
8. M. Nelson, W. Hillen, R. A. Greenwald, Eds., *Tetracyclines in Biology, Chemistry and Medicine* (Birkhauser Verlag, Boston, 2001).
9. D. E. Brodersen *et al.*, *Cell* **103**, 1143 (2000).
10. M. Pioletti *et al.*, *EMBO J.* **20**, 1829 (2001).
11. P.-E. Sum, P. Petersen, *Bioorg. Med. Chem. Lett.* **9**, 1459 (1999).
12. K. Bush, M. Macielag, M. Weidner-Wells, *Curr. Opin. Microbiol.* **7**, 466 (2004).
13. J. J. Korst *et al.*, *J. Am. Chem. Soc.* **90**, 439 (1968).
14. A. I. Gurevich *et al.*, *Tetrahedron Lett.* **8**, 131 (1967).
15. H. Muxfeldt *et al.*, *J. Am. Chem. Soc.* **101**, 689 (1979).
16. K. Tatsuta, T. Yoshimoto, H. Gunji, Y. Okado, M. Takahashi, *Chem. Lett. (Jpn.)* **2000**, 646 (2000).
17. G. Stork, J. J. La Clair, P. Spargo, R. P. Nargund, N. Totah, *J. Am. Chem. Soc.* **118**, 5304 (1996).
18. W. Rogalski, in *Handbook of Experimental Pharmacology*, J. J. Hlavka, J. H. Boothe, Eds. (Springer-Verlag, New York, 1985), vol. 78, chap. 5.
19. A. M. Reiner, G. D. Hegeman, *Biochemistry* **10**, 2530 (1971).
20. A. G. Myers, D. R. Siegel, D. J. Buzard, M. G. Charest, *Org. Lett.* **3**, 2923 (2001).
21. G. Stork, A. A. Hagedorn III, *J. Am. Chem. Soc.* **100**, 3609 (1978).
22. D. M. Vyas, Y. Chiang, T. W. Doyle, *Tetrahedron Lett.* **25**, 487 (1984).
23. P. Pevarello, M. Varasi, *Synth. Commun.* **22**, 1939 (1992).
24. S. H. Pine, *Org. React.* **18**, 403 (1970).
25. A. G. Myers, B. Zheng, *Tetrahedron Lett.* **37**, 4841 (1996).
26. M. Frigerio, M. Santagostino, *Tetrahedron Lett.* **35**, 8019 (1994).
27. E. J. Corey, H. Cho, C. Rucker, D. H. Hua, *Tetrahedron Lett.* **22**, 3455 (1981).
28. F. A. Davis, M. C. Weismiller, C. K. Murphy, R. T. Reddy, B.-C. Chen, *J. Org. Chem.* **57**, 7274 (1992).
29. E. N. Prilezhaeva, *Russ. Chem. Rev.* **70**, 897 (2001).
30. T.-L. Ho, *Tandem Organic Reactions* (Wiley, New York, 1992).
31. F. J. Leeper, J. Staunton, *J. Chem. Soc. Chem. Comm.* **1978**, 406 (1978).
32. F. M. Hauser, R. P. Rhee, *J. Org. Chem.* **43**, 178 (1978).
33. J. H. Dodd, S. M. Weinreb, *Tetrahedron Lett.* **20**, 3593 (1979).
34. J. D. White, E. G. Nolen Jr., C. H. Miller, *J. Org. Chem.* **51**, 1150 (1986).
35. F. M. Hauser, R. P. Rhee, S. Prasanna, S. M. Weinreb, J. H. Dodd, *Synthesis (Mass.)* **1980**, 72 (1980).
36. W. E. Parham, L. D. Jones, Y. A. Sayed, *J. Org. Chem.* **41**, 1184 (1976).
37. S. C. Berk, M. C. P. Yeh, N. Jeong, P. Knochel, *Organometallics* **9**, 3053 (1990).

38. We thank D. Kahne and C. Walsh for helpful discussions and W. Brubaker (Farmington Pharma Development) and C. Thoma and J. Thanassi (Achillion Pharmaceuticals) for antibacterial screening. This work was supported by NIH grant AI48825, NSF predoctoral graduate fellowships (M.G.C. and J.D.B.), and the Deutscher Akademischer Austausch Dienst (C.D.L.). A.G.M. serves on the scientific advisory boards of Vicuron Pharmaceuticals and Miikana Therapeutics and is a consultant for Pfizer. The research described here is independent.

Supporting Online Material

www.sciencemag.org/cgi/content/full/308/5720/395/DC1
Materials and Methods
References

13 January 2005; accepted 1 March 2005
10.1126/science.1109755

Hypoxia, Global Warming, and Terrestrial Late Permian Extinctions

Raymond B. Huey* and Peter D. Ward

A catastrophic extinction occurred at the end of the Permian Period. However, baseline extinction rates appear to have been elevated even before the final catastrophe, suggesting sustained environmental degradation. For terrestrial vertebrates during the Late Permian, the combination of a drop in atmospheric oxygen plus climate warming would have induced hypoxic stress and consequently compressed altitudinal ranges to near sea level. Our simulations suggest that the magnitude of altitudinal compression would have forced extinctions by reducing habitat diversity, fragmenting and isolating populations, and inducing a species-area effect. It also might have delayed ecosystem recovery after the mass extinction.

A catastrophic extinction marks the end of the Permian (*1*, *2*) and is attributed to an acute climate crisis, among other causes (*3*–*5*). However, background extinction rates and ecosystem turnover were elevated throughout much of the Late Permian (*6*, *7*), and recovery after extinction was slow (*1*, *2*). Thus, environmental degradation likely occurred both before and after the final catastrophe, perhaps caused by major shifts in atmospheric chemistry (*8*). Indeed, modeling, isotope, and paleontological evidence (*9*–*13*) suggests that O_2 levels plummeted in the Late Permian and Early Triassic (Fig. 1A) and would have restricted the supply of O_2 to organisms. At the same time, CO_2 levels were rising (Fig. 1A), and climate warming (*14*) would have increased metabolic demand for O_2. Severe hypoxia was inevitable (*9*, *15*, *16*).

Here, we explore a biogeographic consequence of presumed low O_2 levels during the Late Permian and Triassic: Terrestrial animals

would have been restricted to low altitude, because even moderate altitudes would have insufficient O_2. We simulate the magnitude of altitudinal compression and evaluate its contributions to the high background extinction rate, the catastrophic extinction, and the delayed recovery (*1*, *2*).

Terrestrial animals attempting to live at moderate to high altitude are physiologically challenged by declining temperatures, food supply, habitat area, and O_2 levels, along with increased respiratory water loss (*17*). The upper altitudinal limits of species likely reflect the influence of these factors as well as ecological, geological, and biogeographic factors (*18*).

The relative contribution of O_2 in limiting altitudinal ranges has no doubt changed over time because O_2 levels fluctuated so drastically (Fig. 1A). For example, when O_2 levels appear to have been at their zenith during the cold Early Permian [~300 million years ago (Ma), Fig. 1A], the partial pressure of inspired O_2 (PIO_2) even at an altitude of 6 km may have matched that at sea level in today's atmosphere (*19*). In this glaciated and O_2-rich environment, altitudinal ranges would have been constrained by extreme cold or ice, not by O_2 levels. But when O_2 levels are calculated to be at their nadir during the hot Early Triassic (~240 and ~200 Ma), PIO_2 even at sea level may have been equivalent to that at ≥5.3 km in today's atmosphere (Fig. 1B). If estimates of O_2 (Fig. 1A) and climate are correct, the combination of low PIO_2 and high temperature would have induced hypoxia and restricted terrestrial vertebrates to low altitudes.

We simulated the impact of O_2 levels on maximum altitudinal ranges of vertebrates having a presumed mid-Permian physiology (*20*). The actual hypoxia tolerance of mid-Permian ectotherms is of course unknown but was probably lower than that of present-day vertebrates. Mid-Permian vertebrates not only had primitive respiratory systems (*9*) but also had been evolving in an O_2-rich atmosphere for millions of years (Fig. 1A) and could not have become adapted to altitude (hence, to low O_2 levels) because of icehouse temperatures during that time.

We start by deriving a reference set of hypothetical species living in the mid-Permian and having maximum altitudes ranging from 2.0 to 8.0 km, in 1-km intervals. We assume that the maximum altitude of each species was set by—or at least strongly influenced by—the critical PIO_2 occurring at that altitude. Then, assuming that hypoxia tolerances were constant over time (i.e., always had the same critical PIO_2), we calculate how maximum altitudes (Fig. 1C) changed with O_2 levels (Fig. 1A). This involves estimating the average PIO_2 at each altitude during the mid-Permian and then computing (at intervals of 10 million years) the altitude where each PIO_2 would have occurred (*20*).

The presumed drop in O_2 levels during the Late Permian (Fig. 1A) would have drastically compressed the altitudinal ranges of all hypothetical species (Fig. 1C). If O_2 levels dropped to ~16% at the end of the Permian (*8*), PIO_2 at sea level would have been equivalent to that found today at 2.7 km. Animals with limited hypoxia tolerance would have gone extinct (Fig. 1C). To survive, a species would have needed to tolerate a PIO_2 at least equivalent to that found at 6.0 km (red line, Fig. 1C) in the mid-Permian (*21*, *22*).

O_2 levels are thought to have continued to drop into the Early Triassic and to have stayed relatively low for the next 100 million years (Fig. 1A). In addition, CO_2 levels (Fig. 1A) and global temperatures (*14*) remained high. Thus, hypoxia and the resultant altitudinal compression likely persisted into the early Cretaceous (Fig. 1, A and C) and may have contributed to a slow recovery after the mass extinction (*1*, *2*).

Our simulations (Fig. 1, B and C) focus on O_2 levels, but rising temperatures in the Late Permian and Early Triassic (*14*) would have exacerbated hypoxia. To reduce the impact, ectotherms could have dispersed along sea-level corridors to high latitudes, thereby lowering their body temperatures. Alternatively, they could have invaded relatively cool aquatic habitats. Indeed, air-breathing aquatic reptiles (e.g., ichthyosaurs, phytosaurs) diversified at this time.

Freshwater-breathing ectotherms were also probably restricted to low altitudes during O_2 lows. Reduced atmospheric O_2 levels

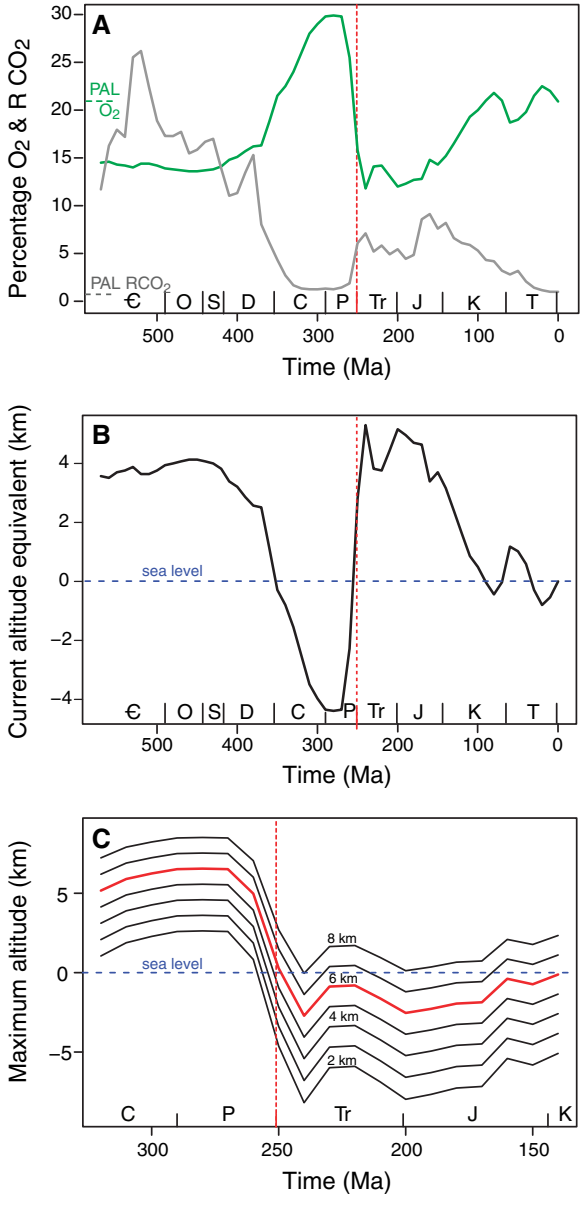

Fig. 1. (**A**) Percent O_2 over time (green) and the concentration of CO_2 (gray) relative to present-day level (PAL) of each gas is indicated. Global hypoxia would have occurred in the Late Permian and Triassic because of dropping O_2 combined with rising temperatures [data from (*4*, *37*)]. The mass extinction at the Permian-Triassic boundary is indicated by a red dashed line. (**B**) Present-day altitude with PIO_2 equivalent to that at sea level in the Phanerozoic. Thus, PIO_2 at sea level at the Triassic O_2 minimum would be found today at ~5 km. (**C**) Predicted maximum altitude over time for hypothetical species having graded tolerances (2 to 8 km) to hypoxia. From the Late Permian through the Jurassic, however, PIO_2 was sufficiently low that ranges would have been compressed to near sea level, and some species would have gone extinct. Period codes: Є, Cambrian; O, Ordovician; S, Silurian; D, Devonian; C, Carboniferous; P, Permian; Tr, Triassic; J, Jurassic; K, Cretaceous; T, Tertiary.

Department of Biology, University of Washington, Box 351800, Seattle, WA 98195, USA.

*To whom correspondence should be addressed. E-mail: hueyrb@u.washington.edu

plus warm water temperatures would lower aquatic O_2 levels, but warm body temperatures increase O_2 demand. Thus, water-breathing ectotherms would likely have been O_2 challenged, even near sea level.

Insects, which suffered major extinctions during the Late Permian (*23*), might also have experienced some hypoxia and altitudinal compression. Insect development is slowed by low PO_2 plus warm temperatures (*24*). Interestingly, giant dragonflies, which evolved during the Permian O_2 high, are thought to have gone extinct in the Late Permian because of limitations on O_2 diffusion (*9*). However, today's large adult insects rely on convective ventilation and are remarkably hypoxia tolerant (*25*); thus, the aquatic larvae of giant insects may have been the primary targets of hypoxia-induced extinction.

Altitudinal compression would have had important biogeographic consequences. Animals specialized for upland habitats could not have survived, as they would have been physiologically excluded from them. Moreover, mountain passes would have seemed physiologically higher to animals (*26*) than are passes of equivalent altitude today. Thus, populations would have become fragmented and isolated (fig. S2), and rates of local extinction may have increased (*27*).

Altitudinal compression plus rising sea levels at the very end of the Permian (*14*, *28*) would have also reduced the land surface physiologically accessible to animals. This loss would have caused additional extinctions via a species-area effect (*29*) and also would have delayed the recovery.

Topographic maps for the mid-Permian to Late Permian (*30*) enable us to estimate (*20*), albeit with substantial uncertainty, the percentage of the land surface that was physiologically accessible to animals with specified hypoxia tolerance (Fig. 2). During the O_2 high in the Permian, virtually the entire surface of Earth had sufficient O_2 to sustain populations of our hypothetical species. By the Triassic, however, hypoxia would have reduced accessible land area for all but the most hypoxia-tolerant species (Fig. 1C). For example, a species physiologically capable of surviving up to 6.0 km in the mid-Permian would have been restricted to below 0.3 km by the Triassic; thus, it would have been excluded from more than half of the available land surface (gray dotted line in Fig. 2). By the early Triassic (Fig. 1A), even a species that could tolerate 8.0 km in the mid-Permian would have likely gone extinct (Fig. 1C) in the absence of compensatory adaptation. Thus, altitudinal compression could have had substantial effects on extinction and recovery rates, given the huge loss in land for all but the most hypoxia-resistant taxa (Fig. 2).

The reasonableness of our scenario of hypoxia-induced altitudinal compression depends fundamentally on the accuracy and timing of estimates of percent O_2 (*8*). Those estimates, of course, have uncertainty (*8*, *20*), and other models can yield somewhat different estimates (*12*, *13*).

Our analyses also assume that O_2 restricted the upper altitudinal limits during the Late Permian and Triassic, that terrestrial vertebrates then had modest hypoxia tolerance, and that adaptation to hypoxia was limited. None of these assumptions can be directly tested as yet, but our compression hypothesis leads to predictions and patterns that are subject to test:

1) Terrestrial vertebrates that did survive the Late Permian should show respiratory adaptations for hypoxia. Indeed, morphological traits of *Lystrosaurus*, one of the few surviving therapsids, and of other Triassic dicynodonts have been interpreted as adaptations to hypoxia (*16*, *31*).

2) Hyperventilation in response to hypoxia would have elevated respiratory water loss during the Late Permian. Maxilloturbinates, which reduce respiratory water loss, first evolved at that time in mammal-like reptiles (*32*). Turbinates have been interpreted as indicating high respiratory rates associated with endothermy (*32*), but they might also be indicators of high respiratory rates induced by hypoxia.

3) Fossil sites for terrestrial ectotherms by the Triassic should be located predominantly at high latitude, where relatively cooler temperatures would reduce metabolic requirements for O_2 and ameliorate hypoxia. Distributional data for therapsids are consistent (*33*). However, therapsids might also have been restricted to high latitude simply because low-latitude sites were hot, dry, and had a depauperate flora (*34*).

4) The compression-forced isolation of taxa into refugia could help to explain Late Permian endemism (*33*), which is surprising for a Pangaean supercontinent. It could also help to explain the "Lazarus effect" (i.e., the reappearance of taxa that disappeared from the fossil record) noted in this period (*1*, *35*).

The extinctions during the Late Permian were the largest ever during the history of life on Earth. An abrupt climate change is thought to be responsible for the catastrophic extinction. Nonetheless, hypoxia may have contributed to the high background extinctions and high faunal turnover occurring before the mass extinction, to the final catastrophe itself, and to the delayed recovery. Low O_2 levels would have promoted extinction and delayed recovery directly via physiological stress (*16*) and indirectly via altitudinal compression.

Note added in proof: A forthcoming paper (*36*) provides new and fine-scaled estimates of O_2 levels during the Late Permian and Early Triassic. The drop in O_2 during the Late Permian is slightly more recent than that in Fig. 1A, but still suggests that hypoxia and altitudinal compression were influential both before and after the mass extinction.

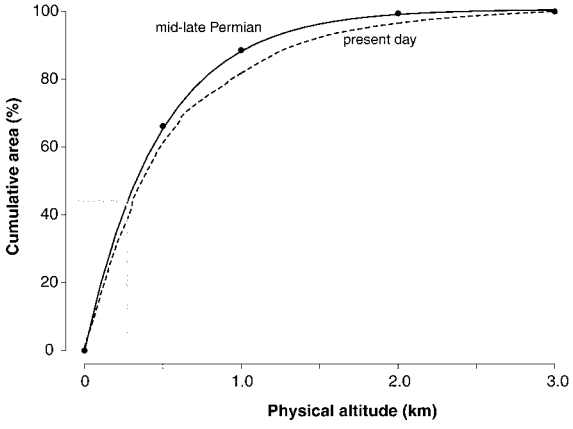

Fig. 2. Plot of cumulative land area versus physical altitude during the mid-Permian to Late Permian [solid line (*30*)] and for the present day [dashed line (*20*)]. This relationship enables us to estimate the percentage of the land surface that was physiologically tolerable (*20*) for the hypothetical species shown in Fig. 1C. A species capable of surviving up to 6.0 km in the mid-Permian would been restricted to below 0.3 km by the end of the Permian (gray dotted line) and thus would have been able to occupy less than half of the available land area. Less hypoxia-tolerant species would have gone extinct; more tolerant ones would have suffered minimal area loss.

References and Notes

1. D. H. Erwin, *The Great Paleozoic Crisis* (Columbia Univ. Press, New York, 1993).
2. S. A. Bowring, D. H. Erwin, Y. Isozaki, *Proc. Natl. Acad. Sci. U.S.A.* **96**, 8827 (1999).
3. A. H. Knoll, R. K. Bambach, D. E. Canfield, J. P. Grotzinger, *Science* **273**, 452 (1996).
4. R. A. Berner, *Proc. Natl. Acad. Sci. U.S.A.* **99**, 4172 (2002).
5. M. J. Benton, R. J. Twichett, *Trends Ecol. Evol.* **18**, 358 (2003).
6. M. J. Benton, V. P. Tverdokhlebov, M. V. Surkov, *Nature* **432**, 97 (2004).
7. P. D. Ward *et al.*, *Science* **307**, 709 (2005); published online 20 January 2005 (10.1126/science.1107068).
8. R. A. Berner, *Geochim. Cosmochim. Acta* **65**, 685 (2001).
9. J. B. Graham, R. Dudley, N. Aguilar, C. Gans, *Nature* **375**, 117 (1995).
10. A. C. Lasaga, H. Ohmoto, *Geochim. Cosmochim. Acta* **66**, 361 (2002).
11. N. D. Sheldon, G. J. Retallack, *Geology* **30**, 919 (2002).
12. N. M. Bergman, T. M. Lenton, A. J. Watson, *Am. J. Sci.* **304**, 397 (2004).
13. R. A. Berner, *The Phanerozoic Carbon Cycle: CO_2 and O_2* (Oxford Univ. Press, Oxford, 2004).
14. D. L. Kidder, T. R. Worsley, *Palaeogeogr. Palaeoclimatol. Palaeoecol.* **203**, 207 (2004).
15. R. A. Berner, D. J. Beerling, R. Dudley, J. M. Robinson, R. A. Wildman Jr., *Annu. Rev. Earth Planet. Sci.* **31**, 105 (2003).
16. G. J. Retallack, R. M. H. Smith, P. D. Ward, *Geol. Soc. Am. Bull.* **115**, 1133 (2003).

17. P. Bouverot, *Adaptation to Altitude-Hypoxia in Vertebrates* (Springer-Verlag, Berlin, 1985).
18. K. J. Gaston, *The Structure and Dynamics of Geographic Ranges* (Oxford Univ. Press, Oxford, 2003).
19. We estimate PIO_2 rather than PO_2, because the addition of respiratory water vapor reduces the partial pressure of O_2 in the lung (*20*).
20. See supporting data on *Science* Online.
21. Estimates of maximum altitudes for the Late Permian and Triassic are somewhat low because warm temperatures would have elevated barometric pressure at altitude. However, the impact on O_2 would have been small: Substituting PO_2 and temperature estimates in the hypsometric equation demonstrates that our altitudinal estimates for the Triassic O_2 low (Fig. 1C) underestimate actual limits by at most 0.1 km (*22*). Similarly, our estimates of maximum altitudes in the cold mid-Permian (Fig. 1C) overestimate actual limits by at most ~0.2 km (*22*). Because these effects are relatively small, we ignore them in our simulations.
22. D. Battisti, personal communication.
23. C. C. Labandeira, J. J. Sepkoski Jr., *Science* **261**, 310 (1993).
24. M. R. Frazier, H. A. Woods, J. F. Harrison, *Physiol. Biochem. Zool.* **74**, 641 (2001).
25. K. J. Greenlee, J. F. Harrison, *J. Exp. Biol.* **207**, 497 (2004).
26. D. H. Janzen, *Am. Nat.* **101**, 233 (1967).
27. I. A. Hanski, *Metapopulation Ecology* (Oxford Univ. Press, Oxford, 1999).
28. A. Hallam, P. B. Wignall, *Earth Sci. Rev.* **48**, 217 (1999).
29. M. L. Rosenzweig, *Species Diversity in Space and Time* (Cambridge Univ. Press, Cambridge, 1995).
30. D. B. Rowley, R. T. Pierrehumbert, B. S. Currie, *Earth Planet. Sci. Lett.* **88**, 253 (2001).
31. K. Angielczyk, personal communication.
32. W. J. Hillenius, J. A. Ruben, *Physiol. Biochem. Zool.* **77**, 1019 (2004).
33. C. A. Sidor *et al.*, *Nature*, in press.
34. P. M. Rees, *Geology* **30**, 827 (2002).
35. P. B. Wignall, M. J. Benton, *J. Geol. Soc. London* **156**, 453 (1999).
36. R. A. Berner, *Geochim. Cosmochim. Acta*, in press.
37. R. A. Berner, Z. Kothavala, *Am. J. Sci.* **301**, 182 (2001).
38. We thank R. Berner for providing data, advice, and discussion; K. Angielczyk, M. Benton, R. Buick, C. Carey, T. Daniel, R. Dudley, D. Erwin, J. Graham, T. Hornbein, D. Rowley, J. Ruben, A. Smith, M. Stoeck, and J. West for discussion; D. Battisti for computing the impact of temperature on critical altitudes; and D. Rowley and G. Wang for calculating hypsometric data. Supported by NSF grant IBN-0416843 (R.B.H.) and the NASA Astrobiology Institute (University of Washington Node, P.D.W., principal investigator).

Supporting Online Material
www.sciencemag.org/cgi/content/full/308/5720/398/DC1
Materials and Methods
Figs. S1 and S2
References

29 November 2004; accepted 15 February 2005
10.1126/science.1108019

Open-System Coral Ages Reveal Persistent Suborbital Sea-Level Cycles

William G. Thompson*† and Steven L. Goldstein

Sea level is a sensitive index of global climate that has been linked to Earth's orbital variations, with a minimum periodicity of about 21,000 years. Although there is ample evidence for climate oscillations that are too frequent to be explained by orbital forcing, suborbital-frequency sea-level change has been difficult to resolve, primarily because of problems with uranium/thorium coral dating. Here we use a new approach that corrects coral ages for the frequently observed open-system behavior of uranium-series nuclides, substantially improving the resolution of sea-level reconstruction. This curve reveals persistent sea-level oscillations that are too frequent to be explained exclusively by orbital forcing.

The idea that Quaternary climate cycles are linked to changes in Earth's orbit is central to climate change theory (*1*). The primary evidence for this comes from the marine oxygen isotope ($\delta^{18}O$) record (*2*) and early dating of coral terraces (*3*). However, there is abundant evidence for abrupt climate change that was too frequent to be explained by orbital changes (*4*). Here we attempt to reconstruct sea level between 70 and 240 thousand years ago (ka) with a resolution sufficient to detect suborbital-frequency oscillations, using a new approach to U/Th coral dating (*5*). Several recent lines of evidence suggest that sea level may be more variable than previously thought. An example is the conversion, via a hydraulic model, of a salinity record from the Red Sea into a sea-level curve for the past 470 thousand years (ky) (*6*). This record suggests fairly large (~35 m) suborbital-frequency sea-level changes during glacial periods such as marine isotope stage 3 (MIS 3) and more modest (~15 m) changes during interglacials (for example, during MIS 5). This new Red Sea record augments a growing body of evidence for suborbital sea-level fluctuations in coral records. At the Huon Peninsula of Papua New Guinea, multiple coral terraces were formed during MIS 3, with highstands occurring about every 6 ky (*7*, *8*). There are also more Huon terraces associated with MIS 5 than can be accounted for by orbital variability (*9*). Such evidence is not restricted to New Guinea; closely spaced terraces on Barbados suggest suborbital period changes in sea level during MIS 5a and MIS 5c (*9*, *10*).

The construction of a high-resolution sea-level record requires a large number of accurate coral ages from a limited geographic area, and this has not been possible with standard dating methods. The conventional equations for U/Th age determination (*11*) require that loss or gain of U and Th have not occurred except by radioactive decay after coral death. This closed-system requirement is often violated in fossil corals as a result of the alpha-recoil mobility of U-series nuclides (*12*), and an initial coral $^{234}U/^{238}U$ ratio that is significantly different from that of modern seawater is taken as evidence of open-system behavior and an unreliable age (*13*). Building on earlier attempts to correct for open-system behavior (*14*), we have derived a set of decay equations that corrects coral ages for these effects (*5*). Although conventional U-series coral ages from a single stratigraphic level often differ substantially, open-system ages of these corals are in much better agreement (Fig. 1, A to C), which illustrates the dramatic improvement in the accuracy of coral ages achieved through open-system dating. It has long been known that many conventional coral ages are unreliable, prompting screening for open-system effects (*13*). Such screening improves accuracy but often results in the rejection of up to 90% of measured ages, degrading the resolution of sea-level reconstructions (fig. S1, A and B). By recovering accurate ages for most corals, the open-system method greatly improves the resolution of the resulting record (fig. S1C).

We have constructed (*15*) a high-resolution uplift-corrected sea-level curve for Barbados (Fig. 2), with open-system ages calculated from published isotope ratio data (*5*, *13*, *16*, *17*) and other measurements (table S1). Corals defining this curve are almost entirely *Acropora palmata*, a reef-crest species. An average data density approaching one age per 1000 years during MIS 5 highstands and one age per 2500 years during MIS 7 (to 220 ka) resolves sea-level fluctuations occurring over a few thousand years. For the most part, clearly separated peaks constrained by multiple coral ages define the oscillations characterizing suborbital sea-level variability. However, in mid-MIS 7, between 200 and 220 ka, three potential sea-level peaks are poorly resolved because of overlapping error envelopes. The best constrained portion of the sea-level curve is during MIS 5c, where minor highstands at 100, 103, and 105.5 ka are evident in coral ages from a

Lamont-Doherty Earth Observatory (LDEO) and Department of Earth and Environmental Sciences, Columbia University, Palisades, NY 10964, USA.

*Present address: Department of Geology and Geophysics, 118 Clark Lab, Mail Stop 23, Woods Hole Oceanographic Institution, Woods Hole, MA 02543, USA.
†To whom correspondence should be addressed. E-mail: wthompson@whoi.edu

single outcrop at Salt Cave Point. These three peaks are independently confirmed by coral ages from the University of West Indies and South Point sites. Reproducibility at this level of detail suggests that our method is robust.

We compared our record to four recent sea-level reconstructions from $\delta^{18}O$ records (Fig. 3) that use different approaches to isolate sea level from the other components of the $\delta^{18}O$ signal. At orbital time scales, there is fairly good correspondence between the $\delta^{18}O$ records, which is expected because their chronologies are linked either directly or indirectly to orbital tuning. However, discrepancies between records (for example, during MIS 6) arise from differences in correlation or tuning and illustrate the difficulty of establishing a detailed and precise chronology. Although there are varying degrees of suborbital variability in the $\delta^{18}O$-derived records, it is difficult to find much correspondence between records. This points to the difficulty in extracting the portion of the $\delta^{18}O$ signal that is attributable to sea level and in resolving suborbital variability. Measurement uncertainty and smoothing of the record by bioturbation also limit the resolution of such records. A coral-derived sea-level record is much less ambiguous, because each coral provides a direct sea-level index and a precise radiometric age. Our record resolves the timing and magnitude of the millennial-scale variability that is suggested in some of the $\delta^{18}O$ records.

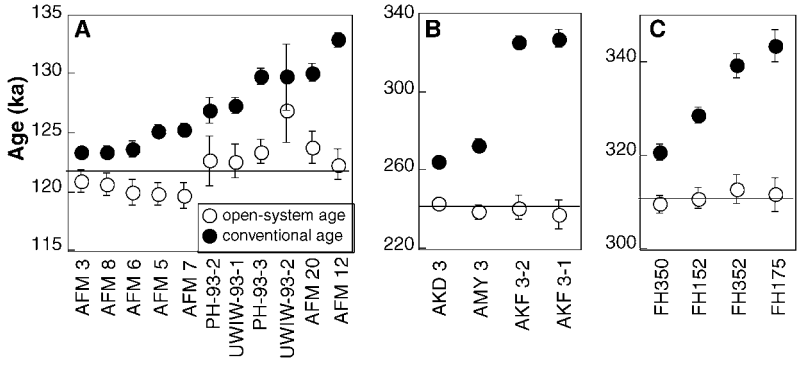

Fig. 1. A comparison of conventional and open-system ages calculated from the same isotope ratio data (*5, 13, 16, 27*). Each group of corals is from a stratigraphically restricted interval, where ages might be expected to be very similar. (**A**) Corals from the top of the University of West Indies terrace, Barbados. (**B**) Corals from the top of St. David's terrace, Christ Church Ridge, Barbados. (**C**) Corals from the 24-m level of the fossil lagoon, Henderson Island, Pacific Ocean.

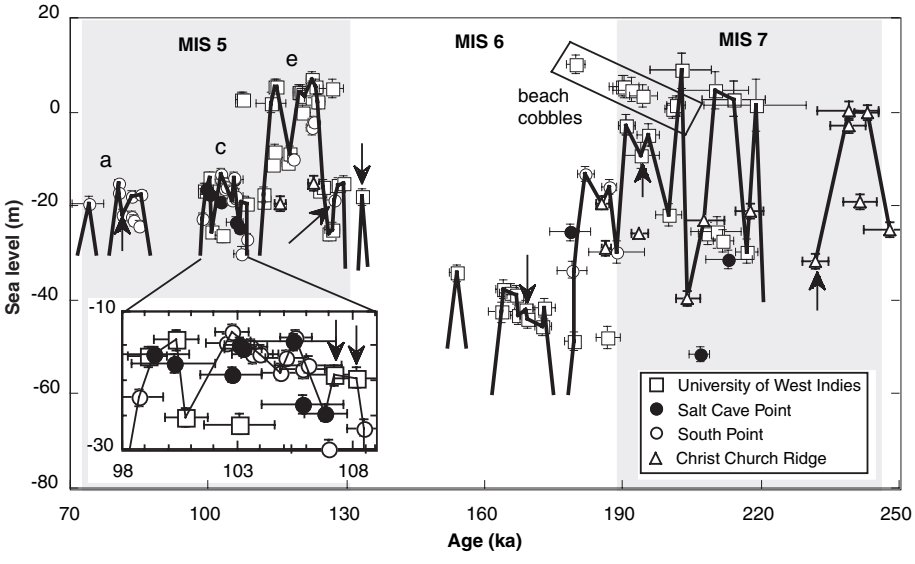

Fig. 2. A high-resolution sea-level curve constructed from Barbados coral data (*5, 13, 16, 17*) using open-system age equations. Plot symbols indicate sample location. Arrows identify the eight corals that are not the reef-crest species *A. palmata*. In general, the sea-level curve is drawn through the highest corals of a given age (*15*). Gaps in the sea-level curve represent large age gaps between closely spaced corals in a single outcrop, where age differences of several thousand years are observed over distances of a few meters. These hiatuses suggest that sea level was lower than the dated strata during these intervals. In all figures, error bars are 2σ and those not visible are smaller than the plot symbols, and MIS boundaries are placed at the orbitally tuned ages of (*28*).

It is useful to compare our record to sea-level and climate records obtained from speleothems (Fig. 4), because U/Th speleothem dating is affected much less by the open-system behavior that disturbs coral ages (*18*). Speleothems recovered from submarine caves provide independent sea-level constraints. Such cave deposits form only when the sea is below the cave's elevation. Therefore, the ages and elevations of such speleothems provide sea-level maxima that should plot above a sea-level curve (Fig. 4A). Although there is some minor conflict with the speleothem data around 200 ka and with a single point during MIS 6 near 165 ka, our sea-level reconstruction is remarkably consistent with these speleothem constraints. Two speleothem data points, at ~130 ka and –50 m, taken together with the coral data, confirm a dramatic oscillation of sea level first indicated by Huon Peninsula corals (*19*) and indicate a minimum sea-level change of >30 m. Furthermore, one speleothem age suggests a minor lowstand in the middle of the broad peak at ~240 ka, which is suggested by the coral data but is not well resolved (Fig. 2). The good agreement of our record with speleothem sea-level constraints provides independent support for the chronology of our sea-level reconstruction. Speleothem growth can also be sensitive to climate change. There are five well-dated records covering the interval under consideration, where the presence or absence of speleothem growth has been linked to climate change. We compared our sea-level reconstruction to these continental speleothem records from Spannagel Cave (Austrian Alps), Clamouse and Villars Caves (France), Newdegate Cave (Tasmania), and several caves in northeastern Brazil (Fig. 4B). In the first four records, speleothem growth ages, indicating a warm and/or wet climate, agree quite well with periods of high sea level. Slowing or cessation of speleothem growth, which are indicative of colder and/or drier climate, correspond to times of lower sea level. The Brazil record, which has been demonstrated to have an antiphase relationship with Greenland temperature, also agrees well with our sea-level record; growth ages (cold Greenland) correspond with times of lower sea level, and brief hiatuses correspond to short-lived sea-level highstands in our record. The good general correspondence of high sea levels with times of warm climate, and lower sea levels with times of colder climate, also increases confidence in our chronology. It is particularly encouraging that several second-order lowstands characterizing suborbital variability in our record correspond closely with independently dated climate reversals documented by hiatuses in speleothem growth (Fig. 4B, arrows).

Our sea-level curve is in good agreement with records we derived from independent coral data. Sea level inferred from Last

Interglacial patch reefs in the Bahamas agrees extremely well with our record (Fig. 5A), indicating two brief highstands at about 125 to 118 ka and 116 to 115 ka. Detailed maps of sample locations combined with open-system ages reveal that these reefs are age-coherent units in stratigraphic order, with the younger reef to seaward. Underlying these patch reefs is a "rubblestone" unit with a wider range of ages that are not in stratigraphic order. This implies that these corals are not in place, although they are reported to be in growth position, which is not unexpected because transported corals have at least a 50% chance of landing upright. This illustrates that open-system ages are useful for distinguishing in situ deposits from transported ones. The stratigraphically inconsistent ages of the rubblestone unit suggest a transgressive beach deposit incorporating older corals from lower stratigraphic levels during storm events, creating the false impression that the Last Interglacial highstand began as early as 127 ka. A substantial fraction of open-system coral ages from Australia also agree well with our record (Fig. 5B), although there is a handful of slightly older corals. Open-system coral ages from an Australian drill core are not in stratigraphic order, suggesting that transported corals may be a problem for this data set as well. Unfortunately, a detailed map of all sample locations is not available to check the stratigraphic consistency of the samples. It is possible that, as in the Bahamas example, the transport of corals from lower stratigraphic levels during storms is extending the apparent duration of the highest sea levels in the Australian record.

An independent sea-level curve for MIS 5a and MIS 5c was constructed using recent Barbados data (Fig. 5C) and the same methods that produced Fig. 2. The detailed reproducibility of minor sea-level changes where data sets overlap in MIS 5c is striking, although the timing of changes during MIS 5a appears slightly different. New data between 80 and 73 ka indicate relatively stable sea level where lower sea levels were inferred from a data gap in our record, suggesting that further work is needed to resolve the discrepancy. In a similar manner, a sea-level curve for MIS 6/5e was constructed from Huon Peninsula data. Four distinct oscillations in sea level are implied (Fig. 5D), agreeing reasonably well with our record, particularly considering the uncertainty of single-point maxima in the Huon record. The major reversal of sea level during the MIS 6/5 transition is very similar to the interpretation of the original investigators (*19*), based on uncorrected ages, but the timing is slightly different. Our curve is also in good general agreement with previous sea-level interpretations from carefully screened conventional ages (Fig. 5E) but resolves much more detail. These differences may be crucial for those using sea-level curves to interpret other data, such as studies of ocean salinity (*20*) or primate evolution (*21*). The agreement of our Barbados record with sea-level records from around the globe suggests that detailed sea-level changes can be resolved with confidence.

Although it is probable that further work will result in revisions of the detailed sea-level curve presented here, the record as a whole strongly suggests that suborbital variability is a persistent feature of the record during both glacial and interglacial periods. This variability falls into a broad suborbital band, with second-order highstands occurring every 3 to 9 ky. Similar variability, observed in $\delta^{18}O$ records from the Atlantic and Pacific (*22*, *23*), has been attributed to changes in sea level (*23*), and our results support this idea. With amplitudes of 6 to 30 m, inferred rates of change approach 10 m per 1000 years, surpassing estimates of the current rate of sea-level rise (*24*) and approximating the average rate of the most recent deglaciation. Although some coral records suggest suborbital fluctuations for parts of MIS 3 and MIS 5 (*8*, *9*, *19*, *25*, *26*), our high-resolution record indicates that this variability persists throughout MIS 5, MIS 6, and MIS 7. Suborbital sea-level variability during glacial periods has been linked to ice-sheet dynamics (*7*, *8*). If interglacial variability is to be attributed to the same cause, it suggests instability in the remaining ice sheets

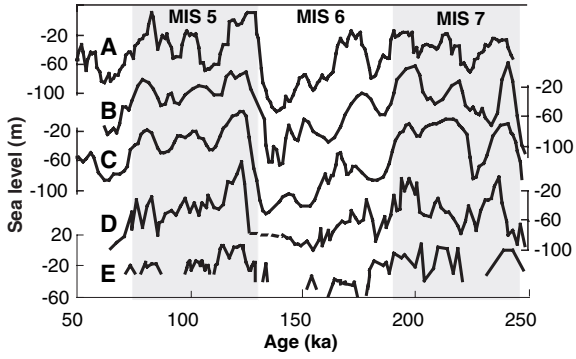

Fig. 3. A comparison of five sea-level records, each on its own time scale. (**A**) Sea-level estimates derived from the Vostok atmospheric $\delta^{18}O$ record and a marine $\delta^{18}O$ record (*29*). (**B**) Sea-level estimates from marine $\delta^{18}O$ data, corrected for temperature with Mg/Ca ratios (*30*). (**C**) Sea-level estimates from $\delta^{18}O$ using regression analysis of coral sea-level and $\delta^{18}O$ data (*31*). (**D**) Sea-level estimates from Red Sea salinity (*6*). (**E**) The coral sea-level record from this work.

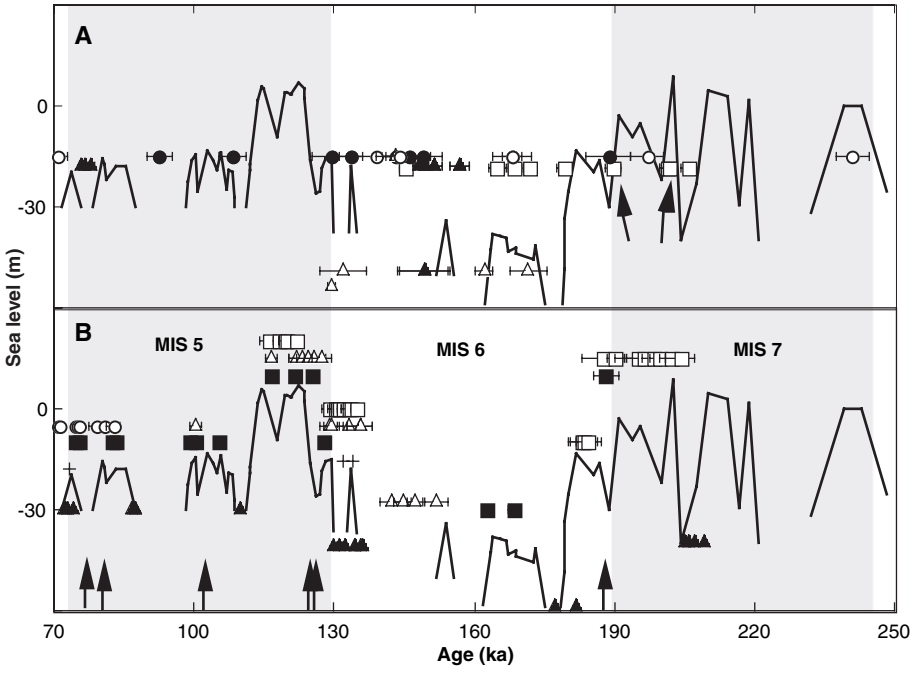

Fig. 4. A comparison of our high-resolution sea-level record (solid line) with the U/Th ages and elevations of speleothem deposits. (**A**) Speleothem sea-level constraints (*32*). Open squares are from (*33*), solid circles from (*34*), open triangles from (*35*), solid triangles from (*36*), and open circles from (*37*). The growth of the speleothems indicates that sea level must have been below the elevation of the cave. Therefore, data points should plot above the sea-level curve (*38*). Arrows indicate ages bracketing marine crust in the record of (*33*). (**B**) Speleothem climate indicators. Warm climate indicators are plotted above the sea-level curve and cold climate indicators below. Speleothem growth indicating warm and/or wet climate: Open squares are from (*39*), solid squares from (*40*), open circles from (*41*), and open triangles from (*42*). Physically observed hiatuses (arrows) suggest cold and dry climate. Spelothem growth indicating cold climate is from (*43*); solid triangles indicate growth ages and crosses indicate short hiatuses, suggesting brief warming.

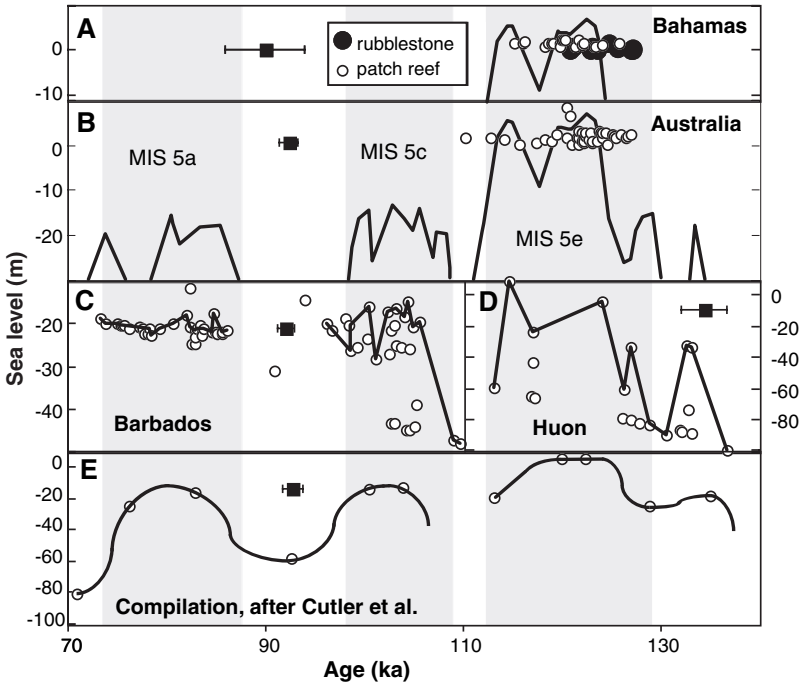

Fig. 5. A comparison of our sea-level record with other coral data (*32*). (**A**) Last Interglacial sea level from open-system ages of Bahamas corals, from isotope ratio data of (*44*). The solid line is our sea-level curve from Fig. 2. (**B**) Last Interglacial sea level from open-system ages of Australian corals, from isotope ratio data of (*45, 46*). Solid lines are our sea-level curves from Fig. 2. (**C**) A relative sea-level curve for MIS 5a and MIS 5c from open-system ages of Barbados corals, from isotope ratio data of (*9*). Solid line is the inferred sea-level change. (**D**) A relative sea-level curve for MIS 6/5 from open-system ages of Huon Peninsula corals, from isotope ratio data of (*19, 47*). Solid line is the inferred sea-level change. (**E**) Sea-level interpretation of (*48*) from a compilation of carefully screened conventional coral ages from Barbados, the Bahamas, and the Huon Peninsula. Solid lines are the sea-level interpretations of (*48*). The solid square symbol in each panel indicates the typical age precision for each data set.

of the far Northern Hemisphere and Antarctica. If substantial sea-level variability is a common feature of previous interglacials, why is there a lack of evidence of similar variations during the Holocene? One difference between the present interglacial and the previous interglacials of MIS 5 and MIS 7 is the modern orbital configuration: The amplitude of the precession cycle is much weaker during the Holocene because of a low in the 413-ky eccentricity cycle. If this is the cause of Holocene sea-level stability, it suggests that orbital configuration plays some role in modulating suborbital sea-level variability.

This study highlights the potential of open-system ages for substantially improving the resolution and accuracy of coral sea-level reconstructions. The ability to generate detailed records from multiple locations is an important strength of this approach, providing a cross-check against stratigraphic complications such as slumping, faulting, differences in coral growth depth, and corals in apparent growth positions that have actually been transported from their original elevations.

References and Notes

1. M. M. Milankovitch, *Serb. Acad. Beorg. Spec. Pub.* **132** (1941).
2. J. D. Hays, J. Imbrie, N. J. Shackleton, *Science* **194**, 1121 (1976).
3. K. J. Mesolella, R. K. Matthews, W. S. Broecker, D. L. Thurber, *J. Geol.* **77**, 250 (1969).
4. W. Dansgaard *et al.*, *Nature* **364**, 218 (1993).
5. W. G. Thompson, M. W. Spiegelman, S. L. Goldstein, R. C. Speed, *Earth Planet. Sci. Lett.* **210**, 365 (2003).
6. M. Siddall *et al.*, *Nature* **423**, 853 (2003).
7. Y. Yokoyama, T. M. Esat, K. Lambeck, *Earth Planet. Sci. Lett.* **193**, 579 (2001).
8. J. Chappell, *Quat. Sci. Rev.* **21**, 1229 (2002).
9. E.-K. Potter *et al.*, *Earth Planet. Sci. Lett.* **225**, 191 (2004).
10. G. Schellmann, U. Radtke, *Earth Sci. Rev.* **64**, 157 (2004).
11. W. S. Broecker, *J. Geophys. Res.* **68**, 2817 (1963).
12. C. Fruijtier, T. Elliot, W. Schlager, *Geol. Soc. Am. Bull.* **112**, 267 (2000).
13. C. D. Gallup, R. L. Edwards, R. G. Johnson, *Science* **263**, 796 (1994).
14. G. M. Henderson, N. C. Slowey, *Nature* **404**, 61 (2000).
15. Materials and methods are available as supporting material on *Science* Online.
16. C. D. Gallup, H. Cheng, F. W. Taylor, R. L. Edwards, *Science* **295**, 310 (2002).
17. R. C. Speed, H. Cheng, *Geol. Soc. Am. Bull.* **116**, 219 (2004).
18. D. A. Richards, J. A. Dorale, in *Uranium-Series Geochemistry*, B. Bourdon, G. M. Henderson, C. C. Lundstrom, S. P. Turner, Eds. (Mineralogical Society of America and Geochemical Society, Washington, DC, 2003), vol. 52, pp. 407–460.
19. T. M. Esat, M. T. McCulloch, J. Chappel, B. Pillans, A. Omura, *Science* **283**, 197 (1999).
20. M. W. Schmidt, H. W. Spero, D. W. Lea, *Nature* **428**, 160 (2004).
21. C. Abegg, B. Thierry, *Biol. J. Linn. Soc.* **75**, 555 (2002).
22. D. W. Oppo, L. D. Keigwin, J. F. McManus, *Paleoceanography* **16**, 280 (2001).
23. D. W. Oppo, B. K. Linsley, Y. Rosenthal, S. Dannenmann, L. Beaufort, *Geochem. Geophys. Geosyst.* **4**, 1001 (2003).
24. S. J. Holgate, P. L. Woodworth, *Geophys. Res. Lett.* **31**, L07305 (2004).
25. K. Sasaki, A. Omura, K. Murakami, N. Sagawa, T. Nakamori, *Quat. Int.* **120**, 51 (2004).
26. E.-K. Potter, K. Lambeck, *Earth Planet. Sci. Lett.* **217**, 171 (2004).
27. C. H. Stirling *et al.*, *Science* **291**, 290 (2001).
28. D. G. Martinson *et al.*, *Quat. Res.* **27**, 1 (1987).
29. N. J. Shackleton, *Science* **289**, 1897 (2000).
30. D. W. Lea, P. A. Martin, D. K. Pak, H. J. Spero, *Quat. Sci. Rev.* **21**, 283 (2002).
31. C. Waelbroeck *et al.*, *Quat. Sci. Rev.* **21**, 295 (2002).
32. The comparison of sea levels from different locations around the globe must be treated with some caution because of global isostatic effects from the loading and unloading of ice over glacial/interglacial cycles. However, comparison of the frequency of suborbital sea-level oscillations in relative sea-level curves should be valid.
33. E. Bard, F. Antonioli, S. Silenzi, *Earth Planet. Sci. Lett.* **196**, 135 (2002).
34. J. Lundberg, D. C. Ford, *Quat. Sci. Rev.* **13**, 1 (1994).
35. P. L. Smart, D. A. Richards, R. L. Edwards, *Cave Karst Sci.* **25**, 67 (1998).
36. D. A. Richards, P. L. Smart, R. L. Edwards, *Nature* **36**, 357 (1994).
37. W.-X. Li *et al.*, *Nature* **339**, 534 (1989).
38. Several investigators have assumed continuous speleothem growth between dated samples. Although the presence of a visible hiatus is proof positive of a discontinuity in the record, the absence of such a hiatus is not evidence of continuous growth. The potential for large hiatuses to escape visual detection is illustrated by the variable preservation of the white biogenic crust marking the 10-ky MIS 7.1 hiatus in the speleothem of (*33*). This crust pinches out laterally along the growth layer, leaving a single growth lamina of ~1 mm that looks very much like sections of the speleothem that are assumed to represent continuous growth. Such a hiatus, particularly one of shorter duration, could not be detected without much closer spacing of dated samples.
39. C. Spotl, A. Mangini, N. Frank, R. Eichstadter, S. J. Burns, *Geology* **30**, 815 (2002).
40. V. Planges, C. Causse, D. Genty, M. Paterne, D. Blamart, *Earth Planet. Sci. Lett.* **201**, 87 (2002).
41. D. Genty *et al.*, *Nature* **421**, 833 (2003).
42. J.-x. Zhao, Q. Xia, K. D. Collerson, *Earth Planet. Sci. Lett.* **184**, 635 (2001).
43. X. Wang *et al.*, *Nature* **432**, 740 (2004).
44. J. H. Chen, H. A. Curran, B. White, G. J. Wasserburg, *Geol. Soc. Am. Bull.* **103**, 82 (1991).
45. C. H. Stirling, T. M. Esat, M. T. McCulloch, K. Lambeck, *Earth Planet. Sci. Lett.* **135**, 115 (1995).
46. C. H. Stirling, T. M. Esat, K. Lambeck, M. T. McCulloch, *Earth Planet. Sci. Lett.* **160**, 115 (1998).
47. M. Stein *et al.*, *Geochim. Cosmochim. Acta* **57**, 2541 (1993).
48. K. B. Cutler *et al.*, *Earth Planet. Sci. Lett.* **206**, 253 (2003).

49. We thank W. Broecker, G. Henderson, and S. Hemming for many productive discussions and M. Stein and the late R. Speed for guidance and debate in the field. McGill University's Bellairs Research Institute of Barbados provided logistical support. Grants from the Lamont Climate Center, the Comer Science & Educational Foundation, and the Goodfriend Prize and start-up funds from LDEO and Columbia University for S.L.G. supported this work. The LDEO Deep-Sea Sample Repository curated some of the corals used for this sea-level reconstruction. Support for this facility is provided by NSF (grant OCE00-02380) and the Office of Naval Research (grant N00014-02-1-0073). This is LDEO contribution no. 6745.

Supporting Online Material

www.sciencemag.org/cgi/content/full/308/5720/401/DC1
Materials and Methods
Fig. S1
Table S1
References

13 August 2004; accepted 3 March 2005
10.1126/science.1104035

Fragmentation and Flow Regulation of the World's Large River Systems

Christer Nilsson,[1]*† Catherine A. Reidy,[1]* Mats Dynesius,[1] Carmen Revenga[2]

A global overview of dam-based impacts on large river systems shows that over half (172 out of 292) are affected by dams, including the eight most biogeographically diverse. Dam-impacted catchments experience higher irrigation pressure and about 25 times more economic activity per unit of water than do unaffected catchments. In view of projected changes in climate and water resource use, these findings can be used to identify ecological risks associated with further impacts on large river systems.

Humans have extensively altered river systems through impoundments and diversions to meet their water, energy, and transportation needs. Today, there are >45,000 dams above 15 m high, capable of holding back >6500 km^3 of water (*1*), or about 15% of the total annual river runoff globally (*2*). Over 300 dams are defined as giant dams, which meet one of three criteria on height (>150 m), dam volume (>15 million m^3), or reservoir storage (>25 km^3) (*3*). The recently constructed Three Gorges Dam on the Chang Jiang (Yangtze) in China is the largest, 181 m high and with a reservoir storing >39 km^3 (*4*, *5*). Although statistics summarizing the world's large dams are available (*3*, *4*, *6*, *7*), detailed multiscale data have not been synthesized globally.

Catchment-scale impacts of dams on ecosystems are generally well known, with both upstream and downstream effects stemming from inundation, flow manipulation, and fragmentation (*8*–*10*). Inundation destroys terrestrial ecosystems and eliminates turbulent reaches, disfavoring lotic biota. It can cause anoxia, greenhouse gas emission, sedimentation, and an upsurge of nutrient release in new reservoirs (*6*, *11*, *12*). Resettlement associated with inundation can result in adverse human health effects and substantial changes in land use patterns (*13*, *14*). Flow manipulations hinder channel development, drain floodplain wetlands, reduce floodplain productivity, decrease dynamism of deltas, and may cause extensive modification of aquatic communities (*15*–*18*). Dams obstruct the dispersal and migration of organisms, and these and other effects have been directly linked to loss of populations and entire species of freshwater fish (*19*–*21*). The World Commission on Dams produced the most comprehensive review of dam impacts yet (*22*), with illustrative catchment-scale case studies. However, data were not available for a global analysis based on subcatchment-scale resolution, integrating hydrologic, ecological, and socioeconomic data. Such a synthesis is needed to understand the multiple spatial, temporal, and interactive impacts of dams.

Here, we present a global overview of flow regulation and channel fragmentation in the world's largest river systems, which comprise a total virgin mean annual discharge (VMAD, the discharge before any substantial human manipulations) of some 790,000 m^3 s^{-1}, or 60% of the world's river runoff. We proceeded by (i) identifying 153 large river systems (LRSs) in Latin America, Africa, Asia, and Australasia that we had not previously assessed (*23*), (ii) locating and gathering storage capacity data for their dams, (iii) quantifying channel fragmentation by dams, (iv) and quantifying flow regulation by relating storage capacity to discharge. We also updated these same data for 139 systems that we had previously assessed in the Northern Hemisphere (*23*), combined the two data sets for a total of 292 river systems, and, on the basis of these data, classified the river systems as either unaffected, moderately affected, or strongly affected (*24*). We were unable to assess rivers in most of Indonesia and a small part of Malaysia (because of a lack of reliable discharge data). We included irrigation data for all 292 LRSs and analyzed global distribution of impact relative to terrestrial biomes and economic activity.

We defined an LRS as a system that has, anywhere in its catchment, a river channel section with a VMAD of ≥350 m^3 s^{-1} (*23*, *25*). By river system, we mean entire networks of stream and river channels interconnected by surface freshwater, from the headwaters to the sea (*26*). The 292 LRSs (table S1 and Fig. 1) drain 54% of the world's land area. North and Central America contain more LRSs (88 total) than any other continent, but on average these systems contribute less water and have smaller catchment areas than do those of Asia, Africa, and South America. Of the 10 LRSs with highest discharge, 6 lie in Asia, 2 in South America, 1 in Africa, and 1 in North and Central America.

The catchments of LRSs encompass at least some part of all 16 of the world's nonmarine biomes as classified by Olson *et al.* (*27*) and >50% of 11 of these biomes, including 87% of all boreal forests and 83% of all flooded grasslands and savannahs. The biomes with least proportion of their surface area in LRSs are rock and ice (1%); mangroves (17%); and Mediterranean forests, woodlands, and scrub (19%). In all, 72 LRSs span only one biome, whereas the Ganges-Brahmaputra system (AS-65) encompasses the widest diversity (10 biomes), followed by the Amazonas-Orinoco (SA-11; these rivers have a natural cross-channel), Amur (AS-20), Yenisei (AS-5), Zambezi (AF-6), and Indus (AS-73) systems, each spanning eight.

Nearly half (139) of all LRSs (48%) remain unfragmented (*28*) by dams in the main channel, 119 systems (41%) have unfragmented tributaries, and 102 systems (35%) are completely unfragmented. Europe contains the smallest number of completely unfragmented LRSs (just three rivers in northwestern Russia). The continent with the greatest number (35) of unfragmented LRSs is North and Central America, and the greatest proportion is in Australasia (74%). Twelve LRSs (9 in Europe and 3 in the United States) have <25% of the main channel's length left unfragmented.

The greatest flow regulation (*29*) was for the Volta river system in Africa (AF-19, 428%). In North and Central America, both the Manicougan (NA-35) and Colorado (NA-70) systems are regulated >250%, and in South America the most highly regulated system is the Rio Negro in Argentina (SA-22, 140%). The most highly regulated systems in Asia are the Shatt Al Arab (or Euphrates-Tigris) in the Middle East (AS-74, 124%) and the Mae Khlong in Thailand (AS-58, 130%). Flow regulation does not exceed 100% in any LRS in Europe or Australasia. A flow regulation of 100% indicates that the entire discharge of one year could be held back and released by the dams in the river system.

The numbers of unaffected and strongly affected LRSs are roughly equal (120 and 104, respectively), whereas moderately affected systems represent just 23%, or 68 of the 292 LRSs (Fig. 1). Of the 10 LRSs with highest discharge, 6 are moderately affected and 4 are strongly affected. The world's two largest discharges, the Amazonas-Orinoco and Congo, are moderately affected, and the third largest discharge, the Chang Jiang, is strongly affected (table S1). The largest unaffected LRS is the

[1]Landscape Ecology Group, Department of Ecology and Environmental Science, Umeå University, SE-901 87 Umeå, Sweden. [2]Global Priorities Group, Nature Conservancy, 4245 North Fairfax Drive, Arlington, VA 22203, USA.

*These authors contributed equally to this work.
†To whom correspondence should be addressed. E-mail: christer.nilsson@emg.umu.se

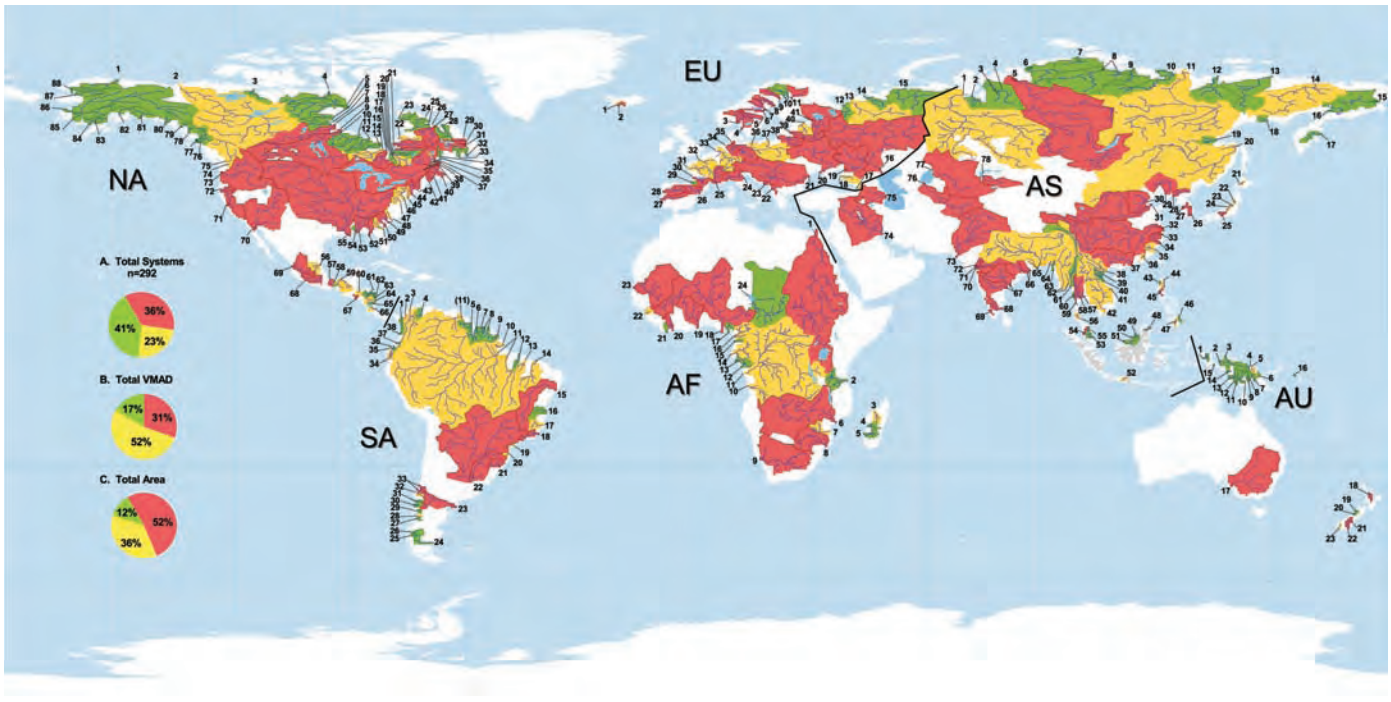

Fig. 1. Impact classification based on river channel fragmentation and water flow regulation by dams on 292 of the world's large river systems. River systems are treated as units and are represented on the map by their catchments. Numbers refer to the list of LRSs in table S1. Green, yellow, and red indicate unimpacted, moderately impacted, and strongly impacted catchments, respectively. White areas indicate land not covered by LRSs. Systems excluded from the study for lack of data are shown in gray. Diagrams at left show A, total number of LRSs; B, total VMAD of LRSs; and C, total surface area of LRSs. NA, North and Central America; SA, South America; AF, Africa; EU, Europe; AS, Asia; AU, Australasia.

Yukon (22nd highest VMAD). Strongly affected systems constitute the majority (52% or 41.2 × 10^6 km^2) (Fig. 1) of total LRS catchment area, despite contributing less water per system (2326 m^3 s^{-1}) and per system catchment area (396 × 10^3 km^2) than moderately affected LRSs. Among continents, the highest number (40) of unaffected LRSs is in North and Central America, whereas Australasia contains the highest proportion (74%) of unaffected systems. Europe has both the smallest number (five) and smallest proportion (12%) of unaffected LRSs (Fig. 2).

Fourteen unaffected or moderately affected LRSs nearly meet fragmentation and regulation criteria for higher impact classification (NA-14, 47, 48, 54, and 80; SA-28 and 32; EU-18, 29, and 33; and AS-1, 24, 35, and 36). Small increases in flow regulation caused by irrigation could change these classifications. Although many dams provide water for irrigation, nonreturned withdrawal from a river's flow for irrigation is a separate and additional form of flow regulation to that caused by retention and release of water by dams. To assess this, we constructed an irrigation index representing the area equipped for or under irrigation (*30*) within each LRS per unit of water in the system (table S1).

Strongly affected systems account for the 25 highest irrigation index values, 15 of which lie in Asia, with the Haihe in China (AS-30)

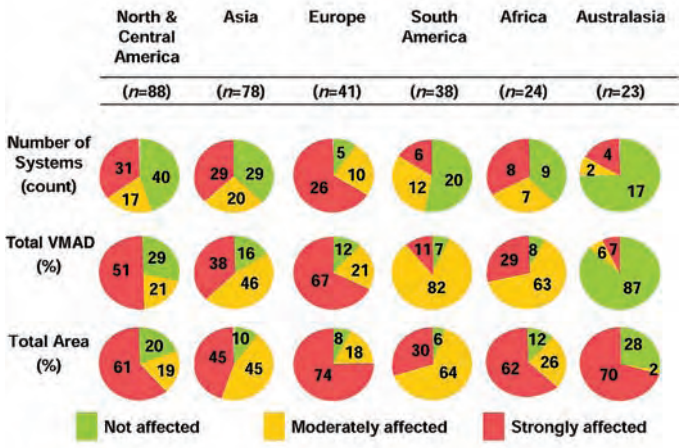

Fig. 2. Total number of systems, total water discharge, and total basin area of strongly affected, moderately affected, or unaffected within each continent's LRSs. Percentages may not total 100% because of independent rounding.

scoring the highest (2194 km^2 per annual km^3 of discharge) (table S1). Of the five borderline unaffected systems, index values only suggest reclassification (to moderately affected) for the Adour in France (EU-29). Of the nine borderline moderately affected systems, index values were high enough to suggest reclassification (to strongly affected) for five systems: Bío-Bío in Chile (SA-32), Kuban in western Russia (EU-18), Agano-Gawa in Japan (AS-24), and Min Jiang and Han Jiang in China (AS-35 and 36, respectively).

Most of the unaffected LRSs are situated in just four biomes (tundra; boreal forests; tropical and subtropical moist broadleaf forests; and tropical and subtropical grasslands, savannahs, and shrublands) (Fig. 3), constituting small proportions of each biome. Tundra, which is sparsely populated, relatively flat, and thus unfavorable to dam construction, is the only biome in which LRS catchment area (29% of total biome area) is predominantly unaffected (73%). Even if unassessed river systems are assumed to be unaffected (a best-case scenario), the maximum proportion of unaffected biome area is still <40% for each of boreal forests; tropical and subtropical moist broadleaf forests; and tropical and subtropical grasslands, savannahs, and shrublands.

Catchment area of strongly affected LRSs constitutes >50% of three biomes (temperate

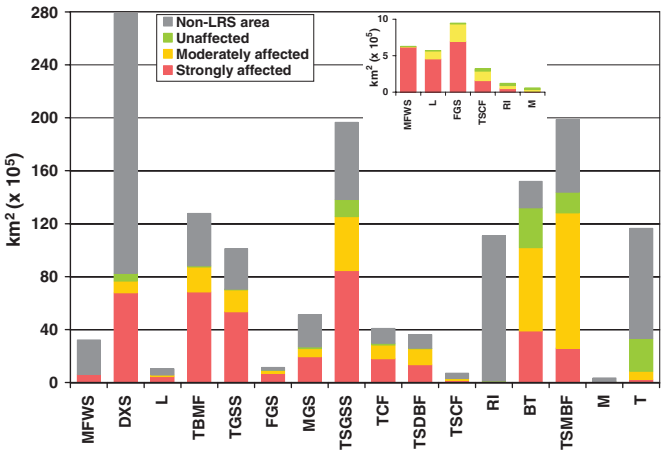

Fig. 3. Distribution of surface area within each of the world's 16 nonmarine biomes among the catchments of unaffected, moderately affected, or strongly affected LRSs; gray represents a non-LRS area, including potential LRSs in Indonesia and Malaysia. Biomes are listed in descending order from left to right by proportion of strongly affected area within LRS-covered area. (**Inset**) Increased resolution of impact class distribution for six biomes with little LRS-covered area. MFWS, Mediterranean forests, woodlands, and scrub; DXS, desert xeric shrubs; L, lakes; TBMF, temperate broadleaf mixed forests; TGSS, temperate grasslands, savannahs, and shrublands; FGS, flooded grasslands and savannahs; MGS, montane grasslands and shrublands; TSGSS, tropical and subtropical grasslands, savannahs, and shrublands; TCF, temperate conifer forests; TSDBF, tropical and subtropical dry broadleaf forests; TSCF, tropical and subtropical coniferous forests; RI, rock and ice; BT, boreal forests/taiga; TSMBF, tropical and subtropical moist broadleaf forests; M, mangroves; and T, tundra.

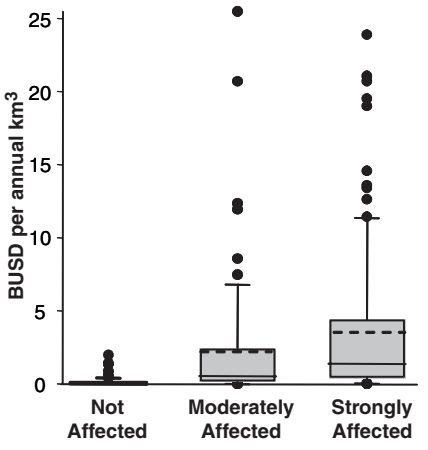

Fig. 4. Distribution of GLP [in billions U.S. dollars (BUSD)] within not affected (n = 120), moderately affected (n = 68), and strongly affected (n = 104) LRSs. Percentile divisions are 10 (not visible), 25, 50, 75, and 90; means are shown as dotted lines.

broadleaf and mixed forests; temperate grasslands, savannahs, and shrublands; and flooded grasslands and savannahs). Within the catchment area of LRSs, 82% is strongly affected in deserts and xeric shrublands, and 99% in Mediterranean forests, woodlands, and scrubs. Flow regulation, implying reduced flooding and less productive floodplains, may be especially harmful in the dry and cold biomes where species are particularly dependent on the riparian resource (*31*, *32*).

The eight LRSs that span seven or more biomes are all moderately or strongly impacted (SA-11; AS-1, 5, 20, 62, 65, and 73; and AF-6) (table S1). Of the 37 LRSs that span five or more biomes, only five remain unaffected (Catatumbo, SA-4; Salween, AS-61; Rufiji, AF-2; Mangoky AF-5; and the Chari, AF-24) (table S1). In these biogeographically diverse LRSs, the impacts of dams are more widespread than those in less diverse systems, because more ecotones are affected by fragmentation.

Moderately and strongly affected LRSs already dominate several biomes, and those biomes may become totally devoid of unaffected river systems if this pattern persists in the smaller basins and subbasins. Indeed, previous results from the Nordic countries show that the regional distribution of impact classes is similar between LRSs and small- and medium-sized river basins (*23*).

In the past century, dam construction has coincided with economic development at the national and regional scales (*22*). To examine the current state of this relationship at the basin scale, we calculated a per-discharge gross LRS product (GLP) accounting for basin population, associated national economies, and VMAD (*33*). Results show that basin impact increases with economic activity, and average GLP of unaffected LRSs is 25 times lower than that of both moderately and strongly affected LRSs (Fig. 4). There are five strongly affected LRSs with negligible GLPs [<$1 million (U.S.) km^{-3}] (table S1), all in northern Canada. These systems lie in sparsely populated regions (driving the low GLPs), and dam benefits (hydropower) are exported to other basins (*34*).

There are 46 LRSs for which large dams are planned or under construction, with anywhere from 1 to 49 new dams per basin (*35*). Forty of these LRSs are in non-OECD (Organization for Economic Cooperation and Development) member nations, indicating that future dam development does not depend on strong national economies. Almost half of the new dams are located on just four rivers, i.e., 49 on the Chang Jiang (AS-32), 29 on the Rio de la Plata (SA-22), 26 on the Shatt Al Arab (AS-74), and 25 on the Ganges-Brahmaputra (AS-65) (*35*). New dams are also planned for several unaffected LRSs, including the Jequitinhonha (SA-16), Cá (AS-40), Agusan (AS-46), Rajang (AS-51), and Salween (AS-61). For each impact class, LRSs with weak economies (*36*) experience greater per-discharge population pressure (*37*) than economically strong LRSs, contributing to greater demand for dam construction among poorer basins. As in northern Canada, interbasin exchange of dam benefits will continue to influence decisions about dam construction. For example, more than 13 dams are planned or proposed for the currently unaffected Salween, the most imminent of which (the Tasang on the main stem) aims to provide international and interbasin benefits (*38*).

As noted, we excluded from our analysis most systems in Indonesia and several in Malaysia. This is unfortunate, because the region is one of the world's top three hotspots for biodiversity (*39*). Additionally, our definition of LRS depends solely on discharge, neglecting spatially large river systems in arid regions that carry little water on an annual basis (e.g., the Rio Grande in North America). Our classification features two limitations. First, it does not address within-basin variations in impacts, which could be substantial in large basins. For example, the moderately affected Mackenzie and Amazonas-Orinoco systems include extensive, virtually pristine areas as well as strongly affected areas. Second, our data often represent minima. We stopped gathering reservoir data once a system reached classification as strongly affected (although any outstanding dams are likely few and small).

As demands on water resources increase, our data can help address the ecological risks associated with further impacts on LRSs. For example, in free-flowing rivers, biodiversity can persist because organism dispersal can be effective in both upstream and downstream directions (*40*, *41*) and because many organisms are likely to adapt to climate change by concomitant shifts in distributions. But in fragmented and regulated rivers, such dispersal can be strongly limited (*10*). These facts need to be accounted for in global planning for sustainable river management.

References and Notes

1. A. B. Avakyan, V. B. Iakovleva, *Lakes Reserv. Res. Manag.* **3**, 45 (1998).
2. V. Gornitz, in *Sea Level Rise: History and Consequences*, B. C. Douglas *et al.*, Eds. (Academic Press, San Diego, CA, 2000), pp. 97–119.
3. P. McCully, *Silenced Rivers* (Zed Books, London, 1996).
4. *World Register of Dams 2003* (International Commission on Large Dams, Paris, 2003).
5. D. Qing, Ed., *The River Dragon Has Come! The Three Gorges Dam and the Fate of China's Yangtze River and Its People* (M. E. Sharpe, Armonk, NY, 1998).

6. V. L. St. Louis, C. A. Kelly, E. Duchemin, J. W. M. Rudd, D. M. Rosenberg, *Bioscience* **50**, 766 (2000).
7. A. Shiklomanov, "Comprehensive assessment of the freshwater resources of the world: Assessment of water resources and water availability in the world" (World Meteorological Organization and Stockholm Environment Institute, Stockholm, 1997).
8. C. Humborg, V. Ittekkot, A. Cociasu, B. VonBodungen, *Nature* **386**, 385 (1997).
9. C. Nilsson, K. Berggren, *Bioscience* **50**, 783 (2000).
10. R. Jansson, C. Nilsson, B. Renöfält, *Ecology* **81**, 899 (2000).
11. S. P. Chang, C. G. Wen, *Water Sci. Technol.* **37**, 325 (1998).
12. L. P. Rosa, M. A. dos Santos, B. Matvienko, E. O. dos Santos, E. Sikar, *Clim. Change* **66**, 9 (2004).
13. R. M. Gillett, P. V. Tobias, *Am. J. Hum. Biol.* **14**, 50 (2002).
14. H. Indrabudi, A. De Gier, L. O. Fresco, *Land Degrad. Dev.* **9**, 311 (1998).
15. K. Tockner, J. A. Stanford, *Environ. Conserv.* **29**, 308 (2002).
16. T. D. Prowse *et al.*, *Water Int.* **27**, 58 (2002).
17. N. L. Poff *et al.*, *Bioscience* **47**, 769 (1997).
18. A. D. Lemly, R. T. Kingsford, J. R. Thompson, *Environ. Manag.* **25**, 485 (2000).
19. A. H. Arthington, R. L. Welcomme, in *Condition of the World's Aquatic Habitats*, N. B. Armantrout, R. J. Wolotira Jr., Eds. (Science Publishers, Lebanon, NH, 1995).
20. P. C. Gehrke, D. M. Gilligan, M. Barwick, *River Res. Appl.* **18**, 265 (2002).
21. T. Penczak, A. Kruk, *Ecol. Freshw. Fish* **9**, 109 (2000).
22. "Dams and development. A new framework for decision-making," *Report of the World Commission on Dams* (Earthscan Publishing, London, 2000).
23. M. Dynesius, C. Nilsson, *Science* **266**, 753 (1994).
24. Following (*23, 25*), we synthesized our data on channel fragmentation and flow regulation to classify the river systems as strongly affected, moderately affected, or not affected (table S2). When reclassifying the northern 139 LRSs, we updated data on dams and excluded previously reported data on irrigation consumption. We excluded previously assessed irrigation data because a global, more consistent data set became available, which we analyzed for all 292 LRSs. We did, however, continue to consider data on interbasin diversions when reclassifying the northern LRSs, because no global and consistent data were available for analysis. Data on interbasin diversions for the 153 nonnorthern LRSs were largely unavailable and thus not considered during impact classification for those systems.
25. Information on materials and methods is available on *Science* Online.
26. Watershed boundaries were taken from (*42*) and modified in several cases to accommodate our definition of a river system. Operational navigation charts of the world (*43*) were consulted for boundary modifications.
27. D. M. Olson *et al.*, *Bioscience* **51**, 933 (2001).
28. We considered all dams except low weirs to fragment rivers [see (*25*) for data sources]. We measured the longest segment of the main channel that was without dams (but that frequently included reservoir water tables) and reported whether dams were absent in all tributaries, present only in minor tributaries, or present in the major tributary (*23*) (table S1).
29. We calculated flow regulation as the sum of reservoir capacity within a river system [see (*25*) for data sources] and expressed this measure as the percentage of the LRS's volumetric annual discharge that can be contained and released by the reservoirs (live storage). One-half of the gross capacity was used as a substitute for live storage for reservoirs that lacked live storage data. The gross capacity is the total water volume that can be retained by a dam, including the bottom water that cannot be released through the lowest outlet. Live storage is the gross capacity excluding this bottom water.
30. S. Siebert, P. Döll, J. Hoogeveen, *Global Map of Irrigated Areas Version 2.0* (Center for Environmental Systems Research, University of Kassel, Kassel, Germany, and Food and Agriculture Organization of the United Nations, Rome, 2001).
31. M. St. Georges, S. Nadeau, D. Lambert, R. Décarie, *Can. J. Zool.* **73**, 755 (1995).
32. B. J. Pusey, A. H. Arthington, *Mar. Freshw. Res.* **54**, 1 (2003).
33. GLP was calculated in a first step as the basin sum of U.S. dollars assigned to each river system inhabitant according to his or her nationality (*44*) and corresponding 2003 per-capita gross domestic product (GDP) (*45*). We then divided this sum by VMAD (expressed in annual km^3), resulting in a per discharge GLP, referred to simply as GLP.
34. "Canadian electricity exports and imports: an energy market assessment" (National Energy Board, Calgary, Canada, January 2003); available online at www.neb-one.gc.ca/energy/EnergyReports/EMA-ElectricityExportsImportsCanada2003_e.pdf.
35. "Rivers at Risk: Dams and the future of freshwater ecosystems" (World Wide Fund for Nature, Godalming, UK, 2004); available online at www.panda.org/downloads/freshwater/riversatriskfullreport.pdf.
36. We considered the minimum 2003 per-capita GDP of OECD member nations (*46*) as a cutoff between weak and strong economies. An LRS's economy was considered strong if its GLP (calculated per capita in this case, rather than per discharge) was greater than or equal to the cutoff. LRSs with GLPs lower than the cutoff were considered to have weak economies. (Mexico's per-capita GDP of $9300, second to lowest among all OECD member nations, was selected as the cutoff. Turkey represented the actual minimum, but data used to calculate Turkey's per-capita GDP were inconsistent with those used for the other OECD member nations; thus Turkey was excluded from selection.)
37. Population pressure was calculated as basin population (*44*) divided by VMAD (expressed in annual km^3).
38. More information is available online at www.salweenwatch.org.
39. N. Myers, R. A. Mittermeier, C. G. Mittermeier, G. A. B. da Fonseca, J. Kent, *Nature* **403**, 853 (2000).
40. J. M. Levine, *Ecology* **84**, 1215 (2003).
41. D. H. Bubb, T. J. Thom, M. C. Lucas, *Freshw. Biol.* **49**, 357 (2004).
42. B. Fekete, C. J. Vörösmarty, W. Grabs, "Global, composite runoff fields based on observed river discharge and simulated water balance" (World Meteorological Organization Global Runoff Data Center Report No. 22, Koblenz, Germany, 1999).
43. "Operational navigation charts 1:1,000,000" (Defense Mapping Agency, Aerospace Center, St. Louis Air Force Station, MO, eds. 2 to 19).
44. "Population LandScan 2000 global population database" (Oak Ridge National Laboratory, Oak Ridge, TN, 2000); an updated version is available online at http://sedac.ciesin.columbia.edu/plue/gpw/landscan.
45. *The World Factbook* (U. S. Central Intelligence Agency, 2003); the current version is available online at www.cia.gov/cia/publications/factbook/index.html.
46. More information is available online at www.OECD.org.

47. We thank K. Berggren, E. Carlborg, P. Hansson, M. Svedmark, and S. Xiong for assistance with data collection; J. M. Helfield for valuable input on this manuscript; and S. L. Pimm for support. This work was economically supported by the Swedish WWF, the United Nations Educational, Scientific, and Cultural Organization/World Water Assessment Programme, the United Nations Environment Programme, and the World Resources Institute.

Supporting Online Material
www.sciencemag.org/cgi/content/full/308/5720/405/DC1
Materials and Methods
Tables S1 and S2

24 November 2004; accepted 28 January 2005
10.1126/science.1107887

Crystal Structure of the Malaria Vaccine Candidate Apical Membrane Antigen 1

Juan Carlos Pizarro,[1] Brigitte Vulliez-Le Normand,[1] Marie-Laure Chesne-Seck,[1] Christine R. Collins,[2] Chrislaine Withers-Martinez,[2] Fiona Hackett,[2] Michael J. Blackman,[2] Bart W. Faber,[3] Edmond J. Remarque,[3] Clemens H. M. Kocken,[3] Alan W. Thomas,[3] Graham A. Bentley[1]*

Apical membrane antigen 1 from *Plasmodium* is a leading malaria vaccine candidate. The protein is essential for host-cell invasion, but its molecular function is unknown. The crystal structure of the three domains comprising the ectoplasmic region of the antigen from *P. vivax*, solved at 1.8 angstrom resolution, shows that domains I and II belong to the PAN motif, which defines a superfamily of protein folds implicated in receptor binding. We also mapped the epitope of an invasion-inhibitory monoclonal antibody specific for the *P. falciparum* ortholog and modeled this to the structure. The location of the epitope and current knowledge on structure-function correlations for PAN domains together suggest a receptor-binding role during invasion in which domain II plays a critical part. These results are likely to aid vaccine and drug design.

Apical membrane antigen 1 (AMA1) is currently in clinical trials as a vaccine against *P. falciparum*, the species causing the most serious forms of malaria in humans. AMA1 is present in all *Plasmodium* species examined (*1*), and orthologs exist in other *Apicomplexa*, including *Toxoplasma* (*2*) and *Babesia* (*3*). Although little is known about its molecular function, genetic evidence indicates a role in maintaining parasite growth during the blood-stage cycle (*4*). Antibodies raised against AMA1 can inhibit erythrocyte invasion and protect against the disease in animal-model systems of malaria (*5–9*). Furthermore, invasion-inhibitory antibodies to AMA1 have been affinity-purified from human sera of donors from malaria-endemic regions (*10*). AMA1 is stored in the microneme organelles after synthesis and is translocated to the parasite surface just before or

during invasion (*11*). It is a type I integral membrane protein with an N-terminal ectoplasmic region, a single transmembrane region, and a small C-terminal cytoplasmic domain (*1*). In all characterized *Plasmodium* AMA1 genes, 16 invariant Cys residues are encoded in the ectoplasmic region, and analysis of the disulfide-bond pattern suggests a division into three distinct domains (*12, 13*). Correct disulfide pairing in the recombinant protein is essential for inducing a protective immune response (*6*). The effectiveness of an AMA1-based vaccine therefore depends critically on maintaining authentic conformational epitopes. We report here the crystal structure of the AMA1 ectoplasmic region from *P. vivax* (PvAMA1) and the epitope mapping of an invasion-inhibitory monoclonal antibody specific for the *P. falciparum* ortholog PfAMA1. Together, these results suggest that domain II is important for the biological function of AMA1.

The crystal structure of the PvAMA1 ectoplasmic region, comprising residues Pro^{43} to Leu^{487}, was determined in two crystal forms, monoclinic and orthorhombic (*14*), and refined at 1.8 Å and 2.0 Å, respectively (*15*). The structure confirms the division of this region into three structural domains, denoted I, II, and III (Fig. 1 and figs. S1 and S2). Several breaks occur in the main-chain tracing of all three domains as a result of absent or poorly defined electron density; these regions correspond to 15% of the polypeptide chain (fig. S2). Of particular note, no electron density was present for the 40-residue segment 295 to 334 in domain II, showing that this region is disordered or mobile. We refer to this region as the domain II loop.

To further understand the function of AMA1, we mapped the epitope recognized by the invasion-inhibitory monoclonal antibody 4G2 (*16*), specific for PfAMA1, and related this to a model of PfAMA1 constructed by homology from the PvAMA1 structure. Different domain combinations of PfAMA1 (I-II, II-III, and I-II-III; and I, II, and III separately) expressed in *Pichia pastoris* (*9*, *15*) were used to test 4G2 binding. Only the I-II and I-II-III combinations were reactive under nonreducing conditions and none were reactive under reducing conditions, which shows that 4G2 recognizes a conformational epitope requiring both domain I and domain II. We further mapped the 4G2 epitope using a series of mutations (mainly replacements by Ala) introduced into domains I and II of PfAMA1 expressed on the surface of COS-7 cells (*15*). Correctly folded mutants, as detected by reactivity with polyclonal antibodies specific for conformational epitopes, were then tested for recognition by 4G2. All but one of the mutations that abrogated PfAMA1 recognition by 4G2 occur in the region between residues 348 and 389 (equivalent to residues 293 to 334 in PvAMA1). This contains the domain II loop, which is disordered or mobile. The 4G2 epitope includes residues from the base of the loop at both the N- and C-terminal ends (PfAMA1 residues Asp^{348}, Lys^{351}, Gln^{352}, Glu^{354}, Gln^{355}, His^{356}, Phe^{385}, Asp^{388}, and Arg^{389}) but not from the central region (fig. S2). Of note, all residues except Asp^{348} fall within the disordered region and, accordingly, were not modeled. Lys^{280} in domain I (Lys^{225} in PvAMA1) was the only 4G2-sensitive residue detected outside the domain II loop. This residue, which is invariant in *Plasmodium* species, is buried, and its amino group forms hydrogen bonds to the main-chain atoms in domains I and II and an invariant Asn on helix α7 in domain II (Asn^{338} in PfAMA1, Asn^{283} in PvAMA1). Replacement of Lys^{280} in PfAMA1 by Ala is thus likely to induce structural changes at the domain I–domain II interface. This would explain our observation that both domains I and II are necessary to maintain the conformational 4G2 epitope, because the base of the domain II loop interfaces with domain I. In addition, the Lys^{280}Ala mutant did not show full recognition by conformation-sensitive polyclonal antibodies, indicating some effect on global folding. We conclude that the invasion-inhibitory 4G2 epitope is confined essentially to the base of the domain II loop.

Comparison of the PvAMA1 structure with other known three-dimensional structures using a distance matrix alignment procedure (DALI) (*17*) reveals that domains I and II are structurally similar to each other and belong to the PAN module superfamily (Fig. 2 and figs. S3 and S4). No previously determined polypeptide fold, however, was identified for domain III. PAN domains are found in proteins with diverse adhesion functions, binding to protein or carbohydrate receptors (*18*). They generally show low sequence identity within the superfamily and have been recognized largely by the cystine pattern and the observed or predicted secondary structure. The closest correspondence of domains I and II of PvAMA1 to known structures bearing PAN domains was found with leech antiplatelet protein (LAPP) (*19*). The PvAMA1 domains are compared with LAPP in Fig. 2, showing preservation of the canonical PAN secondary structure elements and the connectivity between them. The PAN disulfide-bridge pattern is less well preserved in AMA1; only Cys^{162} to Cys^{192} in domain I

Fig. 1. A stereo view of the ectoplasmic region of orthorhombic PvAMA1 in ribbon representation showing domain I (green), domain II (blue), and domain III (magenta). Residues Gln^{294} and Phe^{335} indicate the limits of the disordered domain II loop. Figures were generated using MOLSCRIPT (*27*) and Raster3D (*28*).

[1]Unité d'Immunologie Structurale, Centre National de la Recherche Scientifique, URA 2185, Institut Pasteur, 25 rue du Docteur Roux, 75724 Paris, France. [2]Division of Parasitology, National Institute for Medical Research, The Ridgeway, Mill Hill, London NW7 1AA, UK. [3]Department of Parasitology, Biomedical Primate Research Centre, 2280 GH Rijswijk, Netherlands.

*To whom correspondence should be addressed. E-mail: bentley@pasteur.fr

and Cys^{282} to Cys^{354} in domain II (fig. S4), equivalent to the disulfide bridge between β4 and the helix in LAPP, conform to the PAN motif (*18*). The structural similarity between AMA1 domains I and II suggests that they may originate from an ancient gene duplication. The structure of domain III from PfAMA1, expressed alone, has been analyzed in solution by nuclear magnetic resonance (NMR) (*13*). A significant fraction of the NMR structure is disordered, which can be explained by the absence of domains I and II that interact with these regions of domain III.

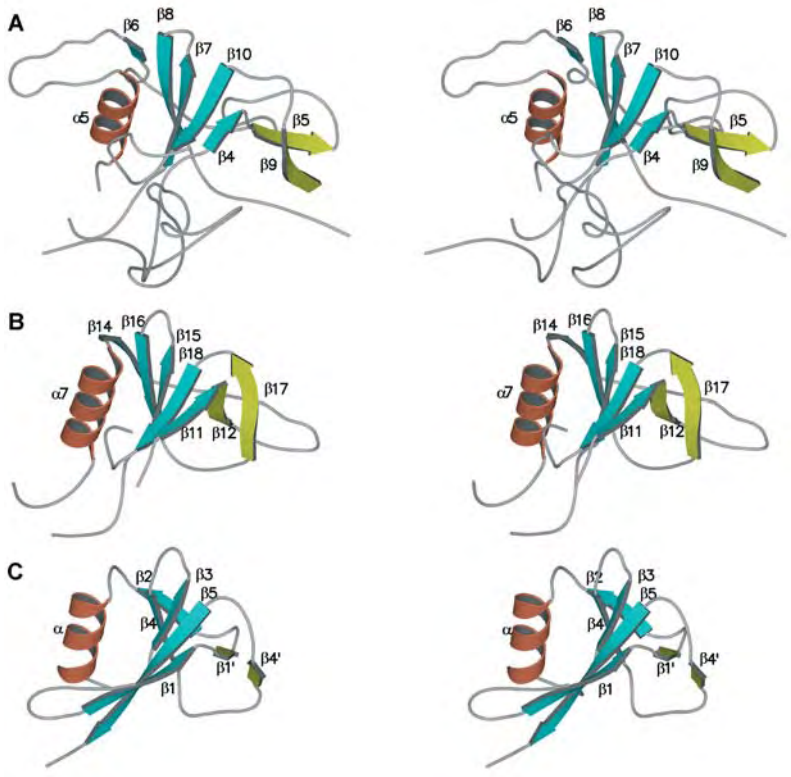

Fig. 2. Comparison in stereo of domain I and domain II of PvAMA1 with LAPP (PDB entry 1i8n). Components characterizing the PAN motif are illustrated as follows: the helix in brown, the 5-stranded β sheet in blue, and the double β strand from the joining segments in yellow. The three domains are viewed from a common orientation: (**A**) domain I, (**B**) domain II, and (**C**) LAPP. Strands β4-β10-β7-β8-β6 of domain I and β11-β18-β15-β16-β14 of domain II correspond to the central 5-stranded β1-β5-β3-β4-β2 sheet of the PAN motif in LAPP, whereas α5 and α7 correspond to the PAN helix in the two respective domains. The inner and outer crossing segments, occurring between β4 and β6, and β8 and β10, respectively, in domain I, and between β11 and β14, and β16 and β18, respectively, in domain II, also conform to the PAN module organization. PvAMA1 domain I residues 92 to 238 superimpose on LAPP residues 46 to 122, with a root mean square (RMS) difference of 2.3 Å between 70 structurally equivalent Cα atoms (DALI *z* score 4.0). PvAMA1 domain II residues 249 to 376 superimpose on LAPP residues 47 to 22, with a RMS difference of 2.6 Å between the 70 structurally equivalent Cα atoms (*z* score 5.1). PvAMA1 domain I residues 93 to 243 optimally position onto PvAMA1 domain II residues 249 to 381, with a RMS difference of 2.7 Å between 83 structurally equivalent Cα atoms (*z* score 6.0).

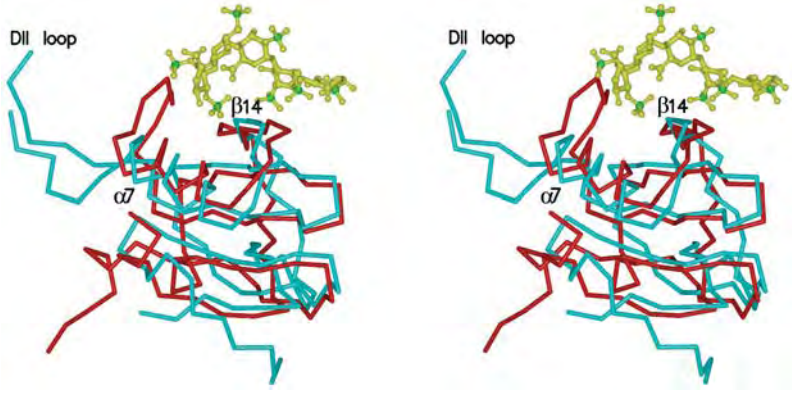

Fig. 3. A stereo view of domain II of AMA1 (blue), with the N domain of NK1 (red) complexed to heparin (yellow with sulfur atoms in green) superimposed. The regions of AMA1 domain II that, by analogy with NK1, may potentially form a ligand-binding site are helix α7, strand β14, and the domain II (DII) loop. The disordered domain II loop (not modeled) could conceivably close upon this site once the putative ligand is in place.

The structural similarity of a protein with unknown function to one with well characterized properties can sometimes provide useful insights into its biological role (*20*). The splice variant of hepatocyte growth factor NK1 is the only protein of known structure with a PAN domain that has been studied in association with its receptor (*21*). NK1, comprising an N-terminal PAN domain and a C-terminal Kringle domain, binds heparin. The crystal structure of NK1 in complex with heparin shows that the ligand binds largely to the PAN domain. The heparin-binding site on the NK1 PAN domain is formed by β2, the helix, and the loop region connecting the helix to β3. Arg and Lys residues are involved in charged interactions with sulfate groups of heparin, and their importance has been confirmed by binding studies with mutants.

To determine whether AMA1 could accommodate ligands or receptors in a similar way, we compared the heparin-binding site on the PAN domain of NK1 with the equivalent surfaces on domains I and II. Docking of the NK1-heparin complex onto PvAMA1 domain I showed that such an interaction is sterically hindered by helix α3 and the loop that precedes β6 and thus would not form an NK1-like binding site. For domain II, however, heparin could be docked without engendering steric hindrance with the antigen (Fig. 3). This putative receptor-binding site on domain II is formed by strand β14 (equivalent to β2 in NK1) and helix α7 (the PAN domain helix). The loop connecting α7 and β15 (equivalent to the helix and β3 in NK1), by contrast, is not positioned for direct contact with the ligand as in NK1. Interestingly, however, this latter region includes the disordered domain II loop, and we do not exclude the possibility that the mobile 40-residue peptide segment closes upon the putative receptor once the latter is in place (Fig. 3). This conjecture is compatible with our observation that the epitope recognized by the invasion-inhibitory antibody 4G2 maps to the base of this loop. Although we are aware that the distribution of charged residues at this postulated binding site on AMA1 does not favor fixation of negatively charged ligands such as heparin, we speculate that other glycans or proteins might be candidates for interaction with domain II.

Other micronemal proteins from *Apicomplexa* include PAN or Apple (a subfamily of PAN) motifs in their structural organization (*22*, *23*). Micronemal proteins play important roles in host-cell invasion (*23*), and several

lines of evidence imply a similar function for AMA1 (*24*–*26*). The presence of PAN motifs in AMA1 and other micronemal proteins may indeed suggest a common phylogenetic origin. Although these diverse observations are consistent with receptor binding by AMA1, direct confirmation of such a role and the nature of the putative ligand remain elusive. The presence of PAN domains in PvAMA1 and our mapping of a protecting epitope to the structure nonetheless provide support for this role by highlighting a functionally important region of the molecule. These results establish a conceptual basis for future experiments to probe the function of AMA1; moreover, they should contribute to further development of vaccine and drug design strategies against malaria.

References and Notes

1. A. P. Waters *et al.*, *J. Biol. Chem.* **265**, 17974 (1990).
2. A. B. Hehl *et al.*, *Infect. Immun.* **68**, 7078 (2000).
3. F. R. Gaffar, A. P. Yatsuda, F. F. J. Franssen, E. de Vries, *Infect. Immun.* **72**, 2947 (2004).
4. T. Triglia *et al.*, *Mol. Microbiol.* **38**, 706 (2000).
5. J. A. Deans *et al.*, *Parasite Immunol.* **10**, 535 (1988).
6. R. F. Anders *et al.*, *Vaccine* **16**, 240 (1998).
7. D. L. Narum, S. A. Ogun, A. W. Thomas, A. A. Holder, *Infect. Immun.* **68**, 2899 (2000).
8. A. W. Stowers *et al.*, *Infect. Immun.* **70**, 6961 (2002).
9. C. H. M. Kocken *et al.*, *Infect. Immun.* **70**, 4471 (2002).
10. A. N. Hodder, P. E. Crewther, R. F. Anders, *Infect. Immun.* **69**, 3286 (2001).
11. J. Healer, S. Crawford, S. Ralph, G. McFadden, A. F. Cowman, *Infect. Immun.* **70**, 5751 (2002).
12. A. N. Hodder *et al.*, *J. Biol. Chem.* **271**, 29446 (1996).
13. M. Nair *et al.*, *J. Mol. Biol.* **322**, 741 (2002).
14. B. Vulliez-Le Normand *et al.*, *Acta Crystallogr.* **D60**, 2040 (2004).
15. Materials and methods are available as supporting material on *Science* Online.
16. C. H. M. Kocken *et al.*, *J. Biol. Chem.* **273**, 15119 (1998).
17. L. Holm, C. Sander, *J. Mol. Biol.* **233**, 123 (1993).
18. H. Tordai, L. Banyai, L. Patthy, *FEBS Lett.* **461**, 63 (1999).
19. E. G. Huizinga *et al.*, *Acta Crystallogr.* **D57**, 1071 (2001).
20. J. M. Thornton, A. E. Todd, D. Milburn, N. Borkakoti, C. A. Orengo, *Nature Struct. Biol.* **7**, 991 (2000).
21. D. Lietha, D. Y. Chirgadze, B. Mulloy, T. L. Blundell, E. Gheradi, *EMBO J.* **20**, 5543 (2001).
22. P. J. Brown, A. C. Gill, P. G. Nugent, J. H. McVey, F. M. Tomley, *FEBS Lett.* **497**, 31 (2001).
23. F. M. Tomley, D. S. Soldati, *Trends Parasitol.* **17**, 81 (2001).
24. A. W. Thomas, J. A. Deans, G. H. Mitchell, T. Alderson, S. Cohen, *Mol. Biochem. Parasitol.* **13**, 187 (1984).
25. T. S. Fraser, H. I. Stefan, D. L. Narum, K. M. VanBuskirk, J. H. Adams, *Mol. Biochem. Parasitol.* **117**, 49 (2001).
26. G. H. Mitchell, A. W. Thomas, G. Margos, A. R. Dluzewski, L. H. Banister, *Infect. Immun.* **72**, 154 (2004).
27. P. Kraulis, *J. Appl. Crystallogr.* **24**, 946 (1991).
28. E. A. Merritt, M. E. P. Murphy, *Acta Crystallogr.* **D50**, 869 (1994).

29. This work was funded by the European Commission (contracts QLK2-CT-1999-01293 and QLK2-CT-2002-01197), the European Malaria Vaccine Initiative, the Pasteur Institute, the Centre National de la Recherche Scientifique, the Biomedical Primate Research Centre, and the Medical Research Council (MRC), UK. C.R.C. is in receipt of an MRC Graduate Studentship grant. We thank the staff of the European Synchrotron Radiation Facility, Grenoble, and Martin Dubbeld for technical assistance. Coordinates and structure-factor amplitudes have been deposited in the Protein Data Bank (PDB): 1w8k (monoclinic) and 1w81 (orthorhombic).

Supporting Online Material

www.sciencemag.org/cgi/content/full/1107449/DC1
Materials and Methods
Figs. S1 to S4
Table S1
References
Movie S1

12 November 2004; accepted 7 February 2005
Published online 24 February 2005;
10.1126/science.1107449
Include this information when citing this paper.

A Homolog of *Drosophila grainy head* Is Essential for Epidermal Integrity in Mice

Stephen B. Ting,[1]* Jacinta Caddy,[1]* Nikki Hislop,[1] Tomasz Wilanowski,[1] Alana Auden,[1] Lin-lin Zhao,[1] Sarah Ellis,[2] Pritinder Kaur,[3] Yoshikazu Uchida,[4] Walter M. Holleran,[4] Peter M. Elias,[4] John M. Cunningham,[5] Stephen M. Jane[1]†

The *Drosophila* cuticle is essential for maintaining the surface barrier defenses of the fly. Integral to cuticle resilience is the transcription factor *grainy head*, which regulates production of the enzyme required for covalent cross-linking of the cuticular structural components. We report that formation and maintenance of the epidermal barrier in mice are dependent on a mammalian homolog of *grainy head*, *Grainy head–like 3*. Mice lacking this factor display defective skin barrier function and deficient wound repair, accompanied by reduced expression of transglutaminase 1, the key enzyme involved in cross-linking the structural components of the superficial epidermis. These findings suggest that the functional mechanisms involving protein cross-linking that maintain the epidermal barrier and induce tissue repair are conserved across 700 million years of evolution.

Despite substantial structural differences, the surface epithelium of flies and that of mice exhibit notable functional parallels. Genetic studies in both organisms have identified highly conserved pathways regulating cell movement and polarity (*1*, *2*), wound healing (*3*), and innate immunity (*4*). Less is known about the molecular and functional conservation of genes involved in assembly and maintenance of the impermeable surface barrier in the two organisms. In mammals, epidermal barrier function is largely provided by the stratum corneum (SC), a tough, insoluble layer composed of structural proteins and lipids covalently cross-linked by the enzyme transglutaminase 1 (TGase1) (*5*). In the fly, the epidermal epithelium deposits the embryonic cuticle, a rigid, waterproof layer essential for maintaining the structural integrity and microbial resistance of the organism (*6*). A limited number of genes have been linked to the regulation of cuticle formation in the fly embryo (*7*). One of these, *grainy head* (*grh*) (*8*), maintains the integrity of the cuticle through the regulation of *Dopa decarboxylase* (*Ddc*), which generates quinones that cross-link the cuticular proteins and chitin (*9*–*11*), similar to the function of TGase1 in mammals. We, and others, have recently identified homologs of *grh* that are highly conserved from *Caenorhabditis elegans* to human (*12*–*15*). We have demonstrated that mice lacking one of these genes, *Grainy head–like 3* (*Grhl3*) (*12*), display neural tube defects (*16*). During these studies, we noted that expression of *Grhl3* during mouse embryogenesis was largely restricted to the surface ectoderm, being expressed throughout this layer from embryonic day 12.5 (E12.5) onward (fig. S1), prompting us to examine the role of this factor in the maintenance of epidermal integrity.

We initially examined whether skin barrier function was perturbed in *Grhl3*-null mice. Changes in skin dye penetration reflect differences in the rates of embryonic acquisition of barrier function (*17*). *Grhl3*$^{-/-}$ and control embryos were exposed to 0.1% toluidine blue at various time points, and the ability of the embryos to prevent penetration of the dye was assessed (Fig. 1A). In agreement with previous studies, dye exclusion was not observed in either wild-type or *Grhl3*-null E16.5 embryos. Subsequently, the permeability bar-

[1]Rotary Bone Marrow Research Laboratories, c/o Royal Melbourne Hospital Post Office, Grattan Street, Parkville, Victoria, Australia 3050. [2]Microscopy Imaging Facility, [3]Epithelial Stem Cell Biology Laboratory, Peter MacCallum Research Institute, East Melbourne, Victoria, Australia 3001. [4]Dermatology Service and Research Unit, Department of Veterans Affairs Medical Center, and Department of Dermatology, School of Medicine, University of California, San Francisco, CA 94121, USA. [5]Division of Experimental Hematology, St. Jude Children's Research Hospital, Memphis, TN 38101, USA.

*These authors contributed equally to this work.
†To whom correspondence should be addressed. E-mail: jane@wehi.edu.au

rier was established as a progressing front in the wild-type embryos between E17.5 and E18.5 (Fig. 1A, top row). In contrast, *Grhl3*$^{-/-}$ embryos demonstrated an inability to exclude dye, as shown by uniform blue staining at E17.5 and E18.5 (Fig. 1A, bottom row), reflecting their defective epidermal barrier.

The skin barrier is critical for the key physiological function of fluid retention by the organism. Epidermal water loss can be measured by differential weight loss between wild-type and null mice under constant environmental conditions. Because the presence of thoracolumbosacral spina bifida in *Grhl3*$^{-/-}$ embryos may have confounded this total body weight analysis, we performed a transepidermal water loss (TEWL) assay on sections of skin from wild-type (+/+) and null (–/–) E18.5 embryos (Fig. 1B) (*17*). The cumulative TEWL from wild-type sections was less than 0.1 mg/mm^2 over a 5-hour period. In contrast, water loss from the *Grhl3*$^{-/-}$ skin was 6.5 times this amount, with more than 0.5 mg/mm^2 lost over the corresponding period. No statistical difference in water loss was observed between the wild-type and *Grhl3*$^{+/-}$ samples.

Because wound repair is another key function of the surface epithelium, we also examined this process in the *Grhl3*-null embryos. We harvested wild-type and *Grhl3*$^{-/-}$ embryos with their yolk sac intact at E12.5 (to assess embryonic wound healing) and E16.5 (to assess adult wound healing) (*18*). After wounding, the embryos were cultured for up to 24 hours in roller bottles and then analyzed by scanning electron microscopy (SEM) (Fig. 2A). Under these ex vivo conditions, the embryos are viable and continue to develop for up to 24 hours (*19*). In both E12.5 and E16.5 wild-type embryos, partial wound closure was observed after 6 hours, and this was largely complete after 24 hours. In contrast, the *Grhl3*$^{-/-}$ embryos of both gestations displayed minimal signs of healing at 24 hours.

The molecular events underlying the defects observed in the *Grhl3*-null epidermis presumably reflected altered expression of target genes of this transcription factor. To date, none of these targets had been identified, and the consensus DNA binding sequence of this factor remained unknown. To further define the molecular mechanisms involved in *Grhl3*-dependent barrier formation and wound healing, we initially compared the phenotype, histology (fig. S2), and ultrastructural features (fig. S3) of the *Grhl3*-null mice with the features reported for mice deficient in other factors known to be critical for barrier formation. These included the fatty acid transport protein Fatp4 (*20*); Pig-a, which is responsible for glycosylphosphatidylinositol (GPI)-anchor synthesis (*21*); the transcription factors Arnt (*22*) and Klf4 (*23*); and the cornified envelope (CE) protein cross-linking enzyme, TGase1 (*24*, *25*). Although all of these deficient mouse lines displayed some features that were shared with the *Grhl3*-null mice, there was a marked similarity between mice lacking *Grhl3* and the animals deficient in either *Klf4* or *TGase1*. Both lines displayed marked thickening of the SC with loss of corneocyte layering (fig. S2), loss of intact CEs, and defects in the SC lipid structures, with incomplete and irregularly deformed lamellae (fig. S3). We therefore examined the expression of *Klf4* and *TGase1* in wild-type and *Grhl3*-null epidermis by Northern analysis (Fig. 3A). The expression of *TGase1* in the *Grhl3*$^{-/-}$ epidermis was reduced to less than one-fifth that of the wild-type control, but the levels of *Klf4* RNA were identical in both samples. No change in expression between wild-type and *Grhl3*$^{-/-}$ epidermis was observed for the previously referred to "barrier" genes (*26*).

To determine whether *TGase1* was a potential Grhl3 target gene, we performed cyclic amplification and selection of targets (CASTing) (*27*) to define the DNA consensus binding site of *Grhl3*, using cellular extracts from an epidermoid carcinoma cell line (A431) transfected with a hemagglutinin epitope–tagged *Grhl3*-containing expression vector (*28*). After six cycles, the population of selected binding sites was cloned and individual isolates sequenced and aligned (Fig. 3B and fig. S4, A and B). The defined Grhl3 DNA binding consensus sequence matched the consensus sequence for *Drosophila grh* DNA binding, which we had previously identified by alignment of multiple *grh*-responsive gene-regulatory regions (*12*).

Recent studies have defined a region of the *TGase1* promoter that is critical for its tissue-specific expression in epidermis and other epithelium (*29*). Scrutiny of this region (between –1.6 and –1.1 kb 5′ of the CAP site) identified a potential *Grhl3* binding site, altered by the presence of one additional nucleotide. Further analysis of the upstream regions of the *TGase1* gene identified a second potential *Grhl3* binding site, 6 kb from the transcriptional start site. We examined these sites in electrophoretic mobility shift assays with the cellular extract from the A431 cells. As shown in Fig. 3C (and fig. S4C), a single specific protein/DNA complex was observed with the Grhl3 consensus probe defined in the CASTing experiment (lane 1). This complex was specifically competed with an unlabeled Grhl3 consensus probe (lane 2), but was

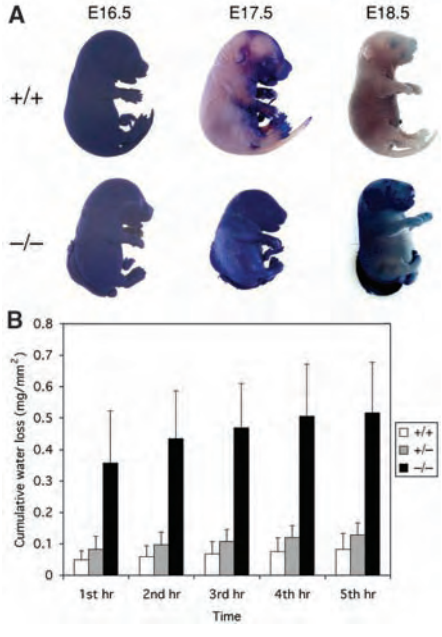

Fig. 1. Impairment of the epidermal barrier in *Grhl3*-null mice. (**A**) Skin permeability assay with 0.1% toluidine blue on *Grhl3*$^{+/-}$ intercross litters taken at the ages indicated. Wild type (+/+, top row); mutant (–/–, bottom row). (**B**) Transepidermal water loss over time on multiple equivalent skin sections from three separate E17.5 embryonic litters was analyzed. Wild type (+/+, $n = 4$); heterozygous (+/–, $n = 10$); mutant, (–/–, $n = 5$). Values are shown as the mean ± SD for each genotype at each time point. The differences between wild type and mutant were significant ($P < 0.01$, Student's t test) at each time point.

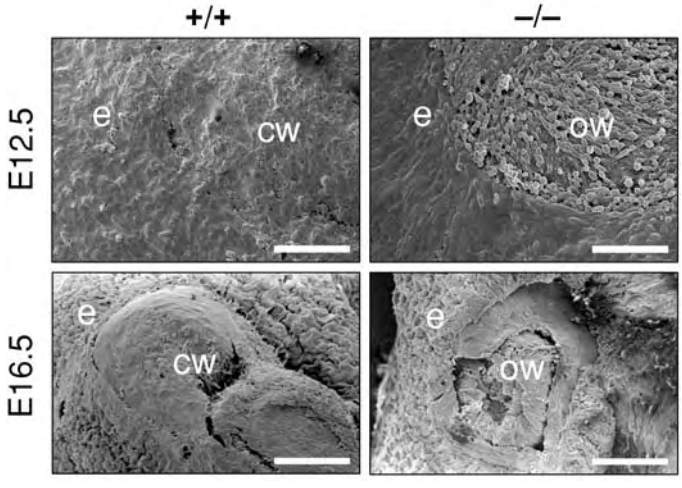

Fig. 2. Failed wound healing in *Grhl3*-null mice. SEM of a hindlimb amputation wound in wild-type (+/+) and mutant (–/–) embryos. The images are representative of the results obtained from six embryos in each group. E12.5 embryos (top row) were photographed 18 hours after amputation, and E16.5 embryos (bottom row) 24 hours after amputation. e, epidermis; cw, closed wound; ow, open wound. Scale bar, 86 μm at E12.5 and 170 μm at E16.5.

not competed with the addition of an unlabeled mutant probe in which the two invariant nucleotides defined in the CASTing selection were altered (lane 3). Addition of either unlabeled *TGase1* probe resulted in a reduction in Grhl3 binding to its consensus sequence (lanes 4 and 5). Taken together, these results suggest *TGase1* as a putative target gene of Grhl3. The link between *TGase1* and *Grhl3* provides a mechanism that unifies the skin phenotypes of the *Grhl3*-deficient mice. *TGase1*-deficient mice also die early in neonatal life with markedly impaired barrier function and ultrastructural defects in their SC lipid lamellae (*24*, *25*). Skin from these animals also displays marked delays in wound repair (*30*). However, differences also exist between these two deficient strains, particularly in the expression patterns of the CE precursor proteins and in the response to skin grafting (*24*), suggesting that the phenotype of the *Grhl3*-null mice may be influenced by the altered expression of additional target genes.

The abnormal barrier in the *Grhl3*-null mice appears comparable to the phenotype seen in *Drosophila grh* mutants, which exhibited fragile cuticles (*7*). Similarly, *C. elegans* embryos in which expression of a *grainy head*–like gene had been reduced by RNA interference failed to hatch and displayed a cuticle defect consistent with a loss of rigidity (*14*). *Grh* was initially identified as a factor involved in the transcriptional regulation of *Ddc* (*9*), which functions to pigment and harden the insect cuticle through the generation of quinones that cross-link the cuticular proteins (*10*). The identification of TGase1, the predominant enzyme involved in the generation of high molecular weight polymers of cross-linked CE proteins (*30*), as a putative target of *Grhl3* indicates that the *grh* family is involved in the regulation of protein cross-linking in barrier formation across 700 million years of evolution. The *grh* mutant cuticular defects are unlikely to be caused solely by *grh* regulation of the *Ddc* gene, because null *Ddc* mutants do not express the above cuticular phenotype, and the hypopigmentation of cuticular structures in the *grh* mutants is not as severe as that in the null *Ddc* mutants. Similarly, the *Grhl3*-null epidermal defects suggest the presence of additional target genes other than *TGase1*. It is conceivable that some of these genes may be conserved from fly to human, a hypothesis strengthened by the demonstration of identical DNA binding consensus sequences for *grh* and *Grhl3*.

The recent identification of wound response enhancers in the *Drosophila Ddc* and *pale* (*ple*) genes that mediate protective functions of the epidermal wound response and require binding sites for *grh*, and *grh* genetic function, provides an additional compelling link between *grh* family members, cross-linking enzymes, and the integrity of the surface epithelium (*31*). *Ple* encodes tyrosine hydroxylase, which is also involved in the generation of quinones for protein/chitin cross-linking (*10*, *11*). It is of interest that the regulation of cross-linking enzyme genes by *grh*-like factors has been conserved, even though the cross-linking genes themselves have diversified from fly to human. We found no change in *Ddc* gene expression in the *Grhl3*-null mice, consistent with the fact that this gene is not linked to protein cross-linking in the mammalian epidermis.

These studies identify an essential function for the *grh* family in maintenance of the integument barrier in diverse species. However, the *grh* gene is also critical for other aspects of epidermal and epithelial development in the fly, including cell polarity (*32*) and tubular morphogenesis (*33*). The complexity of gene function in the fly may also be seen in the mouse Grhl factors.

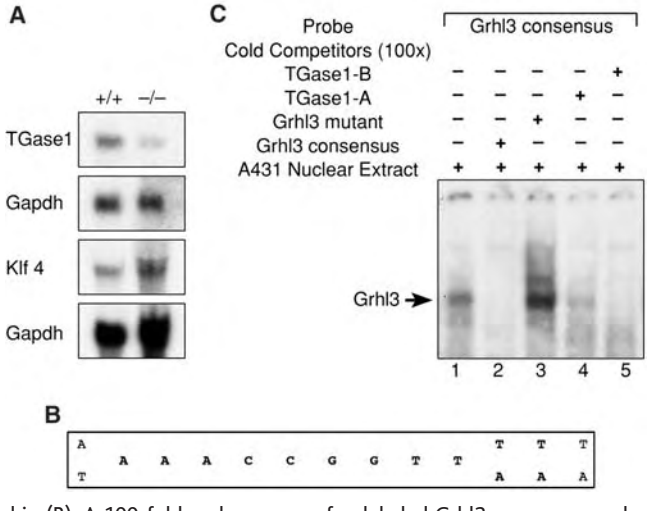

Fig. 3. *TGase1* is a putative target gene of Grhl3. (**A**) Northern analysis of *TGase1* and *Klf4* mRNA expression in skin from wild-type (+/+) and *Grhl3*-null (–/–) embryos. (**B**) Identification of a consensus sequence for recognition by Grhl3. The sequences from 49 clones obtained by CASTing (fig. S4, A and B) were aligned from positions −12 to +12. The consensus sequence was determined by the percent frequency of each nucleotide at each position. (**C**) DNA binding of Grhl3. Extract from the A431 cell line was studied with the Grhl3 consensus probe defined in (B). A 100-fold molar excess of unlabeled Grhl3 consensus probe or mutant probe or the two potential Grhl3 binding sites in the *TGase1* promoter were added in the indicated lanes. The migration of the specific Grhl3/DNA complex is indicated with an arrow. The image shown in this figure has been cropped, and the full image is shown in fig. S4C.

References and Notes

1. N. Harden, *Differentiation* **70**, 181 (2002).
2. M. Mlodzik, *Trends Genet.* **18**, 564 (2002).
3. P. Martin, S. M. Parkhurst, *Development* **131**, 3021 (2004).
4. J. A. Hoffmann, J. M. Reichhart, *Nat. Immunol.* **3**, 121 (2002).
5. A. E. Kalinin, A. V. Kajava, P. M. Steinert, *Bioessays* **24**, 789 (2002).
6. F. Payre, *Int. J. Dev. Biol.* **48**, 207 (2004).
7. S. Ostrowski, H. A. Dierick, A. Bejsovec, *Genetics* **161**, 171 (2002).
8. S. J. Bray, F. C. Kafatos, *Genes Dev.* **5**, 1672 (1991).
9. S. J. Bray, B. Burke, N. H. Brown, J. Hirsh, *Genes Dev.* **3**, 1130 (1989).
10. S. B. Scholnick, S. J. Bray, B. A. Morgan, C. A. McCormick, J. Hirsh, *Science* **234**, 998 (1986).
11. J. Schaefer *et al.*, *Science* **235**, 1200 (1987).
12. T. Wilanowski *et al.*, *Mech. Dev.* **114**, 37 (2002).
13. S. B. Ting *et al.*, *Biochem. J.* **370**, 953 (2003).
14. K. Venkatesan, H. R. McManus, C. C. Mello, T. F. Smith, U. Hansen, *Nucleic Acids Res.* **31**, 4304 (2003).
15. E. I. Kudryavtseva *et al.*, *Dev. Dyn.* **226**, 604 (2003).
16. S. B. Ting *et al.*, *Nat. Med.* **9**, 1513 (2003).
17. M. J. Hardman, P. Sisi, D. N. Banbury, C. Byrne, *Development* **125**, 1541 (1998).
18. P. Martin, *Science* **276**, 75 (1997).
19. J. McCluskey, P. Martin, *Dev. Biol.* **170**, 102 (1995).
20. T. Herrmann *et al.*, *J. Cell Biol.* **161**, 1105 (2003).
21. M. Tarutani *et al.*, *Proc. Natl. Acad. Sci. U.S.A.* **94**, 7400 (1997).
22. S. Takagi *et al.*, *J. Clin. Invest.* **112**, 1372 (2003).
23. J. A. Segre, C. Bauer, E. Fuchs, *Nat. Genet.* **22**, 356 (1999).
24. M. Matsuki *et al.*, *Proc. Natl. Acad. Sci. U.S.A.* **95**, 1044 (1998).
25. N. Kuramoto *et al.*, *J. Clin. Invest.* **109**, 243 (2002).
26. S. B. Ting *et al.*, data not shown.
27. W. E. Wright, M. Binder, W. Funk, *Mol. Cell. Biol.* **11**, 4104 (1991).
28. Materials and methods are available as supporting material on *Science* Online.
29. M. A. Phillips *et al.*, *BMC Dermatol.* **4**, 2 (2004).
30. R. Inada *et al.*, *Am. J. Pathol.* **157**, 1875 (2000).
31. K. A. Mace, J. C. Pearson, W. McGinnis, *Science* **308**, 381 (2005).
32. H. Lee, P. N. Adler, *Mech. Dev.* **121**, 37 (2004).
33. J. Hemphala, A. Uv, R. Cantera, S. Bray, C. Samakovlis, *Development* **130**, 249 (2003).

34. We thank W. McGinnis for sharing of data before publication; members of the Jane lab for helpful discussions; S. Vasudevan, S. Duoangpanya, L. Leypold, and Ozgene Inc. (Perth, Australia) for technical assistance; and B. Mesiti for help with figure preparation. Animal support was provided by staff from the Walter & Eliza Hall Institute. S.M.J. is a Principal Research Fellow of the Australian National Health and Medical Research Council (NHMRC). S.B.T. is a scholar of the Cancer Council of Victoria. J.M.C. is supported by the Cancer Center Support CORE Grant P30 CA 21765, the American Lebanese Syrian Associated Charities, and the Assisi Foundation of Memphis. This work was supported by PO1 HL53749–03 from the National Institutes of Health (USA) and Project Grant 282400 from the NHMRC. Additional support was received from NIH (USA) Grant PO1-AR39448 (W.M.H. and P.M.E.) and from the Department of Veterans Affairs (P.M.E.).

Supporting Online Material

www.sciencemag.org/cgi/content/full/308/5720/411/DC1
Materials and Methods
Figs. S1 to S4
References

15 November 2004; accepted 22 February 2005
10.1126/science.1107511

Reconstitution of Circadian Oscillation of Cyanobacterial KaiC Phosphorylation in Vitro

Masato Nakajima, Keiko Imai, Hiroshi Ito, Taeko Nishiwaki, Yoriko Murayama, Hideo Iwasaki, Tokitaka Oyama, Takao Kondo*

Kai proteins globally regulate circadian gene expression of cyanobacteria. The KaiC phosphorylation cycle, which persists even without transcription or translation, is assumed to be a basic timing process of the circadian clock. We have reconstituted the self-sustainable oscillation of KaiC phosphorylation in vitro by incubating KaiC with KaiA, KaiB, and adenosine triphosphate. The period of the in vitro oscillation was stable despite temperature change (temperature compensation), and the circadian periods observed in vivo in KaiC mutant strains were consistent with those measured in vitro. The enigma of the circadian clock can now be studied in vitro by examining the interactions between three Kai proteins.

Circadian rhythms allow organisms to coordinate their lives according to the alteration of their environments by day and by night (*1*). In most model organisms, transcription-translation–derived oscillatory (TTO) processes based on negative feedback regulation of clock genes are proposed as the core generator of self-sustaining circadian oscillations (*1*, *2*). Cyanobacteria are the simplest organisms that exhibit circadian rhythms. In the cyanobacterium *Synechococcus elongatus* (PCC 7942), three genes (*kaiA*, *kaiB*, and *kaiC*) are essential components of the circadian clock (*3*). Negative-feedback regulation of the expression of the *kaiBC* operon by Kai proteins was proposed as a core loop of prokaryotic TTO (*3*). In the cyanobacterial TTO model, Kai proteins do not regulate a specific set of circadian-controlled genes, but they regulate genomewide gene expression, including that of the *kaiBC* operon (*4*). However, how this transcription-translation feedback loop achieves circadian periodicity and how it stabilizes circadian oscillation against alterations in temperature and metabolic activity (collectively referred to as circadian characteristics) have not been clear. These circadian characteristics are essential for the oscillator to adapt to the environment, so understanding their molecular basis is an important goal in circadian biology.

The phosphorylation state of KaiC robustly oscillates in the cell with a 24-hour period, even under conditions where neither transcription nor translation of *kaiBC* operon was permitted, raising doubts about the TTO model in cyanobacteria (*5*). The circadian characteristics of this oscillator suggested that the pacemaker for the cyanobacterial circadian system was not a transcription-translation feedback loop but the KaiC phosphorylation cycle itself. KaiC has both autophosphorylation and autodephosphorylation activities, and KaiA enhances KaiC autophosphorylation (*6*), whereas KaiB attenuates the effect of KaiA (*7*, *8*). These results imply that, without additional kinases or phosphatases, an autonomous oscillation of KaiC phosphorylation could be generated by cooperation between KaiA and KaiB.

Recombinant KaiC protein was incubated with KaiA and KaiB at a ratio similar to that measured in vivo [KaiA:KaiB:KaiC=1:1:4 (by weight), (*7*)] in the presence of 1 mM ATP. To our surprise, KaiC phosphorylation robustly oscillated with a period of about 24 hours for at least three cycles without damping (Fig. 1A). The ratio of phosphorylated KaiC to total KaiC cycled between 0.25 and 0.65 (Fig. 1C). The amplitude of this in vitro KaiC phosphorylation rhythm was smaller than that observed in vivo under continuous light conditions (*5*). Also the total amount of KaiC remained constant during the incubation (Fig. 1B), which indicated that neither phosphorylated nor unphosphorylated KaiC was degraded during the reaction. Thus, oscillation of KaiC phosphorylation generates autonomously with a circadian period by cooperation of three Kai proteins.

One characteristic of circadian rhythms is that the free-running period remains stable for a relatively broad range of temperatures, referred to as "temperature compensation" of the period (*1*). Such temperature compensation of the in vitro oscillation of KaiC phosphorylation was observed with period lengths of about 22, 21, and 20 hours at 25°, 30°, and 35°C, respectively (Fig. 2A). The thermal sensitivity (Q_{10} coefficient) of the period (Fig. 2B) was about 1.1, consistent with that reported for in vivo gene expression rhythm (*9*). The rates of in vitro KaiC autophosphorylation and autodephosphorylation show a high degree of compensation for changes in temperature (*5*). Thus, temperature compensation of the in vitro rhythm is likely due to these reactions.

Many mutations of *kaiC* shorten or extend the period of circadian rhythm of *Synechococcus* (*3*). To assess whether the in vitro oscillation of KaiC phosphorylation was affected by such mutations, we incubated recombinant mutant KaiC with KaiA and KaiB. Three KaiC

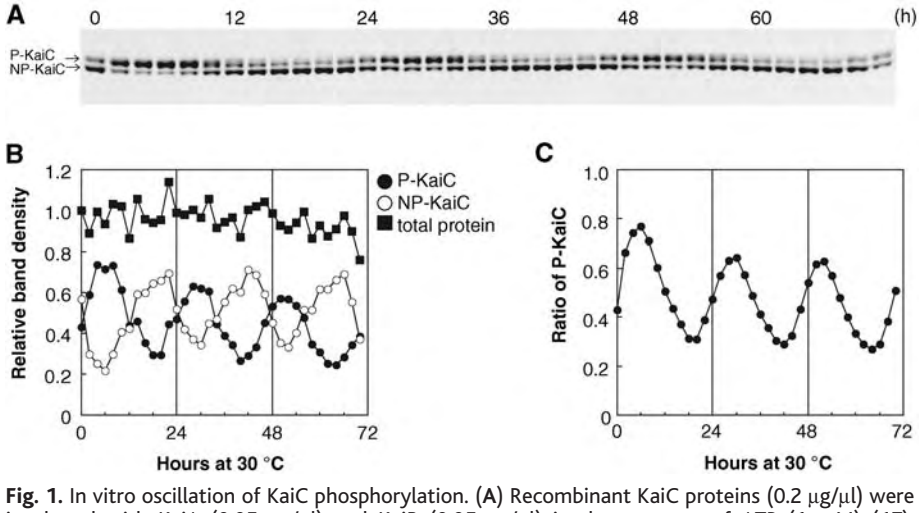

Fig. 1. In vitro oscillation of KaiC phosphorylation. (**A**) Recombinant KaiC proteins (0.2 μg/μl) were incubated with KaiA (0.05 μg/μl) and KaiB (0.05 μg/μl) in the presence of ATP (1 mM) (*17*). Aliquots (3 μl each) of the reaction mixtures were collected every 2 hours and subjected to SDS–polyacrylamide electrophoresis (SDS-PAGE) and Coomassie Brilliant Blue staining. The upper and lower bands correspond to phosphorylated (P-KaiC) and unphosphorylated KaiC (NP-KaiC), respectively (*6*). (**B** and **C**) NIH image software was used to perform densitometric analysis of data (*5*) in (A). The relative densities of total, phosphorylated, and unphosphorylated KaiC are plotted in (B), and the ratios of P-KaiC to total KaiC are plotted in (C).

Division of Biological Science, Graduate School of Science, Nagoya University, and the Core Research for Evolutional Science and Technology (CREST) of the Japan Science and Technology Agency (JST), Furo-cho, Chikusa-ku, Nagoya 464-8602, Japan.

*To whom correspondence should be addressed. E-mail: kondo@bio.nagoya-u.ac.jp

mutants that display high-amplitude bioluminescence rhythms were examined. The period lengths of expression rhythm of *kaiBC* promoter, monitored with a bioluminescence reporter (*3*), were 17, 21, and 28 hours, respectively, in mutant stains with amino acid substitutions of Tyr for Phe^{470} (F470Y), Pro for Ser^{157} (S157P), and Ser for Thr^{42} (T42S). The KaiC phosphorylation profiles, obtained when the mutant proteins were assayed in vitro, were consistent with those observed in vivo (Fig. 3A). We also confirmed that the bioluminescence profiles of these mutant strains were consistent with the in vitro oscillation of phosphorylation for each of the respective mutant KaiC proteins (Fig. 3, A and B). These results indicate that oscillation of KaiC phosphorylation is the molecular timer for the circadian rhythm of *Synechococcus*.

Phosphorylation of clock proteins has been reported in various prokaryotic and eukaryotic model organisms. PERIOD and TIMELESS in *Drosophila* and FREQUENCY in *Neurospora* degraded and/or translocated to the nucleus according to their circadian rhythms of phosphorylation state (*10*, *11*). Because alterations of the phosphorylation of these clock proteins affect the period length, the phosphorylation processes were assumed to be important components of the TTO models, including those for cyanobacteria (*2*, *3*). In these models, phosphorylation only contributes at a specific phase of the circadian cycle. However, our study demonstrates that the oscillation of KaiC phosphorylation is the pacemaker of the cyanobacterial circadian clock. In addition, the in vitro oscillation is generated in a homogenous system, whereas heterogeneous compartments are assumed in eukaryotic models (*2*). KaiC forms hexamers (*12*, *13*) and is phosphorylated at Ser^{431} and Thr^{432} (*14*, *15*). These results imply that KaiC hexamer has multiple phosphorylation states that may have different biochemical characteristics, including autophosphorylation and autodephosphorylation activities and/or binding preferences with other Kai proteins. In addition, the reaction rates of KaiC phosphorylation and dephosphorylation are quite slow, with rate constants of 10^{-3} to 10^{-4} s^{-1} [(*16*), SOM text]. Functionally, this feature would reduce the energy needed for timekeeping.

We propose a model of the cyanobacterial clock in which the autonomous oscillation of KaiC phosphorylation controls the expression of relevant genes including the *kai* genes to generate physiologically functional circadian oscillation (fig. S1). Simultaneously, the in vivo oscillation of KaiC phosphorylation could be amplified by coupling it with periodic changes in the concentrations of Kai protein and/or additional regulatory components of KaiC phosphorylation. The relationship between the phosphorylation of KaiC and the Kai transcription-translation cycle may be similar to that of a pendulum and an escapement mechanism that sustains the pendulum oscillation and transmits time signals to the hands of a wall clock.

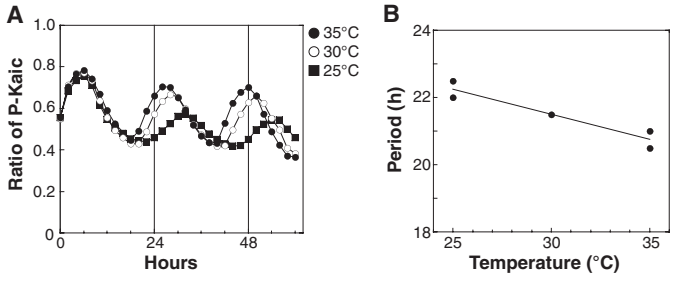

Fig. 2. Temperature compensation of the period of the in vitro oscillation of KaiC phosphorylation. (**A**) Three Kai proteins were incubated as in Fig. 1A at 25°, 30°, and 35°C. SDS-PAGE and densitometric analyses were carried out as in Fig. 1. (**B**) The period of the oscillation of the in vitro KaiC phosphorylation state was plotted against the incubation temperature. Results from two independent experiments were plotted.

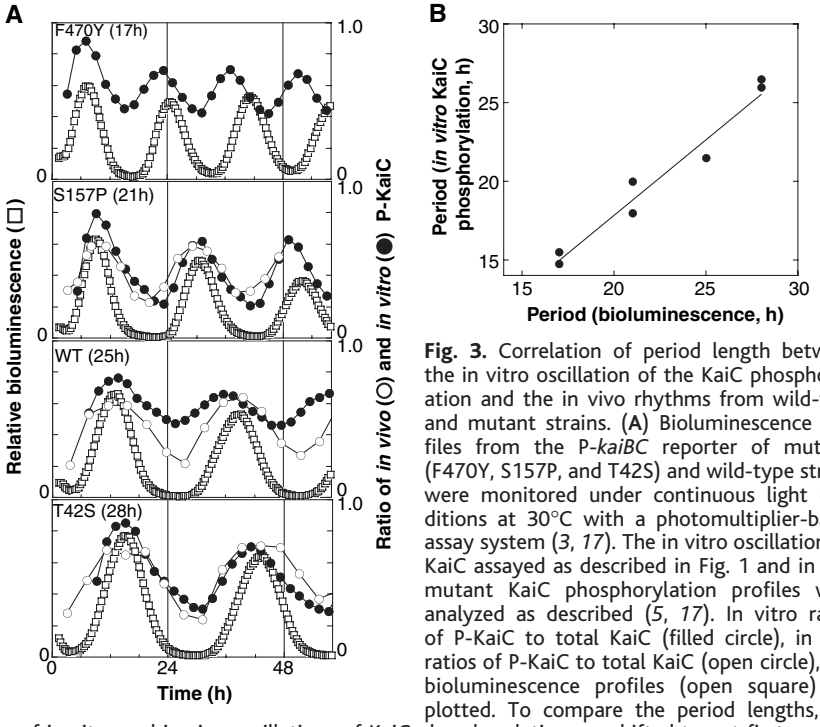

Fig. 3. Correlation of period length between the in vitro oscillation of the KaiC phosphorylation and the in vivo rhythms from wild-type and mutant strains. (**A**) Bioluminescence profiles from the P-*kaiBC* reporter of mutants (F470Y, S157P, and T42S) and wild-type strains were monitored under continuous light conditions at 30°C with a photomultiplier-based assay system (*3*, *17*). The in vitro oscillations of KaiC assayed as described in Fig. 1 and in vivo mutant KaiC phosphorylation profiles were analyzed as described (*5*, *17*). In vitro ratios of P-KaiC to total KaiC (filled circle), in vivo ratios of P-KaiC to total KaiC (open circle), and bioluminescence profiles (open square) are plotted. To compare the period lengths, the phases of in vitro and in vivo oscillations of KaiC phosphorylation are shifted to put first peak of phosphorylation rhythms on that of the corresponding bioluminescence rhythm. Periods of bioluminescence rhythm are shown in parentheses. (**B**) For wild type and each mutant strain shown in (A), the period length of the in vitro oscillation of the KaiC phosphorylation state is plotted against that of the in vivo rhythms of the strain. Results from two independent experiments were plotted.

References and Notes

1. J. C. Dunlap, J. J. Loros, P. J. DeCoursey, *Chronobiology: Biological Timekeeping* (Sinauer, Sunderland, MA, 2004).
2. M. W. Young, S. A. Kay, *Nat. Rev. Genet.* **2**, 702 (2001).
3. M. Ishiura *et al.*, *Science* **281**, 1519 (1998).
4. Y. Nakahira *et al.*, *Proc. Natl. Acad. Sci. U.S.A.* **101**, 881 (2004).
5. J. Tomita, M. Nakajima, T. Kondo, H. Iwasaki, *Science* **307**, 251 (2005); published online 18 November 2004 (10.1126/science.1108451).
6. H. Iwasaki, T. Nishiwaki, Y. Kitayama, M. Nakajima, T. Kondo, *Proc. Natl. Acad. Sci. U.S.A.* **99**, 15788 (2002).
7. Y. Kitayama, H. Iwasaki, T. Nishiwaki, T. Kondo, *EMBO J.* **22**, 2127 (2003).
8. Y. Xu, T. Mori, C. H. Johnson, *EMBO J.* **22**, 2117 (2003).
9. T. Kondo *et al.*, *Proc. Natl. Acad. Sci. U.S.A.* **90**, 5672 (1993).
10. R. Allada, P. Emery, J. S. Takahashi, M. Rosbash, *Annu. Rev. Neurosci.* **24**, 1091 (2001).
11. J. C. Dunlap, J. J. Loros, *J. Biol. Rhythms* **19**, 414 (2004).
12. T. Mori *et al.*, *Proc. Natl. Acad. Sci. U.S.A.* **99**, 17203 (2002).
13. F. Hayashi *et al.*, *Genes Cells* **8**, 287 (2003).
14. T. Nishiwaki *et al.*, *Proc. Natl. Acad. Sci. U.S.A.* **101**, 13927 (2004).
15. Y. Xu *et al.*, *Proc. Natl. Acad. Sci. U.S.A.* **101**, 13933 (2004).
16. The order of rate constant of KaiC phosphorylation was estimated by fitting the model equation $P(t) = P_{equi} + |P(0) - P_{equi}|\exp[-(k_1 + k_2)t]$ (SOM text) to experimental data shown in figure 3, C and D, of our previous report (*5*).
17. Materials and methods are available as supporting material on *Science* Online.

18. This research was supported in part by grants-in-aid from the Japanese Ministry of Education, Culture, Sports, Science, and Technology (15GS0308 to T.K., H.I., and T.O. and 14COEEA01 to T.K.), and the Japanese Society for Promotion of Science (13680778 to H.I.).

8 December 2004; accepted 8 February 2005
10.1126/science.1108451

Representation of Visual Gravitational Motion in the Human Vestibular Cortex

Iole Indovina,[1,2] Vincenzo Maffei,[1] Gianfranco Bosco,[3] Myrka Zago,[1] Emiliano Macaluso,[2] Francesco Lacquaniti[1,3,4]*

How do we perceive the visual motion of objects that are accelerated by gravity? We propose that, because vision is poorly sensitive to accelerations, an internal model that calculates the effects of gravity is derived from graviceptive information, is stored in the vestibular cortex, and is activated by visual motion that appears to be coherent with natural gravity. The acceleration of visual targets was manipulated while brain activity was measured using functional magnetic resonance imaging. In agreement with the internal model hypothesis, we found that the vestibular network was selectively engaged when acceleration was consistent with natural gravity. These findings demonstrate that predictive mechanisms of physical laws of motion are represented in the human brain.

The perception of motion is a fundamental property of the visual system. One of the most frequently encountered stimuli is an object accelerated by gravity, as in free-fall, ballistic, pendulum, or wave motion. Survival in the forest, like success on the sports field, critically depends on the ability to estimate the time to collision [TTC(t)] for accelerated objects, and to react quickly and appropriately as a result. However, psychophysics shows that the human visual system poorly estimates arbitrary accelerations of targets (*1*–*3*), and these accelerations generally are not taken into account in timing manual interceptions (*4*). Moreover, electrophysiological recordings in the monkey show that neurons in a key visual motion area (MT) accurately encode target direction and speed, but they contain only partial information about acceleration (*5*). Yet, visually guided interceptions of objects falling under gravity are accurately timed (*6*–*8*), in contrast with interceptions of objects dropped in microgravity (*9*). Furthermore, visual gravity cues contribute to perception of causality and naturalness of motion (*10*, *11*) and to perception of distance and size for falling objects (*12*) or biological motion (*13*). Gravity cues also influence the realism of special effects in cinematography (*12*). The ability to detect gravitational acceleration in visual motion can be demonstrated early in life. Between 5 and 7 months, infants begin to implicitly expect a downwardly moving object to accelerate and an upwardly moving object to decelerate (*10*). Therefore, there is ample evidence that gravitational acceleration is taken into account in visual perception and interceptive responses. However, the neural bases of gravitational visual processing are unknown.

Here we propose that an internal model calculating the effects of gravity (1g model) on seen objects is derived from graviceptive information, is stored in the vestibular cortex, and is activated by visual motion that appears to be coherent with natural gravity [Fig. 1A and (*14*)]. The basis for this hypothesis is that the vestibular system is able to estimate the gravity vector in head coordinates by combining signals from otoliths and semicircular canals (*14*–*16*) and that multisensory neurons in vestibular cortex also respond to visual stimuli (*17*). We surmise that, through experience, the vestibular estimate of Earth's gravity is transformed and stored as an abstract representation of gravity accessible by the visual system. Initial evidence for represented visual gravity was provided by the observation that, in the absence of gravity-determined sensory cues, astronauts initially expect the effects of Earth's gravity on a dropped object when they attempt to catch it in the Spacelab, and they adapt to the new environment only after a few days of flight (*9*). To test the internal model hypothesis, we measured motor performance and brain activity during different visual tasks. We predict that when the acceleration of a visual target is coherent with represented natural gravity, the 1g model will enable subjects to compute TTC(t) accurately, by engaging the vestibular network. Conversely, when target acceleration has the same amplitude as, but opposite direction to, natural gravity, subjects will compute TTC(t) less accurately, relying on visual motion areas that are poorly sensitive to arbitrary accelerations.

A first functional magnetic resonance imaging (fMRI) experiment involved three different tasks with a block design. In all tasks, subjects were presented with the picture of a woman standing in front of a building and were asked to maintain fixation on a dot placed just above the woman's head (*18*) (Movie S1). A ball moved upward from the fixation point at a constant acceleration bounced on the building cornice and returned downward. Initial ball speed was randomized to make flight duration unpredictable from trial to trial. Additionally, the fixation point expanded transiently after a random delay from the end of ball motion. The ball underwent the same average speed changes in all trials, but gravity was directed either toward the ground of the picture (1g trials, natural gravity) or away from it (–1g trials, reversed gravity). No cue was given to identify either trial type, and perceptually overt differences between them were subtle. In different blocks, subjects were asked either to press a button so as to intercept the descending ball at the time of arrival at the fixation point (proactive task), or to press the button as fast as possible after the Go signal corresponding to the expansion of the fixation point (reactive task). By design, response timing was coupled to the law of motion in proactive tasks, but decoupled in reactive tasks (because of the random delay intervening between the end of ball motion and the Go signal). We used these two tasks to verify that differences in brain activity between 1g and –1g trials would not merely reflect the nature of the motor task or motor errors (*19*). Finally, in a baseline condition, subjects simply fixated the expansions of the fixation point, and there was no ball motion in the visual display (No-motion task).

The proactive task required that subjects programmed motor responses before ball landing to compensate for neuromechanical transmission delays (*20*). Analysis of response times showed that the direction of visual gravity significantly affected the subject's ability to intercept the ball (Fig. 1B, black bars). Thus, all subjects correctly estimated TTC(t) in 1g trials only, and in these trials, the response times were explained by the 1g model that incorporates gravity effects on target motion (*21*, *22*). The response times for –1g trials were explained by the τ model that incorporates information about target position and velocity, but ignores acceleration (*4*, *21*–*23*). As expected, the direction of gravity had little effect on response times during the reactive task (Fig. 1B, white bars).

Analysis of fMRI data showed that 1g trials were associated with significantly more activity than –1g trials in a network involv-

[1]Department of Neuromotor Physiology, Scientific Institute Foundation Santa Lucia, via Ardeatina 306, 00179 Rome, Italy. [2]Department of Neuroimaging, Scientific Institute Foundation Santa Lucia, via Ardeatina 306, 00179 Rome, Italy. [3]Department of Neuroscience, University of Rome Tor Vergata, Via Montpellier 1, 00133 Rome, Italy. [4]Center of Space Biomedicine, University of Rome Tor Vergata, Via O. Raimondo 8, 00173 Rome, Italy.

*To whom correspondence should be addressed. E-mail: lacquaniti@caspur.it

ing the insular cortex, temporoparietal junction, premotor and supplementary motor areas (SMA), middle cingulate cortex, postcentral gyrus, posterior thalamus, putamen, and medial cerebellum (main effect of 1*g* motion, Fig. 2, tables S1 and S2). In agreement with the internal model hypothesis, the network processing 1*g* visual motion included the insulae and temporoparietal junctions, which are generally considered the core regions of the vestibular cortex [(*24*, *25*); see also (*17*) for related work in nonhuman primates]. Activation of the vestibular network was observed during both proactive and reactive tasks, which suggests that it depends on the presence of natural gravity in the visual stimuli, rather than on the specific motor task (anticipatory ball interception versus reaction-time response). Anatomical localization of the vestibular cortex was carried out by means of a second experiment. Standard caloric vestibular stimulations (alternating cold irrigations of the left and right ear) were performed blindfolded, resulting in vestibular sensations and nystagmus (*18*) that are known to depend on canal-otolith interactions performed by vestibular internal models (*26*). The resulting pattern of brain activation (tables S1 and S2) closely matched that reported in several previous neuroimaging studies involving caloric or galvanic vestibular stimulations (*18*, *24*, *27*). We statistically assessed what brain regions were activated by both 1*g* visual motion and vestibular stimulation (Fig. 2, A and B; table S1). This analysis revealed a common network composed of insular cortex (posterior insula and retroinsula), temporoparietal junction, ventral premotor area, SMA, middle cingulate cortex, and postcentral gyrus, as well as posterior thalamus and putamen. Our findings demonstrate that the vestibular network is involved in processing visual motion when this is coherent with natural gravity, which supports the hypothesis of an internal 1*g* model.

As for target motion unrelated to natural gravity, our hypothesis predicts that there should be less involvement of the internal 1*g* model and, hence, less activation of the vestibular network. Indeed, fMRI analysis showed that –1*g* trials were associated with significantly greater activity than 1*g* trials in a region located around the lateral occipital sulcus (LOS) in the middle and inferior occipital gyri (fig. S1, table S3), a region previously identified as motion-sensitive (*28*, *29*). In the context of our tasks, LOS may help compute TTC(*t*) from target position and velocity while ignoring acceleration, as implied by the τ model (*4*, *23*, *30*). As expected, vestibular stimulation did not activate this area, which emphasizes the segregation between neural representations of natural visual gravity and those of visual motion unrelated to gravity. Note that in contrast with gravity information, low-level motion cues were comparable between 1*g* and –1*g* trials, because the visual target moved through the same path and with the same average speed changes in both trial types. Accordingly, we found that several visual motion cortical areas were activated by both 1*g* and –1*g* trials when these trials were compared with the baseline (No-motion) condition. Visual motion areas included occipital area hV3a, middle temporal area hMT/V5+, and intraparietal sulcus regions (*28*, *29*). Moreover, several other areas related to the sensorimotor aspects of the tasks were also activated in this comparison (including superior parietal as well as frontal premotor and motor areas).

In summary, we showed that brain regions overlapping with those activated by direct vestibular stimuli are activated when the internal 1*g* model is called into play by visual exomotion coherent with natural gravity, even if there is no time-varying stimulation of the vestibular sensors. In monkeys, the parieto-insular vestibular cortex (PIVC) at the posterior end of the insula is the core region of the vestibular cortex, as it contains the greatest number of vestibular-driven neurons (*17*, *31*). Most PIVC neurons respond jointly to head accelerations and to optokinetic and neck somatosensory stimuli. PIVC is reciprocally connected (via ventroposterior thalamus) with the vestibular nuclei, as well as with the other vestibular cortical regions [in temporoparietal junction, postcentral gyrus, and ventral premotor and cingulate cortices (*17*)]. In addition, PIVC receives anatomical projections from the pulvinar, inferior parietal, and superior temporal areas, and this provides possible routes for visual inputs to vestibular cortex, as implied by the visual responses reported here (Fig. 2, A and B). In humans, lesions of posterior insula and retroinsula (probable homologs of monkey PIVC) lead to a tilt of the perceived visual vertical and rotational vertigo (*25*). Focal electrical stimulation elicits sensations of altered gravity or body tilt (*32*). Accordingly, it has been suggested that the cortical vestibular network is involved in the perception of our spatial orientation relative to the gravitational vertical (*17*, *24*, *25*, *27*).

Here we propose a new function for this network, namely, a representation of the phys-

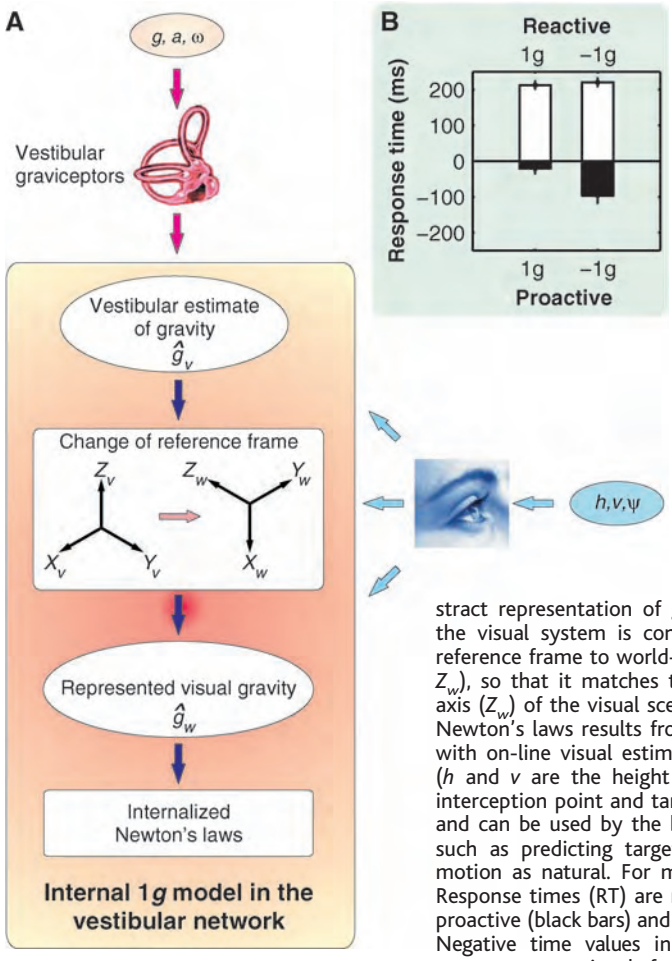

Fig. 1. (**A**) Neural computations predicted by the hypothesis of the internal model of gravity. The vestibular semicircular canals measure the angular velocity of the head (ω); the otolith organs measure both gravity (*g*) and linear acceleration of the head (*a*). Internal model calculations are included within the yellow and pink box. A vestibular estimate of gravity ($\hat{g}_v$) is computed in head-fixed coordinates (X_v, Y_v, Z_v) by the CNS. In general, rotational optokinetic cues (ψ) and extravestibular graviceptive cues may also contribute toward computing $\hat{g}_v$. An abstract representation of gravity ($\hat{g}_w$) accessible by the visual system is constructed by a change of reference frame to world-fixed coordinates (X_w, Y_w, Z_w), so that it matches the perceived top-bottom axis (Z_w) of the visual scene. The internal model of Newton's laws results from the combination of $\hat{g}_w$ with on-line visual estimates about target motion (*h* and *v* are the height of the target above the interception point and target velocity, respectively) and can be used by the brain for different scopes, such as predicting target TTC(*t*), or perceiving a motion as natural. For more details, see (*14*). (**B**) Response times (RT) are means (±SEM, $n = 17$) for proactive (black bars) and reactive (white bars) tasks. Negative time values in proactive correspond to responses occurring before the arrival time of the ball; positive time values in reactive correspond to responses after the Go signal. RT was significantly ($P < 0.001$) different from 0 in –1*g* proactive, 1*g* reactive, and –1*g* reactive trials.

ical laws of motion. Different forms of sensorimotor coordination might share an internal 1*g* model permanently stored in the distributed vestibular network. In this network, sensory processing may not be determined by modality but by the nature of the input, i.e., gravitational acceleration. Thus, the vestibular estimate of gravity helps in discriminating tilt from translation of the head (*15*, *16*), and the 1*g* model removes ambiguity from visual information in TTC estimates (as shown here). Furthermore, the areas of somatosensory cortex and ventral premotor cortex activated by visual 1*g* motion overlap with sensory and motor arm and hand representations, which suggests that the internal 1*g* model is also used to account for gravitational effects on arm position when planning arm movements or sensing arm position (kinesthesia), in agreement with the notion of multimodal processing in the cortical vestibular system (*17*, *24*, *27*). Finally, the internal 1*g* model might influence cognitive processes, transforming gravity into an abstract reference within the brain that contributes to our mind's balance (*33*). The idea that organisms' perception is tuned to environmental constraints by means of their internalization has long been around in psychology (*34*). Here we provided direct evidence that the fundamental physical constraint of Earth's gravity is internalized in the human brain.

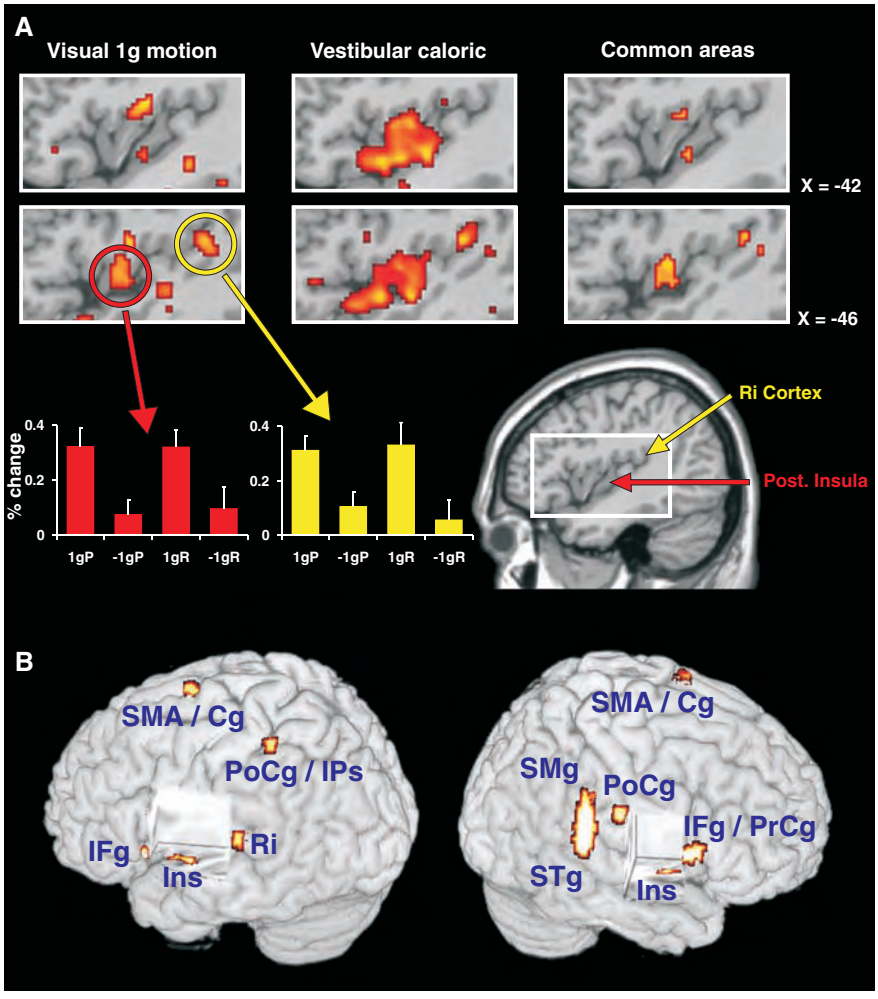

Fig. 2. (**A**) Common areas observed in the insulae for 1*g* visual-motion stimuli and direct vestibular stimuli. (Top) Color-coded areas of activation ($P < 0.05$, corrected for multiple comparisons) at two different parasagittal sections in the left hemisphere. From left to right: main effect of 1*g* motion {[(1*g*P) + (1*g*R)] > [(−1*g*P) + (−1*g*R)]}, main effect of caloric vestibular stimulation [(left stimuli + right stimuli) > baseline], and common activation for visual 1*g* motion and caloric vestibular stimulation. (Bottom) (right) The rectangle delimits the areas depicted in the above panels. Red and yellow arrows point to the anatomical location of the posterior insula and retroinsular cortex on a sagittal section (x = −42 mm) of the Montreal Neurological Institute (MNI) template in stereotactic space. (Bottom) (left) Mean activity (±SEM, $n = 17$) for the left insula cluster (95 voxels centered around the central insular sulcus) and the left retroinsular cluster (196 voxels at the temporoparietal junction). For each active task, averaged activity within these clusters is expressed as activation compared to baseline (No motion), in percentage, with respect to whole-brain mean. For coordinates of peak activations, see table S1. 1*g*P, −1*g*P, 1*g*R, and −1*g*R denote 1*g* proactive, −1*g* proactive, 1*g* reactive, and −1*g* reactive trials, respectively. (**B**) Overall cortical network of common activations for visual 1*g* motion and caloric vestibular stimulation, projected onto the surface-rendered MNI template. A perisylvian volume of brain is removed to show the insular region, deep in the lateral sulcus. *Cg*, middle cingulate gyrus; *IFg*, inferior frontal gyrus; *Ins*, insula; *IPs*, intraparietal sulcus; *PoCg*, postcentral gyrus; *PrCg*, precentral gyrus; *Ri*, retroinsula; *SMA*, supplementary motor area; *SMg*, supramarginal gyrus; and *STg*, superior temporal gyrus. For coordinates of peak activations, see table S1.

References and Notes

1. J. T. Todd, *J. Exp. Psychol. Hum. Percept. Perform.* **7**, 975 (1981).
2. P. Werkhoven, H. P. Snippe, A. Toet, *Vision Res.* **32**, 2313 (1992).
3. A. M. Brouwer, E. Brenner, J. B. Smeets, *Percept. Psychophys.* **64**, 1160 (2002).
4. N. L. Port, D. Lee, P. Dassonville, A. P. Georgopoulos, *Exp. Brain Res.* **116**, 406 (1997).
5. S. G. Lisberger, J. A. Movshon, *J. Neurosci.* **19**, 2224 (1999).
6. F. Lacquaniti, C. Maioli, *J. Neurosci.* **9**, 134 (1989).
7. F. Lacquaniti, M. Carrozzo, N. A. Borghese, in *Multisensory Control of Movement*, A. Berthoz, Ed. (Oxford Univ. Press, Oxford, 1993), pp. 379–393.
8. M. K. McBeath, D. M. Shaffer, M. K. Kaiser, *Science* **268**, 569 (1995).
9. J. McIntyre, M. Zago, A. Berthoz, F. Lacquaniti, *Nat. Neurosci.* **4**, 693 (2001).
10. I. K. Kim, E. S. Spelke, *J. Exp. Psychol. Hum. Percept. Perform.* **18**, 385 (1992).
11. C. R. Twardy, G. P. Bingham, *Percept. Psychophys.* **64**, 956 (2002).
12. J. S. Watson, M. S. Banks, C. von Hofsten, C. S. Royden, *Perception* **21**, 69 (1992).
13. D. Jokisch, N. F. Troje, *J. Vis.* **3**, 252 (2003).
14. The vestibular semicircular canals measure the angular velocity of the head (ω); the otolith organs measure gravitoinertial acceleration ($f = g - a$). A vestibular estimate of gravity ($\hat{g}_v$) is computed by the central nervous system (CNS) as a Bayesian weighted average of multicue information: $\hat{g}_v = \sum_i \hat{g}_i$ where $\hat{g}_i$ is the estimate of g from the ith sensor (*35*). In general, $\hat{g}_v$ can be obtained from (i) the neural solution of the nonlinear integral $\int(\hat{g}_v \times \hat{\omega}_v)dt$ provided by an internal model of how ω and g interact physically ($\times$ designates the vector cross product), (ii) the internal model discrimination between gravity and linear acceleration ($g = f + a$), (iii) the idiotropic vector aligned with the rostrocaudal body axis, (iv) rotational optokinetic cues (ψ), and (v) somatosensory cues. An abstract representation of gravity ($\hat{g}_w$) accessible by the visual system is constructed by a change of reference frame from head-fixed (X_v, Y_v, Z_v) to world-fixed (X_w, Y_w, Z_w) coordinates. The internal model of Newton's laws results from the combination of $\hat{g}_w$ with on-line visual estimates about target motion.

$$\mathrm{TTC}(t) = \frac{-\hat{v}_w(t) + \sqrt{\hat{v}_w(t)^2 + 2\hat{g}_w\hat{h}_w(t)}}{\hat{g}_w} \quad (1)$$

where TTC(t) is the estimate of the remaining time-to-arrival of the target at the interception point at any time t during descent, $\hat{h}_w(t)$ and $\hat{v}_w(t)$ are the visually estimated height of the target above the interception point and target velocity, respectively. Note that $\hat{h}_w(t)$ and $\hat{v}_w(t)$ in Eq. 1 must be in the same reference frame and on the same scale as $\hat{g}_w$. Thus, either all variables are defined in world coordinates by scaling retinal coordinates of the target by perceived extent (or apparent distance) of target trajectory, or all variables are defined in retinal coordinates, and $\hat{g}_w$ must be scaled accordingly. The computations outlined above do not all occur necessarily on-line. In the present experiments, subjects lay supine, $a = \omega = \psi = 0$, and $\hat{g}_w$ was roughly orthogonal to g.
15. D. M. Merfeld, L. Zupan, R. J. Peterka, *Nature* **398**, 615 (1999).

16. D. E. Angelaki, A. G. Shaikh, A. M. Green, J. D. Dickman, *Nature* **430**, 560 (2004).
17. W. O. Guldin, O. J. Grusser, *Trends Neurosci.* **21**, 254 (1998).
18. Materials and methods are available as supporting material on *Science* Online.
19. H. Imamizu *et al.*, *Nature* **403**, 192 (2000).
20. A mean visuomotor processing time of 171 ms was estimated for both 1*g* and –1*g* trials, on the basis of methods described in (*4*, *22*).
21. Both the 1*g* model and the τ model use on-line visual information about target position and velocity to trigger an interceptive movement when TTC(*t*) [see (*14*)] reaches a time threshold equal to the visuomotor processing time (*22*). However, the 1*g* model computes TTC(*t*) under the assumption that the target is accelerated by gravity [Eq. 1 in (*14*)], whereas the τ model assumes that the target moves at constant speed [$\mathrm{TTC}(t) = \hat{h}_w(t)/\hat{v}_w(t)$, see (*4*, *23*)]. Therefore, if the brain uses the 1*g* model to predict target motion, the responses to 1*g* trials will be correctly timed. By contrast, the τ model overestimates the TTC(*t*) of 1*g* trials and predicts that the corresponding responses should be systematically late. As a quantitative test, the time of response was computed separately for the five flight durations and was averaged across all trials of all subjects for a given flight duration. For 1*g* trials, the response times predicted by the 1*g* model were highly correlated with the experimental values in all subjects (mean $r = 0.998$), whereas those predicted by the τ model systematically failed to fit the experimental values (mean $r = -0.5$). The root mean square error (RMSE) of the fit to 1*g* trials was worse by a factor of 1.7 for the τ model than for the 1*g* model. For –1*g* trials, the response times predicted by the τ model were highly correlated with the experimental values in all subjects (mean $r = 0.973$), and adequacy of the fit was demonstrated by the random distribution of the residuals around the mean over the data range. Instead, the 1*g* model fitted the responses to –1*g* trials less adequately, as shown by a systematic bias of the residuals around the mean (thus *r* value was not computed for this fit). Accordingly, the RMSE of the fit was 3.6 times worse for the 1*g* model than for the τ model.
22. M. Zago *et al.*, *J. Neurophysiol.* **91**, 1620 (2004).
23. D. N. Lee, P. E. Reddish, *Nature* **293**, 293 (1981).
24. G. Bottini *et al.*, *Exp. Brain Res.* **99**, 164 (1994).
25. T. Brandt, M. Dieterich, A. Danek, *Ann. Neurol.* **35**, 403 (1994).
26. R. J. Peterka, C. C. Gianna-Poulin, L. H. Zupan, D. M. Merfeld, *J. Neurophysiol.* **92**, 2333 (2004).
27. S. Bense, T. Stephan, T. A. Yousry, T. Brandt, M. Dieterich, *J. Neurophysiol.* **85**, 886 (2001).
28. G. A. Orban *et al.*, *Neuropsychologia* **41**, 1757 (2003).
29. G. Rees, K. Friston, C. Koch, *Nat. Neurosci.* **3**, 716 (2000).
30. H. Merchant, A. Battaglia-Mayer, A. P. Georgopoulos, *Cereb. Cortex* **14**, 314 (2004).
31. O. J. Grusser, M. Pause, U. Schreiter, *J. Physiol.* **430**, 537 (1990).
32. O. Blanke, S. Ortigue, T. Landis, M. Seeck, *Nature* **419**, 269 (2002).
33. V. Smetacek, *Nature* **415**, 481 (2002).
34. R. N. Shepard, *Psychol. Rev.* **91**, 417 (1984).
35. L. H. Zupan, D. M. Merfeld, C. Darlot, *Biol. Cybern.* **86**, 209 (2002).
36. We thank R. Frackowiak, C. D. Frith, G. Galati, C. Porro, G. Rizzolatti, and J. N. Sanes for comments and advice on previous versions of this work. Supported by the Italian Ministry of Health, the Italian Ministry of University and Research (FIRB and PRIN grants), and the Italian Space Agency.

Supporting Online Material
www.sciencemag.org/cgi/content/full/308/5720/416/DC1
Materials and Methods
SOM Text
Fig. S1
Tables S1 to S5
References and Notes
Movie S1

29 November 2004; accepted 31 January 2005
10.1126/science.1107961

Complement Factor H Variant Increases the Risk of Age-Related Macular Degeneration

Jonathan L. Haines,[1] Michael A. Hauser,[2] Silke Schmidt,[2] William K. Scott,[2] Lana M. Olson,[1] Paul Gallins,[2] Kylee L. Spencer,[1] Shu Ying Kwan,[2] Maher Noureddine,[2] John R. Gilbert,[2] Nathalie Schnetz-Boutaud,[1] Anita Agarwal,[3] Eric A. Postel,[4] Margaret A. Pericak-Vance[2]*

Age-related macular degeneration (AMD) is a leading cause of visual impairment and blindness in the elderly whose etiology remains largely unknown. Previous studies identified chromosome 1q32 as harboring a susceptibility locus for AMD. We used single-nucleotide polymorphisms to interrogate this region and identified a strongly associated haplotype in two independent data sets. DNA resequencing of the complement factor H gene within this haplotype revealed a common coding variant, Y402H, that significantly increases the risk for AMD with odds ratios between 2.45 and 5.57. This common variant likely explains ~43% of AMD in older adults.

AMD causes progressive impairment of central vision and is the leading cause of irreversible vision loss in older Americans (*1*). The most severe form of AMD involves neovascular/exudative (wet) and/or atrophic (dry) changes to the macula. Although the etiology of AMD remains largely unknown, implicated risk factors include age, ethnicity, smoking, hypertension, obesity, and diet (*2*). Familial aggregation (*3*), twin studies (*4*), and segregation analysis (*5*) suggest that there is also a substantial genetic contribution to the disease. The candidate gene approach, which focuses on testing biologically relevant candidates, has implicated variants in the *ABCA4*, *FBLN6*, and *APOE* genes as risk factors for AMD. Replication of the *ABCA4* and *FBLN6* findings has been difficult, and in toto these variants explain a small proportion of AMD (*6*–*8*). The alternative genomic approach uses a combination of genetic linkage and association to identify previously unknown genes involved in AMD. We participated in a recent collaborative genomewide linkage screen (*9*) in which chromosome 1q32

[1]Center for Human Genetics Research, Vanderbilt University Medical Center, Nashville, TN 37232, USA. [2]Center for Human Genetics and Department of Medicine, Duke University Medical Center, DUMC Box 3445, 595 LaSalle Street, Durham, NC 27710, USA. [3]Vanderbilt Eye Institute, Vanderbilt University Medical Center, Nashville, TN 37232, USA. [4]Duke University Eye Center and Department of Ophthalmology, Duke University Medical Center, Durham, NC 27710, USA.

*To whom correspondence should be addressed. E-mail: mpv@chg.duhs.duke.edu

Table 1. *CFH* sequence variants identified in neovascular AMD cases and normal controls. All individuals were homozygous for the AMD-associated GAGGT haplotype. The 24 affected individuals selected for sequencing had severe neovascular disease (grade 5) (*12*) with diagnosis before age 74 (mean age at diagnosis: 65.8 years). The 24 control individuals selected for sequencing had no evidence of AMD (grade 1) with age at exam after age 64 (mean age at exam: 69.8 years). The six previously identified SNPs are labeled using standard nomenclature. The five previously unknown variants are labeled given their base pair location on chromosome 1, Ensembl build 35. Five SNPs create nonsynonymous amino acid changes within CFH, and five SNPs create synonymous changes. Exon 1 is not translated. n/a, not applicable.

Location	SNP ID	Effect	Minor allele frequency (%)	
			AMD	Controls
Exon 1	rs3753394	n/a	18	24
Exon 2	rs800292	V62I	0	6
Exon 6	193,380,486 A/G	R232R	0	2
Exon 7	rs1061147	A307A	10	38
Exon 8	193,390,164 C/T	H332Y	0	5
Exon 9	rs1061170	Y402H	94	46
Exon 11	193,414,604 A/G	A473A	0	31
Exon 12	193,416,415 A/G	T519A	0	2
Exon 14	rs3753396	Q672Q	0	23
Exon 18	193,438,299 C/T	H878H	6	2
Exon 19	HGVbase 000779895	E936D	0	23

was identified as a likely region for an AMD risk gene, a location also supported by other studies (*10*, *11*).

To identify the responsible gene on chromosome 1q32, we initially genotyped 44 single nucleotide polymorphisms (SNPs) (*12*) across the 24 megabases (Mb) incorporating this linkage region. We examined two independent data sets: The first contained 182 families (111 multiplex and 71 discordant sibpairs), and the second contained 495 AMD cases and 185 controls. Each SNP was tested for association independently in both data sets. Two SNPs (rs2019724 and rs6428379) in moderate linkage disequilibrium with each other ($r^2 = 0.61$) generated highly significant associations with AMD in both the family-based data set (rs2019724, $P = 0.0001$; rs6428379, $P = 0.0007$) and in the case-control data set (rs2019724, $P < 0.0001$; rs6428379, $P < 0.0001$). These SNPs lie ~263 kilobases (kb) apart.

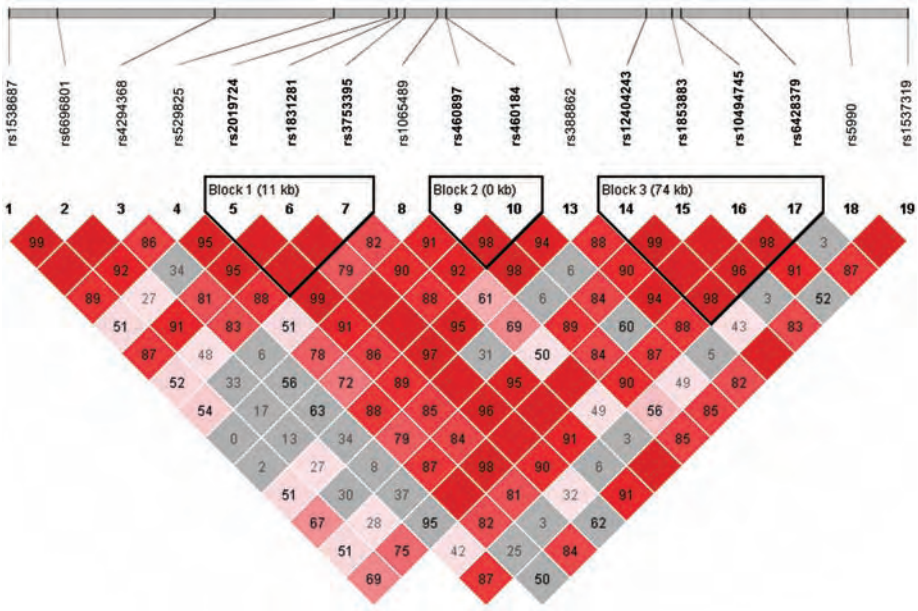

Fig. 1. Haploview plot defining haplotype block structure of AMD-associated region. The relative physical position of each SNP is given in the upper diagram, and the pairwise linkage disequilibrium (D′) between all SNPs is given below each SNP combination. Dark red–shaded squares indicated D′ values > 0.80. D′ = 1.0 when no number is given.

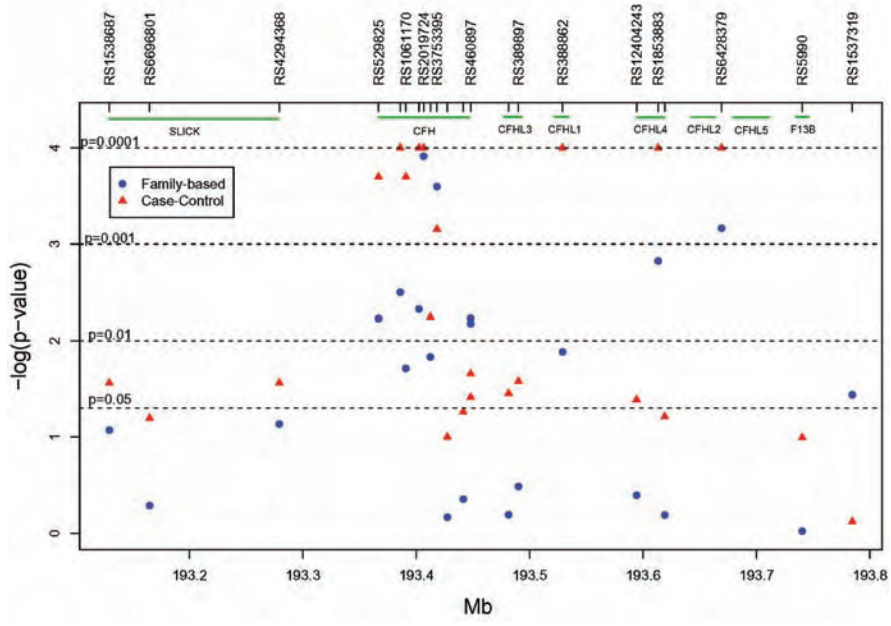

Fig. 2. Plot of family-based and case-control *P* values for all SNPs within the AMD-associated haplotype. The genomic region spanning each gene is indicated in green. $-\log_{10}$ of the nominal *P* values are plotted for each SNP. Results for both the family-based and case-control data sets converge within the *CFH* gene.

To completely define the extent of linkage disequilibrium, we genotyped an additional 17 SNPs across ~655 kb flanked by rs1538687 and rs1537319 and encompassing the 263-kb region. Two linkage disequilibrium blocks of 11 and 74 kb were identified and were separated by 176 kb (Fig. 1). The 11-kb block contained rs2019724, and the 74-kb block contained rs6428379. Association analysis of the 17 SNPs identified multiple additional SNPs giving highly significant associations in one or both of the family-based and case-control data sets (Fig. 2). In the case-control data set, a five-SNP haplotype (GAGGT, defined by SNPs rs1831281, rs3753395, rs1853883, rs10494745, and rs6428279, respectively) constituted 46% of the case and 33% of the control chromosomes ($P = 0.0003$). This same haplotype was also significantly overtransmitted to affected individuals in the family-based data set ($P = 0.00003$). The convergence of the most significant associations to this same haplotype in the two independent data sets strongly suggests that this region contains a commonly inherited variant in an AMD risk gene.

The associated GAGGT haplotype spans ~261 kb. It contains the Complement Factor H gene (*CFH*, OMIM #134370, accession #NM_000186) and the five Complement Factor H–related genes *CFHL1* to *CFHL5*, and lies within the Regulator of Complement Activation (RCA) gene cluster. The most consistent association results (Fig. 2) from both the family-based and case-control data sets converge within the *CFH* gene, implicating *CFH* as the AMD susceptibility gene. The biological role of Complement Factor H as a component of the innate immune system that modulates inflammation through regulation of complement (*13*) enhances its attractiveness as a candidate AMD susceptibility gene. Inflammation has been repeatedly implicated in AMD pathology. C-reactive protein levels are elevated in advanced disease (*14*), antiretinal autoantibodies have been detected in AMD patients (*15*), macrophages are localized near neovascular lesions (*16*), and the hallmark drusen deposits contain many complement-related proteins (*17*).

We screened for potential risk-associated sequence variants in the coding region of *CFH* by sequencing 24 cases with severe neovascular disease and 24 controls with no evidence of AMD. To maximize the likelihood of identifying the risk-associated allele, all sequenced cases and controls were homozygous for the GAGGT haplotype. Five previously unknown and six known sequence variants were detected (Table 1). Only one variant (rs1061170, sequence: T1277C; protein: Y402H) was present significantly more often in cases than controls, occurring on 45 of 48 haplotypes in the cases and on 22 of 48

haplotypes in the controls ($P < 0.0001$). The frequency of sequence variants within the *CFH* coding region on the associated haplotype was significantly reduced in cases compared to controls (12% versus 18%, $P = 0.002$). When the overrepresented T1277C variant was removed from the analysis, this difference became more pronounced (3% versus 16%, $P < 0.00001$). Thus, T1277C is the primary DNA sequence variant differentiating between the case and control haplotypes.

Complete genotyping of T1277C in the family-based and case-control data sets revealed a significant overtransmission in the families ($P = 0.019$) (*12*) and a highly significant overrepresentation in the cases compared to controls ($P = 0.00006$). The odds ratio for AMD was 2.45 [95% confidence interval (CI): 1.41 to 4.25] for carriers of one C allele and 3.33 (95% CI: 1.79 to 6.20) for carriers of two C alleles. When the analysis was restricted to only neovascular AMD, these odds ratios increased to 3.45 (95% CI: 1.72 to 6.92) and 5.57 (95% CI: 2.52 to 12.27), respectively. This apparent dose effect for risk associated with the C allele was highly significant ($P < 0.0001$). There was no apparent allelic or genotypic effect of T1277C on age at AMD diagnosis (mean age at diagnosis: TT, 76.5 years; TC, 77.5 years; CC, 75.5 years). The population attributable risk percent for carrying at least one C allele was 43% (95% CI: 23 to 68%).

The Y402H variant is predicted to have functional consequences consistent with AMD pathology. Residue 402 is located within binding sites for heparin (*18*) and C-reactive protein (CRP) (*19*). Binding to either of these partners increases the affinity of CFH for the complement protein C3b (*20*, *21*), augmenting its ability to down-regulate complement's effect. The observed colocalization of CFH, CRP, and proteoglycans in the superficial layer of the arterial intima suggests that CFH may protect the host arterial wall from excess complement activation (*22*). We hypothesize that allele-specific changes in the activities of the binding sites for heparin and CRP would alter CFH's ability to suppress complement-related damage to arterial walls and might ultimately lead to vessel injury and subsequent neovascular/exudative changes such as those seen in neovascular AMD. Our data support this hypothesis, because the risk associated with the C allele is more pronounced when the analyses are restricted to neovascular AMD. Given the known functional interactions of genes within the RCA gene cluster (*13*), variants within these genes could interact with or modify the effect of the T1277C variant.

Plasma levels of CFH are known to decrease with smoking (*23*), a known risk factor for AMD (*2*). This confluence of genetic and environmental risk factors suggests an integrated etiological model of AMD involving chronic inflammation. Identification of the increased risk of AMD associated with the T1277C variant should enhance our ability to develop presymptomatic tests for AMD, possibly allowing earlier detection and better treatment of this debilitating disorder.

References and Notes

1. Centers for Disease Control and Prevention (CDC), *Morb. Mortal. Wkly. Rep.* **53**, 1069 (2004).
2. J. Ambati, B. K. Ambati, S. H. Yoo, S. Ianchulev, A. P. Adamis, *Surv. Ophthalmol.* **48**, 257 (2003).
3. C. C. Klaver *et al.*, *Arch. Ophthalmol.* **116**, 1646 (1998).
4. C. J. Hammond *et al.*, *Ophthalmology* **109**, 730 (2002).
5. I. M. Heiba, R. C. Elston, B. E. Klein, R. Klein, *Genet. Epidemiol.* **11**, 51 (1994).
6. E. M. Stone *et al.*, *Nat. Genet.* **20**, 328 (1998).
7. S. Schmidt *et al.*, *Ophthalmic Genet.* **23**, 209 (2002).
8. D. W. Schultz *et al.*, *Hum. Mol. Genet.* **12**, 3315 (2003).
9. D. E. Weeks *et al.*, *Am. J. Hum. Genet.* **75**, 174 (2004).
10. G. R. Abecasis *et al.*, *Am. J. Hum. Genet.* **74**, 482 (2004).
11. S. K. Iyengar *et al.*, *Am. J. Hum. Genet.* **74**, 20 (2004).
12. Materials and methods are available as supporting material on *Science* Online.
13. S. Rodriguez de Cordoba, J. Esparza-Gordillo, E. Goicoechea de Jorge, M. Lopez-Trascasa, P. Sanchez-Corral, *Mol. Immunol.* **41**, 355 (2004).
14. J. M. Seddon, G. Gensler, R. C. Milton, M. L. Klein, N. Rifai, *J. Am. Med. Assoc.* **291**, 704 (2004).
15. D. H. Gurne, M. O. Tso, D. P. Edward, H. Ripps, *Ophthalmology* **98**, 602 (1991).
16. M. C. Killingsworth, J. P. Sarks, S. H. Sarks, *Eye* **4**, 613 (1990).
17. R. F. Mullins, S. R. Russell, D. H. Anderson, G. S. Hageman, *FASEB J.* **14**, 835 (2000).
18. T. K. Blackmore, V. A. Fischetti, T. A. Sadlon, H. M. Ward, D. L. Gordon, *Infect. Immun.* **66**, 1427 (1998).
19. E. Giannakis *et al.*, *Eur. J. Immunol.* **33**, 962 (2003).
20. D. T. Fearon, *Proc. Natl. Acad. Sci. U.S.A.* **75**, 1971 (1978).
21. C. Mold, M. Kingzette, H. Gewurz, *J. Immunol.* **133**, 882 (1984).
22. R. Oksjoki *et al.*, *Arterioscler. Thromb. Vasc. Biol.* **23**, 630 (2003).
23. J. Esparza-Gordillo *et al.*, *Immunogenetics* **56**, 77 (2004).

24. We thank all of the study participants and their relatives; M. de la Paz, M. Klein, J. Caldwell, R. Domurath, K. Haynes, V. Mitchell, M. Shaw, and J. Galloway for participant ascertainment; K. Abramson, J. Benton, W. Lambert, B. Love, T. Skelly, E. Tegnell, M. Allen, C. Haynes, R. Chung, and J. Bunch for valuable technical assistance; J. M. Vance and M. Summar for critical reading of the manuscript; and D. J. M. Gass for patient ascertainment and clinical expertise. We also thank the following clinics and clinicians for referring individuals to the study: Southern Retina, L.L.C (C. Harris); Vitreo-Retinal Surgeons (M. Duan and C. Devine); Georgia Retina, P.C.; and The Retina Group of Washington. Supported by grants EY12118 (to M.A.P.-V. and J.L.H.) and EY015216 (to S.S.) from the NIH/National Eye Institute, grant AG11268 from the NIH/National Institute on Aging (to H. Cohen), and grant M01 RR-00095 from the NIH/National Center for Research Resources (to Vanderbilt University).

Supporting Online Material

www.sciencemag.org/cgi/content/full/1110359/DC1
Materials and Methods
Table S1
References

28 January 2005; accepted 23 February 2005
Published online 10 March 2005;
10.1126/science.1110359
Include this information when citing this paper

Complement Factor H Polymorphism and Age-Related Macular Degeneration

Albert O. Edwards,[1*†] Robert Ritter III,[1] Kenneth J. Abel,[2] Alisa Manning,[3] Carolien Panhuysen,[3,6] Lindsay A. Farrer[3,4,5,6,7]

Age-related macular degeneration (AMD) is a common, late-onset, and complex trait with multiple risk factors. Concentrating on a region harboring a locus for AMD on 1q25-31, the *ARMD1* locus, we tested single-nucleotide polymorphisms for association with AMD in two independent case-control populations. Significant association ($P = 4.95 \times 10^{-10}$) was identified within the regulation of complement activation locus and was centered over a tyrosine-402 → histidine-402 protein polymorphism in the gene encoding complement factor H. Possession of at least one histidine at amino acid position 402 increased the risk of AMD 2.7-fold and may account for 50% of the attributable risk of AMD.

AMD is a leading cause of blindness in older individuals (*1*). It is a late-onset, complex trait with hereditary, lifestyle, and medical risk factors (*2*). The condition typically presents in the fifth decade of life with small yellow deposits external to the outer retina and retinal pigment epithelium (RPE) called drusen. Large numbers of drusen and clinical features of damage to the RPE markedly increase the risk of complications (atrophy of the RPE and abnormal neovascularization of the outer retina), leading to severe vision loss (*1*).

Although the primary pathogenic mechanisms of AMD were previously unknown, there is strong evidence that genetics plays a role (*3*–*9*). The first locus for AMD (*ARMD1*) was reported in a single extended family linked to chromosome 1q25.3-31.3 (*5*). Because there was strong evidence for linkage to this region

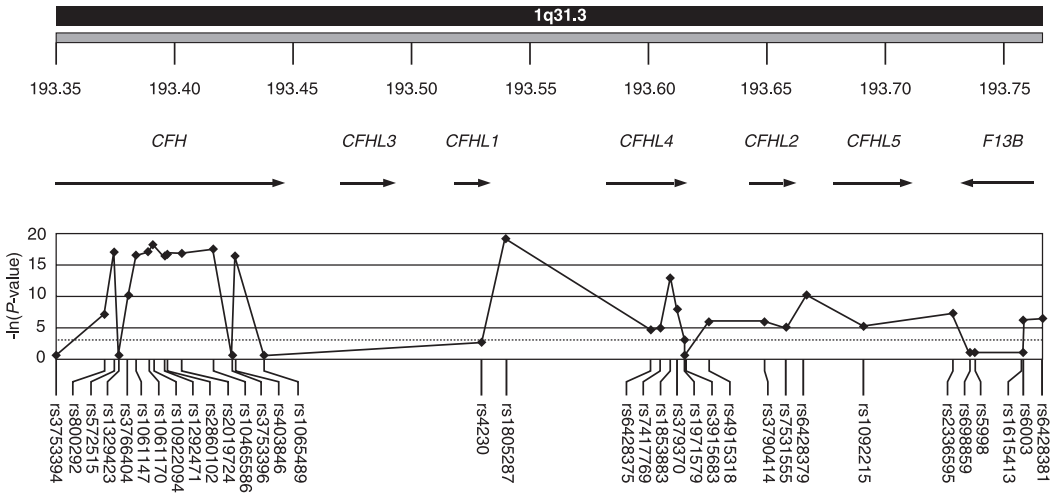

Fig. 1. The regulation of complement activation (RCA) locus located within chromosome 1q31.3 includes the gene for complement factor H (*CFH*), five related genes derived from *CFH* through ancestral duplications, and the gene for factor 13B (*F13B*). A megabase (Mb) scale of this region is provided at the top of the figure. SNPs genotyped across the RCA locus are shown along the bottom of the figure. The negative natural logarithm of the significance of allele association to AMD for each SNP is given in the graph (*10*). The 0.05 significance level is shown by the dotted line. Values greater than 15 on the *y* axis correspond to *P* values less than 10^{-7}.

of chromosome 1 (fig. S1) from subsequently reported small family studies, we focused our efforts on the *ARMD1* locus (*3*, *4*, *6*, *8*, *9*).

We performed an allele association study on a new case-control population that is highly discordant for clinical phenotypes. Cases were enrolled on the basis of ocular features (extensive drusen or pigmentary abnormalities of the macula) placing subjects at high risk for development of the complications of AMD or the presence of those complications in one or both eyes (*10*). Control subjects were from the same patient population and could have no more than four small hard drusen in the central retina (macula) and no known family history of AMD. A subset of 224 cases and 134 controls meeting these criteria were selected as a discovery sample for initial genotyping (table S1). The discovery sample was enriched for AMD cases showing familial clustering of AMD and high-risk, early AMD. A second, replication sample of 176 cases and 68 controls was ascertained at the same clinic following the same protocol (table S1).

Evaluation of the reported $Gln^{5346} \rightarrow Arg^{5346}$ variation in the fibulin 6 gene (*FIBL6*) and 23 single-nucleotide polymorphisms (SNPs) across this gene [supporting online material (SOM) text] gave no evidence for allele or haplotype association in the discovery sample (*11*). To determine whether common coding sequence variation within the *ARMD1* locus was associated with AMD, we searched publicly available databases for nonsynonymous coding SNPs (nscSNPs). We identified 24 nscSNPs with known minor allele frequencies of at least 10% across the 14-Mb *ARMD1* locus. Genotyping of the discovery sample gave significant allele and genotype association between AMD and nscSNPs only within the regulation of complement activation (RCA) locus in chromosome 1q31.3 (table S2). Additional evenly spaced, gene-based SNPs were evaluated across all 31 genes in clusters 1, 3, 4, and 6 at 8-kb to 25-kb density (fig. S1), and no associations with AMD were detected outside of the RCA locus (table S3). These data suggest that the RCA locus contains one or more genetic variants that increase the risk of developing AMD.

The RCA locus spans 388 kb of genomic DNA that contains the gene encoding complement factor H (*CFH*), five genes derived from *CFH* through ancestral duplications, and the gene encoding factor 13B (Fig. 1). A total of 86 SNPs located across the RCA locus and flanking regions were genotyped. Twenty-nine gave evidence for allele association with the majority, and the most significant of these, including the nscSNP rs1061170, concentrated in the *CFH* gene (table S3, GenBank accession no. NM_000186).

Table 1. Association between the $Try^{402} \rightarrow His^{402}$ polymorphism (rs1061170) in *CFH* and AMD. The C allele codes for histidine. The genotype association compares CC with CT and TT.

Sample	Allele distribution			Allele association (*P* value)	Genotype distribution			Genotype association (*P* value)
		Cases	Controls			Cases	Controls	
Discovery	C	0.553	0.340	3.68×10^{-8}	CC	0.320	0.115	7.67×10^{-7}
	T	0.447	0.660		TC	0.467	0.450	
					TT	0.213	0.435	
Replication	C	0.544	0.390	0.0039	CC	0.306	0.186	0.0135
	T	0.456	0.610		TC	0.477	0.407	
					TT	0.218	0.407	
Total	C	0.549	0.355	4.95×10^{-10}	CC	0.314	0.137	1.4×10^{-8}
	T	0.451	0.645		TC	0.471	0.437	
					TT	0.215	0.426	

The genotype frequency data for rs1061170 revealed that the association with AMD was largely due to an excess of CC homozygotes in cases compared with controls (Table 1). A similar pattern of association was evident with seven adjacent SNPs in *CFH* (Fig. 1 and table S3). The strength of the evidence for association diminished markedly with SNPs located immediately proximal to *CFH* and distal to its derivatives *CFHL1* to *CFHL5*, suggesting that the effect was due to one or more polymorphisms in the complement factor genes only (Fig. 1 and table S3).

Haplotype analyses of 34 SNPs spanning 418 kb revealed extensive linkage disequilibrium across the full length of the RCA locus (Fig. 2). The highest level of linkage disequilibrium was discernable among four haplotype blocks across the RCA locus. Thirteen contiguous SNPs in *CFH* (i.e., all but the first two *CFH* SNPs in Fig. 2) form a 64-kb haplotype block. A second 9-kb haplotype block contained SNPs in the proximal

[1]Department of Ophthalmology and McDermott Center for Human Growth and Development, University of Texas Southwestern Medical Center (UTSWMC), 5323 Harry Hines Boulevard, Dallas, TX 75390, USA. [2]Sequenom, Incorporated, 3595 John Hopkins Court, San Diego, CA 92121, USA. [3]Department of Medicine (Genetics Program), [4]Department of Neurology, and [5]Department of Genetics and Genomics, Boston University School of Medicine, and [6]Department of Biostatistics and [7]Department of Epidemiology, Boston University School of Public Health, 715 Albany Street, Boston, MA 02118, USA.

*To whom correspondence should be addressed. E-mail: albert-edwards@swbell.net

†Present address: Institute for Retina Research, 3215 Princess Lane, Dallas, TX 75229, USA.

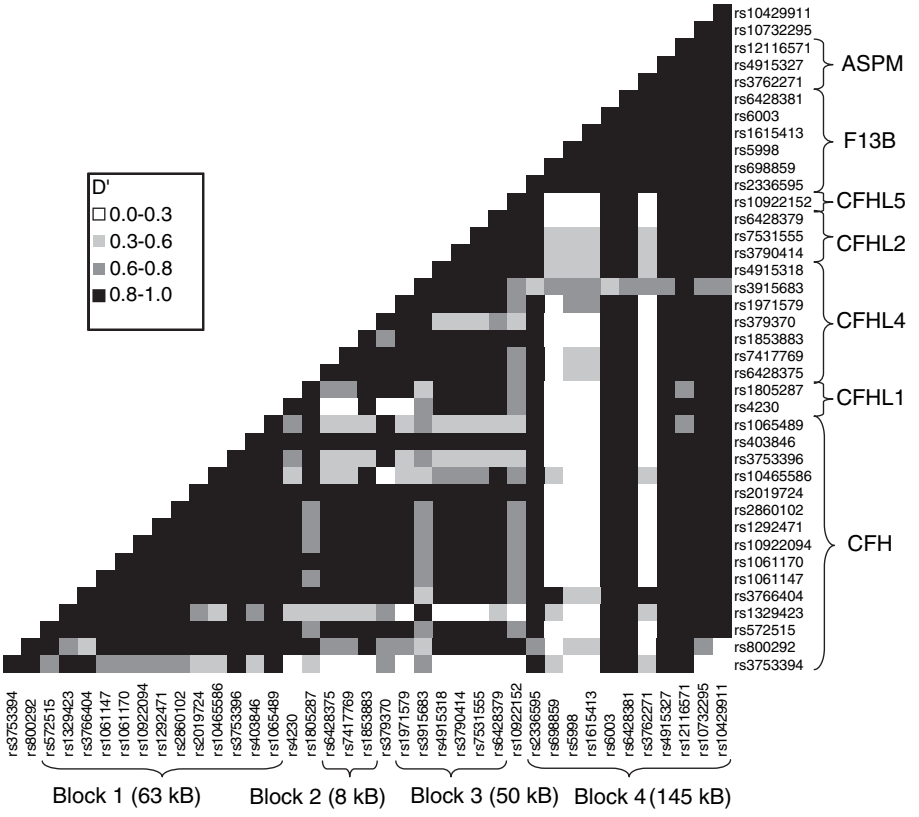

Fig. 2. Pairwise linkage disequilibrium (LD) among 38 SNPs in and surrounding the RCA locus, spanning the region including the 5′ upstream region of *CFH* (represented by the SNP rs3753394) and the proximal portion of *FRBZ1* (represented by the SNP rs10732295), a distance of 516 kb. LD was measured by the D′ statistic with use of data from all subjects in the discovery sample (*10*). A D′ value of 1 indicates complete linkage disequilibrium between two markers, and a D′ value of 0 indicates complete linkage equilibrium. By using the Haploview version 3.0 software, we could divide the RCA locus into four haplotype blocks (*29*). D′ values for all or nearly all pairwise comparisons within a haplotype block are at least 0.8 (black squares). The haplotype block structure is similar to that obtained by the HapMap Project for this region in Caucasians, with the notable difference that blocks 2 and 3 in our structure compose one block in the HapMap report (*10*). The lone SNP (rs379370) between blocks 2 and 3 is a nscSNP in the *CFHL4* gene (table S2) showing moderate LD (gray squares), modest LD (light gray squares), or low LD (white squares) with the SNPs in block 3.

portion of *CFHL4*, a third 50-kb block contained SNPs in the distal portion of *CFHL4* and in *CFHL2*, and a fourth 146-kb block contained SNPs in *F13B*, *ASPM*, and *FRBZ1* (Fig. 2). The SNPs most significantly associated with AMD were in *CFH* or within 221 kb downstream of *CFH* (Fig. 1 and table S3).

The association between AMD and haplotypes comprising two to five contiguous SNPs was evaluated by using the Haplo.stat software and a sliding window approach (*12*, *13*). Additional comparisons were made by using all possible haplotypes formed by pairwise combinations, including at least one nscSNP within the RCA locus. The analysis did not reveal any SNP combination showing greater association with AMD than the individual SNPs. All of the AMD high-risk haplotypes, including a *CFH* SNP from haplotype block 1 and a non-*CFH* SNP from other regions of the RCA locus (Fig. 1), contained the AMD risk allele from the *CFH* SNP but not necessarily the AMD risk allele from the non-*CFH* SNP. These analyses provide further evidence that the multiple signals in the RCA locus are related to a single haplotype and therefore likely caused by a single genetic effect.

To verify these findings, we genotyped 14 SNPs in the RCA locus in the replication sample. Association with AMD was observed with the seven markers that were significant in the discovery sample, including rs1061170, but not with the seven markers yielding negative results in the discovery sample (table S4). Notably, the genotype frequencies for rs1061170 among cases enriched for a positive family history of AMD were nearly identical to the frequencies among cases without this characteristic (Table 1), suggesting that this CFH protein polymorphism is a risk factor for AMD more generally. Taking into account data from the entire sample, a conservative estimation of the relative risk for AMD conferred by having at least one C allele (i.e., having either the CC or CT genotypes) was 2.7 (95% confidence interval of 1.9 to 3.9).

Complement activation has been implicated in the pathogenesis of a number of complex traits, including AMD, and can arise through the classical, lectin, or alternative pathways (*14*). All three pathways lead to the generation of a C3 convertase enzyme and subsequent activation of the immune response, the terminal pathway pore-like membrane attack complex (C5b-9), and cell lysis. The alternative complement pathway is spontaneously activated, and CFH is an essential inhibitor preventing uncontrolled complement activation (*15*). Components of the terminal complement pathway and other markers of inflammation are deposited in drusen and the choroid of eyes with AMD (*16*, *17*). Abnormal regulation of the alternative pathway of complement activation by CFH is consistent with these observations.

The tyrosine-to-histidine polymorphism (rs1061170) at amino acid 402 of CFH may be a primary pathogenic variation increasing the risk of developing AMD. CFH is composed of 20 repetitive units of 60 amino acids called short consensus repeats (SCRs). The $Try^{402} \rightarrow His^{402}$ polymorphism is located within SCR7, which contains the overlapping binding sites for heparin, C-reactive protein (CRP), and M protein (*18*). Serum amounts of CRP were elevated in AMD subjects compared with controls in one large prospective clinical trial (*19*). CRP activates the classic complement pathway but reduces deposition of C5b-9 through the direct binding of CFH (*20*). Risk factors for development of complications of AMD, including cigarette smoking, lack of exercise, hypertension, and obesity (*2*, *21*), increased serum CRP or decreased serum CFH (*22*–*25*). Further, drusen with terminal complement deposition indistinguishable from AMD were observed in eyes from patients with a kidney disease (membranoproliferative glomerulonephritis type II) that can be caused by mutations in *CFH* (*26*, *27*). In principle, altered binding of CFH to CRP or heparin on outer retinal surfaces caused by the $Tyr^{402} \rightarrow His^{402}$ substitution could affect the level of inflammation in the outer retina, thereby contributing to AMD. Although our results are consistent with the $Tyr^{402} \rightarrow His^{402}$ variant causing AMD, they do not rule out the existence of other coding or splice site variants within *CFH* that modulate risk of AMD.

More than 7 million individuals in the United States have retinal features placing them at high risk for developing vision loss from complications of AMD (*28*). The attributable fraction for the C allele derived from the total sample of subjects in this study is 50%, suggesting that persons either homo-

zygous or heterozygous for histidine at amino acid 402 of CFH may account for one-half of AMD cases. Given the rapid aging of the population, an estimated 3 million individuals will have atrophic and exudative complications of AMD by 2020 (*28*). Our findings suggest previously unknown avenues for developing preventative and therapeutic strategies for AMD.

References and Notes

1. R. Klein, B. E. Klein, S. C. Tomany, S. M. Meuer, G. H. Huang, *Ophthalmology* **109**, 1767 (2002).
2. R. Klein, T. Peto, A. Bird, M. R. Vannewkirk, *Am. J. Ophthalmol.* **137**, 486 (2004).
3. G. R. Abecasis *et al.*, *Am. J. Hum. Genet.* **74**, 482 (2004).
4. S. K. Iyengar *et al.*, *Am. J. Hum. Genet.* **74**, 20 (2004).
5. M. L. Klein *et al.*, *Arch. Ophthalmol.* **116**, 1082 (1998).
6. J. Majewski *et al.*, *Am. J. Hum. Genet.* **73**, 540 (2003).
7. J. H. Schick *et al.*, *Am. J. Hum. Genet.* **72**, 1412 (2003).
8. J. M. Seddon, S. L. Santangelo, K. Book, S. Chong, J. Cote, *Am. J. Hum. Genet.* **73**, 780 (2003).
9. D. E. Weeks *et al.*, *Am. J. Hum. Genet.* **75**, 174 (2004).
10. Materials and methods are available as supporting material on *Science* Online.
11. D. W. Schultz *et al.*, *Hum. Mol. Genet.* **12**, 3315 (2003).
12. D. J. Schaid, C. M. Rowland, D. E. Tines, R. M. Jacobson, G. A. Poland, *Am. J. Hum. Genet.* **70**, 425 (2002).
13. H. Zhao, R. Pfeiffer, M. H. Gail, *Pharmacogenomics* **4**, 171 (2003).
14. J. Acosta, X. Qin, J. Halperin, *Curr. Pharm. Des.* **10**, 203 (2004).
15. H. J. Muller-Eberhard, R. D. Schreiber, *Adv. Immunol.* **29**, 1 (1980).
16. R. F. Mullins, S. R. Russell, D. H. Anderson, G. S. Hageman, *FASEB J.* **14**, 835 (2000).
17. L. V. Johnson, W. P. Leitner, M. K. Staples, D. H. Anderson, *Exp. Eye Res.* **73**, 887 (2001).
18. E. Giannakis *et al.*, *Eur. J. Immunol.* **33**, 962 (2003).
19. J. M. Seddon, G. Gensler, R. C. Milton, M. L. Klein, N. Rifai, *JAMA* **291**, 704 (2004).
20. C. Mold, H. Gewurz, T. W. Du Clos, *Immunopharmacology* **42**, 23 (1999).
21. J. M. Seddon, J. Cote, N. Davis, B. Rosner, *Arch. Ophthalmol.* **121**, 785 (2003).
22. J. Esparza-Gordillo *et al.*, *Immunogenetics* **56**, 77 (2004).
23. J. R. Greenfield *et al.*, *Circulation* **109**, 3022 (2004).
24. J. M. Backes, P. A. Howard, P. M. Moriarty, *Ann. Pharmacother.* **38**, 110 (2004).
25. M. H. Wener, P. R. Daum, G. M. McQuillan, *J. Rheumatol.* **27**, 2351 (2000).
26. R. F. Mullins, N. Aptsiauri, G. S. Hageman, *Eye* **15**, 390 (2001).
27. M. A. Dragon-Durey *et al.*, *J. Am. Soc. Nephrol.* **15**, 787 (2004).
28. D. S. Friedman *et al.*, *Arch. Ophthalmol.* **122**, 564 (2004).
29. J. C. Barrett, B. Fry, J. Maller, M. J. Daly, *Bioinformatics* **21**, 263 (2005).

30. We thank the McDermott Sequencing Center at UTSWMC for genotyping assistance and T. Hyatt for technical advice and assistance. Supported by the National Eye Institute (EY014467), a center grant from the Foundation Fighting Blindness, and Research to Prevent Blindness.

Supporting Online Material

www.sciencemag.org/cgi/content/full/1110189/DC1
Materials and Methods
Fig. S1
Tables S1 to S4
References

25 January 2005; accepted 22 February 2005
Published online 10 March 2005;
10.1126/science.1110189
Include this information when citing this paper.

New Products

http://science.labvelocity.com

Drug Permeability Measurements

The Biomek FX ADMETox Workstation for in vitro drug permeability measurements automates the parallel artificial membrane permeability analysis (PAMPA) method for the determination of passive absorption of a drug candidate through an artificial lipid membrane. The PAMPA method is significantly faster than the Caco-2 cell-based method, which takes three weeks to complete. With PAMPA, data collection can occur in less than five hours. The PAMPA method mimics the permeability of drug candidates across the intestinal wall in the human gastrointestinal tract. It can also be run to mimic the permeability across the human blood-brain barrier or can be used for pesticide research in plants.

Beckman Coulter For information 800-742-2345 www.beckmancoulter.com

Kinase Substrate Array

The PepChip Kinase Substrate Array is a high-density peptide array containing unique addressable kinase substrates. The chip allows drug discovery scientists to profile more than 80% of the human kinome. PepChip enables broad kinase activity screening in complex mixtures, substrate profiling of know and unknown kinases, and specificity testing of kinase inhibitors. It is a research tool to investigate the specificity of kinase inhibitors in the context of total kinase activity of the target cells using cell lysates. It offers proof of inhibitor specificity of kinases involved in signal transduction pathways and kinase substrate-dependent inhibition.

Shleicher & Schuell For information 603-352-3810 www.schleicher-schuell.com

Semi-Micro Balances

The Phoenix series of analytical, semi-micro balances includes 5 models to suit various analytical weighing applications. The Phoenix GH-252 is the flagship model, offering dual capacity, including 0.01-mg resolution up to 101 g and 0.1-mg resolution to 250 g. The one-touch automatic calibration function with its motor-driven mass offers easy calibration. The Phoenix also incorporates automatic self-calibration when it detects ambient temperature changes. Standard RS-232C and WinCT data collection software is included with the balance.

A&D Weighing For information 800-726-7099 www.andweighing.com

Whole Genome Amplification

The REPLI-g Kits provide highly uniform DNA amplification across the entire genome, with minimal sequence bias. Various samples can be used, including genomic DNA, fresh or dried blood, buffy coat, and tissue culture cells. Typical DNA yields from a REPLI-g Kit reaction are about 40 μg per 50 μl reactions. A uniform yield of amplified DNA is usually achieved regardless of the quantity of template DNA, enabling immediate downstream genetic analysis, including single nucleotide polymorphism genotyping, protein immunoblotting, restriction fragment length polymorphism analysis, subcloning, and DNA sequencing. The REPLI-g Service provides amplification of unlimited amounts of DNA from limited samples.

Qiagen For information +49 2103 29 12400 www.qiagen.com

Hybrid Phosphoinositide Analogs

Hy-PIPs are a novel class of hybrid phosphoinositide analogs for use in lipid signaling research and drug discovery. They are superior to labeled phosphoinositides because they behave like endogenous phosphoinositides and offer improved aqueous solubility. Hy-PIPs allow better cell staining, improved in vitro assay performance, and increased protein–lipid interaction. Hy-PIPs have potential for use in reporter-based, in vitro biochemical activity screens or for monitoring real-time in vivo distribution and function in living cells. Hy-PIPs are available with biotin or fluorophore labels.

Echelon Biosciences For information 866-588-0455 www.echelon-inc.com

Pre-Separation Filters

MACS Pre-Separation Filters can be used to filter cell suspensions for removal of cell clumps and aggregates before magnetic cell separation. This can improve the separation performance, especially when isolating very rare cells. The filters are equipped with a 30 μm nylon mesh, and can be used for any other application in which removal of particles larger than 30 μm is desired. The filters fit on a variety of MACS Separation Columns as well as on 15 mL tubes.

Miltenyi Biotec For information +49 2204-8306-0 www.MiltenyiBiotec.com

Chiral Stationary Phases

A new generation of immobilized polysaccharide chromatography phases for large-scale chiral separations is available. This new class of chiral stationary phases was designed to improve the productivity of simulated moving bed manufacturing processes for single enantiomer pharmaceuticals. The first product, 20-μm Chiralpak IA, offers significantly broader solvent choices while maintaining the high loading capacity and selectivity of the widely used coated polysaccharides.

Chiral Technologies For information 800-6-CHIRAL www.chiraltech.com

Rat Bioarray

The CodeLink ADME Rat 16-Assay bioarray features a multi-assay chamber that allows up to 16 samples to be processed in parallel on every slide, making it suitable for the high throughput needs of absorption, distribution, metabolism, and excretion (ADME) and toxicity studies in drug discovery in a rat model. Every slide has 16 arrays, each containing more than 1200 carefully selected and functionally validated oligonucleotide probes targeting unique and well-characterized genes involved in ADME processes.

GE Healthcare For information 732-457-8149 www.gehealthcare.com

---

Newly offered instrumentation, apparatus, and laboratory materials of interest to researchers in all disciplines in academic, industrial, and government organizations are featured in this space. Emphasis is given to purpose, chief characteristics, and availability of products and materials. Endorsement by *Science* or AAAS of any products or materials mentioned is not implied. Additional information may be obtained from the manufacturer or supplier by visiting www.science.labvelocity.com on the Web, where you can request that the information be sent to you by e-mail, fax, mail, or telephone.

EDITORIAL FEATURE

Keys to Independence in the U.K. and Ireland

Funding bodies are coming to the aid of young scientists with a variety of programs aimed at helping them become independent investigators

Scientific independence—the freedom to pursue one's own research ideas—is the dream of many ambitious young scientists. But postdocs everywhere find it difficult to escape their indenture and go their own way, and many plow away on their adviser's projects long after they have paid their dues.

What young researchers need is a little career and income stability, a little time to do their own work, and above all, some cold, hard research cash in their own name. Fortunately, their predicament is starting to be noticed. Just last month, the U.S. National Research Council highlighted the struggles of postdoc biomedical researchers to gain independence in the United States, pointing out that only 4% of awards from the National Institutes of Health are granted to new investigators. In 2002, a similar wake-up call was issued in the United Kingdom by the so-called Roberts Review, a report on "the supply of people with science, technology, and engineering skills" commissioned by three U.K. government departments.

The U.K. government has since provided funding to make career paths more stable for postdocs, launching a fellowship program to complement existing ones aimed at scientists making the transition to independent investigators. In Ireland, too—aided by the late '90s economic boom—the government has started to increase the opportunities for scientific independence available to the country's early career scientists. In this special feature, *Science*'s Next Wave, the online publication about science careers (www.nextwave.org), examines these efforts, provides details of some of the top programs (p. 429), and reports on the experiences of young scientists in the United Kingdom and Ireland who are benefiting from them (p. 428).

The power of money

Most agree that the key to unlocking the postdoc shackles is money—independent money. But in the United Kingdom, a standard rule is that postdocs can only apply for major research grants as co-investigators, which keeps them in thrall to a more experienced scientist. In Ireland, postdocs have been eligible to apply for research grants, but until recently funding bodies did not have enough money for postdocs to have a reasonable chance at winning substantial funding.

Still, money has little value without space. In the United Kingdom and Ireland, all researchers applying for grants first have to identify an institution willing to offer them lab space and other essential research support. And that is why, according to Joanne Ross, university interface manager at the U.K.'s Engineering and Physical Sciences Research Council (EPSRC), "the main route for a young researcher to become independent is to get an academic [faculty] position at a university." Such positions usually come with lab space and—especially relevant to U.K. postdocs—"make young researchers eligible to apply for research grants," says Ross.

Unfortunately, junior faculty positions—termed "lectureships" in the United Kingdom and Ireland—are few and highly competitive. The Roberts Review reported that less than 20% of postdocs will ever get a permanent university post. As a result, the transition from postdoctoral serfdom to the scientific equivalent of land ownership—a faculty position with an independent lab—is very slow, often rocky, and rare.

Even those chosen few have a tough row to hoe. Most lectureships come with limited funds to set up labs, so the first thing new lecturers have to do—in between lecture preps and administrative duties—is to write enough research grant proposals that at least one or two will be funded. All this leaves little time for research, at precisely the time when scientists are called upon to make their marks as independent research scientists.

Just last year, the U.K. government introduced a new initiative—the Academic Fellowship Programme—aimed at smoothing the transition from postdoc to lecturer. With this scheme, the government is allocating funding for 1000 positions over the coming 5 years directly to universities so that they may recruit fellows based on their anticipated needs for lecturing staff. Fellows will be expected to take on teaching duties and project management responsibilities gradually as they spend most of their time developing their own independent research. The support is modest—£25,000 per fellow per year for 5 years—so the universities and funding bodies must supplement the fellows financially. The real payoff for academic fellows—and it's a big one—is the promise of a faculty position at the end of the fellowship, after a probationary period.

The U.K. Academic Fellowships are a new approach, but the basic idea—giving young researchers some cash of their own and a boost toward research independence—isn't new. Indeed, in the United Kingdom, the personal fellowship is a long-established, prestigious, more robust career trajectory for early career scientists aspiring to become independent researchers. These grants provide a big chunk of research money and immediate independence. The U.K. Biotechnology and Biological Sciences Research Council (BBSRC) David Phillips Fellowships, for example, pay the fellow's salary for 5 years and a one-off research support grant of up to £200,000. Some of these schemes are also open to junior lecturers, so that they may buy time away from lecturing and concentrate on putting their research career on track.

In Ireland, following a funding boost from the government, Science Foundation Ireland (SFI)—the country's major research funding agency—began to offer a funding scheme

Published by AAAS

comparable to the United Kingdom's personal fellowship, the President of Ireland Young Researcher Awards (PIYRA). These are generous, paying up to €1.2 million to each researcher over 5 years.

The Irish funding boost also had repercussions on mainstream research grants. The tangible difference for young scientists now is that funding bodies have sufficient resources to give them their share of the money pot. In particular, the SFI Investigator Programme offers successful candidates between €100,000 and €250,000 per year, with an overall success rate last year of 28%. Both PIYRA and Investigator grants focus on Ireland's key areas of strategic interest—biotechnology and information and communication technologies—although these grants are available for work in any area that "underpins" these fields.

These fellowships and other independent-funding schemes intended to ease the transition to scientific independence are still rare in the United Kingdom and Ireland, as they are elsewhere. Yet, for the few young scientists who manage to get one, they can make becoming independent much less harrowing. And because they tend to go to the best and the brightest, the scientific significance of these awards is probably much greater than their numbers indicate. But perhaps most encouraging is that these programs are evidence that U.K. and Irish funding bodies are aware of the obstacles early career scientists face as they approach scientific independence and are taking some initiative to help them solve these problems. As SFI Director General Bill Harris puts it, "Today's young researchers will be leading the research teams of tomorrow; we want them to have good career paths."

–ANNE FORDE AND ELISABETH PAIN

Anne Forde is an editor based in Cambridge, U.K., and Elisabeth Pain is a contributing editor based in Barcelona, Spain, for *Science*'s Next Wave.

EDITORIAL FEATURE

Views From the Trenches

Making the transition from postdoc to independent investigator is tough. Scientists who received prestigious fellowships or grants relate their experiences—and offer some advice

Karin Hing has her own research team at the Interdisciplinary Research Centre in Biomedical Materials at Queen Mary University in London. She also has independent funding, her research into bone graft substitutes has led to the formation of a spinoff company, and at home she has a budding family. In short, she could be mistaken for a successful senior lecturer at any U.K. research university. But one thing she doesn't have—yet—is a permanent faculty position.

Hing is one of a few early career scientists in the United Kingdom and Ireland who have won grants that allow them to work independently, even before they have attained lectureships (the equivalent of assistant professorships in the United States). These grants may come in the form of a fellowship in the United Kingdom or an independent research grant in Ireland, but whatever the name and particular strategy, they all provide a much-needed kick-start for an academic research career. Grants like these offer generous, independent research support, which gives highly talented young scientists some leverage to negotiate with universities for lab space and other support usually available only to lecturers and more experienced scientists. This in turn allows them to build their own research teams and—most importantly—to pursue their own research ideas. Despite their relative youth and inexperience, these lucky few are able to work as principal investigators (PIs) while greatly improving their prospects for more permanent academic employment. Call them "junior PIs."

Making the break. Karin Hing's fellowship has brought independence to pursue her work on bone graft substitutes.

CREDIT: TOM BUCKLAND

Finding the right host

Funding bodies in the United Kingdom and Ireland offer a variety of schemes that provide young scientists at least some of the advantages that Hing enjoys (see story, p. 427, and box, p. 429). These diverse programs all have a common goal: to free young scientists from dependence on a more senior scientist or even a university.

First, however, applicants for these coveted awards must find a university willing to provide lab space and other institutional support. In the United Kingdom, applicants approach a prospective host institution seeking an endorsement of their projects. Working out the nitty-gritty details of space and equipment and securing them permanently comes later. "In my experience, it is very unusual for a fellow to be promised an empty lab by their host before applying for a fellowship," Hing says. "But once you have your fellowship, you are then in a position to barter with your host for extra space—or to find a better offer!"

In Ireland, institutions tend to commit earlier, but this doesn't mean more casually. As Ruth Davis, research support officer at University College Cork, says, "We have to know up front—at the proposal stage—what the candidate needs." While they always look to choose the best scientific candidates, she notes, they must also consider whether "we can deliver the space and additional resources they need."

For the prospective junior PI, there is more to picking an institution than lab space and equipment. "People have to look at the support and inspiration [the host institution may offer them]," says Kevin Ryan, a Cancer Research UK senior cancer research fellow investigating how regulating factors in programmed cell death may be used as potential targets for therapy. Also important, Ryan says, is whether junior PIs feel comfortable with the departmental and institutional administrators they will have to work under, because "you will ask them for support and need to know that any concerns you may

Published by AAAS

have will be heard." Ryan chose the Beatson Institute for Cancer Research in Glasgow because he knew the institute well, having worked there as a Ph.D. student.

Cormac Taylor of University College Dublin (UCD) Conway Institute of Biomolecular and Biomedical Research has a lot of experience with this kind of negotiation. Taylor won a Wellcome Trust Career Development Fellowship,

"The biggest challenge is to manage people and know what everyone is doing."
–Cormac Taylor

which he used to start his work on oxygen sensing in human disease, after which he secured a Science Foundation Ireland (SFI) Investigator grant. Taylor's advice: Use your fellowship and grant money as leverage to negotiate good working conditions. "Don't underestimate your own value, and don't undersell yourself."

Boost your chances

That advice could apply equally well to researchers entering the hot competition for independent grants. Apart from an excellent track record, review panels look for a carefully conceived, interesting research plan that the applicant is well prepared to execute. SFI Director General Bill Harris says the main criteria are the "quality of the idea, quality of the recent track record of the researcher, and the strategic relevance of the research."

Kristina Downing of the Department of Biochemistry at the University of Oxford believes that the novelty of a project and its relevance to the funding body's mission are key. She should know; she has won two fellowships. In 1996, she received a Research Career Development Fellowship from the Wellcome Trust, a funding body in the United Kingdom primarily interested in understanding human health and disease. Downing proposed to study the structure of fibrillin 1, a large cell-membrane modular protein, and to examine how structural changes in the protein relate to human disease. In 2000, she applied for a Senior Research Fellowship in Basic Biomedical Science, also from the Wellcome Trust, and was successful again. This time her research project extended her findings to other proteins and diseases.

CREDITS (TOP TO BOTTOM): SCIENCE FOUNDATION IRELAND; K. DOWNING

A potential for commercial applications may also tip the balance in an applicant's favor. Fergal O'Brien won a President of Ireland Young Researcher Award (PIYRA) from SFI to launch his research at the Department of Anatomy at the Royal College of Surgeons in Dublin. He is using his award to look into developing a physical collagen matrix that could be used clinically as an artificial tissue scaffold. O'Brien feels that the combination of basic research and commercial potential in his project attracted SFI's interest.

Showing that you will bring scientific knowledge back to the United Kingdom or Ireland is another factor that can play an important role, or so thinks UCD's Taylor. His Wellcome Trust Fellowship and SFI grant allowed him to return to his native Ireland after spending 5 years at Harvard Medical School in the United States. Taylor believes that the key to both of his funding successes was his desire and ability to "take expertise or technology from an international institution" and inject it into a local institution.

The bumpy road to independence

Once you have independent funding, a host institution, and lab space, then comes the really hard part: building up a research team. "Setting up my own lab was really hard," says Downing. "I had come from a pretty computational background and didn't know any molecular biology." She was helped by her first postdoc, who had more molecular-

"Setting up my own lab was really hard. … I had come from a pretty computational background and didn't know any molecular biology."
–Kristina Downing

biology experience. Still, Downing estimates that by the time the old lab she was allocated was refurbished, the lab space arranged, and the equipment bought and delivered, 6 months had elapsed. "Fortunately, I was able to work in a different lab during this time, so no one's work suffered," she says.

Newly independent scientists also must hire—and support—people for the first time. PIYRA awardee O'Brien, who currently has three Ph.D. students and one postdoc, encour-

Find a Fellowship

Several government and private organizations offer fellowships to bridge the divide from postdoc to independent investigator. The following programs provide salary and other support. For more details, including deadlines, success rates, and how to apply, go to www.nextwave.org

UNITED KINGDOM AND IRELAND

Wellcome Trust Research Career Development Fellowships in Basic Biomedical Science
For scientists with 3 to 6 years of postdoctoral experience. Covers salary for fellow and a graduate research assistant or technician, and research expenses for up to 4 years.
www.wellcome.ac.uk/node2129.html

Wellcome Trust Senior Research Fellowships in Basic Biomedical Science
For scientists with 5 to 10 years of postdoctoral experience. Covers salary for fellow, research staff, and technical support and expenses for equipment, consumables, and travel for 5 years.
www.wellcome.ac.uk/node2130.html

UNITED KINGDOM

Biotechnology and Biological Sciences Research Council (BBSRC) David Phillips Fellowship
Up to 10 fellowships for scientists with less than 5.5 years of postdoctoral research experience. Covers the fellow's salary (£27,000 to £30,000 a year) and a one-off support grant of up to £200,000 for technical support, equipment, consumables, and travel expenses, for up to 5 years.
www.bbsrc.ac.uk/funding/fellowships/Welcome.html

Medical Research Council New Investigator Award
Up to 30 fellowships for senior postdocs or newly appointed academics. Covers salary for fellow and a researcher or technician, and research and travel costs for 3 years. Maximum value of the award is £300,000.
www.mrc.ac.uk/index/funding

Medical Research Council Career Development Award
About 10 fellowships for scientists with 3 to 6 years of postdoctoral experience. Covers salary for the fellow and research staff, and research and travel expenses for up to 4 years.
www.mrc.ac.uk/index/funding

Royal Society University Research Fellowships
Up to 40 fellowships for scientists with 2 to 7 years of postdoctoral research experience. £50,000 to £60,000 a year for 5 years covers the fellow's salary and goes toward staff and research costs.
www.royalsoc.ac.uk/funding.asp?id=1121

Engineering and Physical Sciences Research Council (EPSRC) Advanced Research Fellowships
About 49 fellowships for scientists with at least 3 years of postdoctoral experience who were awarded their Ph.D.s less than 10 years ago. Covers the fellow's salary for up to 5 years. Fellows will have the option to apply for research funds for research staff, equipment, and consumables for up to 3 years.
www.epsrc.ac.uk/ResearchFunding/FundingOpportunities/Fellowships/default.htm

Cancer Research UK Career Development Fellowship
Up to four fellowships for scientists with 3 to 6 years of postdoctoral experience. Covers salary for fellow and a postdoc and a technician, and research expenses for 6 years, plus a one-off equipment grant of up to £25,000.
science.cancerresearchuk.org/gapp/grantapplications/tcdb/tcd_cdf?version=1

Senior Cancer Research UK Fellowship
Up to four fellowships for scientists with 6 to 10 years of postdoctoral research experience. Covers salary for fellow, a postdoc, a Ph.D. student, and a technician; research expenses for 6 years; and a one-off equipment grant of up to £50,000.
science.cancerresearchuk.org/gapp/grantapplications/tcdb/tcd_scrf?version=1

IRELAND

Science Foundation Ireland (SFI) President of Ireland Young Researcher Award
Up to 10 fellowships for scientists in fields that underpin biotechnology and information and communications technologies who have received a Ph.D. within the last 5 years. Provides up to €1.2 million for salaries and funding for equipment, consumables, travel, and collaboration for 5 years.
www.sfi.ie/content/content.asp?section_id=418&language_id=1

SFI Investigator Programme Grants
About 22 fellowships for scientists in fields that underpin biotechnology and information and communications technologies with at least 3 years of postdoctoral experience. Provides €100,000 to €250,000 per year for salaries and funding for equipment, consumables, travel, and collaboration for 4 years.
www.sfi.ie/content/content.asp?section_id=188&language_id=1

Health Research Board Research Project Grants
About 50 fellowships for scientists with more than 3 years of postdoctoral experience. Provides €55,000 to €70,000 per year for 3 years for salary costs and small items of equipment, consumables, travel, and training.
www.hrb.ie/display_content.php?page_id=99

Bird in the hand. Mark Whittingham hopes his fellowship to study foraging and distribution patterns in birds will lead to a permanent post.

ages new PIs to "take their time to pick the right people," because "it will pay off." O'Brien was "stunned" when his advertisement for a postdoc drew about 100 responses from around the world. O'Brien feels that he could hire a highly skilled candidate because he had 5 years of research funding. "That was a big selling point," he says.

Like any other newly independent scientist, independent-grant winners soon find themselves managing people, something they aren't trained to do. Taylor thinks that "science is the [relatively] easy part; the biggest challenge is to manage people and know what everyone is doing." Taylor started with a single technician, and he advises other scientists to "start small [in order] to learn people management." His team now has seven members.

Next destination: a permanent post?

With a substantial publication record and the experience of getting a lab up and running and launching an independent research team, independent grant winners are in good shape when the time comes to compete for permanent positions. "A fellowship is very valuable in terms of offering you 5 years and leverage to apply for a lectureship at a university," says Mark Whittingham, who joined the Department of Biology at the University of Newcastle upon Tyne, U.K., in 2004. Whittingham received a David Phillips Fellowship from the Biotechnology and Biological Sciences Research Council to investigate foraging decisions and distribution patterns of birds and the implications for conservation.

Importantly, U.K. fellowships require host institutions to help recipients integrate into the regular academic staff. "I haven't signed anything, but there is an informal agreement that as long as I do well, I will get a position," says Whittingham.

For some independent-funding recipients, integrating into the regular permanent staff isn't a problem. Ryan applied for a lectureship at the Beatson Institute at the same time he applied for his Cancer Research UK Fellowship. "I got offered the job before getting the fellowship," he says. When he won the fellowship shortly after that, the institute offered him a new package, tailored for his position, and he was able to hire a couple of extra people. Yet Ryan is confident he would have benefited if things had happened in the opposite order. "If you want to have a job, a fellowship is a very good thing to bring with you," he says. "It is very attractive to employers, because you have a salary, it is quite prestigious, and it indicates you are able to write a research plan that has already been vetted."

Still, the picture may not be as rosy for everybody, given the current dearth of faculty positions. Justin McCarthy, an SFI Investigator in the Department of Biochemistry at University College Cork, fears that some who have impressive PI funding but no tenure may be left in the lurch when their funding dries up. He, fortunately, won't be in that position; he already holds a lectureship.

Hing's position is not as secure. "Once I had the fellowship, they gave me a lectureship [immediately]," she says. But this was a fixed-term lectureship. Although it topped up her fellowship salary and added to the prestige without requiring onerous teaching and administrative duties, "there was no guarantee of employment beyond the end of my fellowship," she says.

Now reaching the end of her fellowship, Hing is negotiating with her institution for a permanent position. "I have been led to believe I will get a permanent position, but I am not 100% sure," she says. She advises new grantees to make a clear arrangement about what is going to happen when their independent funding runs out. "You should negotiate a permanent position with your host from the beginning, so that you can relax and concentrate on your research throughout your fellowship," she says. And if it should prove impossible to get a firm promise from the host institution, she advises looking into what other career prospects may be offered by other institutions—another great advantage of having funding in your own name.

–ANNE FORDE AND ELISABETH PAIN

CREDIT: M. J. WHITTINGHAM